DEVELOPMENT OF AN ENERGY MANAGEMENT SYSTEM FOR FUEL CELL/LITHIUM-ION BATTERY HYBRID ELECTRIC VEHICLES

by

OBU SAMSON SHOWERS

Thesis submitted in fulfilment of the requirements for the degree

Doctor of Engineering: Electrical Engineering

in the Faculty of Engineering

at the Cape Peninsula University of Technology

Supervisor: Prof AK Raji

Bellville Campus

October 2022

DECLARATION

I, **Obu Samson Showers**, declare that the contents of this dissertation/thesis represent my own unaided work, and that the thesis has not previously been submitted for academic examination towards any qualification. Furthermore, it represents my own opinions and not necessarily those of the Cape Peninsula University of Technology.

20th October 2022

Signed **Date**

ABSTRACT

The growing interest in fuel cell hybrid electric vehicle (FCHEV) is largely supported by the decline in fossil fuel production and the need to operate eco-friendly transport system. This interest has triggered significant research on various aspects of FCHEV. Again, environmental pollution associated with internal combustion engine (ICE) vehicles, advancement in fuel cell technology, improvement in power electronics, and cutting-edge energy management systems (EMSs) are additional reasons why FCHEV has received significant attention by both the transportation and environment sectors including researchers and vehicle manufacturers. However, having an effective EMS improves the performance of fuel cell hybrid electric vehicle by enhancing the optimisation of individual components within the system. However, to overcome the complex task of optimisation, factors such as component degradation, straight-line performance, fuel consumption and driveability must be considered in detail. Hence, the primary purpose of EMS in a FCHEV is to reduce the electrical stress exerted on the fuel cell, increase the productive lifespan and to minimise the fuel consumption. This is informed by the fact that the durability and cost of fuel cell stack is the main obstacle preventing massive adoption of FCHEVs.

Therefore, an EMS is designed and developed under the MATLAB/Simulink environment and Typhoon HIL software for Real-Time simulation primarily to optimise power regulation and distribution for a fuel cell/ lithium-ion battery hybrid electric vehicle. The EMS is developed to exploit the advantages of fuel cell and lithium-ion battery hybridisation for improved performance while offsetting the individual setbacks. The system consists of a 100 kW proton exchange membrane fuel cell stack (PEMFC), DC-DC boost converter, 30 kW lithium-ion battery, DC-DC bidirectional converter, an inverter, permanent magnet synchronous motor (PMSM), vehicle body (including chassis, tires, gears) and controllers that ensured effective power distribution.

To demonstrate the effectiveness of the developed EMS in terms of power distribution and performance, it was implemented using Federal Test Procedure-75 (FTP-75) drive cycle to highlight transient load and regenerative braking. In addition, the EMS is modelled with fuel cell control component and battery control component respectively using PI controller, battery SOC and power demand by the electric vehicle (EV). This was implemented using external voltage loop and internal current control loop of the bidirectional converter and current loop control and the voltage loop of the DC-DC boost converter. The results showed a precise response to the load demand and improved performance throughout the drive cycle. The lithium-ion battery was able to supply power during transient loads when the power supply from the fuel cell was less than the load demand. Furthermore, validation of the MATLAB/Simulink result was required to authenticate it by implementing the model in real-time using Typhoon

HIL software. The real-time result was similar to the ones obtained in MATLAB/Simulink environment thereby confirming the effectiveness of the EMS.

Keywords: Fuel Cell, Lithium-ion battery, Energy Management System, Hybrid Electric Vehicle, MATLAB/Simulink, Typhoon HIL software.

ACKNOWLEDGEMENTS

I wish to express my honest thanks to Almighty God for giving me perfect health coupled with clarity of purpose from the start of this journey to the end.

A special thanks to my supervisor (Prof AK Raji) for his immense contribution, support, motivation, guidance and encouragement. His guidance helped me from the beginning to the end of this research journey. I could not have imagined having a better supervisor and mentor. Prof, your excellent and well-guided supervision ensured the success of this thesis.

I would like to thank all my siblings for the support and words of encouragement whenever required. Your show of love during this period cannot be overemphasized.

My genuine thanks also go to all members of Faculty of Engineering, staffs at the centre for distributed power electronics system (CDPES) and energy institute and friends for their immeasurable suggestions and contributions throughout this work.

I would also want to thank the Cape Peninsula University of technology and University Research Fund (URF) for their financial assistance.

DEDICATION

This thesis is dedicated to the SHOWERS dynasty for all your support and nurturing.

TABLE OF CONTENTS

TABLE OF FIGURES

LIST OF TABLES

GLOSSARY OF TERMS

AC	Alternative Current
AEV	All-Electric Vehicles
AFC	Alkaline Fuel Cells
ANN	Artificial Neural Network
BEV	Battery Electric Vehicle
CHP	Combined Heat and Power
CSI	Current Source Inverter
DC	Direct Current
DMFC	Direct Methanol Fuel Cell
DP	Dynamic Programming
ECMS	Equivalent Cost Minimization Strategy
EDLC	Electrochemical Double Layer Capacitor
EIA U.S.	Energy Information Administration US
EM	Electric Motor
EMS	Energy Management System
EREV	Extended Range Full-HEV
ESS	Energy Storage System
EV	Electric Vehicle
FC	Fuel Cell
FCEV	Fuel Cell Electric Vehicle
FCHEV	Fuel Cell Hybrid Electric Vehicle
FES	Flywheel Energy System

FLC	Fuzzy Logic Controller
Full-HEV	Full Hybrid Electric Vehicle
GHG	Green House Gases
HESS	Hybrid Energy Storage System
HEV	Hybrid Electric Vehicle
HF	Hybridization Factor
ICE	Internal Combustion Engine
ICEV	Internal Combustion Engine Vehicle
IEA	International Energy Agency
MCFC	Molten Carbonate Fuel Cell
MES	Main Energy Source
MHEV	Mild Hybrid Electric Vehicle
NN	Neural Network
PAFC	Phosphoric Acid Fuel Cells
PEMFC	Proton Exchange Membrane Fuel Cell
PHEV	Plug-In Hybrid Electric Vehicle
PI	Proportional Integral
PID	Proportional Integral Derivative
PPS	Primary power supply
SMC	Sliding Mode Control
SOC	State of Charge
SOFC	Solid Oxide Fuel Cell
UC	Ultracapacitor

UDSE	U.S. Department of Energy
VRLA	Valve Regulated Lead Acid
VSI	Voltage Source Inverter

CHAPTER 1: INTRODUCTION

1.1 Background

Fuel cell as a source of power for electromobility has been a major topic of academic and technical discussions in the electric transportation industry in the past decade and has contributed significantly to the increase in the deployment of electric vehicles. A report from the International Energy Agency (IEA) showed that the number of electric vehicles increased significantly from 2010 to 2021. Presently, the number of electric car stock globally is 16.5 million according to the last report by the IEA at the end of 2021 (IEA, 2022). This number according to regions, countries and type is presented in Figure 1.1.

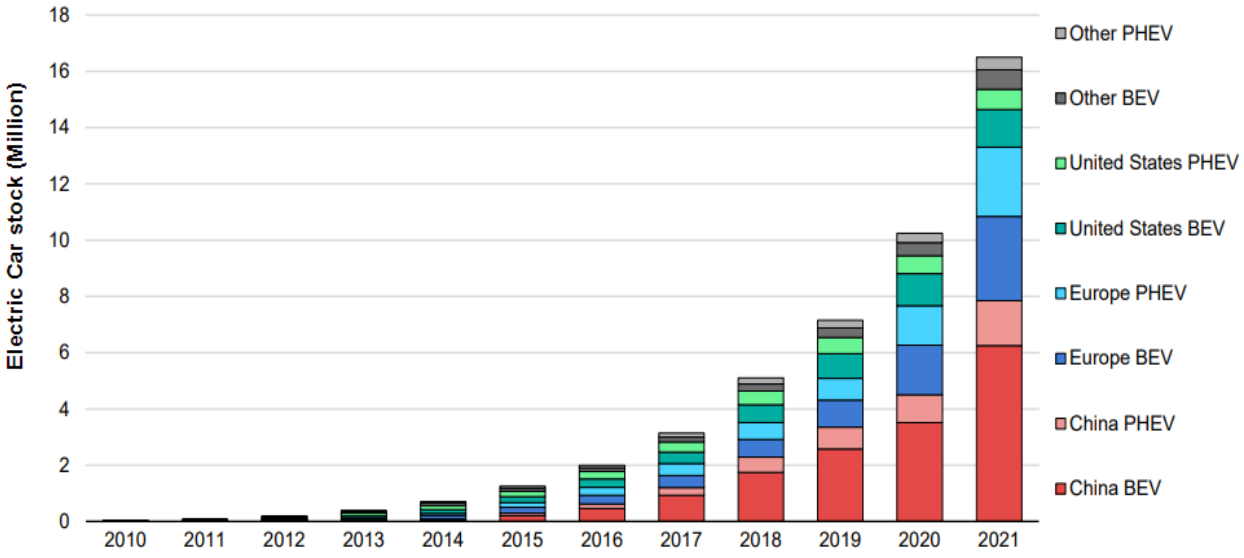

Figure 1.1: Electric car stock by region and technology (IEA, 2022)

The general interest in electric vehicles and fuel cell is largely supported by the decline in fossil fuel and the need to operate an eco-friendly transport system. This interest has equally triggered extensive research in the application of fuel cell in electric transportation industry. Furthermore, environmental pollution associated with internal combustion engine (ICE) vehicles, advancement in fuel cell technology, improvement in power electronics and cutting-edge energy management techniques has contributed significantly to the deployment of fuel cell/lithium-ion battery hybridisation in electric vehicle application (Zeiaee, 2016; Salet, 2018; Yue, 2019; Erensoy, 2018; Pittini, 2014). International policy on public transportation, electromobility and renewable energy adoption has also supported and contributed to the growth of fuel cell applications in electric transportation (Gao et al., 2019; Shang, 2013; Jeon, 2020; Felgenhauer et al., 2016; EG&G Technical Services, 2004; Vaz, 2015).

There are several in-depth technical literature and research on electromobility conducted in the past ten years that studied the use of fuel cell, supercapacitor and batteries as the primary

and secondary sources of power for electric vehicles (Hosseini & Butler, 2020; Sulaiman et al., 2018; Weyers & Bocklisch, 2018; Panday & Bansal, 2016; Böhme & Benjamin, 2017). However, the use of fuel cell and lithium-ion battery requires further investigation with regards to its suitability and energy management system processes. According to Mokrani et al. (2014), the hybridisation of fuel cell and supercapacitor has the capacity to supply both active and reactive power to electric vehicles if the energy management system is optimised. In addition, the study also indicated that with the inclusion of lithium-ion battery, the delay in response time associated with the former can be addressed and the entire system improved significantly.

The quest to operate environmentally friendly transport system with well modelled energy management systems and advancement in semiconductors has presented a novel advantage in the use of fuel cell/ lithium-ion battery powered electric vehicles. It has shown to be a reliable source of primary power supply to electric vehicles hence, supporting the electric transport initiative aimed at discouraging the over-reliance on fossil fuel which many studies have shown to be a major contributor to environmental pollution (Behdani & Naseh, 2017; Zhi-ling et al., 2010; Xu et al., 2015; Wu, 2014; Waag et al., 2014).

FCHEV has exhibited significant potential and travel range advantage over battery electric vehicle (BEV) due to less mass and packaging volume cost while still retaining all the advantages of a complete EV (Wang et al., 2006). This is because fuel cell system has better energy density in relation to its mass batteries and permits more chemical energy to be stored without an increase in the vehicle mass. In addition, hydrogen has a very high energy density and the energy storage conversion components of a fuel cell are entirely separated. This means that the tanks can be resized according to the storage demand while the stack is sized to handle the prevailing power demand (Benyahia et al., 2014; Tazelaar et al., 2013; Sulaiman et al., 2015; Ates et al., 2010; Manoharan et al., 2019; Fletcher, 2017; Carnevali, 2017). Again, several studies have shown that fuel cell is a suitable choice for electric vehicles application, but a lot of research is still required to address obvious technological glitches (Hosseini & Butler, 2020; Weyers & Bocklisch, 2018; Sulaiman et al., 2018; Azidin, 2016; Han et al., 2014). Some of these challenges include high production cost, durability of the stack, proper modelling of the energy management system (EMS) and high energy density by mass of hydrogen storage fuel cell (Ehsani et al., 2018; Okba, 2015; Bendjedia et al., 2016; George, 2018).

Presently, there are few technical literatures available on distributed parameter model-based control (Han et al., 2014; Azidin, 2016; Arabul et al., 2015; Fletcher et al., 2016; Gou et al., 2010; Ehsani et al., 2010; Sahu, 2017). However, a time-dependent analysis and linear control strategies for fuel cells in general and PEMFC in particular, using distributed model-based was presented in 2017 (Sahu, 2017; Carnevali, 2017; Das et al., 2017; Behdani & Naseh, 2017). The research used a ratio control strategy and a Multi-Input Multi-Output (MIMO) control

system. The main objective, however, was to control the power density and temperature hence, the results showed that by selecting the appropriate controlled variables, the PEMFC did not reveal any sign of variation in gain and thus can be regulated by a linear controller. This was limited to the control strategies and did not investigate the proficiency of the model.

According to Becherif et al (2015), Uzunoglu & Alam (2007), Herb et al (2013), Alloui et al (2015), Smithson Bell (2016), Feroldi (2012), Kolli et al (2015) and Abd El Monem et al (2014), improved energy management systems, efficient modelling of fuel cells and selecting the right size of lithium-ion batteries, which are seen to be the basic components of a FCHEV, can be used to solve some of the challenges hindering the massive rollout of electric vehicles globally. The present fuel cell hybrid technology together with suitable energy management system has shown huge potential in creating a reliable electric transportation system devoid of environmental pollution (Gao, Jin, Liu, et al., 2016; Das et al., 2017; Strahl, 2014; Hernandez et al., 2014; Fonseca, 2013).

A study on the impact of effective energy management system, proper control and correct operating parameters of PEMFC during the load-up process and its relevant application on vehicles is necessary as it relates to the adoptability of PEMFC application in vehicles (Salet, 2018; Jeon, 2020). This will assist researchers understand and analyse the changing characteristics of current output and corresponding voltages in the flow field of PEMFC. All the principles of dynamic electric output during the load-up process achieved during the research will assist and be beneficial for optimising, controlling, operating, and modelling an appropriate energy management system for PEMFC application on vehicles.

The above in-depth, current and technical literatures have clearly highlighted the significance and urgent need for this research even as the world is moving towards electric transportation and trying to reduce the over dependence on fossil fuel powered transport system. Therefore, this research supports meaningful initiatives by government, policy makers and researchers aimed at increasing the adoption of more fuel cell/lithium-ion battery powered electric vehicles on the road by modelling an efficient energy management system.

1.2 Statement of the research problem

Globally, the depletion of fossil fuel deposits is occurring faster than they are replenished. It is predicted that the available fossil fuel can only meet the world energy demand for the next 40 years because of the lack of capacity to get the fossil fuel out of the ground in no distant future (Azidin, 2016). Additionally, the use of fossil fuel and internal combustion engine (ICE) vehicles has contributed significantly to environmental pollution and looming concerns of anthropogenic (man-made) climate change. Because of the above problems and more, it is critical to adopt and develop a transportation system that will not depend on fossil fuel as the primary source

of energy hence, the adoption of electric vehicles. The acceleration of electric vehicle (EV) adoption in the past decade has been significant due to technology maturity, anticipated scarcity of fossil fuel and government policies on environmental protection. Although commercial hybrid electric vehicles are widely accessible in the market at the moment and considered as better alternative to conventional internal combustion engine (ICE) vehicle. Fuel cell/lithium-ion battery powered EV still exhibit some notable limitations but not in the increasing fossil fuel prices nor environmental pollution rather within the energy management system of the vehicle. Some of such limitations are slow charging time, short travel distance, high temperature, self-discharge, low battery capacity level and slow power response by the fuel cell during sudden energy demand (Suh, 2006; Khayyer, 2008; Sahu, 2017; Okba, 2015). Therefore, a proper hybridisation and energy management system of fuel cell/lithium-ion battery powered EV will definitely improve the dynamic behaviour and self-sufficiency of the EV power supply and distribution. Hence, a smart energy management system (EMS) for a fuel cell/lithium-ion battery hybrid EV is required to enhance its functionality.

1.3 Significance of the Research

Having identified the technical hitches associated with the operation of a fuel cell/lithium-ion battery hybrid systems, this research adds value to existing academic literature geared towards evaluating the different types of energy management systems available for automotive applications. This allows for the optimisation of variables such as efficiency, robustness, effective power distribution and durability using existing knowledge of fundamental operating principles with the potential to accelerate the adoption and use of fuel cell/lithium-ion battery hybrid systems for automotive applications.

Again, the proposed energy management system is an efficient, durable, and practicable model that provides a complete outcome capable of helping electric vehicle manufacturers to better understand the dynamics of fuel cell/lithium-ion hybridisation system. In addition, the research will promote and support the use of fuel cell/lithium-ion battery hybrid system as effective sources of power for automotive applications hence, discouraging over dependence on fossil fuel transportation system rather embracing cleaner sources of energy for the transportation sector. In conclusion, the results will help electric vehicle manufacturers, Government agencies, academics, and other stakeholders to better understand the benefits of fuel cell thereby making a well-informed decision on the best sustainable and eco-friendly source of power for electromobility applications.

1.4 Aims and Objectives of the research

Even though several authors have demonstrated the importance of fuel cell in electric vehicle applications, only limited literature is available on the energy management system of fuel

cell/lithium-ion battery hybrid system for automotive applications. Hence, the aim of this research is to model an energy management system that will optimise power supply and distribution of fuel cell/lithium-ion battery hybridisation system for electric vehicle applications.

To accomplish the above aim, the following objectives will be achieved:

- To undertake a literature review of fuel cells, lithium-ion batteries, and electric vehicles.
- To develop a system and method capable of assessing the practicability of fuel cell/lithium-ion batteries for automotive applications.
- To model an energy management system and experimentally validate series of models of control techniques of fuel cell and lithium-ion battery over time scales relevant to electric vehicle applications.
- To advance an understanding of the operation of fuel cell and lithium-ion batteries that will inform the type of design and control required for electric vehicle applications.
- To determine and study the effect of integrating a fuel cell and lithium-ion battery for automotive applications considering the type of power control implemented.
- To identify the best method of optimising a fuel cell/lithium-ion battery hybridisation system design for electric vehicles.

1.5 Delineation of the research

Due to the vastness of the research areas in electric vehicle, fuel cell and battery systems, some limitations are drawn:

- The study concentrated primarily on energy management system for a fuel cell/lithium-ion battery hybrid electric vehicle
- The research was done on electric vehicles only not trains, three-wheels nor trucks
- The study used Federal Test Procedure drive cycle (FTP-75) data for the simulations
- The study used only lithium-ion battery as the secondary source of power

1.6 Thesis outline

Chapter 1 introduces the thesis by presenting a brief background of the research topic, statement of the research problem, its significance, contributions of the research, aims and objectives of the study and delineation of the research.

Chapter 2 offers detailed literature review on the fundamental knowledge of electric vehicles including types of EV and configuration, types of fuel cell systems with specific electrolysers, types of batteries with special concentration on lithium-ion battery, and energy management systems.

Chapter 3 is centred around mathematical modelling of individual components involved in the system such as fuel cell, electric vehicle body, power electronics converters and lithium-ion battery. Thereafter, the individual components are integrated and executed in the MATLAB/Simulink environment and Typhoon HIL for real time simulation.

Chapter 4 presents the energy management system algorithm developed and implemented according to set conditions.

Chapter 5 presents a summary of results obtained from both MATLAB/Simulink environment and Typhoon HIL software in real time. The result is evaluated accordingly to ascertain the effectiveness of the EMS using available studies.

Chapter 6 concludes the thesis and offers some recommendations for further research.

1.7 Publications

The following publication emanated from this doctoral research:

- Showers, S.O. & Raji, A.K. 2020. August. Benefits of Electric Vehicle as Mobile Energy Storage System. *In IEEE PES/IAS Power Africa Conference,* Virtual 2020.

- Mavoungou D.G.M., Showers, S.O., Luta, D.N., & Raji, A.K. Energy Efficiency Techniques for Residential, Commercial and Industrial Sectors in Sub-Saharan Africa. *In IEEE PES/IAS Power Africa Conference,* Virtual, 2020

- Showers, S.O. & Raji, A.K. 2021. Electric Vehicles in South Africa: Status and Challenges**.** *In IEEE PES/IAS Power Africa Conference,* Virtual, 2021.

- Showers, S.O. & Raji, A.K. 2022. Modelling and Simulation of Fuel Cell Hybrid Electric Vehicle Powertrain. *Southern African Universities Power Engineering Conference (SAUPEC)*, Durban South Africa, 2022.

- Showers, S.O. & Raji, A.K. 2022. State-of-the-art review of fuel cell hybrid electric vehicle energy management systems [J]. *AIMS Energy,* 10(3): 458-485, June. Doi: 10.3934/energy.2022023

- Showers, S.O. & Raji, A.K. 2022. Integrating Electric Vehicles for Grid Ancillary Services: Growth and Perspectives. *Industrial and Commercial Use of Energy Conference.* Cape Town, South Africa, 2022.

1.8 Summary

In this chapter, background information on electric vehicles, fuel cell technology, and various energy management systems are introduced. The statement of the research problem and significance of the research are presented. Thereafter, the aims and objectives followed by the delineation of the research are summarised. Finally, the structure of the thesis is explained and publications that emanated from the research is presented.

CHAPTER 2: LITERATURE REVIEW

2.1 Introduction

In this chapter a comprehensive literature review on the fundamentals of electric vehicle with specific focus on the history and development of electric vehicle, electric vehicle design including a brief description of EV parameters and types of electric vehicle configurations is presented. Subsequently, literature reviews on individual components of a FCHEV is presented. This includes its configuration, the electronic converters such as types of DC-DC converters, bi-directional DC-DC converters and the power control architecture.

Furthermore, different types of electric vehicle power supply sources such as electrochemical batteries and ultracapacitors are discussed. This includes their advantages and disadvantages in automotive applications, various types of battery technologies, electric battery configuration, standard electric model of ultracapacitor and state of charge (SOC) of ultracapacitors.

Thereafter, the operating principles and technical characteristics of some types of fuel cell technologies and corresponding electrolysers including their applications and functionalities in electric vehicles are reviewed. This includes the type of electrolyte used, their efficiency and suitability for vehicular applications. In addition, various energy management strategies and techniques indicating their unique features in electric vehicle are adequately reviewed and presented accordingly.

2.2 Fundamentals of Electric Vehicles

Presently, the development of a new generation vehicle that is more energy efficient and environmentally friendly is advocated loudly by various sectors of the society. This type of vehicle can be divided broadly into two categories, pure electric vehicle (EV) and hybrid electric vehicle (HEV). EVs are seen to be more suitable for urban applications and commuter-town vehicles (Erensoy, 2018). However, to use EV efficiently, it is imperative to design the EV to meet users' technical and economic expectations without ignoring the unique environmental conditions. Hence, the EV must be user friendly, technically robust, and affordable with improved performance and increased travel range, including battery reliability as a major deciding factor. Research on the effective performance of a fuel cell hybrid EV (FCHEV) has experienced significant development in the past decade with much needed on the energy management system down to the level of individual components. Through evaluation of the FCHEV dynamic behaviour on the road: moving resistance and effective performance; and the driving performance such as maximum speed, acceleration and energy consumed by the vehicle are obtained and will be used to optimize the FCHEV performance.

2.2.1 History of electric vehicle

Thomas Davenport from Brandon built the first ever recorded electric vehicle in 1834 in the UK. He built a small battery to supply an electric motor that was later used to power a small vehicle that could only drive for short distance. But in 1881, Gustave who was a Frenchman, built EV that weighed about 160 kg including the driver. The design had a DC motor that was powered by a lead-acid battery. Two British academic professors later built a similar electric vehicle two years later (Okba, 2015). The technology improvement by these British professors did not attract the required attention because the performance of the EV at that point was still less than the horse carriages. Hence, potential customers were neither attracted nor impressed because the speed and range were around 15 km/h and 16 km respectively which was far less than horse carriages. 20 years later, EVs gained some level of public acceptance due to technology improvement and competed favourably with gasoline-powered vehicles. This competition was more evident in America where most of the roads were not properly constructed outside major cities (Erensoy, 2018; Okba, 2015). Although during the same period in Europe, gasoline vehicles were more prevalent because most of the roads were properly paved and therefore required longer range vehicles.

In 1894, the Morris and Salom's Electroboat was introduced to the public as the first commercial electric vehicle in New York city used as a taxi as shown in Figure 2.1. The Electroboat during this period in question showed to be more profitable than horse powered cabs regardless of the cost of EVs (approximately $3000) as against $1200 for horse cabs. These improved EVs were powered using two 1.5 hp motors and drove at maximum speed of 32 km/h and a range of 40 km (Okba, 2015).

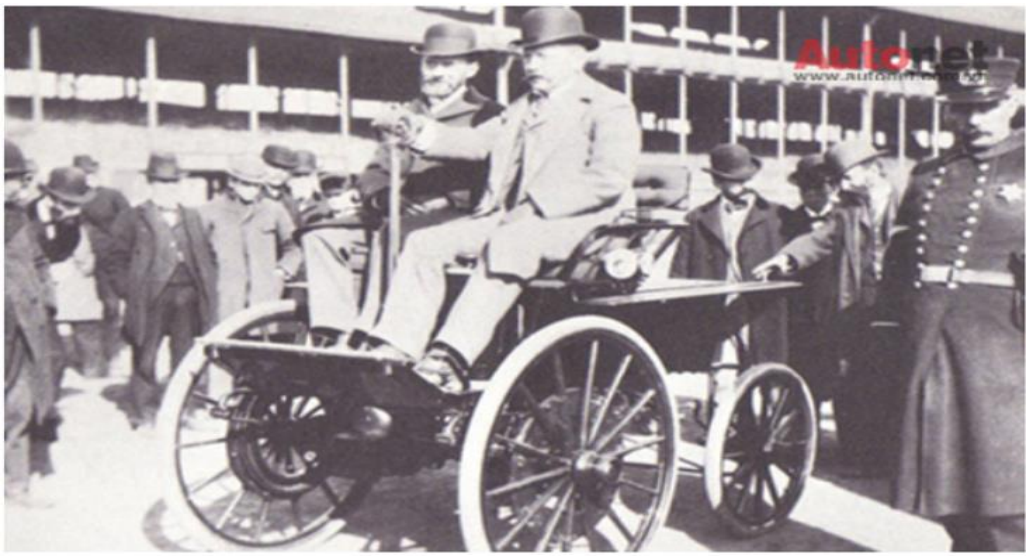

Figure 2.1: Electroboat (Okba, 2015)

The most outstanding technological advancement of this period was the introduction of regenerative braking by M.A Darracq on his 1897 coupe in France. This technique uses the vehicle's kinetic energy that is present during braking to recharge the batteries thereby improving the driving range of the vehicle and boost the energy efficiency in urban driving for both pure electric and hybrid electric vehicles. Furthermore, Camille Jenatzy in 1899, built the first electric vehicle known as "La Jamais Contente" to achieve 100 km/h as shown in Figure 2.2 (Okba, 2015; Fletcher, 2017). This was a significant advancement in electric vehicle in that era before its acceptance started declining. However, the high cost of electric vehicles together with limited driving range and low performance were seen to be the major hindrance in the mass deployment of EVs as against gasoline vehicles, which were more technologically robust and flexible during the same period. The only commercially viable electric vehicles were produced in 1905. These were majorly golf carts and delivery vehicles that were introduced to the public 60 years after the 1899 upgrade (George, 2018).

Figure 2.2: La Jamais contente, 1899 (Okba, 2015)

The electric vehicle industry experienced a significant shift in 1945 when three researchers at the Bell Laboratories introduced the transistors and thyristor that enabled the switching of high currents and voltages. This was significant because it became possible to control the amount of power supplied to an electric motor by avoiding the complexity of using rheostats and provided for easy operation of AC motors at different frequencies (Ehsani et al., 2010). Furthermore, General Motors (GM) in 1966 introduced the Electrovan that was operated by induction motor supplied by inverters constructed using thyristor. But the most outstanding

electric vehicle during this period was the introduction of the “Lunar Roving Vehicle’ which was used by the Astronauts on the moon. The vehicle became popular due to its energy consumption, capacity and light weight. It weighed 209 kg and had the capacity to carry a load of 490 kg while the travel range was approximately 65 km. This was an extra-terrestrial vehicle that had no impact on earth. Hence, the design was simple and easy for engineers because of the absence of air, low gravity in the moon and low speed which contributed to increased travel range (Carnevali, 2017; Ehsani et al., 2010).

Subsequently, in the 1960s and 1980s, environmental protection took the centre stage thereby compelling series of research in electric vehicle. Major automobile manufacturers started the production of prototypes and miniature electric vehicles designated for specific markets and countries. Regardless of the development and several researches carried out on battery technology, power electronics, and electric vehicle during this period, travel range was still a major problem that was considered a hindrance to the mass adoption of electric vehicles (Patel et al., 2021).

The growth of modern-day electric vehicle reached its climax in the 1980s and early 1990s with the introduction of some practical vehicles by firms such as Peugeot Société Anonyme (PSA) with the 106 Electric and GM with the EV1. These EVs revolutionised the entire industry because of the improvement in terms of the capacity, speed, and travel range. However, with these improvements on EVs, it was obvious in the early 1990s that EVs could not match gasoline vehicles because of travel range and total performance. Gasoline had better travel range, improved performance and the technology was advanced (Ehsani et al., 2018). Due to the above reasons, automobile manufacturers abandoned complete electric vehicles and focused more on hybrid electric vehicles. After few years of research and development, hybrid electric vehicles (HEV) were rolled out in mass at the detriment of complete EVs (Ehsani et al., 2010; Okba, 2015; Ehsani et al., 2018).

The past twenty years (precisely starting from 2000) has experienced significant growth in modern electric vehicle design and performance. One of such was the introduction of fuel cell generator stack prototype that replaced the battery. This turned research focus to advanced vehicle technology with specific interest on energy management of hybrid electric vehicle sources such as fuel cell/supercapacitor (SC) and or battery (Azidin, 2016; Felgenhauer et al., 2016; Yue, 2019). Hybridization of the fuel cell powered electric vehicle has shown huge potential in overcoming some of the disadvantages posed by fuel cell alone-powered vehicle. Hence, in the development of electric vehicle, the battery technology and adequate energy management system is seen as the major obstacle on the path of mass adoption of electric vehicle (Carnevali, 2017; Shang, 2013; George, 2018; Wu, 2014; Azidin, 2016). Recently, there have been significant effort in battery technology research to improve the overall

performance suitable for electric vehicle with more research and improvement still required. However, the past five years (starting from 2016) have experienced major improvement in battery technology because of the number of ground-breaking research and relevant results obtained in the sector. This has also demonstrated to major automobile manufacturers and governments around the world that EVs are vehicles of the future as it will help reduce greenhouse gas emissions in the environment. In the USA, the transportation sector alone contributes 25% of environmental pollution thereby making it a major contributor (IEA, 2022). Today most automobile manufacturers produce 50% EVs and 50% gasoline vehicles. Some of the EVs available for sale to the public are, Tesla model 3, BMW i3, BAIC EU-Series, Nissan LEAF, BYD Yuan/S2 EV, SAIC Baojun E-Series as shown in Figure 2.3.

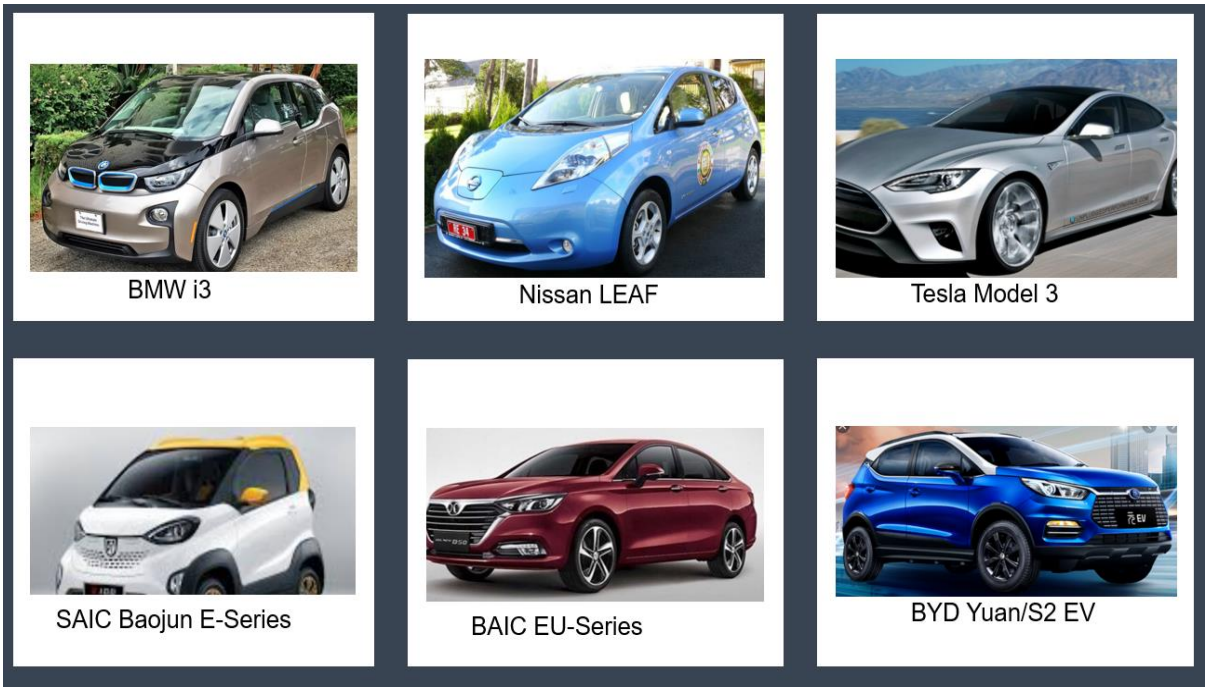

Figure 2.3: Available electric vehicles (Ehsani et al., 2018)

2.2.2 Brief description of EV

What drives a vehicle forward is the tractive force (F_t) present in the contact region between the EV tires and the round surface region of the wheels. This force (F_t) is produced by the power plant torque and enabled via transmission and final drive down to the tires and wheels. However, grading resistance, tire rolling resistance and aerodynamic drag force are some of the internal and external resistances encountered by vehicles that affects its motion. Forces acting on a vehicle in motion in an inclined surface is shown in Figure 2.4 (Okba, 2015; Bendjedia et al., 2017; Ehsani et al., 2018)

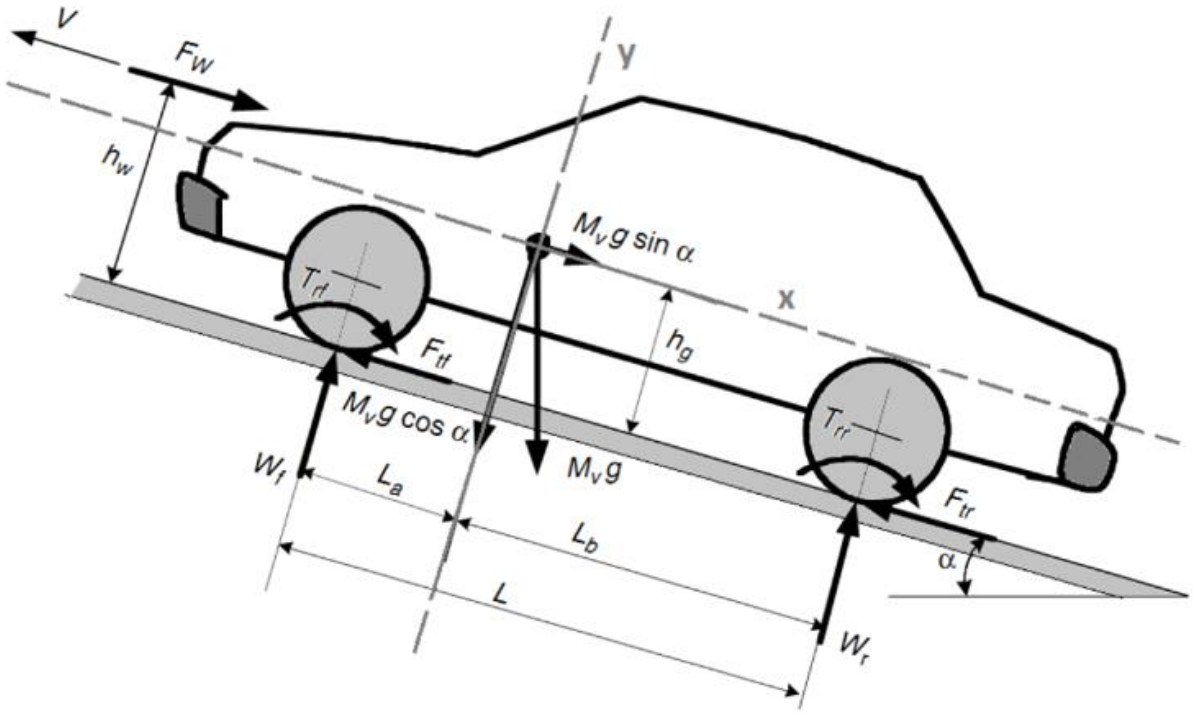

Figure 2.4: Forces acting on an inclined vehicle (Okba, 2015)

Vehicles acceleration can be explained using Newton's second law of motion as expressed in equation 2.1 (Okba, 2015).

$$\frac{dV}{dt} = \frac{\Sigma F_t - \Sigma F_{tr}}{\delta M_v} \tag{2.1}$$

Where;

V = vehicle speed

$\sum F_t$ = total vehicle tractive effort force

$\sum F_{tr}$ = total tractive effort resistance force

M_v = vehicle total mass

δ = mass factor (effect of rotating components in the vehicle)

According to Figure 2.4, there will be no movement in the vertical axis (y-direction) relative to the normal direction because the gravitational force in that direction is cancelled out by the road reaction force. Meaning that the vehicle's wheels are always in contact with the road thereby creating friction. Hence, the velocity relative to the normal (V_y) = 0. The above explanation provided for one-dimensional analysis of vehicle movement in the horizontal direction (x-axis) without considering the vertical forces and all opposing forces.

2.2.2.1 Grading resistance

The weight of a vehicle produces a force in the downward direction whenever it is climbing or descending an inclined surface. This force is vital when calculating or resolving the forces acting on the vehicle at any point as presented in Figure 2.5. The force will either oppose the vehicle movement or support it depending on the direction of force of the vehicle. However, only the uphill resistance is considered when analysing the total performance of a vehicle. This grading force is what is referred to as “Grading Resistance” (F_g) and expressed as (Das et al., 2017; Strahl, 2014).

$$F_g = M_v g sin(\alpha) \tag{2.2}$$

But when the road is small and to ensure easy calculation and simplification of the value of the grading resistance, the road angle “α” is normally substituted with a value. In addition, as shown in Figure 2.5, the grade value can be obtained using equation 2.3 (Ehsani et al., 2010).

$$l = \frac{H}{L} = \tan(\alpha) = \sin(\alpha) \tag{2.3}$$

The tire rolling resistance and grading resistance collectively are referred to as “road resistance” (F_{rd}) in some literature and expressed as (Borkow & Gabbay, 2018)(Okba, 2015; Ehsani et al., 2018):

$$F_{rd} = F_r + F_g = M_v g(\cos(\alpha) + l) \tag{2.4}$$

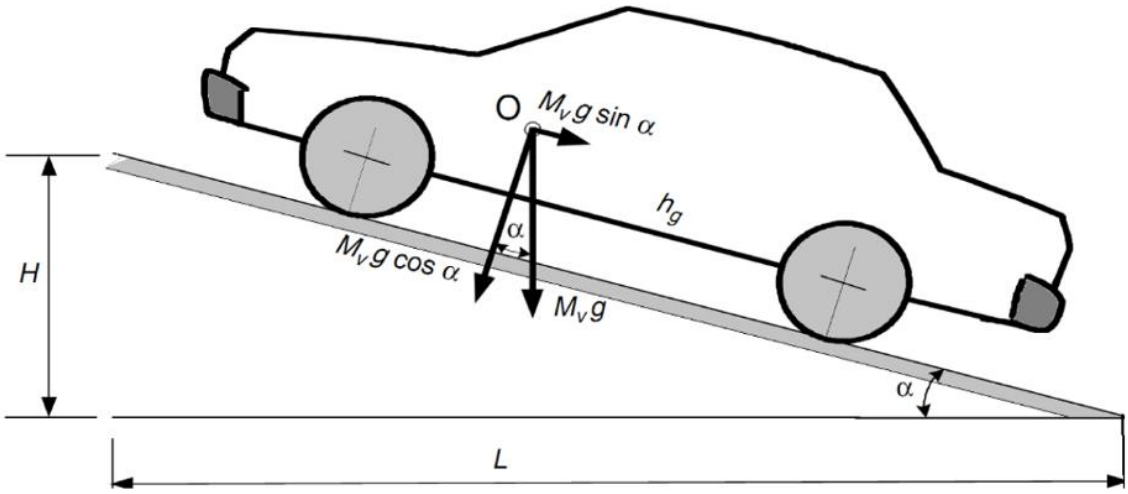

Figure 2.5: An inclined vehicle (Okba, 2015)

2.2.2.2 Rolling Resistance

This is the force required to keep the vehicle tires in motion along a straight line at constant speed. Some literature defines it as “the energy loss per distance travelled by the vehicle due to non-elastic deformations of the tires and losses in the wheel suspension system”. It is simply the friction that exist between the vehicle tires and the road (Shang, 2013; Salet, 2018; Yue, 2019). This force creates a ground reaction force that ensures forward movement which in turn creates a moment that tend to stop the rolling of the wheel as shown in Figure 2.6. This moment is referred to as “rolling resistant moment” and expressed as:

$$T_r = a.P \tag{2.5}$$

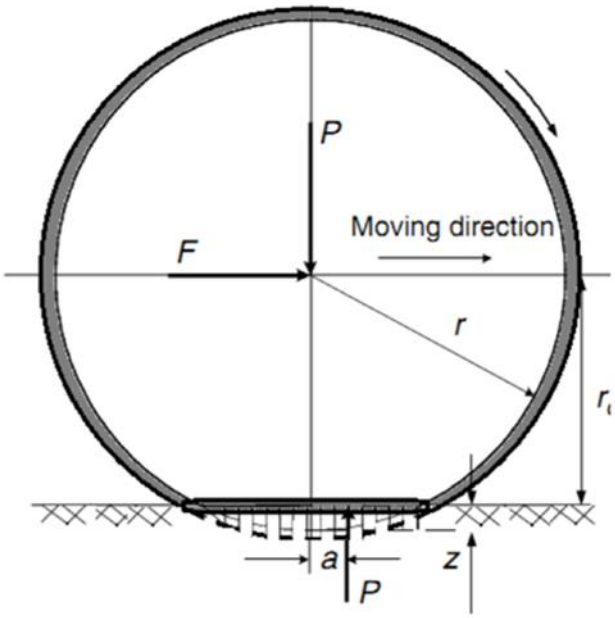

Figure 2.6: Tire deflection and rolling resistance on a road (Ehsani et al., 2010)

However, to maintain the wheel rolling, a force F_r, is required at the centre to keep the rolling at equilibrium with the rolling resistant moment. This force is expressed as:

$$F_r = \frac{T_r}{r_{dyn}} = \frac{Pa}{r_{dyn}} = pf_r \tag{2.6}$$

Where:

$T_r = rolling\ resistance\ [Nm]$

$P = Normal\ load\ acting\ on\ the\ centre\ of\ the\ rolling\ wheel\ [N]$

$r_{dyn} = dynamic\ radius\ of\ the\ tyre\ [m]$

$f_r = rolling\ resistance\ coefficient$

In addition, the rolling resistant moment can be substituted using a corresponding force on the x-axis acting on the centre of the wheel in anticlockwise direction of the wheel movement. This corresponding force is referred to as "rolling resistance" with defined magnitude and expressed as (Khayyer, 2008):

$$F_r = f_r P \tag{2.7}$$

Where P is the normal load acting on the centre of the rolling wheel. The value of P should be replaced by the horizontal force that is perpendicular to the surface of the road when a vehicle is operated in an inclined surface using the expression in equation 2.8 (Khayyer, 2008).

$$F_r = f_r P cos(\alpha) \tag{2.8}$$

The value for rolling resistance coefficients differs according to the vehicle weight, tire design and threading, type of road surface and design, material composition and level of friction. Hence, tires with less friction provides improved traction on dry surfaces and flat roads. Rolling resistance coefficient for different types of surfaces and tires are shown in Table 2.1.

Table 2.1: Rolling resistance coefficients of some roads (Khayyer, 2008)

Rolling resistance coefficient	Description
0.001 - 0.0025	Train steel on steel with tatz-mounted electric traction. The acceptable theoretical limit possible is 0.001.
0.0015 - 0.0025	Low resistance tubeless radial tire used for solar cars/eco marathon cars made specifically by Michelin
0.005	Tramrails standard dirty with straights and curves
0.0055	Normal BMX bicycle tire used for solar cars
0.006 - 0.01	Low rolling resistance car tire on a smooth road and truck tires on a smooth road
0.010 – 0.015	Normal car tires on concrete
0.020	Car on stone plates
0.030	Car/bus on tar/asphalt

2.2.2.3 Aerodynamic drag force

Aerodynamic drag is a resistive force that acts against the direction of thrust of a vehicle as shown in Figure 2.7. However, the air density, coefficient of vehicle drag, vehicle design, square of the vehicle speed, and the function of the vehicle frontal area can be used to calculate the drag force under certain or established vehicle conditions using equation 2.9 (Ehsani et al., 2010). But, the vehicle coefficient is determined by the vehicle shape and design (Howell, 2014; Okba, 2015; Ehsani et al., 2010). Aerodynamic drag force of a light vehicle is highly dependent on its wheels and tyres. On a typical light (passenger) vehicle, aerodynamic drag force produces approximately 25% of the total drag. Hence, this is an important factor in the design and modelling of electric vehicles because aerodynamic losses exercise significant impact on the travel range of EVs (Howell, 2014).

$$F_w = \frac{1}{2} p A_f c_d (V_{veh} + V_w)^2 \qquad 2.9$$

Where:

$c_d = Aerodynamic\ drag\ coefficient$ (Determined by vehicle shape)

$V_{veh} = Vehicle\ velocity$

$\rho = air\ mass\ density$

$A_f = front\ area\ of\ the\ vehicle$

$V_w = Wind\ speed\ component\ of\ a\ vehicle's\ moving\ direction\ \ (positive\ when\ component\ is\ opposite\ to\ the\ vehicle\ speed\ and\ negative\ when\ it\ is\ in\ the\ same\ direction\ with\ the\ vehicle\ speed)$

It is technically vital to note the relationship between the drag force and vehicle speed. The vehicle speed has a cubic relation with the force of drag which means that little change in the vehicle speed will require significant amount of engine power to overcome the force of drag. Furthermore, this relationship also shows that aerodynamics of the vehicle does not have much impact on the vehicle at lower speed, but its impact is more noticeable and significant at highway (high) speed.

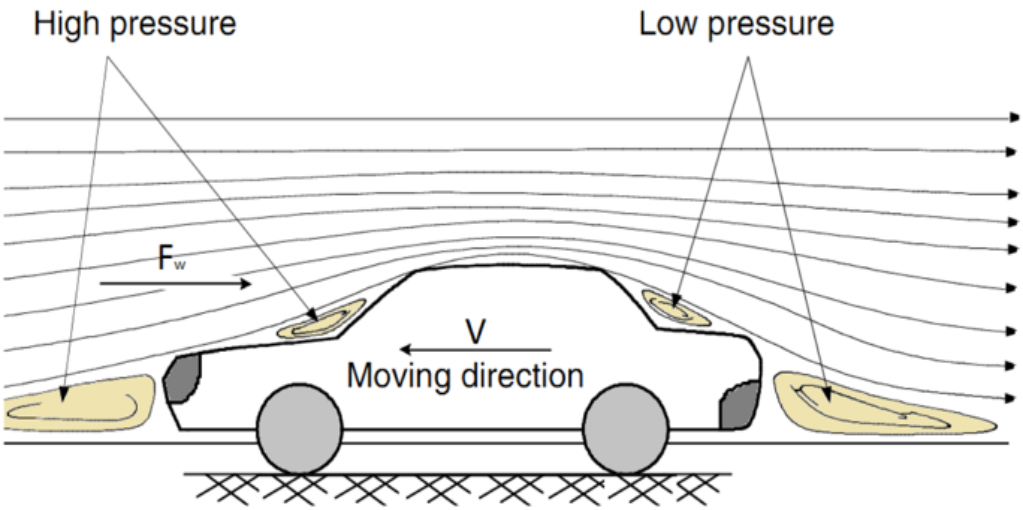

Figure 2.7: Aerodynamic drag force acting on a vehicle (Okba, 2015)

Table 2.2 shows the aerodynamic drag coefficient "C_d" for some vehicle body shapes. These type of body shapes are not the only types available but for this research, only these types are highlighted just to introduce the concept and point out the impact it has on vehicles (Howell, 2014; Bendjedia et al., 2017; Khayyer, 2008).

Table 2.2: Aerodynamic coefficient for different vehicle body shape (Khayyer, 2008)

Vehicle type	Aerodynamic coefficient
Van body	0.5 - 0.7
Open convertible	0.5 – 0.7
Buses	0.6 – 0.7
Motorcycles	0.6 – 0.7
Streamlined buses	0.3 – 0.4
Trucks/Trains	0.8 – 1.5
Optimum streamed design	0.15 – 0.20
Wedge-shaped body	0.3 – 0.4
K-shaped	0.23
Ponton body	0.4 – 0.55

2.3 Electric Vehicle design

According to Ehsani et al., (2010), Lorf, (2014), Sims-williams, (2014), and Okba, (2015), the effective design of an EV is largely dependent on the torque (i.e. vehicle speed power), features of the traction motor, and efficient power distribution. The vehicle driving performance is normally assessed using the acceleration time, gradeability and the maximum speed with significant consideration on the motor power rating and transmission values.

2.3.1 Acceleration time

Vehicle acceleration performance is measured by the time it takes for the vehicle to accelerate from a low speed to a much higher speed. This is normally from zero to approximately 100 km/h for light passenger vehicles. Hence, the vehicle acceleration can be expressed using Newton's second law as:

$$a = \frac{dV}{dt} = \frac{F_t - (F_r + F_w)}{M_v \delta} \qquad (2.10)$$

Where the mass factor "δ" is expressed as:

$$\delta = 1 + \frac{i_w}{M_v r_d^2} \qquad (2.11)$$

Where, i_w is the angular moment of the wheel. Therefore, using equation 2.10, an electric vehicle acceleration time, a_t and distance, d_a, from speed V_0 to V_1 can be expressed separately as:

$$a_t = \int_{V_0}^{V_1} \frac{M_v \delta V}{(P_t/V) - M_v g f_r - (1/2) pcd A_f V^2} dV \qquad (2.12)$$

While,

$$d_a = \int_{V_0}^{V_1} \frac{M_v \delta}{\left(T_p i_g i_0 \eta_t / rd\right) - M_v g f_r - (1/2) pcd A_f V^2} dV \qquad (2.13)$$

Normally, numerical methods are used to obtain the acceleration time and covered distance on the speed of the vehicle because it is technically complex to obtain the analytical solution using equation 2.12. Hence, a typical acceleration time and distance together with speed of vehicle for an electric vehicle is shown on Figure 2.8. To obtain the value of acceleration time against the tractive power P_t with the vehicle mass factor δ kept constant, the aerodynamic drag force and the rolling resistance must be ignored and assumed to have no effect on the vehicle speed.

Therefore, the acceleration time can be achieved using equation 2.14 as:

$$a_t = \frac{\delta M_v}{2P_t} (V_1^2 + V_0^2) \qquad (2.14)$$

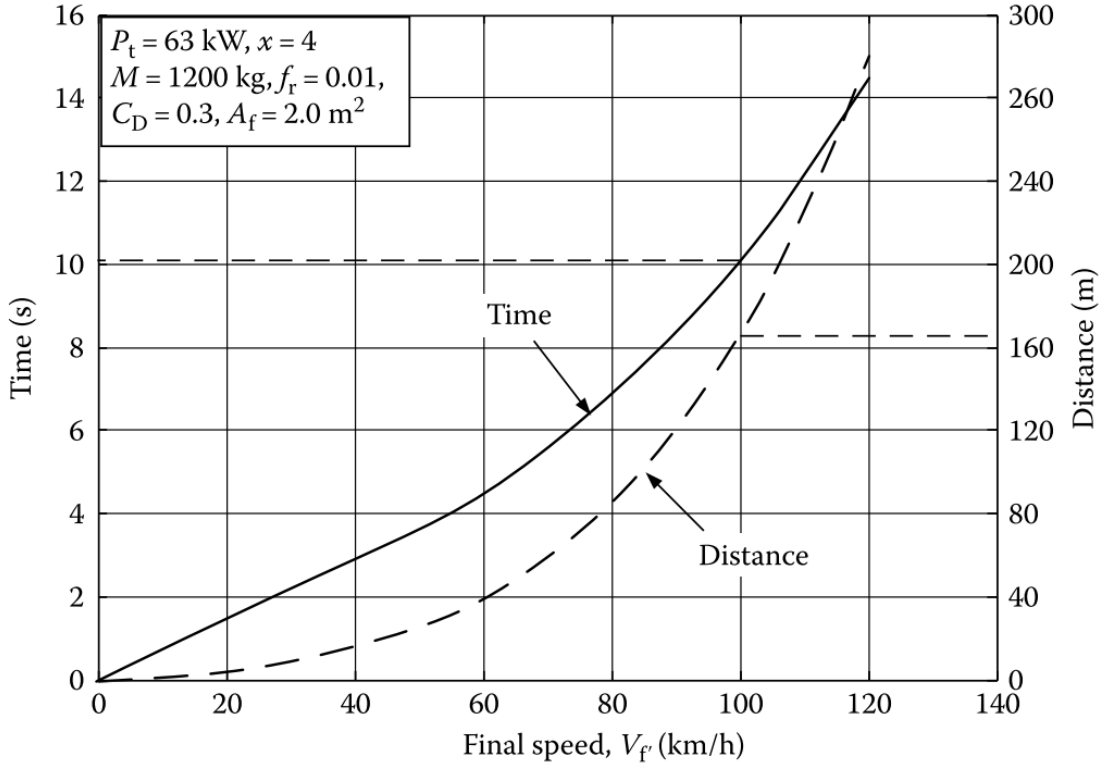

Figure 2.8: Acceleration time and distance versus final speed (Ehsani et al., 2010)

2.3.2 Gradeability

This is the total drag force needed to move a vehicle in a vertical direction (x-axis). It is also described as the grade angle that the electric vehicle can pull at constant speed in an inclined surface. Furthermore, this is achieved by the net tractive effort of the electric vehicle as: $F_{t_{net}}(F_{t_{net}} = F_t - F_r - F_w)$ and expressed in equation 2.15. Gradeability is less significant at low speed as against mid and high speeds as shown in Figure 2.9 because the highest grade level of a vehicle can overcome at specific speed level can be evaluated based on set conditions and boundaries (Bendjedia et al., 2017; Okba, 2015; Lorf, 2014; Howell, 2014).

$$l = \frac{F_{t_{net}}}{M_v g} = \frac{F_t - (F_r + F_w)}{M_v g} \tag{2.15}$$

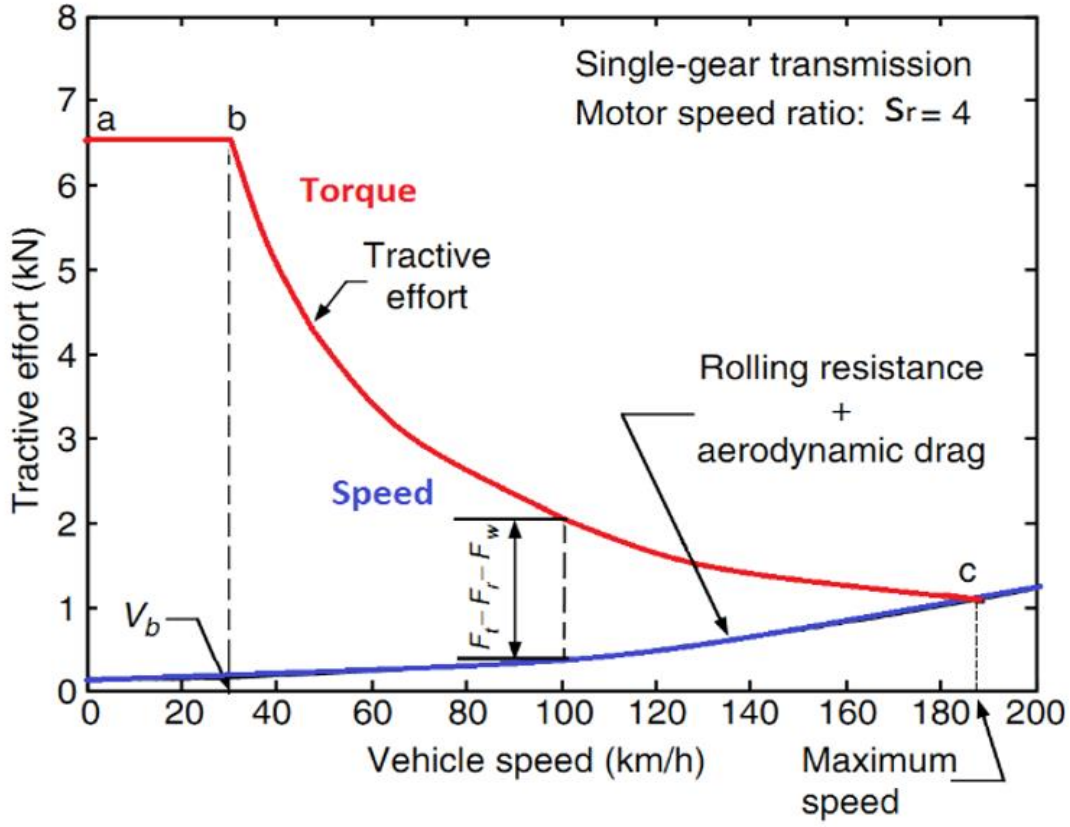

Figure 2.9: A typical tractive drag effort against vehicle speed (s_r = 4, single-gear transmission) (Okba, 2015; Ehsani et al., 2010)

2.3.3 Maximum speed

Fundamental design and operation of any vehicle comprises of the acceleration, driving speed and gradeability. But the maximum driving speed of a vehicle is achieved by identifying the point where the resistance curve which includes the aerodynamic drag force and rolling resistance and the tractive effort curve is connected as shown in Figures 2.8 and 2.9, respectively. Although, some vehicles with bigger traction motor and/or larger gear ratio does not always include the point of intersection in its design. However, in designs where the point of intersection is not shown, then the vehicle speed will be determined by using the maximum speed of the traction motor as expressed in equation 2.16 (Ehsani et al., 2010; Okba, 2015).

$$V_{max} = \frac{\pi W_{max} r_d}{30 i_{gmin} i_0} \tag{2.16}$$

Where:

$r_d = drive\ wheels\ radius$

$W_{max} = maximum\ motor\ speed\ (rev/min)$

$i_0 = gear\ ratio\ of\ final\ drive$

$i_{gmin} = minimum\ gear\ ratio\ of\ transmission$

2.3.4 Characteristics of traction motor

The characteristics of a typical variable-speed electric motor drive used for automotive application and other electric motor devices is shown in Figure 2.10, where at the low-speed region (less than the base speed), the motor has a constant torque (Ehsani et al., 2018). The motor power is always constant during high-speed operation i.e., speed higher than the motor base speed while, the torque is constant at low-speed operation i.e., speed lower than the motor base speed. Typically, the ratio of the maximum speed to the base speed (speed ratio) is used to define the characteristics and expressed as s_r. During low-speed region, when motor supply voltage increases, the speed also increases through the electronic converter while the lux density remains constant (Ehsani et al., 2010). When the motor is operating at the base speed, the motor voltage will be equal to the supply voltage. But, when the motor is operating at a speed higher than the base speed, the motor voltage remains constant while the flux density is reduced and continues in the same trajectory according to the speed and direction. Consequently, the speed increases as the torque decreases when operating at a speed equal to the base speed (Okba, 2015).

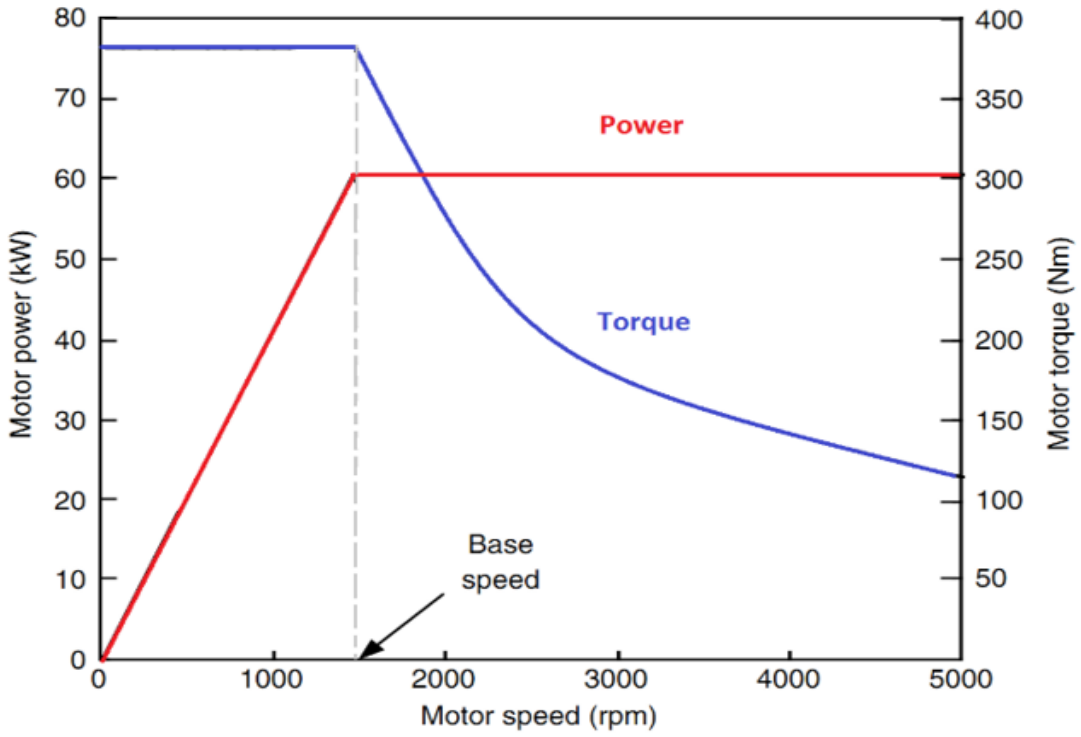

Figure 2.10: Characteristics of a typical variable-speed electric motor (Ehsani et al., 2010)

The torque speed shape directly affects the electric motor torque, rolling resistance, aerodynamic drag and the variable speed ratio. Hence, it is obvious that the vehicle acceleration and gradeability output can be enhanced with simplified transmission and the motor maximum torque can be improved substantially within the elongated constant power range (Bendjedia et al., 2017) . Although, allowable maximum speed ratio is set for individual motor within specified operational conditions that will enhance optimization. For instance, because a permanent magnet is included in the motor design, the field created will deteriorate over time if the speed ratio is very small such as $s_r = 2$ in the permanent magnet while switched reluctance motors possess the potential of achieving $s_r = 6$ and the induction motors is approximately $s_t =$ 2,3 and 4 respectively (Okba, 2015; Bendjedia et al., 2017; Ehsani et al., 2018).

2.3.5 Tractive power of a motor

The tractive power of a motor P_t is written as:

$$P_t = \frac{\delta M_v}{2t_a}(V_1^2 + V_0^2) \tag{2.17}$$

To adequately define the tractive power of a motor, the power utilized in overcoming the dynamic drag and the rolling resistance must be established within the allowable conditions of operation. However, during the acceleration period, the standard drag power is usually expressed as (Ehsani et al., 2010; Ehsani et al., 2018):

$$P_{drag} = \frac{1}{t_a}\int_0^{t_a}\left(M_v g f_r V + \frac{I}{2}\rho c_d A_f V^2\right)dV \tag{2.18}$$

Where the vehicle speed “V” can be expressed with respect to time “t” as:

$$V = V_1\sqrt{\frac{t}{t_a}} \tag{2.19}$$

Simplifying equations 2.18 and 2.19 and integrating gives:

$$P_{drag} = \frac{3}{2}M_v g f_r V_1 + \frac{1}{5}\rho c_d A_f V_1^3 \tag{2.20}$$

Hence, the total tractive power of the motor used in accelerating the vehicle from speed V_0 to speed V_1 in time t seconds can be expressed as:

$$P_t = \frac{\delta M_v}{2t_a}(V_1^2 + V_0^2) + \frac{2}{3}M_v g f_r V_1 + \frac{1}{5}\rho c_d A_f V_1^3 \quad (2.21)$$

2.3.6 EV energy consumption

The energy consumption of a vehicle is measured per unit over a specific distance covered in kilowatt-hour per kilometre (kWh/km). This unit is used to assess the energy efficiency of the vehicle, power supply and travel range. In EVs, this is a fundamental design parameter that has and is still attracting several research aimed at increasing the travel range (Ehsani et al., 2010). But for battery electric vehicles (BEVs), the energy consumption unit is expressed in kWh. It is normally measured at the battery terminals and used to calculate the vehicle travel range thereby making it a very vital factor in EV design. Power losses present during transmission and in the motor drive together with the power losses in electronic devices in the vehicle is equal to the total power delivered by the battery required for propulsion. The motor drive and power transmission losses are usually represented by their efficiencies as (Ehsani et al., 2010; Noel et al., 2019; Arcos-Vargas Editor, 2021):

$$motor\ drive\ losses = h_m\ \ \&\ \ power\ transmission\ losses = h_t$$

Therefore, the output power of the battery without the inclusion of the non-traction load otherwise referred to as “auxiliary load” can be represented as:

$$\bar{P}_{Bout} = \frac{V}{h_m h_t}\left[(M_v g f_r + i) + \frac{1}{2}\rho c_d A_f V^2 + M\delta\frac{\delta V}{dt}\right] \quad (2.22)$$

In addition, at the battery terminals, the regenerative braking power can be further utilized by operating the motor drive as a generator and restoring the power to the battery during an actual braking process on EVs. Such power is normally wasted in ICE vehicles but can be utilized in EVs and expressed as (Noel et al., 2019; Arcos-Vargas Editor, 2021):

$$P_{B_{in}} = \frac{\beta V}{h_m h_n}\left[(M_v g f_r + i) + \frac{1}{2}\rho c_d A_f V^2 + M\delta\frac{dV}{dt}\right] \quad (2.23)$$

$$where;\ i = road\ side\ grade\ and\ \ \frac{dV}{dt} = acceleration\ are\ both\ negative,$$
$$\beta = regenerative\ braking\ factor\ (function\ of\ applied\ braking\ strenght\ of\ the\ EV\ design)$$

Therefore, the net energy consumption from the battery can further be expressed as:

$$\int_{traction} P_{Bout}dt\ +\ \int_{braking} P_{Bin}dt \quad (2.24)$$

Again, the battery must be recharged whenever the net battery energy consumption equals the total energy produced by the battery as measured at the battery terminal. This process is highly important to avoid running the battery flat. The effective travel range is determined by the resistive power, the efficiency of the regenerative braking factor (β), and the total energy resident in the battery (Okba, 2015; Noel et al., 2019; Arcos-Vargas, 2021). However, the efficiency of the traction motor depends on its operating position on the speed-power diagram as shown in Figure 2.11.

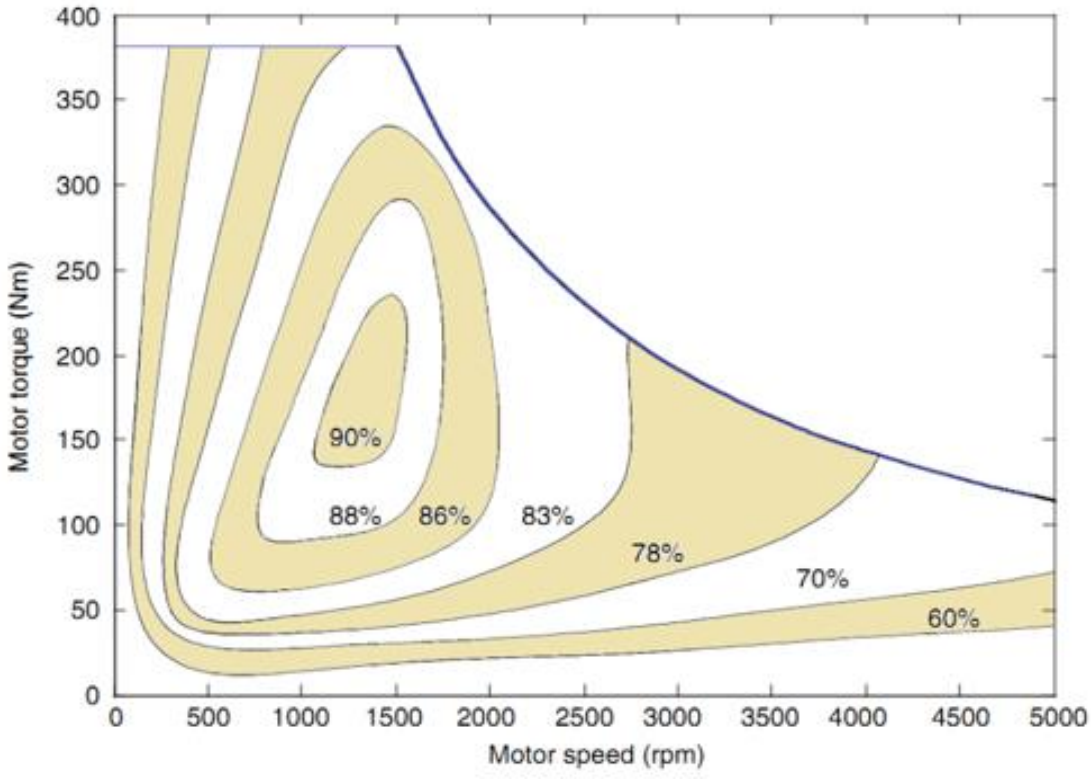

Figure 2.11: Characteristics of standard electric motor efficiency (Ehsani et al., 2018)

2.4 Types of EV configurations

EVs have different configurations based on the type of energy sources and design used. Each of these configurations has its unique advantage, disadvantage, and limitations in terms of power density, emission rate, cost, energy density, safety, fuel efficiency, performance, size and weight. However, EVs are broadly categorized as: hybrid electric vehicles (HEV), battery electric vehicle (BEV), plug-in hybrid electric vehicle (PHEV), and fuel cell hybrid electric vehicle (FCHEV).

2.4.1 Hybrid EV

Hybrid electric vehicles (HEVs) are vehicles powered by two or more sources of power for its operation (Noel et al., 2019). The power sources are categorized as primary and secondary

power sources and, in most cases mechanical power from internal combustion engine and power from either battery, ultracapacitors, fuel cell, etc. This type of configuration has low emissions as compared to ICE vehicles for the same travel range and does not require plugging-in for recharging because it recharges when driving (Arcos-Vargas, 2021; Noel et al., 2019). Therefore, HEVs possesses the advantages of high fuel economy, low tailpipe emissions with the power and travel range of ICE vehicles and are technically designed and configured as either parallel HEV, series HEV or series-parallel HEV (Gang et al., 2006; Opila et al., 2014).

2.4.1.1 Parallel HEV configuration

Parallel HEV is configured to ensure that two or more energy sources can always provide propulsion power to the vehicle. A typical parallel HEV is shown in Figure 2.12, where the electric motor and internal combustion engine (ICE) are connected in parallel with a mechanical link that synchronize the torque emanating from both sources (Ehsani et al., 2018; Ehsani et al., 2010).

Advantages of parallel HEV

- It uses smaller engine and traction motor size to achieve the same performance.
- Increased efficiency.
- HEV can operate as generator/motor and ICE. i.e., it can be used as either of them.
- Improved travel range

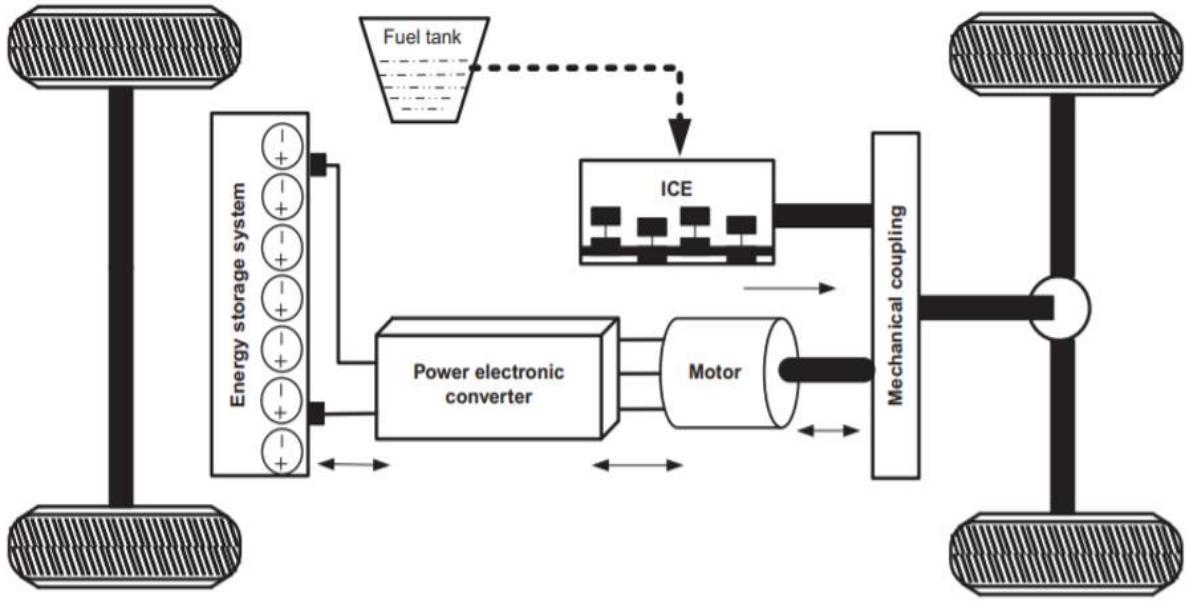

Figure 2.12: Parallel HEV configuration (Ehsani et al., 2018)

Drawbacks of parallel HEVs

- Synchronizing the power from the ICE and the motor creates a complex mechanical system.
- Increased cost due to additional components.
- Complex energy management system is created because power from two parallel sources must be controlled.

2.4.1.2 Series HEV configuration

A series HEV uses two power sources, which feeds a single electric motor that propels the vehicle. However, one energy converter can provide propulsion in a series HEV. The ICE is mechanically connected with an electric generator that is coupled to the electric motor and battery pack through a power electronic converter as shown in Figure 2.13. The fuel tank is a unidirectional energy source while the electrochemical battery pack is a bidirectional energy source connected to the power bus through a DC/DC power converter (Li & Liu, 2009).

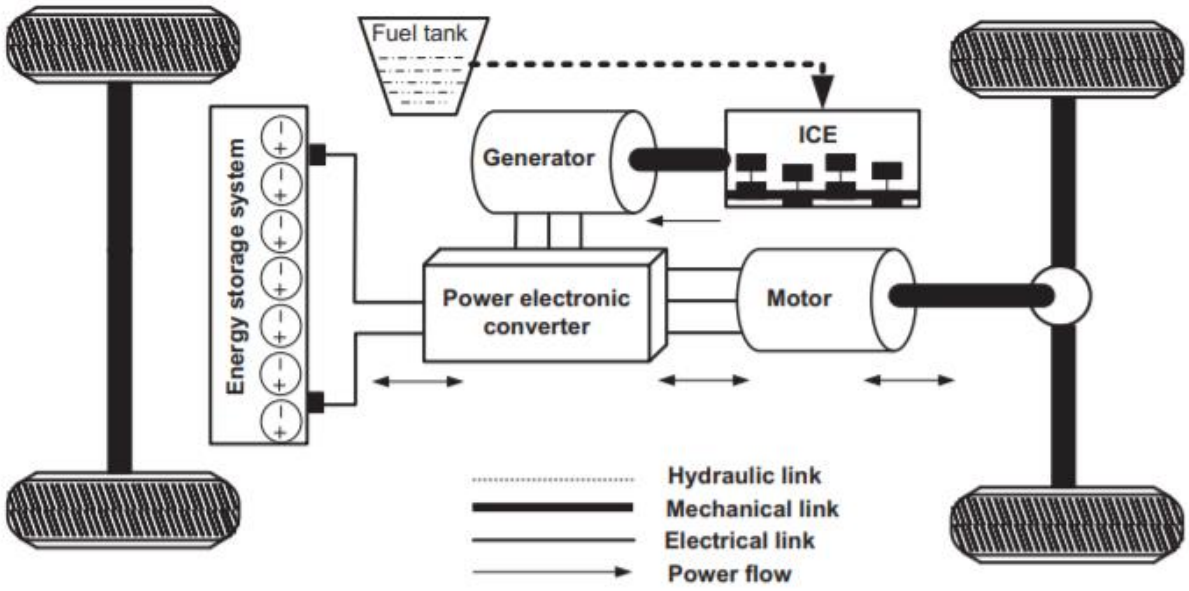

Figure 2.13: Series HEV configuration (Jain & Kumar, 2018)

Advantages of Series HEV

- Electric motor possesses close to ideal torque-speed characteristics
- It is adequate for short travel range
- Simple to design and operate
- It reduces harmful gas emissions
- Smaller and more efficient engine

Drawbacks of series HEV

- The motor must be designed to operate at maximum power demand of the vehicle even though vehicles do not always operate at the maximum power demand.
- The battery pack and other components must be designed for maximum power and maximum driving speed for long travel range else, the battery pack will discharge quickly.
- The design must include motor, generator, and ICE for effective operation
- More costly

2.4.1.3 Series-parallel HEV configuration

Series-parallel HEV configuration is a combination of both series and parallel HEV configurations for practical application on roads. This unique configuration enjoys the advantages of both series and parallel HEV configurations in its operation. In addition, this type of configuration can also be used to recharge the battery during waiting periods such as traffic jam and traffic lights with specific consideration on the trade-offs between performance and cost. However, additional electrical and mechanical components (mechanical link and generator) are introduced thereby contributing to its weight, cost, and design complexity as shown in Figure 2.14 (Jain & Kumar, 2018; Okba, 2015; Ehsani et al., 2010).

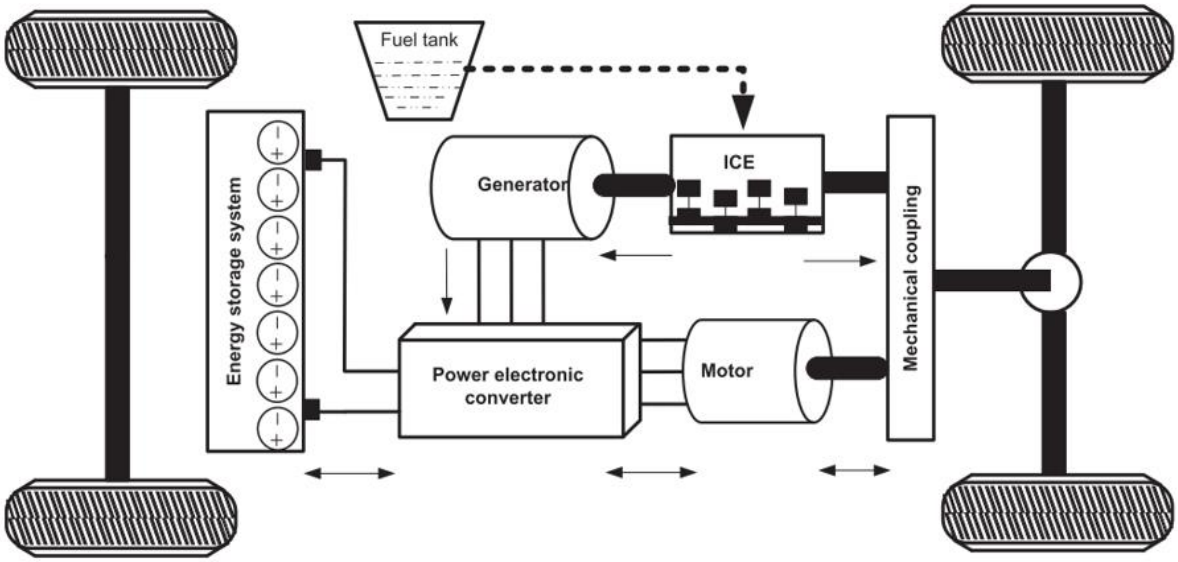

Figure 2.14: Series-parallel HEV configuration (Jain & Kumar, 2018; Ehsani et al., 2010)

Series-parallel HEV is further categorised as engine-intensive and electric-intensive as some of the available configurations. In engine-intensive configuration, the ICE is modelled as the dominant power source as against the electric motor and it is only the engine that drives the wheels into motion without any form of support from the electric motor. While, in electric-intensive configuration, the electric motor is the dominant source of power supply but

occasionally assisted by the ICE during moments of high load demand by the vehicle, such as driving on inclined or steep surfaces. The operating modes (start, acceleration, regular driving, deceleration, battery charging, and braking) for both engine-intensive and electric-intensive are the same except in the regular driving mode where the engine is made to operate most efficiently (Sun et al., 2012).

Advantages of Series-parallel HEV

- Environmentally friendly with less pollution
- Increased travel range and high autonomy

Drawbacks of Series-parallel HEV

- Complex drive train
- Higher cost
- Added weight
- Complex components management
- Extra power loss caused by the mechanical coupling and planetary gear unit.

2.4.2 Battery electric vehicle (BEV)

Battery electric vehicle (BEV) is sometimes referred to as pure electric vehicle by some individuals/organizations. This is because, unlike the hybrid electric vehicle (HEV), BEV is completely electric and does not have internal combustion engine (ICE) (Alharbi, 2013). This is still debatable because battery electric vehicles do not emit direct harmful emission or pollute the environment but majority of the power plants which generate the electricity used to recharge BEVs are not from renewable sources and still emit greenhouse gasses. The battery must be recharged when completely or partially discharged because the vehicle is totally dependent on the battery as the primary and only source of power (Ehsani et al., 2010). Although, the travel range in this instance depends on the battery capacity, size and other vehicular dynamics including effective energy management system (EMS). In addition, the operation of electric vehicle is based on the principles of electric drives which comprises a power modulator, electric motor and an inbuilt energy source with corresponding energy management system as shown in Figure 2.15 (Alharbi, 2013).

Advantages of BEV

- It has zero greenhouse emission
- Less noise
- Safer as compared to HEV
- Easy operation

- High efficiency (peak at 90%)
- Does not use fossil fuels
- It can recover waste energy through regenerative braking

Drawbacks of BEV

- Limited operating travel range per cycle battery charge
- Slow battery charging time
- Dynamic performance degradation
- Lower flexibility
- Heavy weight
- High cost

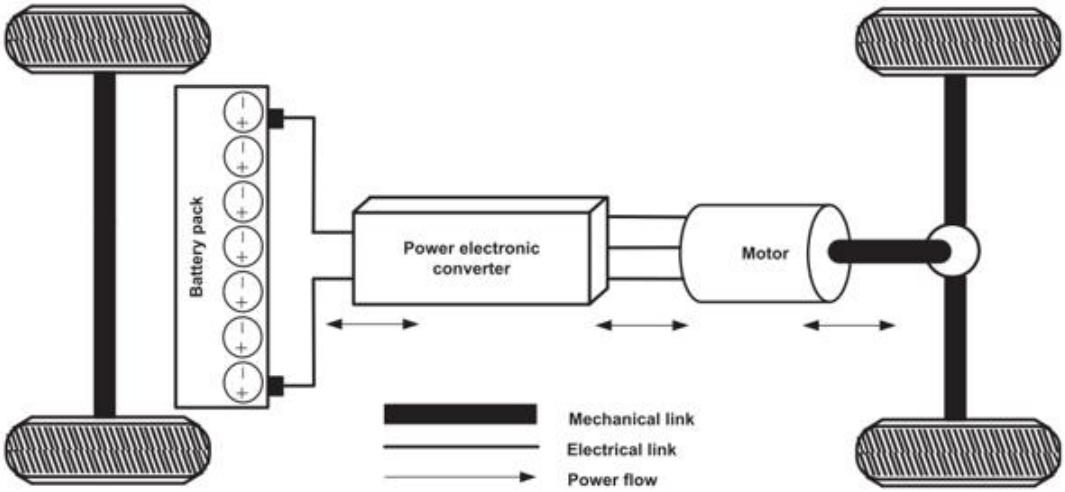

Figure 2.15: BEV configuration (Ehsani et al., 2018)

2.4.3 Plug-in hybrid electric vehicle (PHEV)

Plug-in hybrid electric vehicle (PHEV) technology combines the characteristics of both HEV and BEV in its design and operation as shown in Figure 2.16. According to the board of directors of the IEEE in 20007 after an extraordinary technical meeting on the exact definition of PHEV, they defined PHEV as a hybrid electric vehicle that has a minimum battery capacity of 4 kWh provided the battery can be recharged from an external source and cover a travel range of 16 km in one battery cycle charge without using fossil fuel (Ehsani et al., 2010). Practically, PHEVs have large battery pack unlike HEVs that can be recharged using external sources such as the electricity grid, grid connected renewable energy sources or a standalone renewable energy source. The source of charging the battery contributes to the amount of greenhouse gas emission released by the vehicle. Again, PHEVs operate entirely or almost entirely, on electricity when the battery is fully charged thereafter, switches gradually to hybrid mode based on the predefined SOC of the battery or when the battery is nearly drained or the

vehicle power demand is more than the battery capacity (Alharbi, 2013). However, internal combustion engine powers the vehicle when the battery is completely discharged but, recently, there is the concept of “vehicle-2-grid” (V2G) (Ehsani et al., 2018). This is a condition where the excess power from the vehicle is feed to the grid and vice versa depending on the prevailing power condition through a bidirectional converter according to IEEE standard 1547 for utility connection (Jain & Kumar, 2018; Ehsani et al., 2010).

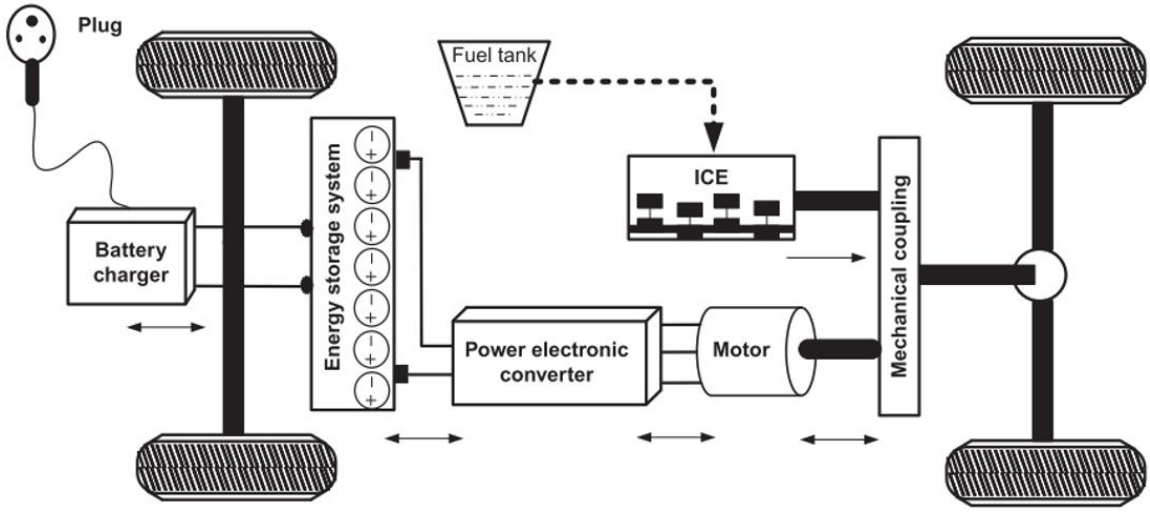

Figure 2.16: PHEV configuration (Jain & Kumar, 2018)

Advantages of PHEVs

- Less greenhouse gas emission
- Increased fuel efficiency
- Increased electric travel range
- V2G or G2V potential
- Developed technology and commercialized

Drawbacks of PHEVs

- More complex
- Grid disturbance due to power supply uncertainty
- High initial cost
- Complicated electronic circuitry
- Difficulty in energy management system and adequate power distribution

2.4.4 Fuel cell hybrid electric vehicle (FCHEV)

In the past eight years, fuel cell hybrid electric vehicles (FCHEVs) have witnessed significant improvement in its performance, efficiency, and design (Ehsani et al., 2018). Furthermore, when compared to ICE vehicles, FCHEVs emit less greenhouse gases but has higher energy efficiency advantages because fuel cells convert freely available fuel directly into electrical energy with no significant energy loss in the system. However, this is not the situation with vehicles powered exclusively by fuel cells due to problems of low power density of the fuel cell, slow response time, heavy weight, and large power unit. Hence, FCHEV configuration with a climaxing power source is a suitable technology with the potential if correctly harnessed that will offset the disadvantages demonstrated by fuel cell powered vehicles. Similarly, in automotive applications, the low output power demand during low-speed driving and significantly large output power during sudden acceleration has led to increased efficiency as shown in Figure 2.17 (Jain & Kumar, 2018).

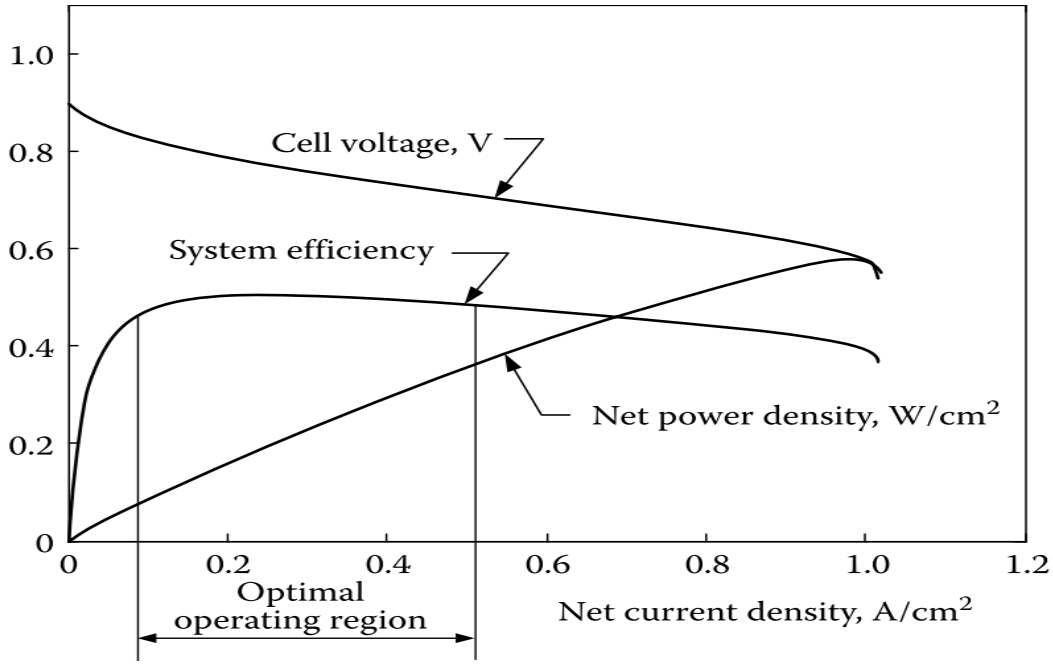

Figure 2.17: Standard operating characteristics of a fuel cell (Jain & Kumar, 2018)

2.4.4.1 FCHEV configuration

A fuel cell hybrid electric vehicle (FCHEV) basically consists of a fuel cell system that serves as the primary source of power, a vehicle controller, peaking power source (PPS), an electric motor drive with specific controller, an electronic interface that links the fuel cell and the PPS as shown in Figure 2.18. The motor output power and corresponding flow of energy between the fuel cell, PPS and the drive train is controlled using the vehicle controller based on the received power from the accelerator or the brake system and other functional signals in the

vehicle (Ehsani et al., 2010; Jain & Kumar, 2018). However, during braking, the electric motor operating as a generator converts a portion of the braking energy into electrical energy then stores it in the PPS. But in sudden acceleration and peak power demand, both the primary energy source (fuel cell) and the peaking power source (PPS) will supply power to the electric motor. When the rated power of the fuel cell is more than the load demand, the excess more will be stored on the PPS for later usage. Hence, with effective energy management system, the PPS will always be charged by the excess power from the fuel cell without requiring external charging system (Ehsani et al., 2018).

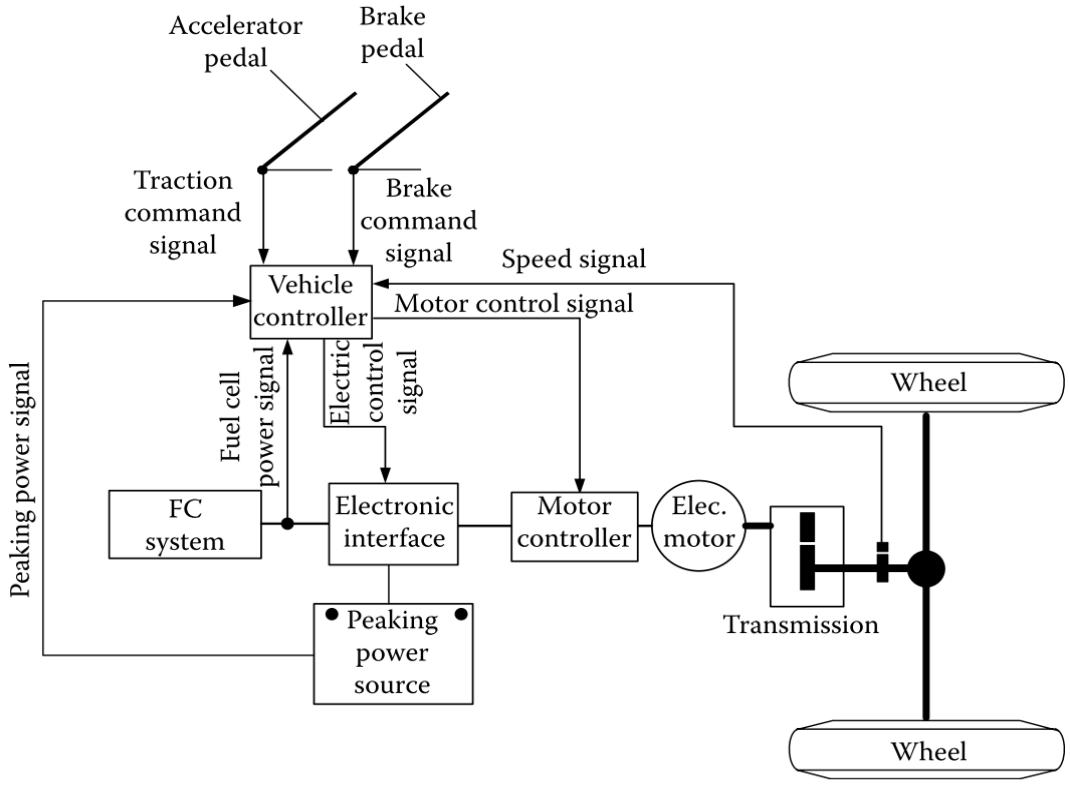

Figure 2.18: Standard fuel cell hybrid drive train configuration (Ehsani et al., 2010)

2.4.4.2 DC/DC converter for FCHEVs

In FCHEVs, a DC-DC converter is required to either step-up or step-down the voltage and to interface the FC and the energy storage system (either battery or supercapacitor) to the DC-link to ensure system optimisation. The DC-DC converter can be designed to operate as unidirectional or bidirectional converter depending on the specific application (Soylu, 2011). Although, in a bidirectional converter, the power can be directed both ways which makes it useful in vehicular applications because of the power demand during vehicle acceleration and regenerative braking. This is implemented to regulate the input current, output current, output voltage or to operate constant power by adjusting the duty cycle. Some downsides of DC-DC converters are electronic noise, increased cost and complications in design (Sorlei et al., 2021;

Soylu, 2011). Hence, DC-DC converters are broadly categorised into isolated and non-isolated converters.

2.4.4.2.1 Isolated Converters

Isolated converters are used in applications where total isolation of the input from the output is required. A typical isolated bidirectional DC-DC converter has the configuration shown in Figure 2.19. This type of configuration has a high transformer and two high frequency switching converters that are basically used to ensure a perfect electric isolation between the two sources under established design constraints. The primary function of the transformer is to ensure that the voltage between various stages is matched for adequate design optimisation (Greeshma & Nayana, 2016). Hence, the standard method of achieving this is the use of high frequency transformer. Presently, there are various configurations available in the market while others are still at the experimental stage with much research time and resources invested. Some of such commercialised configurations are: Full-Bridge, Half-Bridge, Forward and Push-Pull converters. These can either be used as unidirectional or bidirectional converters depending on the application but the percentage of stepping up or stepping down is significant (Sorlei et al., 2021). In addition, isolated DC-DC bidirectional converters are commonly used in fuel cell electric vehicle applications because of the high conversion rate it presents. Amongst the aforementioned converters, the full bridge is always the prime choice configuration for HEVs applications when complete electrical isolation is required because it is effective for high power applications (Soylu, 2011).

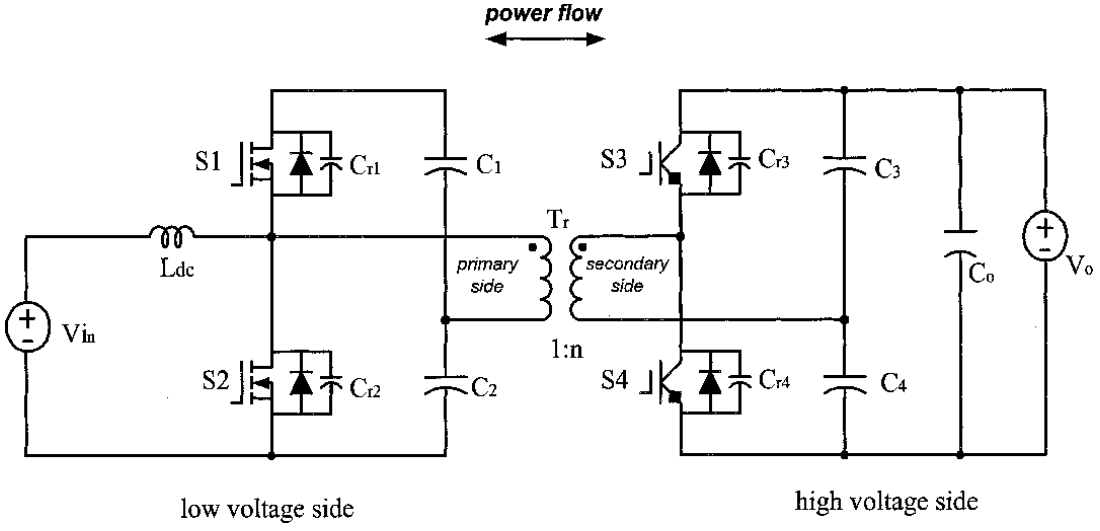

Figure 2.19: A typical Isolated bidirectional DC-DC converter (Soylu, 2011)

2.4.4.2.2 Non-isolated converters

Contrary to isolated DC-DC converters, non-isolated DC-DC converters have DC components in both the input and output. Non-isolated converters are normally used in applications to step-

up or step-down the voltage in relatively low power applications where there is no significant technical challenge between the output and input having no dielectric separation (Greeshma & Nayana, 2016). There are basically five major types of non-isolated converters: buck, boost, Cuk, buck-boost, and charge-pump converters. These converters are used differently but the charge-pump converter can be used to either step-up the voltage or used for voltage inversion, but only in reasonably low power applications. Some of the notable advantages of non-isolated converters are, high efficiency, low cost, high durability, reliability, simple circuit design, small size, low weight, etc (Du et al., 2010; Greeshma & Nayana, 2016). Different types of non-isolated DC-DC converters are shown in Figure 2.20.

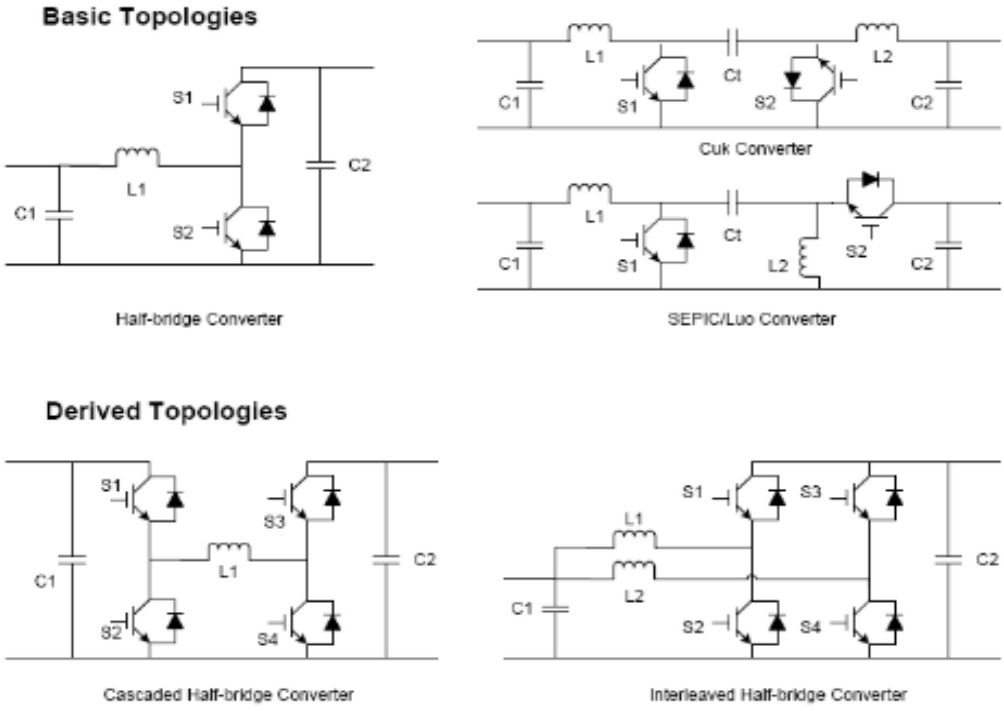

Figure 2.20: Different types of non-isolated bidirectional DC-DC Converters

2.4.4.3 FCHEV control strategy

The primary purpose of vehicle control system is to ensure proper power distribution between the fuel cell, PPS, and the drive train. An effective control system will always ensure the fuel cell system functions optimally, provide adequate power supply to meet the power demand, ensure the energy level in the PPS is constantly kept within acceptable and optimal levels based on the power capacity of the primary and secondary energy sources (Ehsani et al., 2010).

The driver provides a brake command or traction command using a brake pedal or an accelerator pedal based on the power demand and available energy using the following parameters and implemented under the algorithm as shown in Figure 2.21

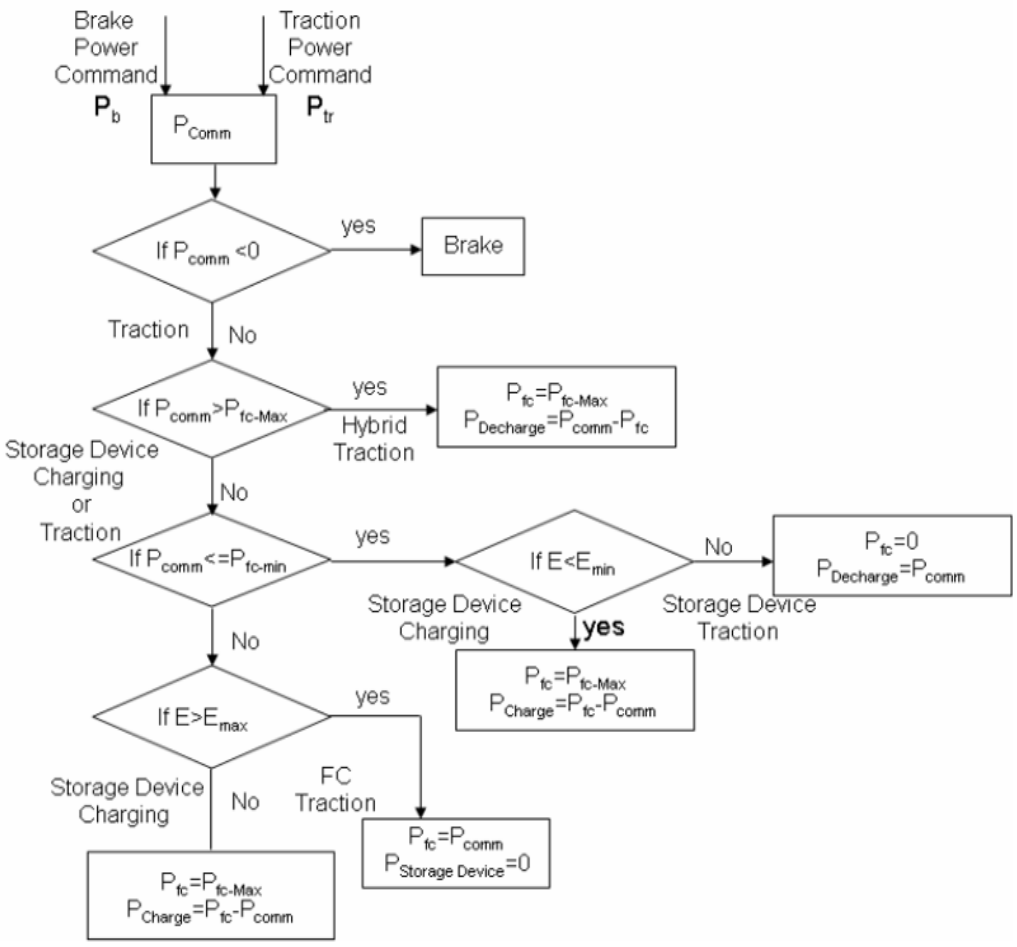

Figure 2.21: Typical control algorithm for FCHEV (Ehsani et al., 2010)

Where:

$P_{comm} = Commanded\ power$

$P_{fc-rated} = Rated\ power\ of\ the\ fuel\ cell\ system$

$P_{fc} = Fuel\ cell$

$P_{fc-min} = Fuel\ cell\ minimum\ power$

$P_{pps-traction} = Traction\ power\ from\ the\ PPS$

$P_{pps-charging} = PPS\ charging\ power$

$E = PPS\ energy\ level$

$E_{min} = Minimum\ energy\ of\ the\ PPS$

$E_{max} = Maximum\ energy\ of\ the\ PPS$

Therefore, in traction mode, the input (electrical power) to the electrical motor drive can be represented as (Ehsani et al., 2010):

$$P_{fc-min} = \frac{P_{comm}}{\eta_m} \tag{2.24}$$

Where; η_m = motor drive efficiency. But operating in braking mode, the electrical motor functions as a generator hence, the motor electrical power output can be represented as:

$$P_{m-out} = P_{mb-comm}\,\eta_m \tag{2.25}$$

Where; $P_{m-out} = motor\ braking\ power$

Using equations 2.24 and 2.25 together with an appropriate flowchart, the different operating modes of the drive train can be explained accordingly using equivalent power control strategies.

- Braking mode: During this mode, the PPS absorbs energy from the regenerative braking system based on the braking system features while the fuel cell is kept idle.
- Standstill mode: This is the condition where none of the power sources (Fuel cell, PPS) supplies power to the drive train.

2.5 EV power supply sources

Hybrid EVs and complete battery EVs will soon dominate the clean vehicle market due to technology improvement and favourable government policies (Okba, 2015). It is projected that by 2025, the total EV sales will reach 11.2 million from the 2.5 million in 2020 then reaching 31.1 million by 2030. EVs would have approximately 32 percent of the total market share for the sale of new cars as shown in Figure 2.22.

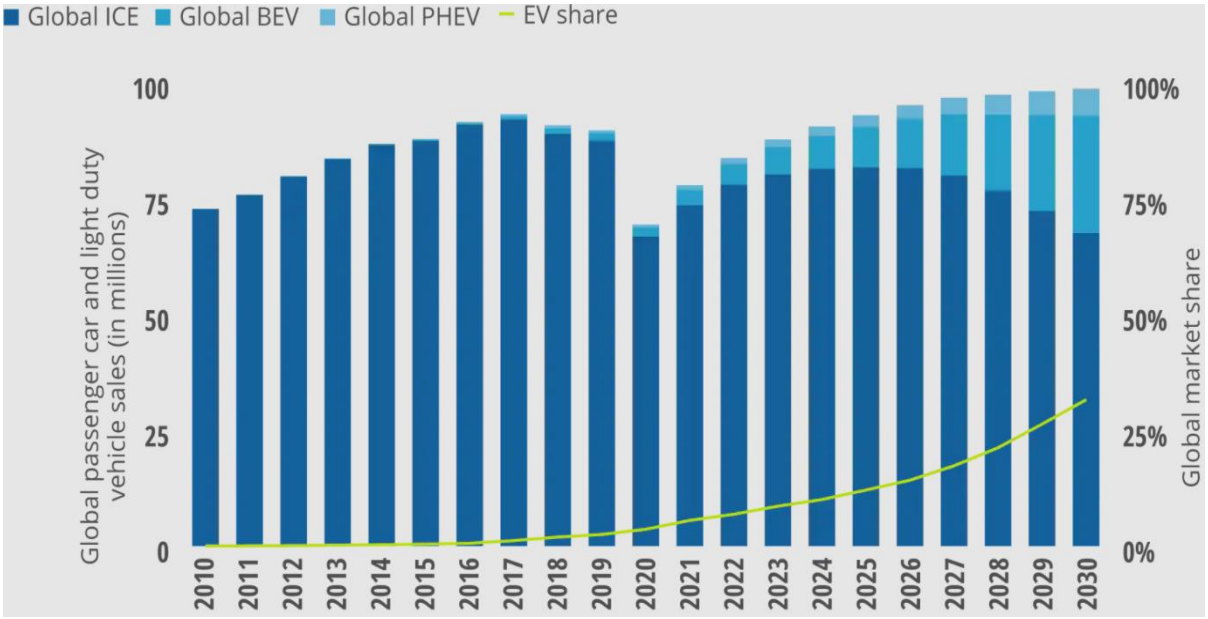

Figure 2.22: Annual global light-duty vehicle and global passenger-car sales (IEA, 2020)

This significant growth on the sale of EVs is underpinned on the advancement in energy storage technology which is considered as the engine or centre of EV growth. Presently, there are several energy storage requirements for automotive application such as cost, adequate maintenance, specified energy, efficiency, specific power, effective energy management, environmental adjustment and friendliness and safety (Rosario, 2007; Mokrani et al., 2016; Zhang & Li, 2019). Specified energy requirement is a critical and primary factor considered when assigning energy source for EV because it determines the vehicle travel range and type of EMS required for optimization. Again, it is vital for EV manufacturers and PPS providers to understand the basic principle of the different energy sources, and specific requirements of the EV supply source and corresponding EMS. These energy storage systems are mainly supercapacitors and chemical batteries. Therefore, this section will present the fundamentals of different types of electrochemical batteries, supercapacitors, and fuel cell technologies including their suitability for specific applications (Hu et al., 2018).

2.5.1 Electrochemical batteries

These are electrochemical devices that convert chemical energy into electrical energy during discharging and convert electrical energy into chemical energy when charging (Corral-Vega et al., 2019; Zhang et al., 2017). A battery is made up of individual cells that are connected in series or parallel or both to achieve a desired output voltage. It is made up of three basic main components connected as shown in Figure 2.23. The anode (negative electrode) is oxidised during electrochemical reaction by releasing electrons to the external circuit, the cathode (positive electrode) accepts the electrons from the external circuit during same period while the electrolyte acts as the conductor that provides the platform for electrons transfer between the anode and cathode. The electrolyte is usually water or other solvents having dissolved salts, acids or alkali with the capacity to trigger ionic conductivity. This can be solid conductor with equal operating cell temperature or liquid electrolyte depending on the type of cell (Khayyer, 2008).

But several kinds of electrochemical batteries, like nickel-metal hydride, lead-acid, lithium-based, etc., are also accessible. But for general automotive application and EV application in particular, lithium-ion battery is the prime choice because of its lightweight, higher efficiency, relative power as well as the energy capacity (Okba, 2015).

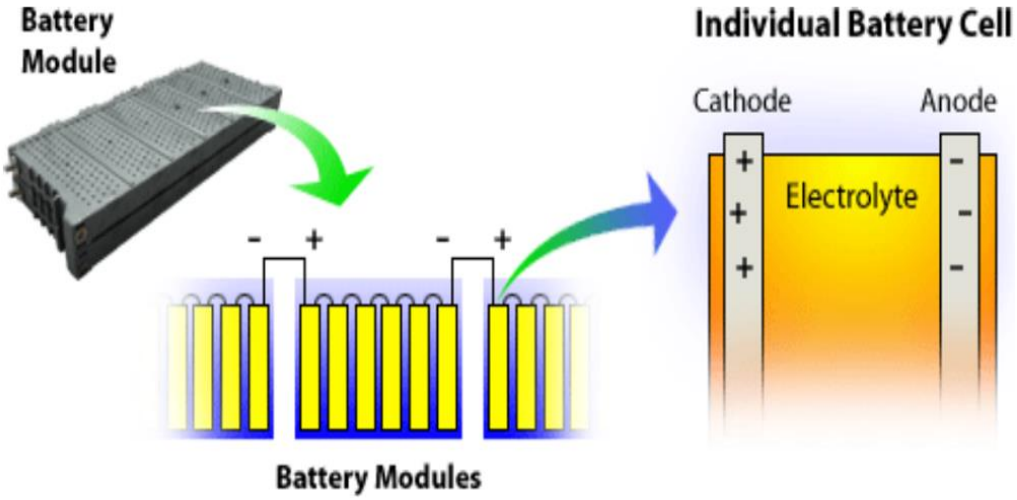

Figure 2.23: Battery module, its schematic, and battery cell (Khayyer, 2008)

2.5.1.1 Nickel-metal hydride (NiMH) battery

Nickel metal has excellent electrochemical properties suitable for battery applications in the automotive sector It is a metal lighter than lead with four different battery technologies: nickel-metal hydride, nickel-cadmium, nickel-zinc, and nickel-iron (Yue, 2019; Williamson, 2013). However, only nickel-metal hydride (NiMH) will be discussed because of its relevance in electric vehicle applications.

NiMH battery is regarded as one of the prime choices for automobile applications in the past ten years. This is because of its high specific energy and relative power capacity which makes it suitable for high power applications. It has low internal resistance but high rates of self-discharge making it unfit for low power applications. Although, it was first used on the Toyota Prius vehicle in the late nineties in Japan, the second-generation GM EV1 and later in the testing of the Solectric GT EV. The battery technology since then has witnessed significant improvement because of the research input by some manufacturers such as: Panasonic, SAFT, GP and YUASA2 (Khayyer, 2008; Alloui et al., 2015)

Advantages of NiMH

- Easy storage and transportation void of major regulatory conditions
- 30-40% higher energy density compared to standard NiCd
- Environmentally friendly with less emissions

Drawbacks of NiMH

- High self-discharge of approximately 12.5% daily at room temperature
- Less discharge currents
- High cost

- Requires difficult charge procedure
- Poor cycle efficiency

2.5.1.2 Lead-acid battery

Lead-acid batteries have been available in the market since the 19th century with various applications in the automotive industry and other electrical energy storage devices (Mkhize, 2019). It is regarded as the battery of choice in applications that requires high-power capacity such as HEVs and most electrical devices because of its low cost, high-power capacity and advanced technology amongst other advantages as highlighted. Presently, there are various types of lead-acid batteries developed and readily available in the market for different applications with different levels of enhanced performance. One of such development is the advancement of the sealed lead-acid battery with specific energy capacity of more than 40 Wh/kg, improved fast charging time and increased life cycle (Sanguesa et al., 2021; Rosario, 2007; Jain & Kumar, 2018). Bipolar and micro-tubular grid designs are some other types of lead-acid technologies that have been improved in recent times. As part of the improvement on these types of technologies is the increase in the specific energy of the battery which is achieved by reducing the inactive components such as the current collector, separators, casing etc. However, “Electro-source Horizon battery” is the most advanced sealed lead-acid battery at the moment. It has an improved energy capacity of 43 Wh/kg, improved life cycle of above 600 cycles for EV application, fast charging system (8 mins - 50% charge capacity and completely charged in 30 mins), low cost, high specific power of 285 W/kg, less environmental pollution, mechanically strong and less operational cost (Shang, 2013; Sundström & Stefanopoulou, 2006).

Advantages

- Low self-discharge rate
- Materials used for the manufacture are low cost compared to other types of batteries
- It requires little maintenance
- Advanced and well-known technology
- High power capacity

Drawbacks

- Low energy density
- Limited full discharge cycles
- Potential runaway due to improper charging
- Poor temperature characteristics below 10◦C
- Significant reduction in specific energy and specific power

The poor temperature characteristics exhibited by lead-acid batteries has limited its use in traction of vehicles in cold climate regions hence, making it one of the major constraints hindering mass adoption of lead-acid batteries in automotive applications. In addition, to address safety challenges inherent in lead-acid batteries, an electrochemical technique is integrated in the design to soak up the hydrogen and oxygen emissions (Ehsani et al., 2010).

2.5.1.3 Lithium based battery

Lithium based batteries possesses good electrochemical characteristics that has made it the battery of choice for electric vehicle applications (Smithson Bell, 2016). Lithium metal is the lightest metals used for battery production. It has significantly high thermodynamic voltage that produces high specific power and corresponding high specific energy. Presently, there are two notable lithium-based batteries available: lithium-polymer and lithium-ion (Ehsani et al., 2018; Okba, 2015; Jain & Kumar, 2018; Wu, 2014; Khayyer, 2008).

2.5.1.3.1 Lithium Polymer (Li-poly) battery

The electrolytes in lithium polymer batteries are solids and that is why it is referred to as “solid state batteries” (Kamarudin et al., 2009). There are different types of lithium polymer electrolyte battery technologies available in the market today. However, each of these technologies are at different stages of technological advancement, but the most advanced technology is the polyethylene oxide which is surrounded by suitable electrolyte salt to improve the specific energy and equivalent specific power (Ehsani et al., 2010). Li-poly has exhibited the highest specific energy and specific power by substituting highly flammable electrolytes in the battery with non-flammable electrolytes. Hence, the replacement of the electrolyte has provided significant benefits, safety and advantages when used for EV applications (Han et al., 2014).

Advantages

- Light weight
- Offered better resistant caused by overheating
- Enhanced safety
- Reduced profile
- More economical

Drawbacks

- Reduced life cycle
- Poor energy density
- Bigger sizes and more expensive to manufacture

2.5.1.3.2 Lithium-ion battery

Presently, lithium-ion batteries are the most commercialised battery technology used in automotive applications because it has higher volumetric and gravimetric energy densities when compared to other battery technologies (Wu, 2014). A standard lithium-ion battery is made up of five different components: a cathode, anode, current collector, ionically conductive electrolyte and insulating separator. Hence, the operating principle and individual components of a standard lithium-ion battery is shown in Figure 2.24.

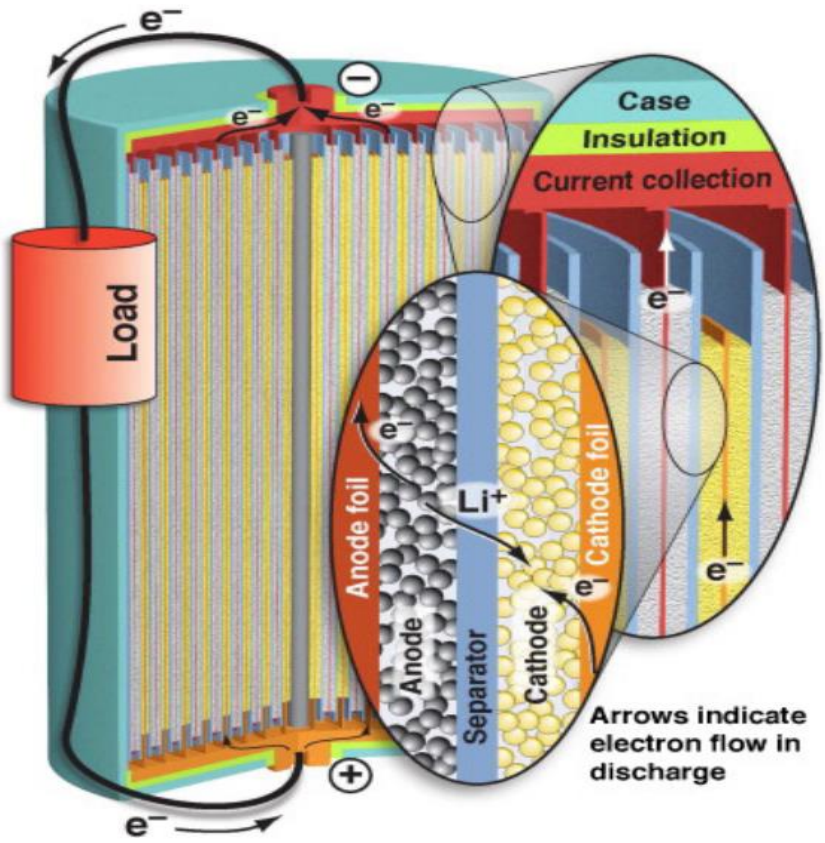

Figure 2.24: Lithium-ion battery structure indicating flow of electrons (Wu, 2014)

Lithium-ion (Li-ion) battery has experienced significant technological advancement since its commercialisation in 1991 because of its electrochemical characteristics. Li-ion based batteries have higher energy and power densities relative to other types of batteries and chemistries of the same size. These benefits have increased the competitiveness of Lithium-ion based battery vehicles against ICE vehicles for short travel range within a city (Fletcher, 2017). In the past decade, Li-ion battery has seen significant growth in technology making it the battery of choice in EV applications and other regular consumer electronics gadgets such as laptops and mobile phones (Ehsani et al., 2018). Furthermore, Li-ion batteries have very high cycling efficiency that helps improve the fuel economy of hybrid vehicles and the charging price of EVs (Khayyer, 2008).

Beginning from 1993, some battery manufacturing companies such as SAFT, Panasonic, SONY, VARTA and GS Hitachi were actively involved in the improvement of Li-ion batteries. Recently, SAFT introduced a new technology on Li-ion battery suitable for EV applications with a specific power of 1350 W/kg and a specific energy density of 85 Wh/kg. Thereafter, a high-energy Li-ion battery of approximately 420 W/kg and 150 Wh/kg operating at 80% SOC was introduced for EV applications. This type of battery has seen applications in the new Nissan Leaf EV amongst others due to the increased lifecycles, less charging time and increased travel range. Li-ion batteries have a better coping mechanism during transient loads than fuel cells mostly due to the lack of an external reactant supply; however, they still show some level of degradation (Ehsani et al., 2010).

Advantages

- High energy density
- Better safety
- Less maintenance
- Considerable low self-discharge rate

Drawbacks

- Very expensive to manufacture
- Requires protection circuit

Finally, recent research have shown that lithium-ion based battery technology has the potential to dominate the EV industry in the next ten years (Wu, 2014). Regrettably, EVs are still very expensive due to the high cost of battery pack which is a major obstacle hindering mass adoption and deployment of EVs globally (Khayyer, 2008; Samrat et al., 2014).

2.5.1.4 Electric battery configuration

To model a standard electric battery requires only the steady state characteristics without incorporating the dynamic behaviour of the battery as shown in Figure 2.25. The model basically comprises of an internal resistance (R_{int}) and an internal voltage source (V_{int}) described as the voltage drop, "ΔV" that are created by the chemical reaction present in the system. The battery current in this case is considered positive as expressed in equation 2.26 (Wu, 2014).

$$V_{bat} = V_{bat_{int}} - R_{int} i \tag{2.26}$$

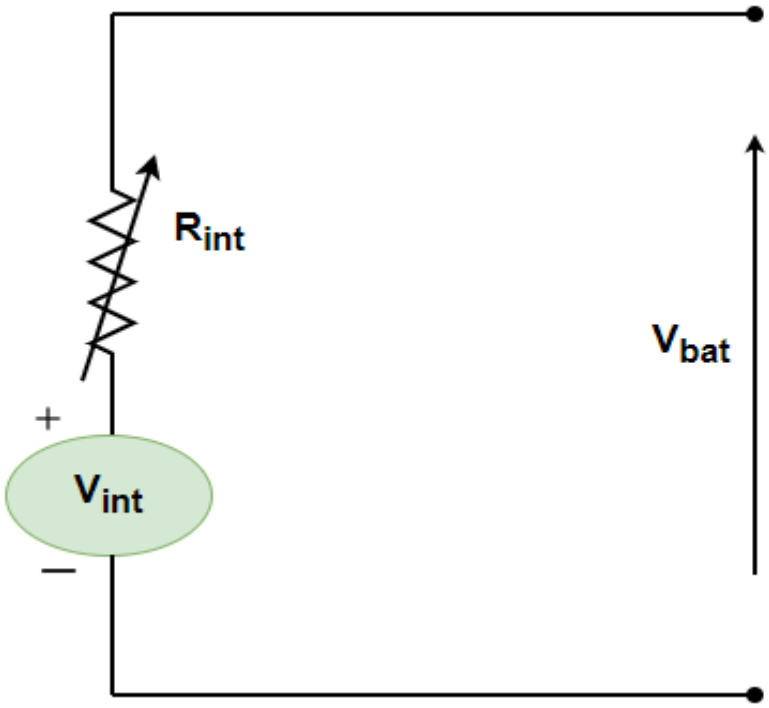

Figure 2.25: Equivalent battery circuit (Wu, 2014)

2.5.1.4.1 Specific energy

The specific energy of a battery is an important parameter required for practical applications and optimal operation because it determines the absolute useful work hence, it is also referred to as “gravimetric energy storage density” of an electrochemical cell. It is the combination of the specific capacity and the voltage range expressed in watt-hour per kilogram (Wh/kg). Mathematically it can be expressed as (Wu, 2014; Khayyer, 2008; Ehsani et al., 2018)

$$Energy = \int EdC \tag{2.27}$$

2.5.1.4.2 Specific power

For any application that requires high power demand for its operation such as complete EV and HEV applications, it is important to know the specific power of the electrochemical cell because it will assist in reducing the battery weight and selecting the other components (Miao et al., 2019). Again, establishing an accurate value of the specific power of a battery will enhance optimal operation of the battery and the entire system. However, it is the internal resistance of the electrochemical cell that determines the specific power which is also referred to as “gravimetric power density” and expressed in watt per kilogram (W/kg) (Panchal, 2014). Using the electric model battery shown in Figure 2.25, the maximum power generated and supplied to the load can be expressed as:

$$P_s = \frac{V_{int}^2}{4(R_c + R_{int})} \quad (W/kg) \tag{2.28}$$

2.5.1.4.3 Battery state of charge (SOC)

The state of charge (SOC) is considered amongst the most critical parameters of a battery. It is generally expressed as the percentage of the present charge (capacity) against the nominal capacity. The nominal capacity is provided by the manufacturer and indicates the maximum amount of charge the battery can store and still operate optimally within established standard. SOC has no unit but expressed in percentage levels. A battery that is fully charged has SOC of 100% while fully discharged battery has SOC of 0% (Panchal, 2014; Wu, 2014). Considering time interval, the battery SOC can be expressed as (Chang, 2013):

$$SOC\ (t) = \frac{Q(t)}{Q_n} \tag{2.27}$$

$Where$:

$Q(t) = available\ charge$

$Q_n = nominal\ capacity$

2.5.1.4.4 Battery energy efficiency

This is the ratio of the operating voltage to the thermodynamic voltage that occurs when the battery charging and discharging energy is the efficiency of the battery. It is described as voltage losses inherent in power or energy losses through charging and discharging in batteries (Wu, 2014). Therefore, the efficiency of the battery (η_c) when charging is expressed as:

$$\eta_c = \frac{v_{int}}{v} \tag{2.28}$$

While the efficiency of the battery (η_d) when discharging is expressed as:

$$\eta_d = \frac{v}{v_{int}} \tag{2.29}$$

In addition, the electrical potential created by the chemical reaction in the battery is greater during charging and lower during discharging. This is significantly dependent on the amount of energy stored in the battery, battery state of charge (SOC) or the current rating of the battery (Wu, 2014; Panchal, 2014). The efficiency of a standard battery when charging and discharging is shown in Figure 2.26. From the figure, it shows that the charging efficiency of

the battery is high at low SOC while the discharging efficiency is high at corresponding high SOC and the net cycle efficiency is highest when the battery SOC is 50% (Okba, 2015).

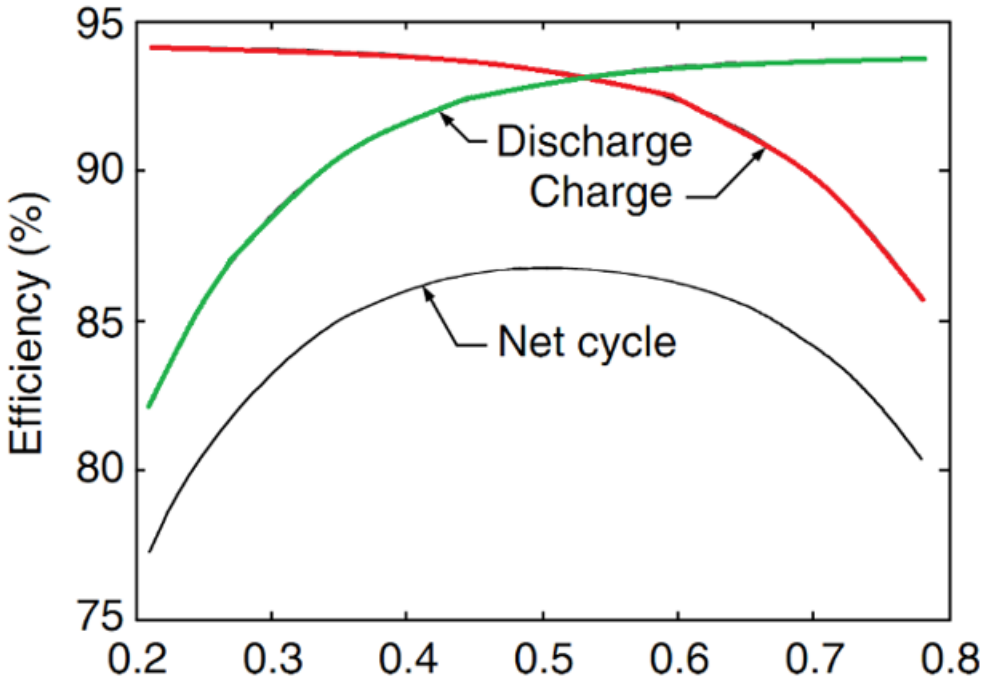

Figure 2.26: Standard battery efficiency when charging and discharging (Okba, 2015)

2.5.2 Ultracapacitor (UC)

General Electric Engineers were the first to observe the electric double-layer capacitor effect in 1957 during an experiment in the laboratory that involved the use of porous carbon electrode. The mechanism and phenomenon at that point was not clear to the engineers but it was observed that an extremely high capacitance energy was stored in the carbon holes (Okba, 2015). Ultracapacitors (UCs) are electrochemical devices with a higher energy density than electrochemical batteries such as lithium-ion and lead-acid, but a lower specific energy. Therefore, it has limited its use in automotive applications because EVs requires transient dynamic performance during acceleration and deceleration (Panchal, 2014; Wu, 2014). Batteries and fuel cells are better deployed in EV applications because of their higher specific energy as compared to UCs. However, the power sources can be recharged using the energy sources during regenerative braking or less driving load (Panchal, 2014; Wu, 2014; Okba, 2015).

2.5.2.1 Fundamental Principles of Ultracapacitor (UC)

An electrochemical UC consists of an electrolyte and two electrodes that are connected electrically. However, the two electrodes are separated by a thin layer (insulator) but when a voltage is applied on both electrodes, an electric double-layer is created on both electrodes

that have negative and positive charges on both plates (Panchal, 2014). These opposite charges create an electric double-layer that charges the plates on both sides of the capacitor as shown in Figure 2.27.

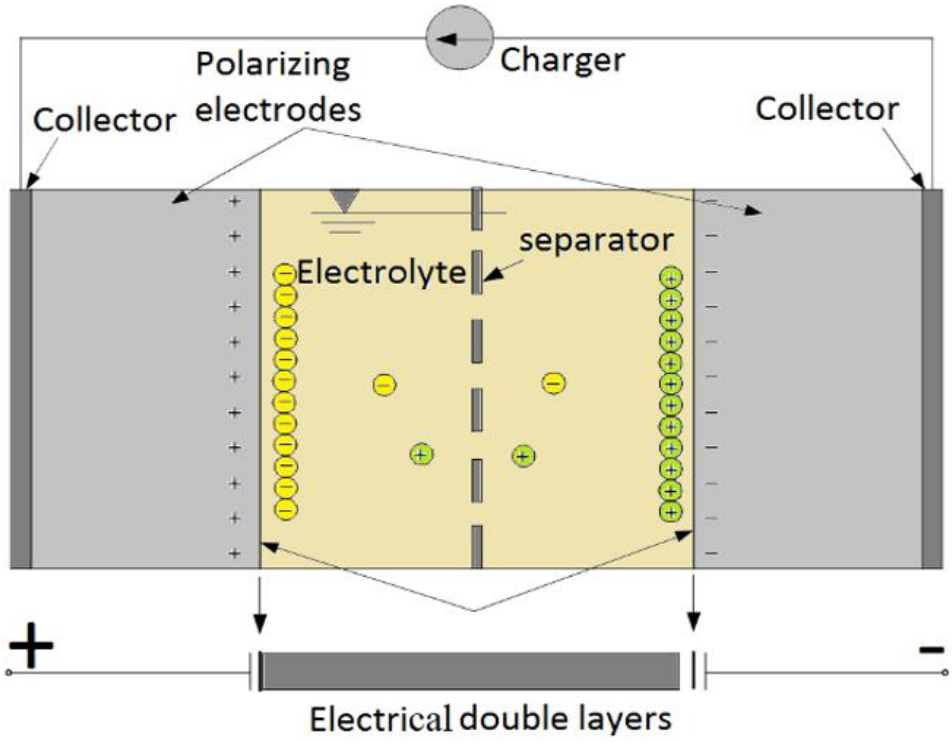

Figure 2.27: Structure of a standard Ultracapacitor (Dusmez & Khaligh, 2014)

In addition, UCs have high power density, high load currents and low equivalent series resistance (ESR) caused by the types of material used and design construction. These qualities have contributed to the low heating losses, high efficiency, high charge and discharge capacity that has characterised UCs. But due to the fast charging and discharging capacitance, the cost of ultracapacitor is higher than electrochemical batteries and other forms of energy sources that are currently available in the industry. However, an increase in the plates area will lead to a decrease between the plates but lead to an increase in the capacitance of the capacitor (Wu, 2014; Alharbi, 2013).

2.5.2.2 Standard electric model Ultracapacitor

Presently, there are different types of equivalent electric circuits of UCs according to type of materials used, design construction and circuit considerations. One of such design is an equivalent electrical circuit shown in Figure 2.28. In this design, the measure of the voltage-dependent capacitance of the non-linear capacitor, i.e., the derivative of charge with respect to potential is replaced by a linear voltage dependent capacitor kV_0 and a fixed capacitor C_0 (Berrueta et al., 2019; Shi & Crow, 2008).

$$\frac{dV_0}{dt} = \frac{1}{C_0 + kV_0} I_{SC} \tag{2.30}$$

while,

$$V_{SC} = R_{SC} I_{SC} + V_0 \tag{2.31}$$

Where, *k* is a constant equivalent to the slope voltage and $C_0 + kV_0 > 0$

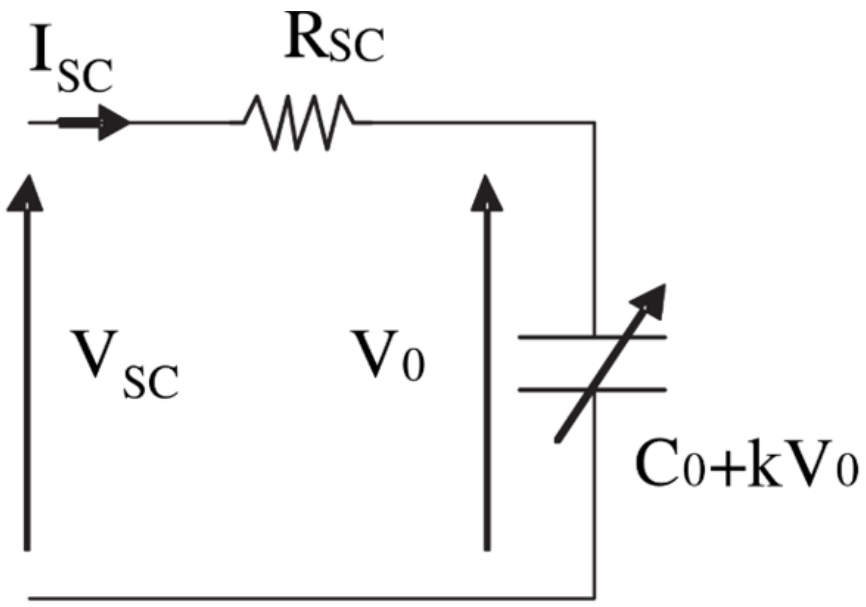

Figure 2.28: Ultracapacitor equivalent circuit (Shi & Crow, 2008)

The total energy stored in the Ultracapacitor is expressed as:

$$E_{SC} = \frac{1}{2} C V_{SC}^2 \tag{2.32}$$

Where, C is the capacitance of the capacitor in Farad (F).

2.5.2.3 State of Charge (SOC) of Ultracapacitor

The SOC of an Ultracapacitor is the ratio of the total amount of energy stored at any particular moment to the maximum energy that can be stored (Berrueta et al., 2019). Again, the stored energy is proportional to the square of the applied voltage. This is normally represented by the base voltage (V_{SC_b}). In addition, the useful energy provided by the UC during operation is

usually less than the potential maximum energy which can be expressed as (Shi & Crow, 2008):

$$E_{SC_u} = \frac{1}{2} C\left(V_{SC_b}^2 - V_{SC_r}^2\right) \tag{2.33}$$

Where, V_{SC_r} is the UC's rated voltage. But at the base voltage, the SOC can be further expressed as (Okba, 2015):

$$SOC = \frac{E_{SC_u}}{E_{SC_c}} = \left(\frac{V_{SC_b}}{V_{SC_r}}\right)^2 \tag{2.34}$$

One of such examples is shown in Figure 2.29, where the cell voltage of UC drops from 60% of the rated voltage then the total available energy also dropped to 64%. This is a typical example of how the UC's SOC is affected during operation which is temperature dependent (Ehsani et al., 2010; Wu, 2014; Okba, 2015; Lorf, 2014).

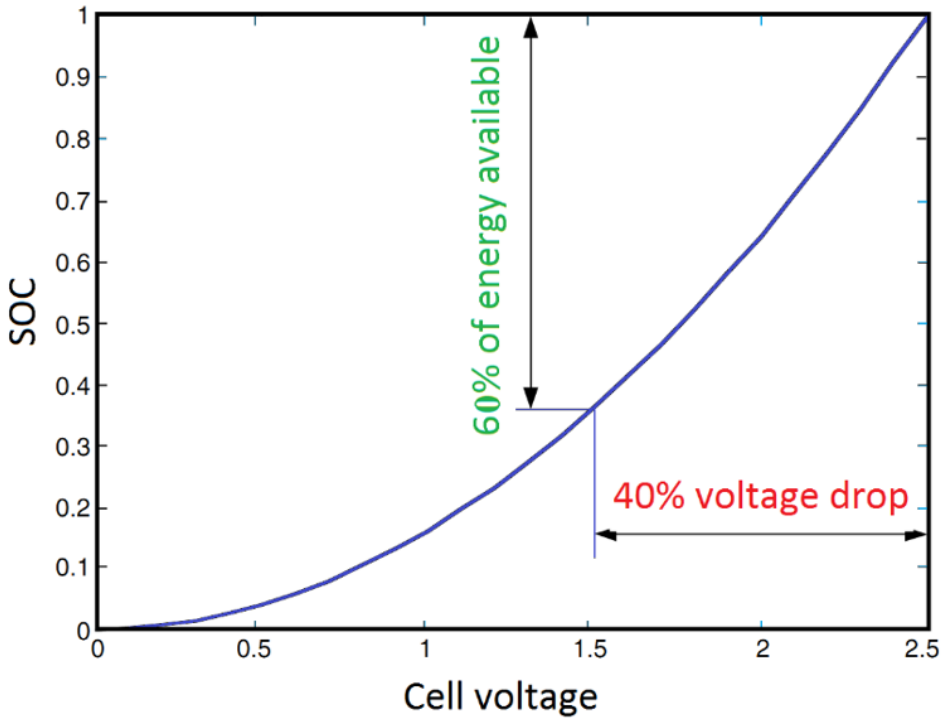

Figure 2.29: Standard SOC of Ultracapacitor (Okba, 2015)

2.5.3 Fuel Cell

The use of fuel cell for vehicular applications has received much attention in the past ten years due to the advancement in technology and its environmental benefits. However, the deployment of fuel cell in vehicular applications is slow because much research is still required

to improve the efficiency and cost (Behdani & Naseh, 2017; Feroldi, 2012; Wu, 2014). Fuel cell is an electrochemical cell that converts chemical energy of a fuel into electrical energy. It accepts fuel and air at the input and produces water and electricity as the output through a chemical reaction (Manoharan et al., 2019). Presently, there are different types of fuels available such as, hydrogen, methanol, ethanol, etc that have advantages of both ICE and batteries (long travel range and high energy density) if only supplied with fuel continuously (Han et al., 2014; Fernandez et al., 2020; Das et al., 2017)

2.5.3.1 Brief history of fuel cell

In 1839, Sir William Grove, a Welsh judge and scientist invented the first fuel cell technology which was before then used basically in experiments in the laboratories. This invention triggered significant interest in the 1960s amongst scientists and engineers at the National Aeronautics and Space Administration (NASA) that made way for the adoption of PEMFC for its space program over nuclear power, solar power and wind power because of the high risks, intermittent power supply and high costs associated with these sources (Manoharan et al., 2019; Okba, 2015). Currently, FCs are the primary power supply to the space shuttle but was also used to power the Apollo and Gemini spacecraft missions by NASA in the 60s. Regardless of the successful applications of FCs in the space industry, it only received significant recognition and commercialisation in the 1980s due to technology maturity and need to operate more environmentally friendly spacecrafts (Okba, 2015). Fuel cells was only implemented in vehicular applications in the 1950s when a group of researchers headed by FT Bacon at the University of Cambridge demonstrated with the use of alkaline FC for short travel range. The FC was operated at above 200℃ and travelled for a very short distance which was not the main interest of the research at that moment rather the ability to propel the vehicle (Manoharan et al., 2019; Vaz, 2015; Strahl, 2014). This development gave rise to the design of an Alkaline FC hydrogen/Oxygen rated at 6 kW in August 1959 to power a forklift and other machine tools. Subsequently, the past decade has experienced a significant prototyping of FCEV and FCHEV which has replaced the battery pack due to increased research in fuel cell energy management and further advancement in technology (Manoharan et al., 2019; Zhi-ling et al., 2010; Vaz, 2015).

2.5.3.2 Fundamental principle of fuel cell

A fuel cell is made up of two electrodes (cathode and anode) with an electrolyte between them. The electrolyte is characterised by a special porous material that allows the free flow of positive ions (protons) while stopping the electrons (cathode) (Luta, 2019). The catalyst ensures that the positive and negative ions are separated when Hydrogen gas passes through the negative

electrode (anode) as shown in Figure 2.30. However, the electrochemical reaction that takes place in a fuel cell is similar to a chemical battery and expressed as (Okba, 2015):

$$2H_2 \Longrightarrow 4H^+ + 4e^- \tag{2.35}$$

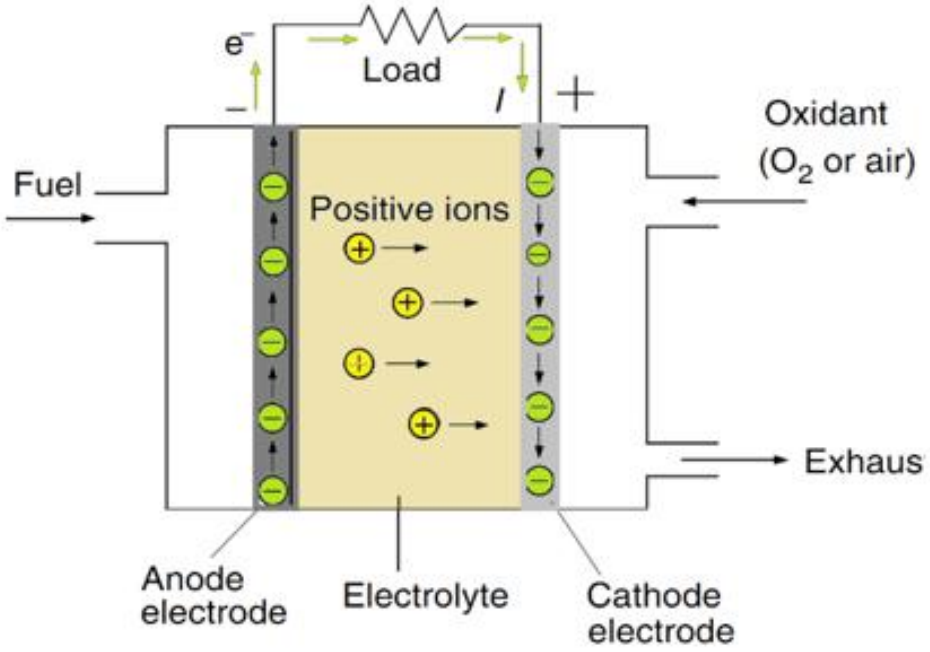

Figure 2.30: Fundamental principle of a fuel cell (Okba, 2015)

The protons drift towards the positive electrode (cathode) through the electrolyte while the electrons gravitate towards the negative electrode (anode) supported by an external circuit thereby generating electricity. The Hydrogen protons and electrons are fused together with oxygen supplied by an external gas-flow to produce water and heat at the electrode as expressed in equation 2.36 (cathode) (Ehsani et al., 2010; Ehsani et al., 2018).

$$O_2 + 4H^+ + 4e^- \Longrightarrow 2H_2O \tag{2.36}$$

Therefore, the general equation of a fuel cell is given as (Luta, 2019):

$$O_2 + 2H_2^+ \Longrightarrow 2H_2O \tag{2.37}$$

Furthermore, the load capacity and other operating conditions of the fuel cell determines the voltage produced by individual fuel cell which is between 0 and 1 V (Ehsani et al., 2010). Under normal conditions, the standard value of the voltage is approximately 0.7 V (Okba, 2015). But, to increase the voltage of a FC, several cells are connected in series then the total voltage is achieved by multiplying the number of cells by the average cell voltage.

As highlighted earlier, the by-products of fuel cell are water and heat, but both can be constantly eliminated to maintain steady power supply and optimal operation of the entire system.

Generally, fuel cell has significant advantages compared to other types of power sources such as electrochemical battery, fossil fuel, coal, natural gas, wind, geothermal, etc. Some of these advantages are (Smithson Bell, 2016):

- Noiseless operation
- Little maintenance required
- High power efficiency
- High power density
- Long life
- Reduced corrosion
- Operates in high temperatures

Fuel cell powered vehicle have longer travel range because FC provides steady electrical energy under normal condition if the fuel supply is maintained. It also has zero emissions as compared to ICE vehicles because of the direct conversion of free energy to electrical energy (Das et al., 2017). However, the use of FC in vehicular applications is slow due to some few challenges such as, inadequate hydrogen storage, slower dynamic performance, existence of high current ripples, inadequate voltage profile compared to current density, pressure regulation, heat management and lack of effective compression mechanism (Wu, 2014; Okba, 2015).

2.5.3.3 Types of fuel cells

Presently, there are various types of FC technologies that are commercially available while others are still at the foundational stage. These technologies are at different stages of research and development hence can be categorised based on the type of electrolyte utilized, power conversion efficiency, output power, operating temperatures, active lifetimes, applications and technology maturity. Some of these include the Molten Carbonate Fuel Cell (MCFC), Solid Oxide Fuel Cell (SOFC), Alkaline Fuel Cell (AFC), Phosphoric Acid Fuel Cell (PAFC), Direct Methanol Fuel Cell (DMFC) and Proton Exchange Membrane Fuel Cell (PEMFC) (Ehsani et al., 2010; Okba, 2015; Luta, 2019). The primary reactant in a FC is hydrogen while the oxidant is oxygen. But presently there are several types of reactants such as by-products of biomass and ethanol being used depending on the type of technology. Each of these technologies have unique advantages and disadvantages.

Presently, PEMFC is the most used fuel cell for various applications because of the technology maturity and flexibility. This high level of acceptance and recognition enjoyed by PEMFC has provided it with significant market share of approximately 97% of all available fuel cell (Erensoy, 2018; Luta, 2019). They are seen to be the best choice for vehicular applications because of its rapid response time, high efficiency, higher power density, low operating temperatures and simple and user-friendly characteristics. Although, the cost of PEMFC and travel range are still the major obstacles hindering its mass adoption for vehicular applications. Phosphoric Acid Fuel Cells (PAFCs) are the most marketed fuel cell for applications that requires standard temperatures. PAFCs are commonly used for cogeneration applications and specific areas that requires high efficiencies. In addition, when operating solely on hydrogen and oxygen, the Alkaline Fuel Cells (AFCs) has the best performance. Although, it is still confronted with setbacks such as short lifetimes and zero tolerance on impurities during operation which has prevented its use in earthly applications but rather useful in extra-terrestrial applications (Han et al., 2014). Solid Oxide Fuel Cells (SOFCs) and Molten Carbonate Fuel Cells (MCFCs) are suitable for high temperature areas and combined-heat and-power (CHP) applications. SOCFs are better suited for base-load grid applications while MCFCs are best deployed in applications that requires high efficiency because of the technology advancement (Han et al., 2014).

2.5.3.3.1 Molten Carbonate Fuel Cell (MCFC)

Molten Carbonate Fuel Cell consists of a molten carbonate cell sandwiched by two porous electrodes that are highly conductive, operates at significantly high temperatures of approximately 600 to 700℃ and mostly used for stationary power generation (Erensoy, 2018). The operating principle of a MCFC indicating the flow of electrons is shown in Figure 2.31. To withstand the high operating temperature, the fuel cell stacks are usually made of stainless-steel materials. However, the hydrogen is insulated from the carbon monoxide fuel thereby ensuring the breakdown of hydrogen through the water shift chemical reaction to produce hydrogen assisted by the internal reforming capability. Again, the high operating temperature of MCFC supports the utilisation of internal reforming where the hydrocarbon fuels produce hydrogen at the output within the cell stack and not the outside processor. The outcome of the chemical reaction generates electricity just like PEMFC (Luta, 2019; Erensoy, 2018; Ehsani et al., 2010). In addition, some of the advantages of MCFC are (Ehsani et al., 2010):

- Metal catalyst and insulated reformers are not required because it operates in high temperature
- Increased efficiency of approximately 50 to 60%
- Appropriate for use as combined cycle
- It has the capacity to be combined with many hydrocarbons such as natural gas

Some drawbacks of MCFCs are:

- It can only be used for average and high-power applications
- Performance degradation in the anode and cathode due to corrosive electrolyte
- High operating temperature aids fast cell component degradation
- MFCFs are vulnerable to poisoning by Sulphur

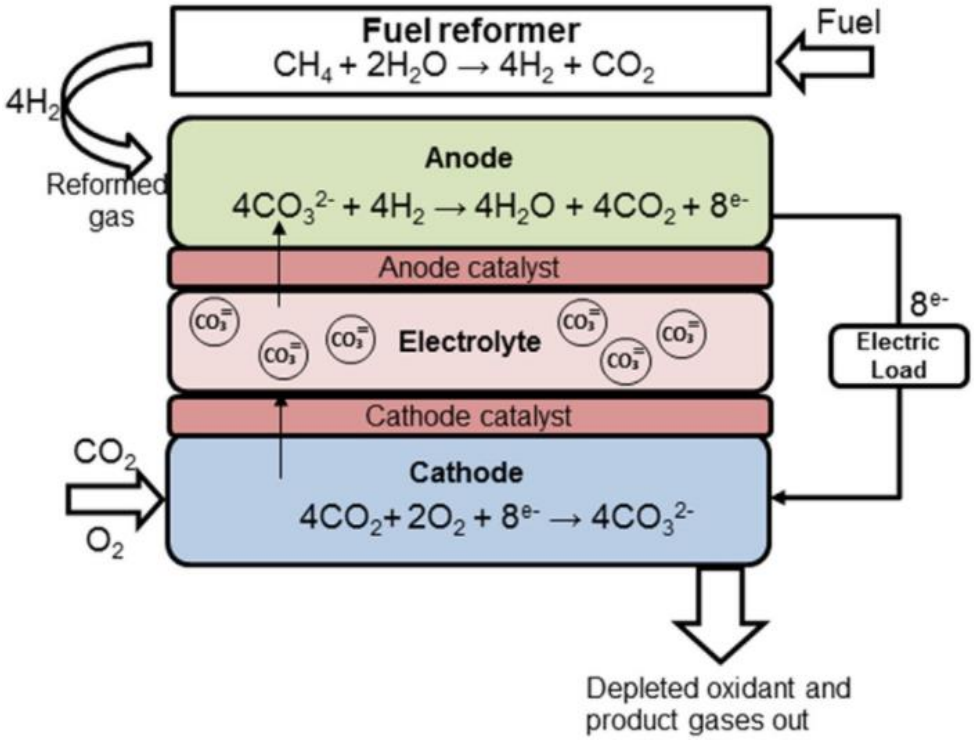

Figure 2.31: Operating principle of Molten Carbonate Fuel Cell (Mehmeti et al., 2017)

2.5.3.3.2 Solid Oxide Fuel Cell (SOFC)

Solid Oxide Fuel Cells (SOFCs) are primarily operated at high temperatures of approximately 800 to 1000℃ depending on the individual systems designs and configurations. Operating at such high temperature has made the material selection of the different parts of the SOFC a daunting task (Luta, 2019). However, in the design, Oxide ion conducting yttria stabilised Zirconia (YSZ) which is strong ceramic material is the material that is generally used for the electrolyte while nickel/YSZ is used for the anode and strontium-doped lanthanum manganate (LSM) for the cathode as shown in Figure 2.32. One of the significant benefits of SOFCs is its effective electricity generation from a range of fuels for different power generation applications (Okba, 2015). Furthermore, SOFCs have high efficiency of around 50 to 60% without the need for a separate reformer to remove the hydrogen from the fuel due to the internal reforming capability. Extra power can be produced using waste and heat through cogeneration process. Nevertheless, SOFCs are still not suitable for larger load demand due to the intermittent power

supply, high cost, average start up and zero tolerance on sulphur. Therefore, they are basically used for medium and high load demand applications (Mehmeti et al., 2017; Minh, 2004).

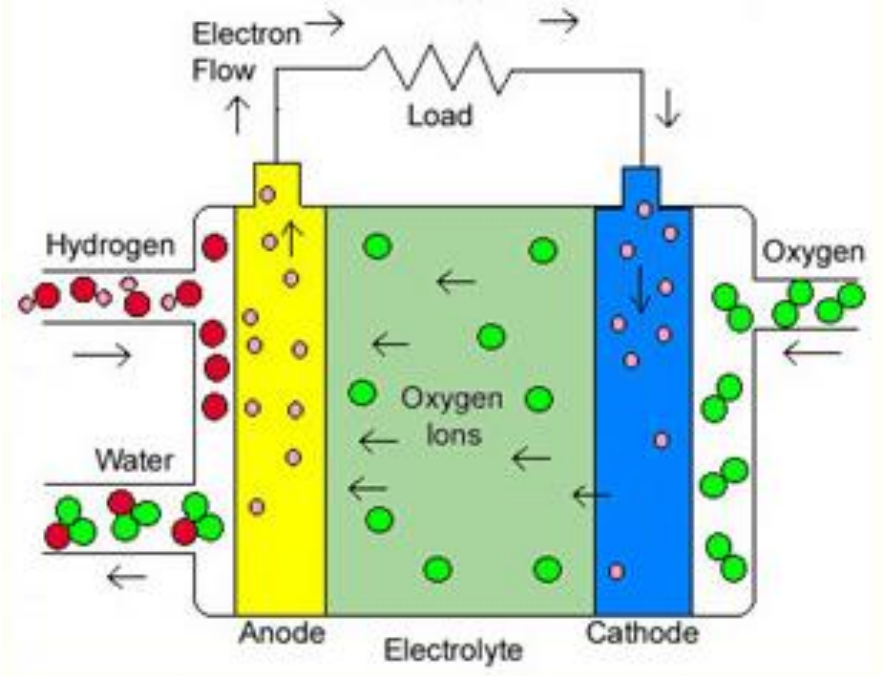

Figure 2.32: Solid Oxide Fuel Cell (Minh, 2004)

2.5.3.3.3 Alkaline Fuel Cell (AFC)

Alkaline fuel cells (AFCs) were initially designed for vehicular applications because it was effective for adequate and fast delivery of power (Uzunoglu & Alam, 2007). However, the work by Francis Thomas Bacon in the 1930s at the University of Cambridge was the first in Alkaline fuel cell technology. Thereafter, several other works were developed from that point that led to the advancement of permeable, sintered nickel electrodes that was later displayed in the 1950s. Hence, it was previously called the Bacon fuel cell after the British scientist. This new technology was the beginning of Alkaline liquid electrolyte that became the primary electrical power source during the Apollo mission and thereafter the space shuttle Orbiter (Bidault & Middleton, 2012; Luta, 2019). AFC has an efficiency of between 60 to 70% and operates effectively at low temperature of about 100℃. It uses a liquid solution of Potassium hydroxide as its electrolyte while the negative charge particles are moved from the anode to the cathode with water been discharged as its by-product as shown in Figure 2.33. The main benefit of this fuel cell technology is its fast-starting characteristics and the major difficulties were the control of the liquid electrolyte and the immobilisation of the absorption of CO_2 in the atmosphere due to precipitation of carbon species and low conductivity (Bidault & Middleton, 2012). Furthermore, during chemical reactions, additional time is usually needed for the alkaline to be consumed in the electrolyte which reduces the hydroxide content. An extra platform is required

to flush out the amount of CO_2 in the ambient air which obviously serves as a drawback because it reduces the lifespan of the system (Luta, 2019).

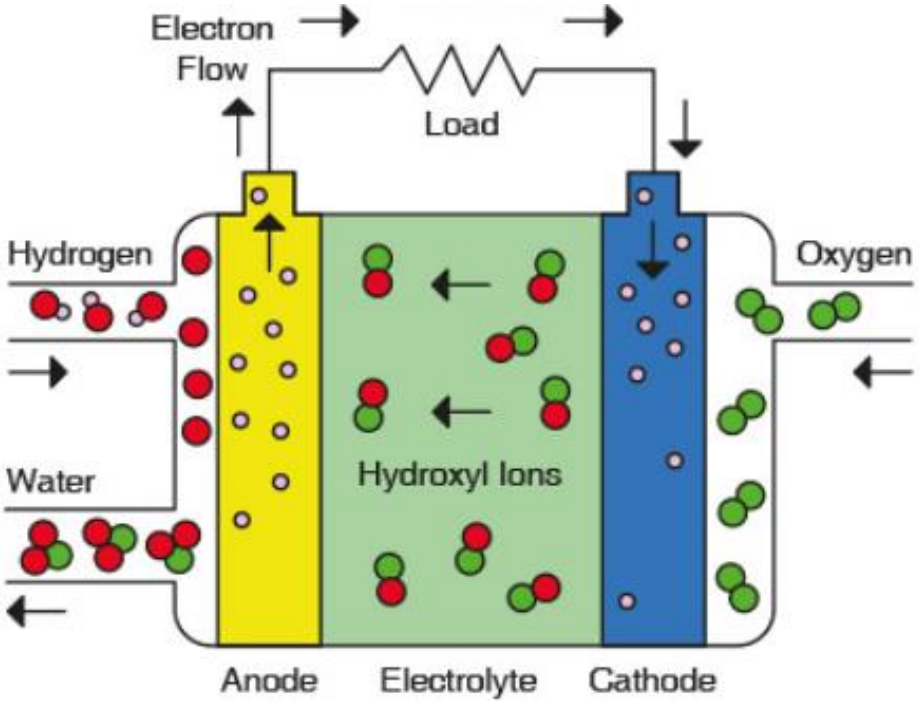

Figure 2.33: Alkaline Fuel Cell (Bidault & Middleton, 2012)

2.5.3.3.4 Phosphoric Acid Fuel Cell (PAFC)

Phosphoric Acid Fuel Cells (PAFCs) were amongst the first commercially developed fuel cells that were intended for terrestrial applications in the mid-1960s to operate at temperatures between 170 to 210℃. It uses highly concentrated (>95%) phosphoric acid as its electrolyte and permeable carbon electrodes that has platinum catalyst as shown in Figure 2.34. The chemical reaction uses CO_2 with air as the oxidant and pure hydrogen as the primary fuel. A porous silicon-carbide matrix is normally used to restrict the electrolyte. The interior parts of PAFC is designed to handle the high corrosive nature of the acid electrolyte. Its operation is like PEMFC but somewhat different because the electrolyte used is significantly lenient to CO_2 impurities from different hydrocarbon fuels. The efficiency of PAFC increases in cogeneration to around 80% as against single generation of about 40 to 50 %. It is mostly used in stationary power plants and heat applications because they are available in different sizes from 100 kW to 500 kW. Nevertheless, the major drawback of PAFC is the high cost arising from the use of platinum as catalyst (Choudhury, 1989).

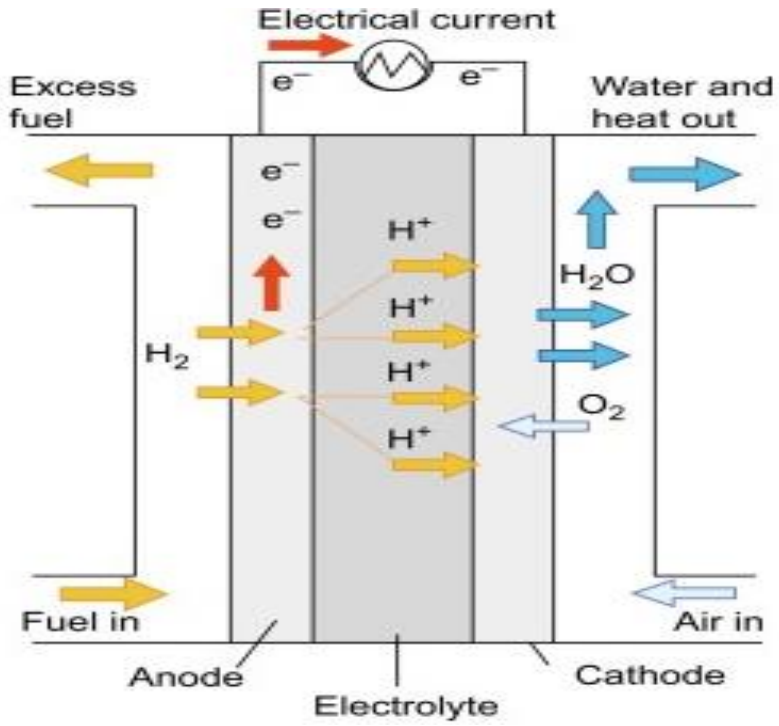

Figure 2.34: Schematic representation of a PAFC (Choudhury, 1989)

2.5.3.3.5 Direct methanol Fuel cell (DMFC)

Direct methanol fuel cell (DMFC) is a developing electrochemical membrane reactor that operates at low temperature with liquid methanol supplied at the anode (Kamarudin et al., 2009). It is an improvement of PEMFC because it utilises polymer membrane electrode like PEMFC, but the major difference is that a liquid methanol is directly oxidised to carbon dioxide at the cathode to produce electricity. The energy density is higher when pure methanol is used at the anode but decreases when a mixture of water and methanol is used (Ong et al., 2017). In situations where a mixture of water and methanol is used, the water is usually returned to the anode to maintain a balanced electrochemical reaction. Presently, its efficiency is still a major concern because it is less efficient than other technologically advanced and less advanced fuel cells. Hence, it is mostly used as power supply for small electronic devices such as laptops, mobiles phones, iPads etc. DMFCs are considered FC of choice in some applications because fuel (methanol) can easily be stored in a suitable container and the reactor is simple to design without fuel reforming (Sundmacher et al., 2001).

At the anode $\Longrightarrow CH_3OH + H_2O \rightarrow CO_2 + 6H^+ + 6e^-$ (2.38)

and

at the cathode $\Longrightarrow 3/2O_2 + 6e^- + 6H^+ \rightarrow 3H_2O$ (2.39)

2.5.3.3.6 Proton Exchange Membrane Fuel Cell (PEMFC)

The proton exchange membrane fuel cell (PEMFC) like other types of fuel cells has a cathode, an anode and an electrolyte membrane as shown in Figure 2.35 (Abd El Monem et al., 2014). The anode and cathode are separated by an electrolyte called “Nafion” used in low-temperature PEMFC. It serves to facilitate the movement of protons from the anode to the cathode while the electrons are moved over through an external circuit load. However, when in operation, the fuel (Hydrogen (H_2)) is electrochemically oxidised at the anode catalyst layer to produce protons and electrons while on the cathode, electrons and protons electrochemically react with oxygen to produce water and heat as its by-product (Carnevali, 2017). In the past decade, PEMFCs have witnessed significant technological advancement hence, drawn much interest because of its notable advantages such as, fast response time, improved and efficient energy conversion rate, high power density, less sensitive to orientation and no polluting by-products (Smithson Bell, 2016). Furthermore, PEMFCs are classified as Low-Temperature PEMFC (LT-PEMFC) or High-Temperature PEMFC (HT-PEMFC) based on the operating temperature. The operating temperature for Low-Temperature PEMFC is between 60-80℃ and it uses a totally fluorinated Teflon-based material as its electrolyte while the catalyst is a standard Platinum material (Lu, 2013). The electrolyte material in a LT-PEMFC is called Nafion and was first produced in the 1960s specifically for space applications by DuPont but has found applications in other sectors such as vehicular applications, boats, etc (Lu, 2013). The High-Temperature PEMFC operates between 110-180℃, uses Polybenzimidazole (PBI) doped in phosphoric acid as its electrolyte and Platinum–Ruthenium as its catalyst. The electrical efficiency of LT-PEMFC is between 40-60% while HT-PEMFC is between 50-60% respectively but both are determined by the operating temperature, type of electrolyte, catalyst and system configuration (Smithson Bell, 2016; Fletcher et al., 2016; Ehsani et al., 2018).

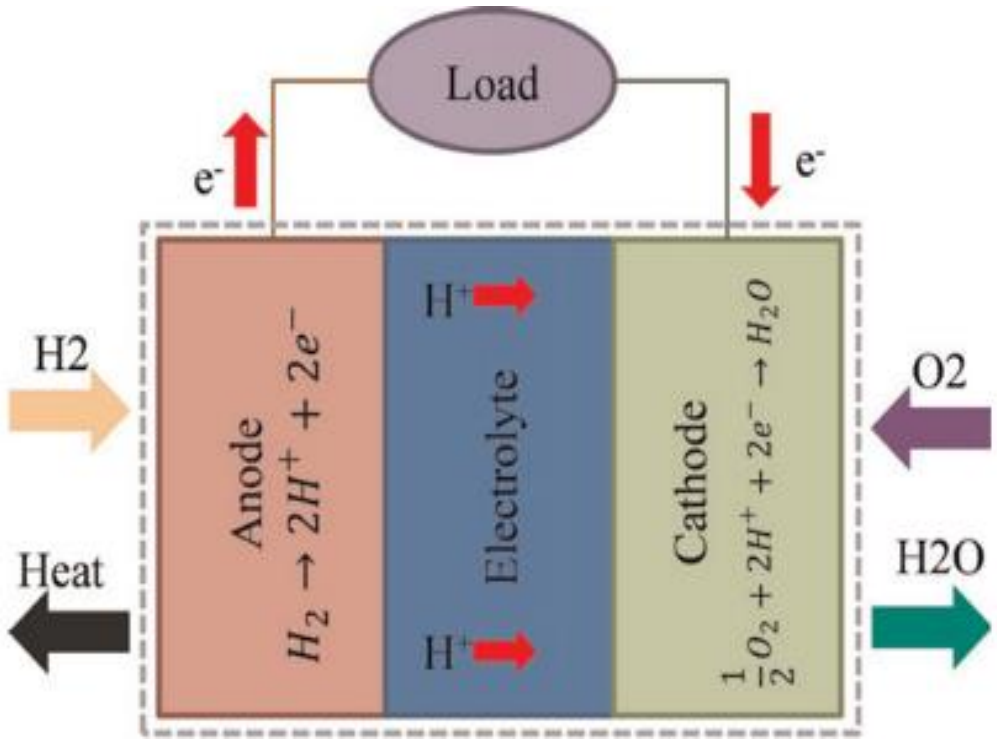

Figure 2.35: Schematic of a PEMFC (Abd El Monem et al., 2014)

2.6 Energy Management Systems (EMS)

The primary function of EMS in a vehicle is to control and ensure effective management of different energy sources and storage devices based on the drive cycle information (Fletcher, 2017; Erensoy, 2018). However, the hybridisation of fuel cells with batteries, ultracapacitors or both in FCHEV is basically to absorb the regenerative braking energy and maintain a balance between the load and fuel cell power. Achieving these two conditions will ensure that the vehicle is always operated optimally and efficiently without overloading individual components in the system. According to Fletcher, (2017), FCHEVs have not achieved its pride of place in the EV sector due to concerns around high cost and fuel cell degradation which with proper EMS can be systematically reduced. The battery can be used to provide additional power to the system thereby ensuring the downsizing of the fuel cell which will lead to reduced cost of materials. Again, the fuel cell degradation challenge can be solved using the battery to supplement power during acceleration or transient loads (Erensoy, 2018). This will enhance the fuel cell lifespan, improve efficiency and operate it at optimal position. But to have an in-depth understanding of EMS control systems for FCHEVs, sufficient literature on EVs, types of EV design, its configuration including different power supply sources and types of FCs is provided in sessions 2.1 to 2.5. Therefore, in this session, a brief literature review on EMS requirements such as dependability, battery cell degradation, fuel economy, and fuel cell degradation are presented. Furthermore, various type of EMS techniques used for vehicular applications are presented.

2.6.1 EMS Requirements

The primary aim of EMS strategies is to offer a dependable, robust, efficient operation, lower fuel consumption, reduce cost and minimise losses. These can be obtained by developing an efficient EMS within established parameters (Fletcher, 2017). A brief literature review on some EMS requirements necessary for optimal operation are presented below.

2.6.1.1 Reliability

This is the term used in electric vehicles to describe availability of power, predictability of parameters and consistency of performance. Vehicles are expected to always respond adequately according to established constraints consistently. It includes a wide range of factors expressed by the driver and the drive cycle considered to enhance performance (Erensoy, 2018). Some of such parameters are pedal response, vibration, acceleration, engine noise, braking mode shifting amongst others. For example, the vehicle performance when accelerating is expected to remain reliable regardless of the battery state of charge (SOC). Reduced battery SOC should not affect the vehicle's ability to provide adequate power or perform optimally considering the characteristics of individual components in the vehicle. Therefore, reliability concerns are normally included as an integral component of EMS when optimisation is considered globally (Fletcher, 2017)

2.6.1.2 Battery Cell Degradation

EMS directly controls a battery's SOC and the current loading of the battery simultaneously at any specific time during its operation thus, having a substantial impact on the battery's rate of degradation (Erensoy, 2018; Fletcher, 2017). This means that having an effective EMS will increase the charge-discharge cycle of a battery. Although, a battery's rate of degradation depends on the chemical configuration, it is mostly affected when it is exposed to a temperature and voltage higher than required. A battery operated within recommended temperature and voltage will lasts longer than the ones operated outside its temperature and voltage (Erensoy, 2018). Therefore, a battery should be operated within allowable voltage and temperature for optimal operation. Operating a battery within its voltage can be achieved by ensuring that an already fully charged battery is not charged further nor allowed to exceed the allowable current. This phenomenon is mostly experienced in traction batteries during regenerative braking. Furthermore, a battery is not allowed to operate below its minimum voltage to prevent deep charging. This happens mostly when trying to draw current beyond the minimum level or from an already depleted battery which occurs during traction. Lastly, the charge-discharge cycles of the battery create gradual damage hence, the EMS must be designed to prevent over cycling of the battery (Roscher et al., 2011; Fletcher, 2017; Erensoy, 2018).

"However, the battery's functionality gradually decreases over its lifetime because of power and capacity losses. Particularly high temperatures, high currents, and high energy throughput are the main factors that force the deterioration of batteries' electric characteristics." (Roscher et al., 2011, p. 98)

2.6.1.3 Fuel Economy

Majority of the research on EMS is centred around fuel economy because of the direct impact it has on the operational cost and travel range of the vehicle because, implementing an effective EMS in FCHEV will significantly reduce the running cost and enhance the travel range without increasing the size of the energy storage system (ESS) (Fletcher, 2017). The efficiency of fuel cell is determined by the power supply and demand (load) ratio such that at low power demand, the percentage of current supply against ancillary (fans, humidifiers, etc) increases compared to useful output thereby reducing the overall system efficiency (Erensoy, 2018). But as the load increases gradually the impact of ancillary current decreases while the ohmic losses increases. The voltage starts to drop substantially at high loads such that the mass transfer of different chemicals across the fuel cell becomes the restricting factor as shown in Figure 2.36 (Rousseau et al., 2004).

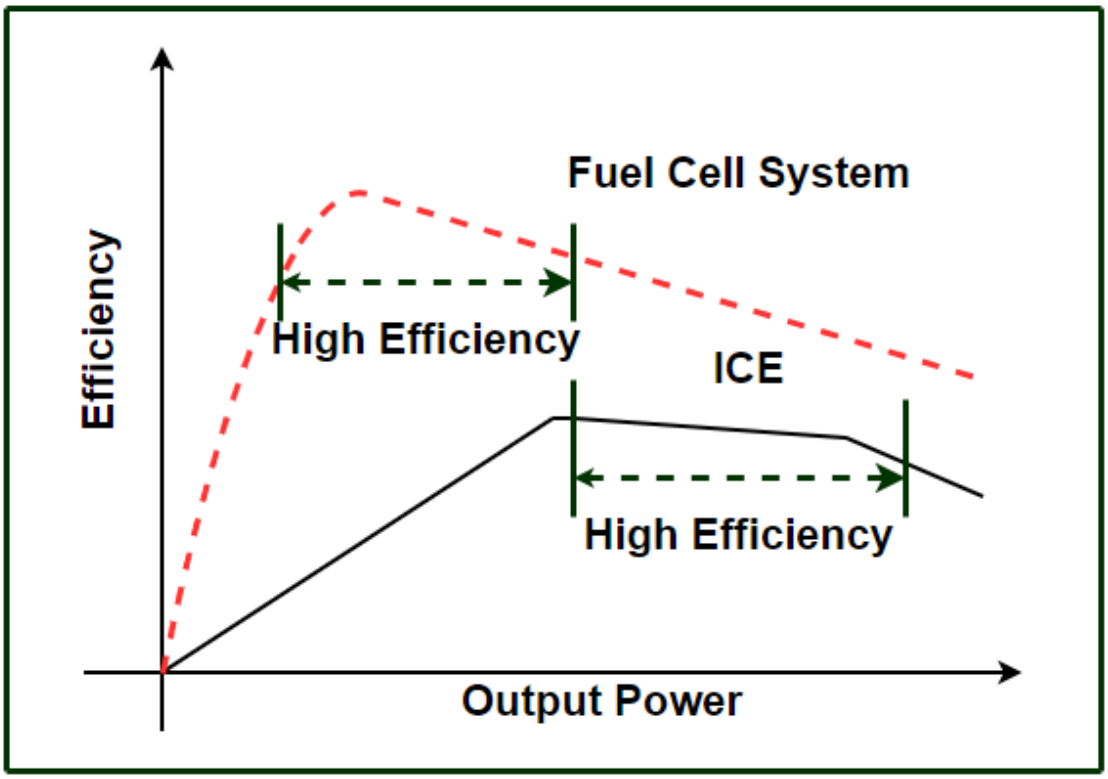

Figure 2.36: Fuel Cell efficiency vs. ICE efficiency (Rousseau et al., 2004)

In addition to ensuring the optimisation of the fuel cell, the efficiency of other components in a FCHEV must be evaluated for overall system efficiency. Some of such components are the DC/DC converters, traction motor, energy storage system, inverters, etc (Fletcher, 2017; Erensoy, 2018; Rousseau et al., 2004). However, it is the SOC of the battery during braking that determines the energy efficiency recovery that arises from braking. So, if the power from braking is greater than the battery capacity or the battery is fully charged, then the energy at that moment will be lost. Hence, it is vital to have a battery with enough capacity to absorb the energy during braking so that the recovered energy can be maximised (Fletcher, 2017).

2.6.1.4 Fuel Cell Degradation

"The durability of each component of a PEMFC is affected by many external factors in an operating fuel cell, including the fuel cell operating conditions (such as humidification, temperature, cell voltage, etc.), impurities or contaminants in the feeds, environmental conditions (e.g., subfreezing, or cold start), operation modes (such as start-up, shutdown, potential cycling, etc.), and the design of the components and the stack." (Yuan et al., 2011, p. 9109)

There are several research on fuel cell degradation that are available stretching from electrochemical modelling to experimental study on accelerated decaying testing to Failure Mode and Effects Analysis (FMEA) (Yuan et al., 2011; Pukrushpan et al., 2006; Zhang et al., 2009; Placca & Kouta, 2011). However, the primary purpose of reducing fuel cell degradation is to detect obtainable levels for supervisory control. Presently, a typical PEMFCs is expected to operate for 3500 hours but with effective EMS, the lifespan of the fuel cell can be enhanced to reduce the normal minimum number of hours by operating it less than required but still competitive with ICE (Wu, 2014). Operating fuel cell efficiently and optimally depends on a variety of factors including impurities of the reactants, environmental conditions, material properties and operating conditions. EMS have no direct impact on some of these factors such as impurities in the cell and environmental conditions, but it can prevent fuel cell degradation by adjusting the operational condition in order to reduce its impact. Lastly, fuel cell degradation is broadly classified into three categories: catalyst layer, membrane layer and Gas Diffusion Layer (GDL) (Fletcher, 2017; Erensoy, 2018; Wu et al., 2008; Zhang et al., 2009; Placca & Kouta, 2011; Pukrushpan et al., 2006; Yuan et al., 2011; Rousseau et al., 2004).

2.6.2 EMS Techniques

The different topologies shown in Figure 2.37 can be implemented on FCHEV using different control strategies depending on the primary purpose of the EMS, optimisation focus, system configuration, etc (Erensoy, 2018). Presently, there are various EMS techniques available that can be used to control FCHEVs with some still at the experimental stage while others are well

developed. The development of some of these strategies are more complex than others, but the level of complexity does not essentially translate to best strategy nor trade-off for the inconsequential gradual advancement. Hence, there should be adequate concentration on the practicality of the chosen algorithm and primary purpose of the EMS and not only the power-train dynamics (Fletcher et al., 2016; Fletcher, 2017; Erensoy, 2018). Practical control techniques employed on hybrid power source for vehicular applications is broadly categorised into machine learning strategy, heuristic strategy, optimisation-based control strategy and passive control as shown in Figure 2.38.

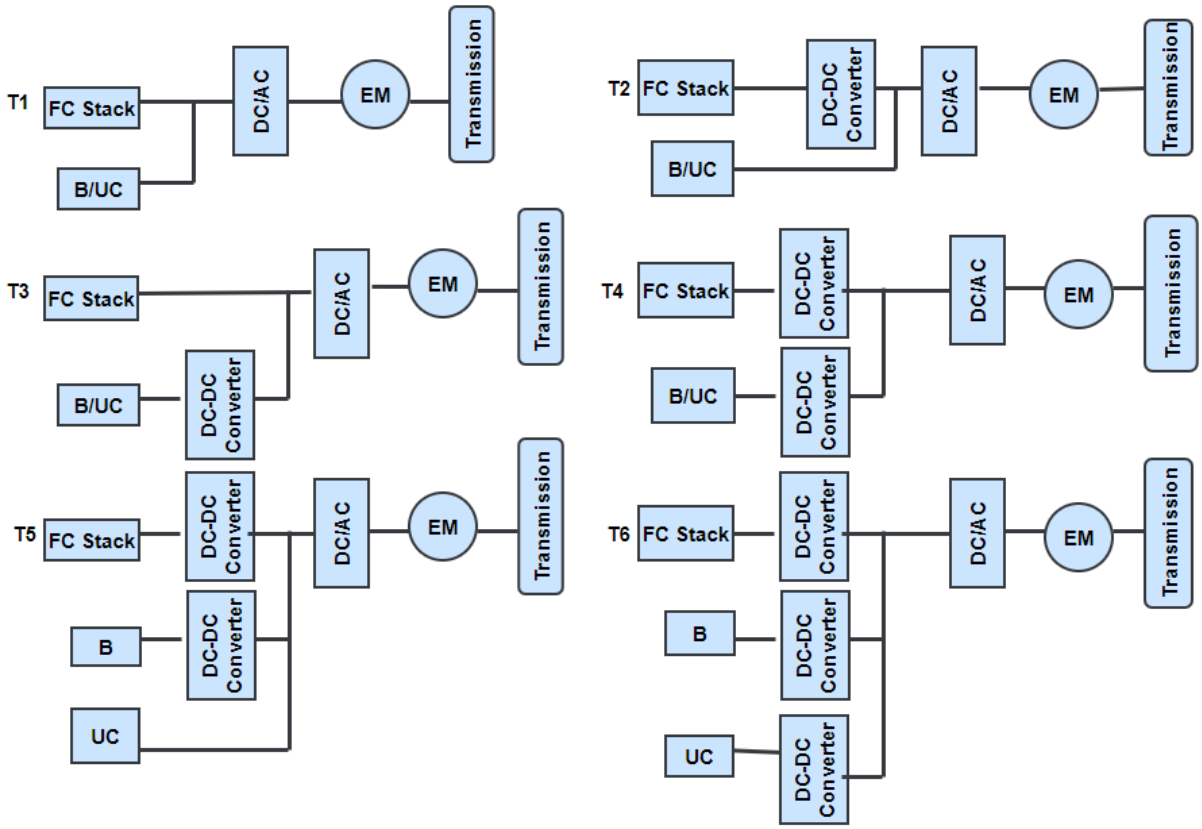

Figure 2.37: FCHEP Topologies (Erensoy, 2018)

2.6.2.1 Machine Learning Strategy (MLS)

The output control of machine learning is less complicated compared to heuristic strategy (HS) because it does not have the series of complex conditions present in HS but it offers an outcome that can be regulated automatically (Showers & Raji, 2022; Fletcher, 2017; Erensoy, 2018). Again, when using MLS, the controllers can be re-enhanced for various power-train configurations with less weight compared to other strategies thereby offering significant operational advantage above rule-based techniques. A typical MLS can be operated off-line and the results implemented on the test vehicle while others can be executed directly on the test vehicle by including little computational algorithm to ensure steady and improved optimisation. Wavelet decomposition, neural networks, and deterministic dynamic

programming (DDP) are three major categories of MLS. Wavelet-based decomposition strategy is implemented using a well-defined algorithm that employs filtering techniques while neural network strategy uses three distinct levels of time interval that ensures load variations, SOC of the DC output power and the inputs from the load power (Erensoy, 2018). Deterministic dynamic programming (DDP) technique is basically designed to execute huge complex problems by splitting it into smaller portions then recombine the result to accomplish the general solution. According to Odeim et al., (2015), when DDP is used for off-line optimisation, the performance of the PI controller is always better than that of fuzzy logic regardless of it having less operational parameters.

2.6.2.2 Heuristic strategy

This is based on the anticipated characteristics of the driving force system and utilizes prearranged sets of conditions to define the operational states of the overall system (Showers & Raji, 2022; Erensoy, 2018). Heuristic strategy is broadly classified into two, Deterministic rule-based technique and fuzzy logic technique as shown in Figure 2.38. Deterministic rule-based technique uses predetermined knowledge of fuel efficiency, behaviour of individual components, power flow in the drive-train and other physical experiences to execute a search table on how available power sources will be distributed in the system. It is categorised into state-based power assisting technique and load levelling technique which will be the focus of this study. However, the number of set conditions are relative and can be improved to reduce the amount of fuel consumed. This technique is mostly used in EMS because it is less complex and can be used for real time operations (Erensoy, 2018; Fletcher, 2017).

2.6.2.2.1 State-based power assisting technique (SBPAT)

Power distribution and current sharing in state-based power assisting control technique is based on the power rating of the electric motor which is informed by the fuel cell power, type of energy storage and its corresponding SOC (Showers & Raji, 2022; Fletcher, 2017). This type of technique is mostly used in FCHEP energy management strategy for various applications where the low voltage from the fuel cell is boosted before connecting to the inverter while the voltage from the ESS is kept at same level. But to optimise such system, the EMS is developed to establish the optimal point of individual components based on predetermined set of rules that measures the load-power relationship at intervals. For example, a PI and low pass filter-controlled DC converter can be implemented to ensure power stability while the reference current of a fuel cell is established using the EMS (Erensoy, 2018).

A study conducted by Han et al., (2014), showed that the efficiency of a power-train operated using real life driving cycle of a boat with SBPAT EMS was enhanced compared to load tracking control. Again, Gao, Jin, Zhang, et al., (2016), whose study was primarily focused on

enhancing fuel economy, eliminating fuel cell degradation and preserving battery lifecycle for a hybrid fuel cell/battery bus while driving showed significant improvement in the fuel economy. The study was modelled for regular start and stop, fast acceleration which increases the fuel cell efficiency during long drives and idle positions. The result of the study showed that when using state-based power assisting technique, the fuel economy increased by 3.5% and the power supply was constant at optimal position.

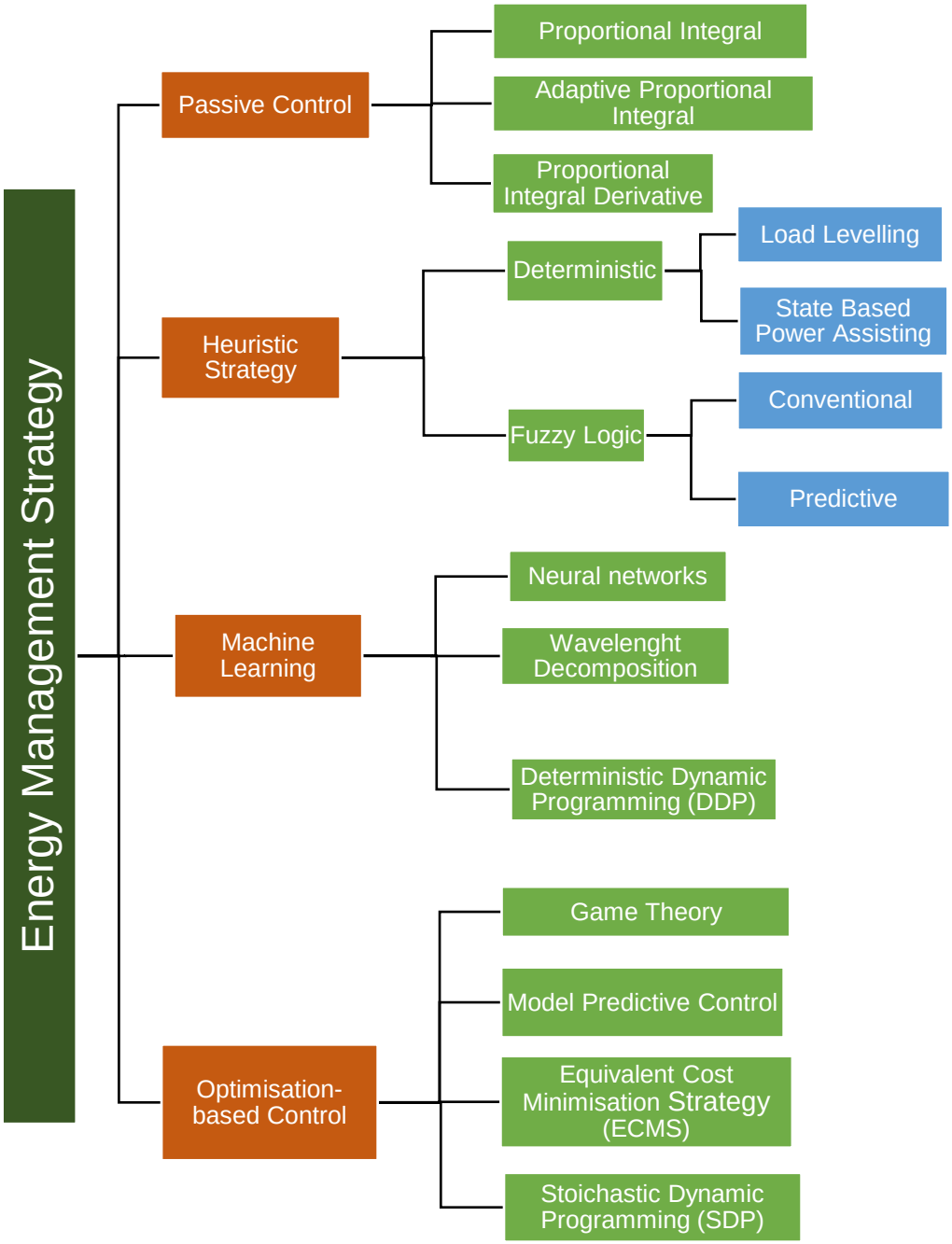

Figure 2.38: Power-trains Energy management control strategies (Erensoy, 2018)

2.6.2.2.2 Load levelling strategy

Load levelling strategy ensures constant power supply from the fuel cell while the ESS functions as a backup for energy storage and management of transient loads (Fletcher et al., 2016). A research group at the Virginia Tech developed a boost converter for a fuel cell-controlled power-train to support the EMS by removing the power transfer regulation from on-board computer while maintaining the fundamental power transfer. This double layer control technique maintains balance using a DC/DC buck converter. It uses a low-level control system and fuzzy logic to regulate the fundamental low inductor current setting it as the reference point while, a high-level strategy is used to optimize the fuel cell operation during transient loads. The ESS in this type of configuration is primarily to handle the load dynamic behaviour while the fuel cell provides the average or base power (Fletcher et al., 2016; Erensoy, 2018). Although, with load levelling strategy, significant power losses are recorded during charge/discharge conditions because of the power flow through the power electronic device (DC-DC converter).

In addition, rather than using deterministic set of rules, fuzzy logic can be used to control the power distribution in real-time which also ensures enhanced performance because of the design flexibility that it enjoys (Grammatico et al., 2010; Fletcher, 2017). The fuzzy logic control system is based on a set of “IF” conditions that sets the operational boundaries that must be met for satisfactory condition. The design flexibility potentially creates variety of complex control conditions that might affect the control system performance. But, if the set conditions are adequately allocated, it can reduce the percentage of control failure in the system. Hence, fuzzy logic strategy aspires to improve the control system by reducing adequate cost function drive cycle by providing the anticipated driving cycle information (Fan, 2011; Fletcher, 2017; Fletcher et al., 2016).

2.6.2.3 Optimisation-based control

Optimisation-based control strategy is used mathematically to establish control boundaries and objectives in a cost function that is based on the cost of fuel consumption, losses in the system and overall cost of the system. This is achieved by employing fundamental global optimisation values to define control techniques that are informed by predetermined drive cycle data (Erensoy, 2018; Felgenhauer et al., 2016; Fan, 2011; Fletcher, 2017). However, there are some setbacks with this method because utilising global optimisation creates design challenges for real-time applications, but it is still a useful design strategy for assessing several control strategies. Optimisation-based control is broadly classified into Stochastic Dynamic Programming (SDP), Equivalent Consumption Minimization Strategy (ECMS), Model Predictive Control (MPC) and Game theory.

2.6.2.3.1 Stochastic dynamic programming (SDP)

SDP is an optimisation-based control strategy that uses time-invariant results based on the vehicle characteristics and the possibility of moving to a different operational condition to develop an effective EMS (Tazelaar et al., 2013). It enjoys a design flexibility that permits the utilisation of several drive cycle data for effective on-board direct implementation and practical (real-time) assessment using Markov Chain (Fletcher, 2017; Erensoy, 2018). However, its major drawback is the computational complexity which affects real-time implementation in some instances. This problem can be solved by representing the cost function as a linear Quadratic Control or a Quadratic equation combined with predetermined drive cycle information.

2.6.2.3.2 Equivalent consumption minimization strategy (ECMS)

ECMS controls the ESS state of charge when supplying the load and ensures that the fuel consumption is operated optimally without over stretching available energy sources in the system (Fletcher, 2017). It ensures localised optimal operation of individual components at all times by taking into consideration the overall energy consumption whilst the SOC is monitored regularly. This type of strategy also enjoys multiple topologies and flexible configuration with energy sources operated at optimal levels (Zhang et al., 2017; Erensoy, 2018). In addition, the equivalent coefficient which is equal to the power ratio of all available power sources in the system must be stated for effective operation using ECMS while the fundamental value of the co-state must be established. The equivalent coefficient is a vital parameter when using ECMS and must be defined for enhanced performance alongside the co-state because they are all linked to the drive cycle (Zhang et al., 2017). However, anticipated drive cycle is adequately defined using multiple set of rules to ensure optimal operation.

2.6.2.3.3 Model predictive control (MPC)

Based on past and present model of a system, model predictive control strategy makes predictions of the future and anticipated outcomes within a defined set of tested rules using a quadratic cost function and components classification based on other tested models (Showers & Raji, 2022). It improves existing strategy whilst maintaining potential outcomes but requires future parameters. However, MPC in most instances are connected with global positioning system (GPS) to offer real-time optimisation by distributing the area of operation of the driving force system against a group of linear configurations combined with established parameters (Fletcher, 2017; Erensoy, 2018; Zhang et al., 2017).

2.6.2.3.4 Game theory (GT)

Game theory energy management strategy offers a unique and encouraging solution in energy management system by introducing an independent optimisation operation for individual control device (Zhang & Li, 2019). Based on its distinctive characteristic of handling problem associated with interfacing components for multiple powered system, GT has gained wide acceptance in smart grid system applications, hybrid electric vehicle and sustainable energy applications. However, to enhance system performance, defined set of rules are mostly optimised utilising offline optimisation algorithm for a specific drive cycle. These may include, dynamic programming algorithm, particle swarm optimization, direct global optimization, genetic algorithm and simulated annealing optimization. Each of this optimisation algorithm is modelled to handle a specific aspect of the optimisation target without affecting other aspects of the system. Furthermore, when used for energy management in a hybrid electric vehicle or any other hybrid power system, each power source is modelled uniquely as a component and decides on a specific amount of power that will ensure its optimisation. This, however, depends on the drive cycle information which can be forecasted using predictive techniques such as, Markov chain models, neural network, support vector machine and sophisticated sensor tools (Showers & Raji, 2022; Zhang & Li, 2019; Zhang et al., 2017; Erensoy, 2018; Fletcher et al., 2016).

2.6.2.4 Passive control

Passive control strategy uses the linear feedback and feed-forward controllers to synchronise the output current of the fuel cell with the bus voltage. Hence, the current is kept at a level that ensures optimal performance of the fuel cell and other sources of power within the system. It utilises the controllers to control the duty cycle of both DC converters (unidirectional DC/DC and bidirectional DC/DC converters). This type of control technique is broadly classified into, Proportional Integral, Adaptive Proportional Integral and Proportional Integral Derivative. All three control strategies are flexible and can easily be implemented without any having an advantage over the another but depends on the purpose of the EMS (Fletcher, 2017; Ehsani et al., 2018; Erensoy, 2018; Zhang et al., 2017).

2.7 Summary

In this chapter, a comprehensive literature review was presented which considered not only fuel cell/lithium-ion hybrid electric vehicle, but also considered fuel cell/supercapacitor hybrid electric vehicle. However, the focus was FCHEV which includes the fundamentals of electric vehicles such as brief history, description of EVs, corresponding parameters, EV design and types of EV configurations such as hybrid EV (parallel HEV and series HEV). Furthermore, different power supply sources such as electrochemical battery and supercapacitor were

reviewed and adequately presented to understand their suitability in vehicular applications. A brief literature review on the history of fuel cell including its fundamental principles and the different types were also presented to provide an insight on their advantages and disadvantages, availability, and technology maturity.

The primary focus of this study is the development of an energy management system which include EMS requirements, reliability, and fuel cell economy. To understand the functionality and configuration of a suitable EMS, literature review on different EMS techniques such as machine learning strategy, heuristic strategy, optimisation-based control and passive control were presented. Hence, the available literature showed that most studies focused on reducing transient load effect using heuristic strategy with very few studies focusing on reducing it by using computational optimisation methods. The reliability of fuel cell for vehicular application is a critical aspect that requires further research because of the significant impact of EMS on the fuel cell lifespan and its control on the operating level of the fuel cell during operation.

CHAPTER 3: FCHEV COMPONENTS MODELLING

3.1 Introduction

The past decade has experienced a rapid development in electric vehicle design and associated energy management systems due to technology advancement. This chapter presents the drive-cycle reference block, longitudinal driver model and individual components of a fuel cell/lithium-ion battery hybrid electric vehicle. These components include the electric vehicle body (comprising the vehicle parameterised friction tires, mechanical differential block, and a simple gear box) as shown in Figure 3.1, fuel cell stack (PEMFC), power electronic converters (DC/DC unidirectional and bidirectional converters), lithium-ion battery and electric motor. Thereafter, the individual components are integrated and executed in the MATLAB/Simulink environment and Typhoon HIL software for real time simulation.

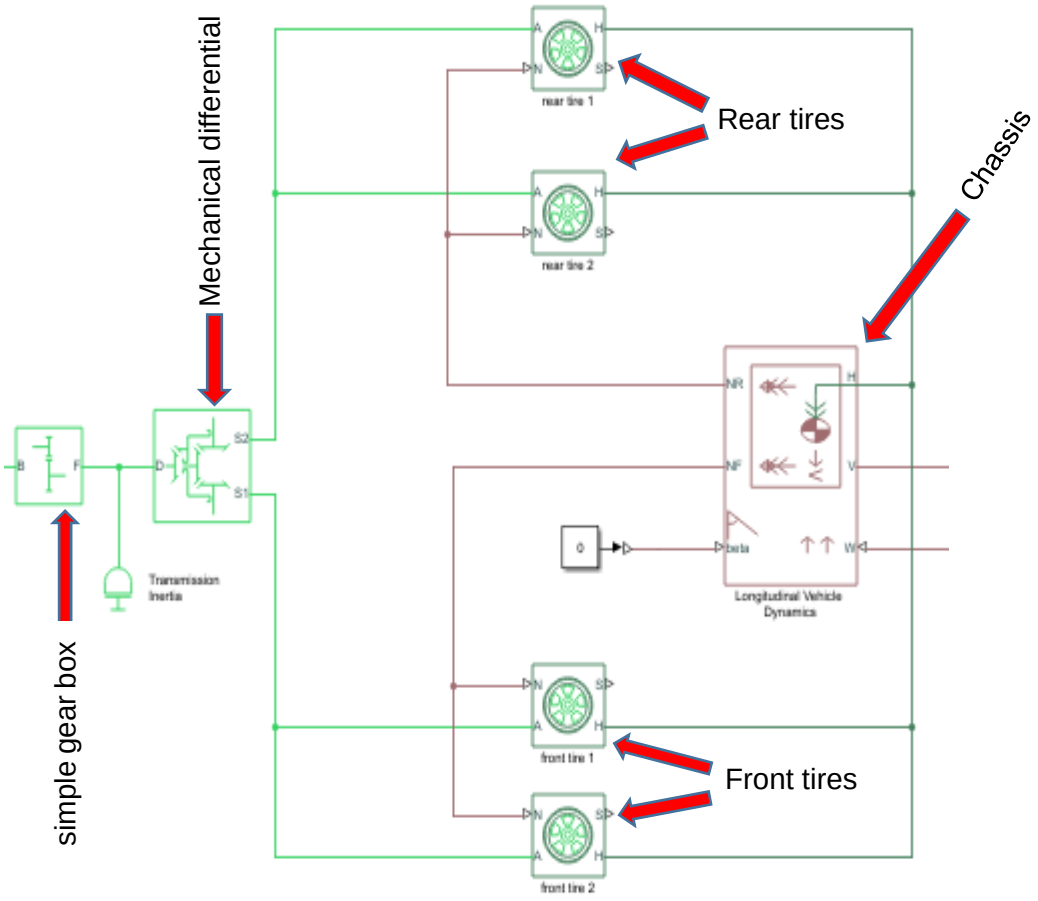

Figure 3.1. Vehicle body in MATLAB/Simulink

3.2 Drive cycle reference block

The drive cycle reference block represents the vehicle velocity over time and provides the duty cycle used for the simulation. There are different pre-defined drive cycles approved by

standard organisations in different countries for vehicle performance testing such as New European Driving Cycle (NEDC) and Extra Urban Driving Cycle (EUDC) used in Europe, Federal Test Procedure-75 (FTP-75) used in the USA, Wide Open Throttle (WOT), and ARTEMIS Driving cycles. However, in this study the FTP-75 was used because of its distance (17787 m), duration (2474 seconds) and average speed (45 km/hr) as shown in Figure 3.2. This block represents the vehicle speed and any associated gradient preestablished by the drive cycle.

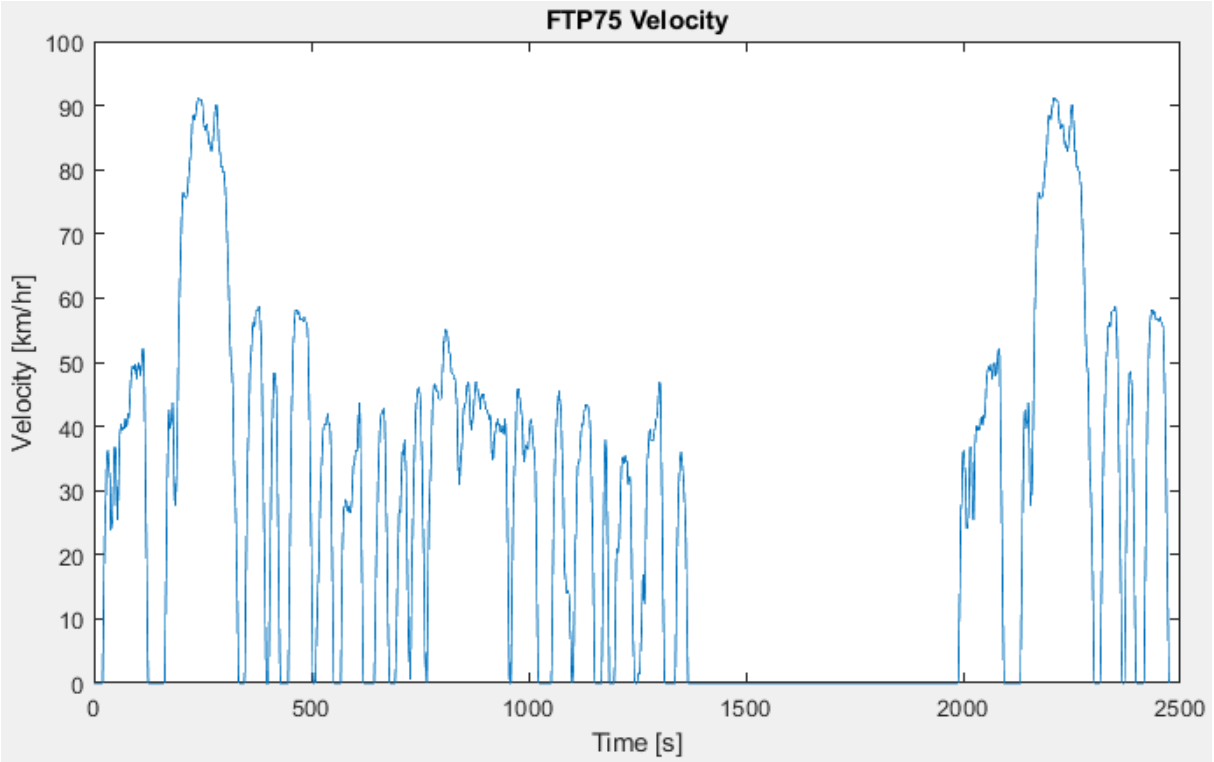

Figure 3.2: Drive cycle source (MATLAB, 2019a)

The drive cycle shows that the velocity was at the lowest range most of the time and acceleration were low. Although, there is a visible large spectrum of acceleration demand that implies a high transient load demand on the power-train as anticipated. The intervals when the velocity is zero are taken as regenerative energy storage to charge the battery and serves as zero load on the power-train.

3.3 Longitudinal driver model

The longitudinal driver model block is used to control the vehicle speed based on the obtained feedback from the actual vehicle and the drive-cycle refence demand as shown in Figure 3.3. It is a speed tracking controller used to generate normalised acceleration and regenerative braking based on the feedback and reference velocities and expressed in km/hr. The communication between the driver and the vehicle is one of the important parameters that ensures accurate drive-ability hence, the driver model is designed to trail the reference speed

tightly and not to implement the actual behaviour of the driver. This model is implemented using a Proportional Integral (PI) controller determined by the error that exist between the reference demand and the feedback from the vehicle model. A positive torque is sent to the vehicle through the electric motor (EM) during acceleration and regenerative braking is implemented during deceleration to ensure that the battery is recharged.

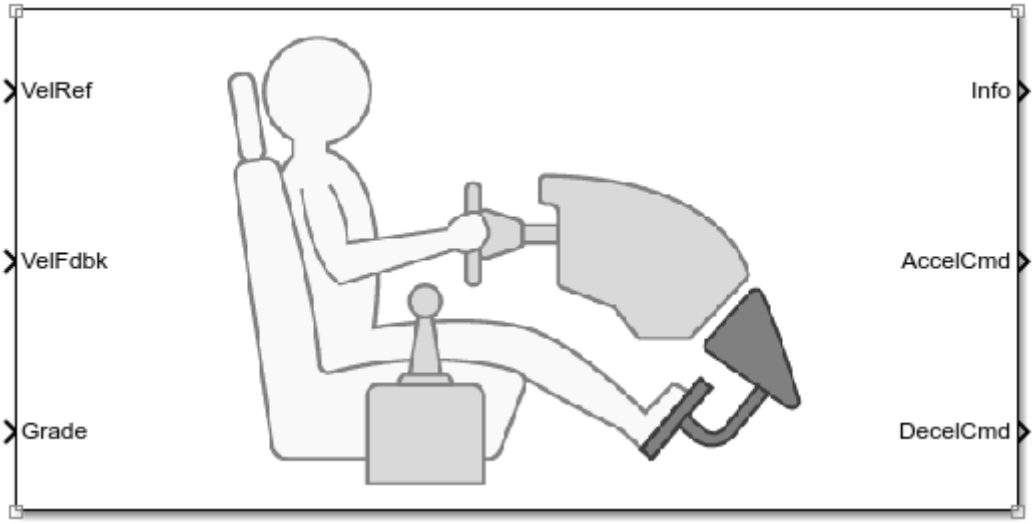

Figure 3.3: Longitudinal driver model

3.4 Electric vehicle body modelling

3.4.1 Studied EV architecture

The physical design of the EV model used in this study is implemented according to applied load experienced when set in motion. The operational characteristics of the vehicle with corresponding parameter coefficients related to the vehicle depends on the drive cycle parameter, road condition, driver behaviour and the vehicle design. To ensure the vehicle is operated optimally with improved vehicle performance, the forces acting on the vehicle when in motion such as motor torque and speed are evaluated accordingly. Although, the torque and speed of the motor are not coupled directly to the linear motion of the vehicle but rather propelled by the electrical motor with the aid of a differential mechanical device coupled to the power sources through the DC/AC inverter (Fletcher, 2017). This is implemented through the gears with a ratio of 1/G and a radius r of the vehicle wheels. The internal and external structure of the vehicle showing how the dynamics of the vehicle body is connected to the electrical motor (EM) is shown in Figure 3.4.

In addition, modelling an EV requires that all the forces (road load and tractive forces) acting on the vehicle must be balanced when the vehicle is in motion. The road load comprises rolling resistance of the tires, gravitational force, aerodynamic drag force and hill-climbing force as shown in Figure 3.5. These forces if wrongly computed and implemented will negatively affect

the performance of the vehicle thereby impairing the optimal performance of different components of the vehicle.

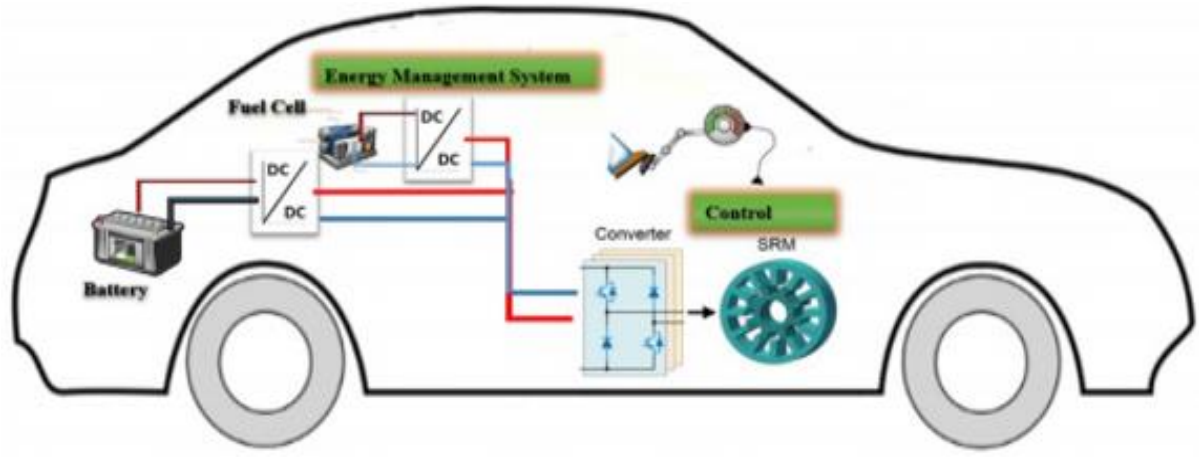

Figure 3.4. Internal structure of the EV (Chaibet et al., 2020)

From Figure 3.3, it is shown that the rate of change with time is equal to the sum of all the forces acting on the vehicle and the momentum is conserved. The momentum is very vital in vehicle modelling and it is defined as (Mkhize, 2019):

$$P = mv \tag{3.1}$$

therefore,

$$\frac{dP}{dt} = m \times \frac{dv}{dt} = F - \mu_{rr} m_g = \frac{1}{2}\rho A C_d v^2 - mgsin\,(\emptyset) \tag{3.2}$$

Re-grouping like terms gives,

$$F = \mu_{rr} mg + \frac{1}{2}\rho A C_d v^2 + mgsin\,(\emptyset) + m\frac{dv}{dt} \tag{3.3}$$

Where g is the gravitational force, m is the mass of the electric vehicle, μ_{rr} is the rolling resistance coefficient, A is the frontal area of the vehicle, ρ is the air density, v is the velocity of the vehicle in motion, $\emptyset$ is the inclined climbing angle, and C_d is the drag coefficient. However, the rolling resistance is generally created by the flattening of the vehicle tire at the point of direct contact with the surface of the road. But the rolling resistance coefficient μ_{rr} is usually determined by the amount of pressure in the tire and the type of tire coupled with its usage. The value of the rolling resistance coefficient is between 0.001 and 0.015 depending on the type of tire and this value can be controlled to ensure optimal performance during motion by ensuring that the tire is adequately inflated with the correct and proper air.

Again, from equation 3.3, the resultant force F will always generate a counteractive torque that acts against the driving force known as the tractive force where the first parameter represents the rolling resistance force, the second parameter represents the aerodynamic drag force, the third parameter represents the hill inclined force and the fourth parameter represents the acceleration force, respectively (Chaibet et al., 2020; Mkhize, 2019).

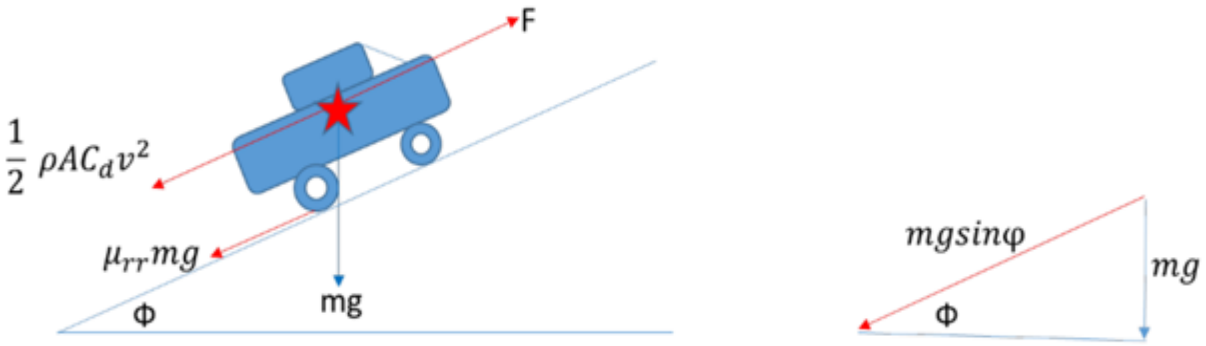

Figure 3.5. Electric vehicle modelling

The parameters of the vehicle body used in this study was systematically selected to reflect the South African road condition, most popular vehicle and driver behaviour as shown in Table 3.1. This includes the vehicle body mass, number of axles, horizontal distance from the axle, drag coefficient, air density, frontal area, etc. for various types of roads such as access and streets roads, local roads, district roads, primary arterials, freeways and expressways.

Table 3.1: Parameters of the Vehicle body used in this study

Parameters	Values
Mass	1000 kg
Number of wheels per axle	2
Horizontal distance from CG to front axle	1.4 m
Horizontal distance from CG to rear axle	1.6 m
CG height above ground	0.5 m
Gravitational acceleration	9.81 m/s^2
Drag coefficient	0.25

Frontal area	2 m^2
Air density	1.18 kg/m^3

3.4.1.1 Front and Rear wheels

When in motion, the four wheels in the vehicles (two in front and two rear) converts the rotational motion into linear motion (Mkhize, 2019). In addition, using the value of the torque of the differential component, the tractive forces can be calculated including the velocity of the vehicle caused by the wheel rotation using equation 3.4 (Okba, 2015).

$$\begin{Bmatrix} F_{left} = \frac{1}{R_{wheel}} T_{diff_{left}} \\ F_{right} = \frac{1}{R_{wheel}} T_{diff_{right}} \\ W_{left} = \frac{1}{R_{wheel}} V_{veh_{left}} \\ W_{right} = \frac{1}{R_{wheel}} V_{veh_{right}} \end{Bmatrix} \quad (3.4)$$

Using the radius of curvature ($Radius_{courv}$) and the corresponding distance between the rear wheels also known as the vehicle width (l_{veh}), one can differentiate the linear velocities of the left and right wheels accordingly.

$$\begin{Bmatrix} F_t = F_{left} + F_{right} \\ v_{veh_{left}} = \frac{R_{courv} + \frac{l_{veh}}{2}}{R_{courv}} v_{veh} \\ v_{veh_{right}} = \frac{R_{courv} - \frac{l_{veh}}{2}}{R_{courv}} v_{veh} \end{Bmatrix} \quad (3.5)$$

3.4.1.2 Mechanical differential

The torque reduction is adequately distributed on the right, left, front and rear wheels as well as the rotational speed as presented in equation 3.6 (Okba, 2015).

$$\begin{Bmatrix} T_{diff_{left}} = \frac{1}{2} T_{gear} \\ T_{diff_{right}} = \frac{1}{2} T_{gear} \\ W_{diff} = \frac{1}{2} (W_{left} + W_{right}) \end{Bmatrix} \quad (3.6)$$

Where, $T_{diff_{left}}, T_{diff_{right}}, \ and \ W_{diff}$ represents the differential rotation speed and torques of the right and left wheels immediately after the differentials, respectively.

3.4.1.3 Chassis

Chassis is the vehicle frame, the part on which the vehicle body is mounted and supports the vehicle gears, wheels, transmission and driver's seat in most instances. It represents a two-axle vehicle body set in longitudinal motion and accounts for the total body mass, road incline, aerodynamic drag and total weight distribution between the axles caused by acceleration and drive cycle as clearly shown in Figure 3.6. However, the velocity of the vehicle V_{veh} can be achieved using Newton dynamic expression based on the total tractive force of the vehicle F_t together with the resistance force F_{tr} as expressed in equation 3.7.

$$M\frac{dV_{veh}}{dt} = F_t - F_{tr} \tag{3.7}$$

Where M is the vehicle mass, and the velocity is selected as a state variable because the chassis is an accumulation element.

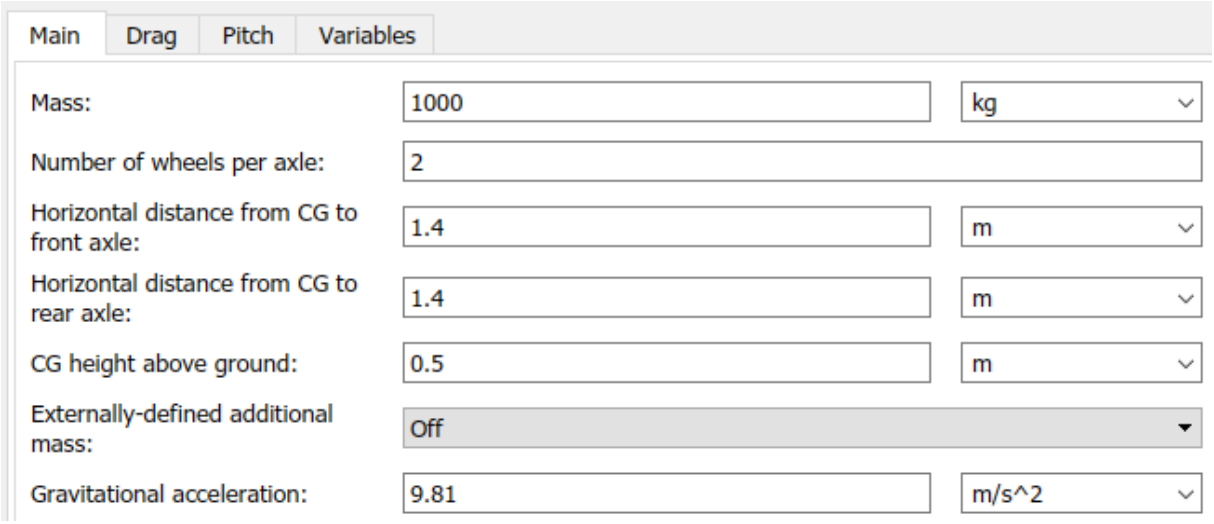

Figure 3.6. Longitudinal vehicle dynamics

3.5 Power-train components modelling

3.5.1 Fuel cell system

Fuel cell can be implemented using different models and techniques with specific concentration on any part such as experimental, thermal, chemical and electrical. The primary objective and intended application of the fuel cell determines the particular model that is most suitable. Fundamentally, experimental modelling depends on experiments to establish practical models of representing fuel cell, thermal models depend on the thermal equilibrium in both steady-state and dynamic operating states of the fuel cell, chemical models include the heat transfer, diffusion of species and mass transport while electrical models are represented in dynamic or steady-state models (Choudhury, 1989). However, each of the aforementioned

models have shown unique weakness depending on the intended application. Experimental models do not incorporate the impacts of pressure created by the gases at the input, temperature, flow rate and the thermodynamic of the fuel cells. Chemical models are very complex for electrical applications because of the unnecessary parameters needed for effective modelling of the fuel cell while the thermal model has a major setback with the heat application required. Hence, the electrical model was chosen in this study because the fuel cell characteristics is represented using electrical components without the inclusion of thermodynamic and chemical parameters (Luta, 2019).

Temperature is one of the most important factors considered when selecting a suitable fuel cell for any application because it has the ability to alter its performance. In this study, Proton-Exchange Membrane Fuel Cell (PEMFC) was the most appropriate fuel cell because it's operational temperature is between 20-100℃ with relatively high efficiency of up to 58% under low operating pressures of between 1-3 bar. The low temperature PEMFC allows quick start-up, which is critical for vehicular application hence, the model used in this study does not consider the dynamics of the reactant flow of the fuel cell. PEMFC has a high-power generation capacity and operational characteristics making it the best option for vehicular application compared to other fuel cells such as Solid Oxide fuel cell (SOFC), Molten Carbonate fuel cell (MCFC), Phosphoric Acid fuel cell (PAFC), and Alkaline fuel cell (ALFC) (Hosseinzadeh, 2012).

3.5.1.1 Fuel cell model

The study made the following assumptions regarding the PEMFC, the PEMFC was supplied with clean hydrogen and oxygen gases at steady state, the temperature was uniformly distributed across the stack under controlled condition, the system was operated according to Nernst equation, the gases were treated as ideal based on ideal gas law, the by-product at the exit is liquid water and at the outlet is shocked orifice. In addition, the internal resistance of the stack was considered constant and the mass connected voltage drops were considered to be reaction kinetics dependent. The humidification of the membrane was considered to be controlled under any load condition. The hydrogen storage tank was not modelled because of the associated dynamic considerations such as piping and weight and the assumption that the air and fuel supply was available when needed at appropriate condition. Again, the fuel cell stack was modelled using the generic MATLAB/Simulink PEMFC model based on first principle. Where, the equivalent circuit of the model showing physical characteristics of the system such as flow rates, pressure and temperature that determines the open circuit voltage (E_0), Tafel slope (A), exchange current (i_0), voltage (V_{fc}) and current (i_{fc}) of the fuel cell including delay function for the error calculations were considered ideal as shown in Figure 3.7 (Hosseinzadeh, 2012).

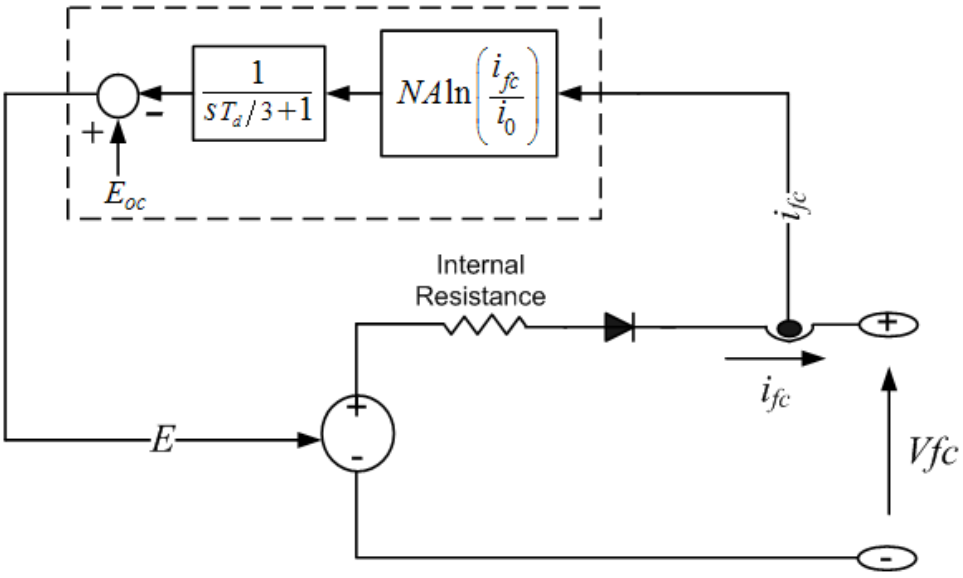

Figure 3.7. Equivalent circuit model of the PEMFC

The voltage is represented using the Nernst equation and the mathematical framework of the model as (Luta, 2019):

$$E_n = 1.229 + (T - 298)\frac{-44.43}{zF} + \frac{RTln(P_{H_2}P_{O_2}^{0.5})}{zF} \qquad \text{when T} \leq 100℃ \tag{3.8}$$

Where, T represent the temperature, R is the ideal gas constant, *F* is the Faraday constant, P_{H_2} and P_{O_2} represent the hydrogen and oxygen partial pressures respectively.

The partial pressures are further represented as a function of the reactant utilisation using equations 3.9 and 3.10 respectively (Erensoy, 2018):

$$P_{H_2} = \left(1 - U_{fH_2}\right)x\%P_{fuel} \tag{3.9}$$

$$P_{O_2} = \left(1 - U_{fO_2}\right)y\%P_{air} \tag{3.10}$$

Where U_{fH_2} and U_{fO_2} are used to represent the hydrogen and oxygen utilisation respectively, P_{fuel} and P_{air} represent the hydrogen and oxygen pressures while x and y represent the percentage of hydrogen and oxygen content.

Furthermore, the rates of reactant utilisation are represented in equation 3.11 and 3.12 respectively:

$$U_{f_{H2}} = \frac{60000RTi_{fc}}{2FP_{hydr}V_{hydr}x\%} \tag{3.11}$$

$$U_{f0_2} = \frac{60000RTi_{fc}}{4FP_{oxyg}V_{oxyg}y\%} \tag{3.12}$$

Where, V_{hydr} and V_{oxyg} represent the hydrogen and oxygen flow rates respectively while i_{fc} represent the cell current.

The open-circuit voltage (E_{OC}) is given by equation 3.13 as follows:

$$E_{OC} = K_c E_n \tag{3.13}$$

where K_c is the voltage constant that depends on the exchange current and Tafel slope.

Again, the Tafel slope is given as follows:

$$A = \frac{RT}{zF\alpha} \tag{3.14}$$

The exchange current is given as:

$$i_0 = \frac{zFke^{-\Delta G/RT}\left(P_{H_2} + P_{0_2}\right)}{Rh} \tag{3.15}$$

However, considering operational losses which comprises of diffusion losses and activation losses, the open-circuit voltage is represented as:

$$V = E_0 - V_{act} - V_r \tag{3.16}$$

where V_r and V_{act} are given by equations 3.17 and 3.18 as follows (Souleman et al., 2009):

$$V_r = r_{ohms}i_{fc} \tag{3.17}$$

$$V_{act} = \frac{RT}{2\alpha F} ln\left(\frac{i_{fc}}{\frac{2FK(P_{H2} + P_{O2})}{Rh} exp\left(\frac{\Delta G}{RT}\right)}\right) \frac{1}{s\frac{T_d}{3} + 1} \tag{3.18}$$

Where, α is the charge transfer coefficient, K is the Boltzmann constant, h is the plank constant, ΔG is the activation energy barrier, T_d is the cell settling time based on current step and r_{ohms} is the cell resistance.

Therefore, the fuel cell (PEMFC) voltage is given as follows:

$$V_{fc} = N.V \tag{3.19}$$

where N is the total number of cells in the fuel cell stack

3.5.1.2 Polarisation curve of the PEMFC

The fuel cell (PEMFC) was selected from the MATLAB/Simulink library and modelled using the parameters shown in Table 3.2 according to equations 3.8 to 3.19. The corresponding voltage against current and power against current are shown in Figures 3.8 (a) and (b) respectively and the fuel cell stack nominal and signal variation parameters are shown in Table 3.3 and Table 3.4 respectively. However, at the nominal operating point, the PEMFC power is 100 kW, voltage is 350 V and the current is 285.7 A respectively.

Table 3.2: Fuel cell stack parameters

Detailed parameters of the fuel cell stack	
Voltage at 0A and 1A [V_0 (V), V_1 (V)]	[150, 200]
Nominal operating point [Inom (A), Vnom (V)]	[285.7, 350]
Maximum operating point [Iend (A), Vend (V)]	[345, 288]
Number of cells	65
Nominal stack efficiency (%)	50
Operating temperature (Celsius)	45
Nominal Air flow rate (lpm)	3000
Nominal supply pressure [Fuel (bar), Air (bar)]	[1.5, 1]
Nominal composition (%) [H2 02 H2O (air)]	[99.95, 21, 1]

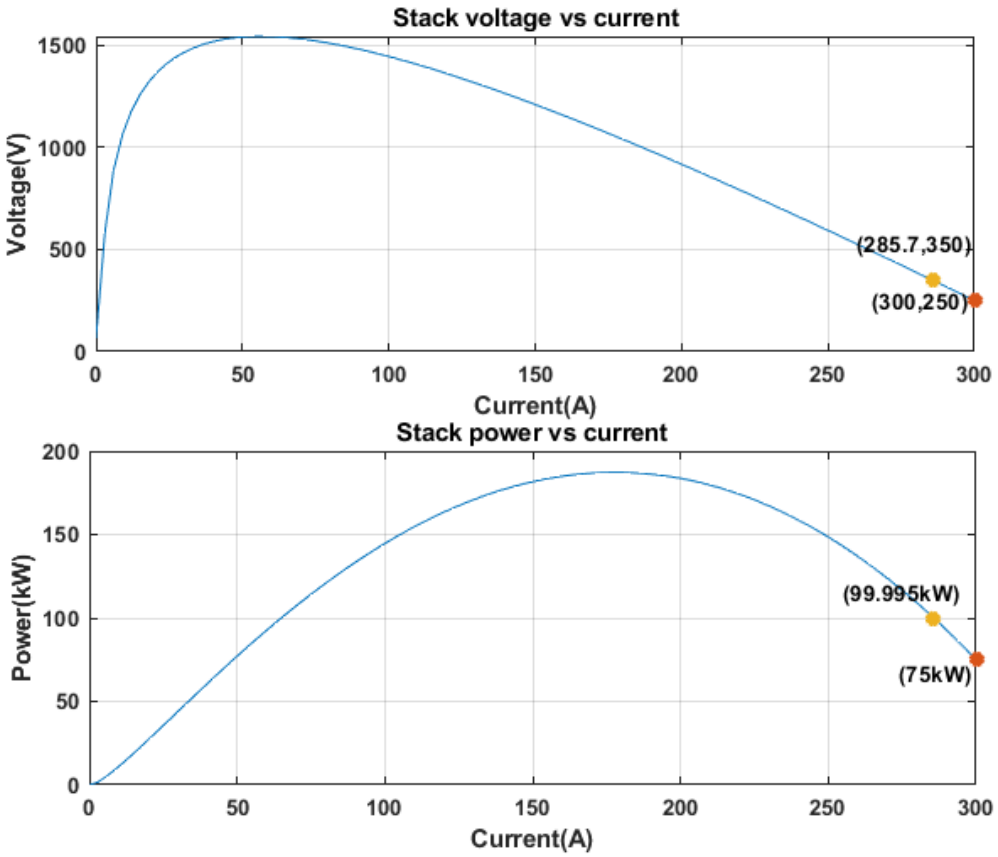

Figure 3.8: Characteristics of the PEMFC

Although the fuel cell was modelled successfully under the aforementioned assumptions, this model does not consider the overall performance of the fuel cell in a long-term. Fuel cell degradation is a major factor that requires the necessary attention considering the significant challenges associated with its operational performance when operated for a long period. But this study focuses on the performance delivery of the fuel cell only at the design stage and operational level without including the operational costs.

Table 3.3: Fuel Cell simulation parameters

Fuel cell stack nominal parameters	
Stack nominal power	100 kW
Stack maximum power	100.02 kW
Fuel cell resistance	0.00334 ohms
Nernst voltage of the cell [En]	1.1736 V
Hydrogen utilization (%)	8.056
Oxidant utilization (%)	9.199
Nominal fuel consumption	99.55 slpm
Nominal air consumption	236.9 slpm
Exchange current [i_o]	0.279055 A
Exchange coefficient [alpha]	0.001636

Table 3.4: Fuel Cell signal variation parameters

Fuel Cell signal variation parameters	
Fuel composition	99.95 %
Oxidant composition	21 %
System temperature (T)	318 K
Fuel supply pressure	1.5 bar
Air supply pressure	1 bar

3.5.1.3 Fuel delivery system

The power management system provides adequate fuel cell current required for optimal performance. According to the model assumptions highlighted earlier, the fuel cell is connected to a DC/DC converter to boost the operational voltage equal to DC bus voltage. To achieve the desired energy management output regarding the amount of current produced, the fuel flow to the fuel cell stack is controlled within the decision constraints. This will ensure that adequate amount of current is supplied to the power electronic converter. Hence, the fuel supply was modelled using equation 3.20 based on the operational assumption that the utilization ratio of the hydrogen is constant, which showed 959.6 slpm at 100 kW production as shown in Table 3.3. This value is equivalent to 3 bar fuel delivery for 0.99 utilization ratio (Xu et al., 2015).

$$V_{lpmf} = \frac{60000RTN_c i_{fc}}{2Fx\%P_{fuel}U_{f_{H_2}}} \tag{3.20}$$

PEMFC has a response time of one second, but it is not practical to assume that the fuel supply system has the capacity to swiftly regulate itself hence, the need for fuel cell stack inclusion. Connecting the fuel cell with a corresponding battery size provides the necessary advantage of utilizing the swift dynamic response time of the battery pack which is in the order of milliseconds. This will compensate the fuel supply system and fuel cell reaction time by providing adequate supply to warm up the fuel cell which is in seconds for PEMFC. Hence, modelling the fuel supply system is necessary because it will decrease the response time and enhance fuel cell performance.

3.5.2 Power electronic converters

The primary purpose of power electronic converters in a circuit is to regulate and control the power flow from available power sources to the load at a suitable voltage and current. During the conversation process, the system usually experiences power losses but selecting adequate components will reduce the losses to an acceptable level. These converters are generally classified according to the type of power conversion such as DC-to-DC, DC-to-AC, AC-to-AC or AC-to-DC. To ensure improved conversion efficiency, the power losses during the conversion must be minimised. However, the choice of converter topology depends on the user's skills, knowledge and simulation objectives because their complexities differ significantly. Hence, this section presents modelling of the DC-to-DC boost converter, DC-to-DC bidirectional converter and DC-to-AC converter together with the closed loop control systems used for each. The boost converter is used to step-up the fuel cell stack voltage from 350 V_{DC} to 400 V_{DC} and the battery from 144 V_{DC} to 400 V_{DC} respectively. In addition, the DC-bus voltage of 400 V_{DC} is reduced to 144 V_{DC} suitable to charge the battery during vehicle

regenerative braking and idle moments. The design of these power converters consists of inductors, capacitors, diodes and switches in different configurations aimed at achieving the set objectives. These switches can be fully-controlled (such as IGBTs, BJTs, GTOs, MOSFETs, etc), partially-controlled (thyristor) or uncontrolled (diodes) but controlled switches are powered by circuits using control signals while the uncontrolled switched are line commutated.

3.5.2.1 Unidirectional (Boost) Converter (UDC)

A simple DC-DC boost converter with semiconductor devices (MOSFET and diode) assumed to be ideal is shown in Figure 3.9. Where, the operating modes of the boost converter are determined by the value of the inductor current. The boost converter is considered to be operating in the continuous conduction mode (CCM) when the inductor current has a value greater than zero else it would be in the discontinuous conduction mode (DCM). Again, when the converter is at steady state, its operation is such that when the MOSFET is "ON", the input voltage will charge the inductor L and the capacitor will supply the load R. But, when the MOSFET is in the "OFF" state, the inductor will discharge the stored energy to the load R through the ideal diode.

To express the relationship between the DC voltage V_C (V_{out}) and the input voltage V_{in}, the DC voltage V_C is assumed to be greater than the capacitor voltage ripple and expressed as (Showers, 2019):

$$V_{out} = \frac{V_{in}}{1 - D} \tag{3.21}$$

Where, the duty cycle D is defined as:

$$D = 1 - \frac{V_{in}}{V_{out}} \tag{3.22}$$

and T_{on} and T_s are used to indicate the portion when Q is on the "ON" position and the switching period respectively.

Again, when operating at steady state, the value of the inductance L is defined using equation 3.23 as (Showers, 2019):

$$L_c = \frac{V_{in} * D}{\Delta_{IL} * f_s} \tag{3.23}$$

Where, f_s, is the switching frequency and defined as:

$$f_s = \frac{1}{T_s} \tag{3.24}$$

To ensure that it is operated in the continuous conduction mode, the value of the inductor is selected to be ten times greater than the calculated value in equation 3.23.

The capacitor in the converter is used to reduce the peak-to-peak ripple that is often present in the output voltage. This value can be defined using equation 3.25 as (Showers, 2019):

$$C_{min} = \frac{I_{out} * D}{f_s * \Delta V_c} \tag{3.25}$$

In this study, the bus voltage of the power-train is designed for 400 V with an allowance of 20% variation due to the vast battery range coupled with the electric motor (EM) controllers designed to regulate the pulse width modulation of the EM. The output voltage of the fuel cell stack is boosted to 400 V because it provides for 350 V as the nominal voltage. This ensures that the fuel cell stack is adequately protected against current and voltage ripples caused by transient loads and in addition boost the voltage to correspond to the bus voltage of the power-train. Again, the voltage can either be regulated using switch mode power supplies (SMPS) or linear regulators based on the design objective. SMPS utilises a switching regulator such as IGBT, MOSFET that has power transistor in implementing the switching mode at high frequency between “ON” and “OFF” position. It has the capacity to step-up or step-down the voltage according to the adopted topology and the linear regulator regulates the output voltage by dissipating extra power in the ohmic losses making it useful for voltage drop control. Most modern applications use SMPS because it has a higher efficiency than linear regulators which can be attributed to reduced power dissipation, less weight and smaller size. Hence, SMPS is most suitable and appropriate for experimental studies.

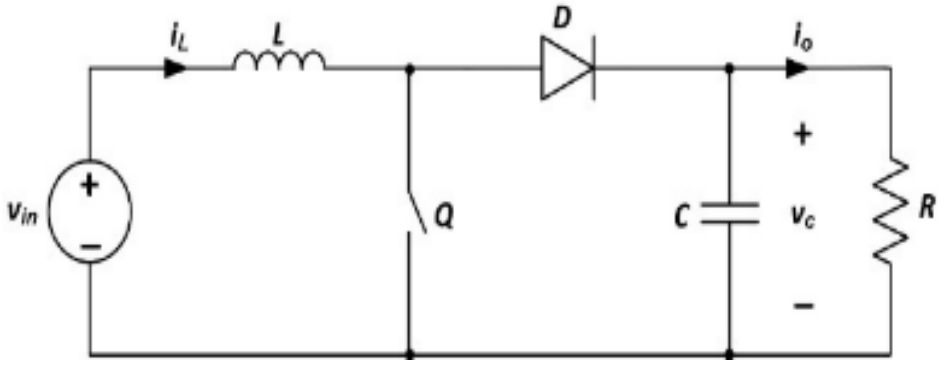

Figure 3.9: A typical boost converter

Efficiency, performance objectives and cost are critical factors when designing any converter for any specific hybrid power-train. In this study, the boost converter was selected because of

the choose of the DC-bus voltage and fuel cell stack voltage respectively. The DC-to-DC boost converter with fuel cell stack connected across it as modelled in the MATLAB/Simulink environment according to the power-train set conditions and operational requirements is shown in Figure 3.10 and the boost converter parameter values are shown in Table 3.5.

The control scheme of a voltage source three-phase inverter is shown in Figure 3.11. It comprises of a voltage and current regulators that provides high-quality power factor. In addition, the voltage regulator ensures that the changes in the DC voltage is controlled by the PI controller and produces a current that corresponds to the DC reference voltage.

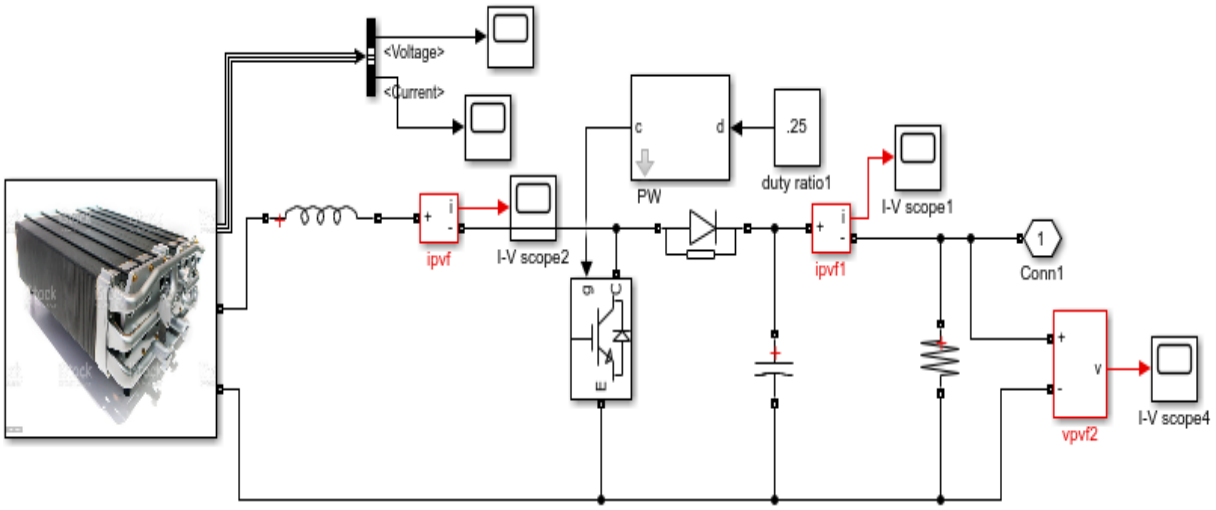

Figure 3.10: Fuel cell stack connected across the boost converter

Table 3.5: Fuel cell DC-DC boost converter parameters

Input voltage	350 V
Output voltage	400 V
Input Power	100 kW
Duty cycle	12.5 %
Switching frequency	40 kHz
Critical Inductance	13 µH
Critical Capacitance	19.5 µF
Output Resistance	3.2 Ω

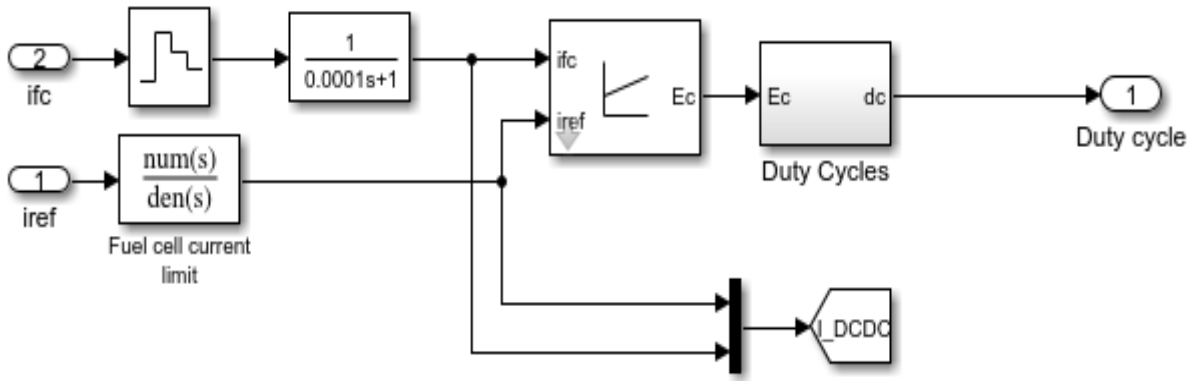

Figure 3.11: Current source inverter control.

3.5.2.2 Bidirectional converter (BDC)

The DC/DC bidirectional converter is used to boost the lithium-ion battery voltage when discharging and buck operation when charging. Presently, there are several types of bidirectional converters topologies, but the commonly used ones are the fundamental non-isolated topologies. These are generally categorised into fundamental topologies such as Half-bridge converter, SEPIC converter, Cúk converter and derived topologies such as interleaved half-bridge converter and cascaded half-bridge converter as shown in Figure 3.12 and Figure 3.13 respectively (Greeshma & Nayana, 2016; Du et al., 2010).

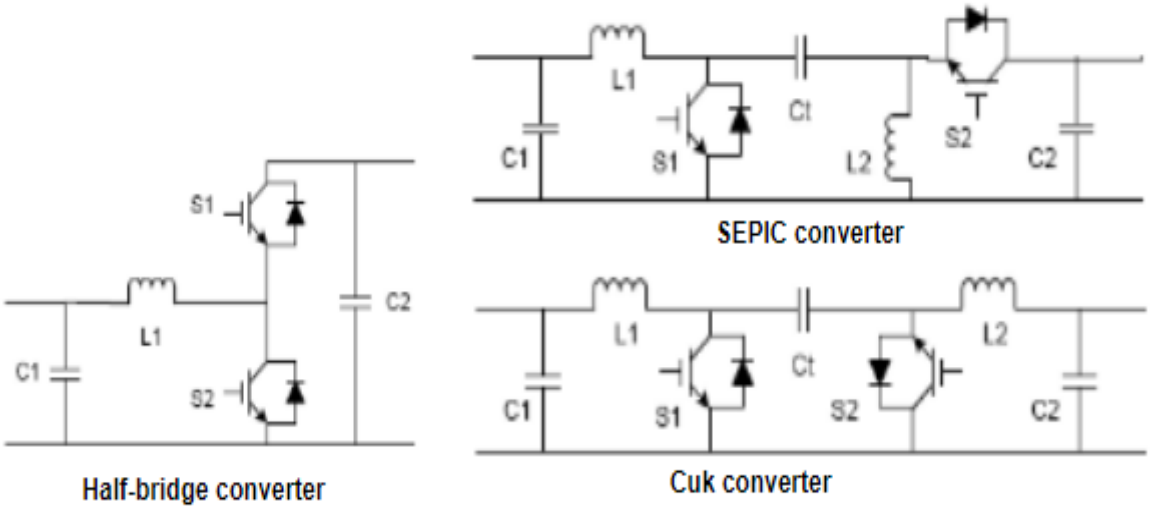

Figure 3.12: Basic non-isolated converter topologies

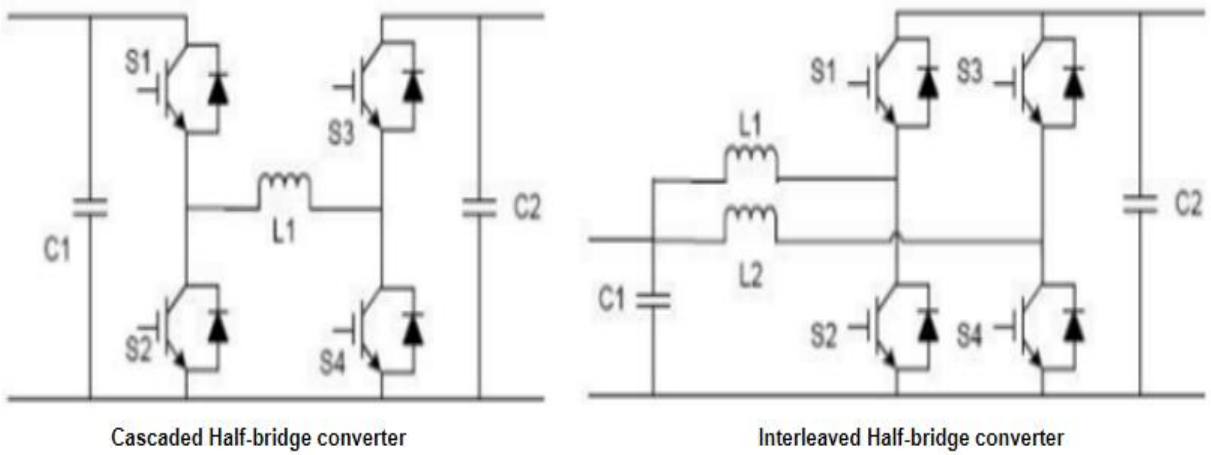

Figure 3.13: Derived non-isolated Converter topologies

The interleaved and cascaded half-bridge bidirectional converters are obtained from basic half-bridge converter and their characteristics is evaluated based on the characteristics of the basic half-bridge converter. But the half-bridge bidirectional converter is mostly used in vehicular applications because of its simple design, operational effectiveness and easy application. Therefore, when using the half-bridge converter, the capacity of the output capacitor and the discontinuous output current is generally affected during the boost mode, but it functions better because it uses only two switches for its operation (Du et al., 2010). Again, the derived interleaved half-bridge converter has reduced stresses and improved efficiency, but the half-bridge converter was carefully chosen in this study because of its light weight, low cost, and easy design.

The Li-ion battery is connected on the low voltage side at 144 V_{DC} and the high voltage side is connected to the 400 V_{DC} bus as shown in Figure 3.14 and the DC/DC bidirectional converter parameters are shown in Table 3.6. Hence, the output voltage of the fuel cell boost converter and DC bus voltage are stepped down to 144 V_{DC} while the battery voltage is boosted to 400 V_{DC} to ensure effective voltage regulation. This topology has the capacity to function in both the boost and buck modes based on the prevailing load demand, fuel cell output power and battery state of charge (SOC). Therefore, the effective control of the bidirectional converter duty cycle will ensure voltage stability during both modes and the charge and discharge protection of the Li-ion battery.

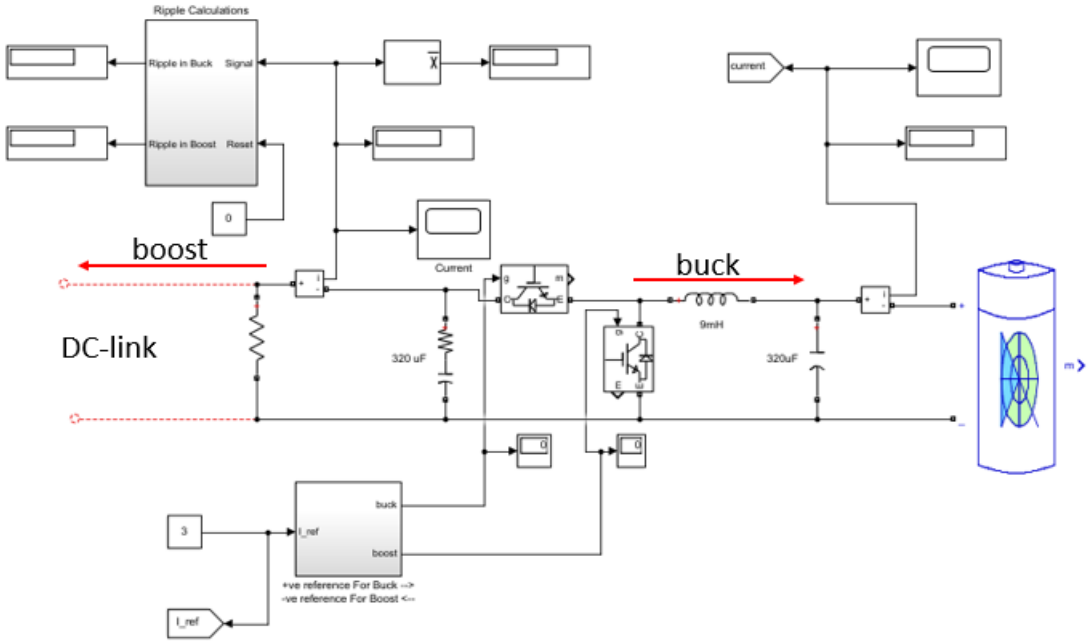

Figure 3.14: Bidirectional converter used in this study

The value of the inductor value of the bidirectional converter is obtained using equation 3.25 as (Showers, 2019):

$$L_{min} = \frac{D(1-D)^2 VH^2}{2Pcf} \tag{3.25}$$

Where:

L_{min} = minimum Inductor value

D = Duty cycle

V_H = high voltage (DC Bus voltage)

Pc = critical load power

f = switching frequency

The capacitor value of the bidirectional converter can be calculated using equation 3.26 as:

$$C_H = C_L = \frac{D}{R_{Hf}(\Delta V_H / V_H)} \tag{3.26}$$

Where:

C_H = capacitor on the high voltage side (DC bus)

C_L = capacitor on the low voltage side (battery side)

D = Duty cycle

$R_H = \frac{L_{min} 2f}{D(1-D)^2}$

f = switching frequency

V_H = voltage on the high side (DC bus voltage)

$\Delta V_H = \frac{V_H D}{R_H C_H f}$

Table 3.6: DC/DC bidirectional converter parameters

Battery voltage	144 V
DC bus voltage	400 V
Input Power	30 kW
Duty cycle	64 %
Switching frequency	100 kHz
Inductance (L_{min})	5.9 µH
$\mathrm{R_H}$	7.96 Ω
$\Delta \mathrm{V_H}$	1.0295
Capacitance	320 µF

The controller is modelled to ensure that the DC/DC bidirectional converter generates both buck and boost signals based on the power dynamics in the system (fuel cell output power and battery SoC) and the vehicle speed as shown in Figure 3.15. The controller is an intelligent system that provides power to the electric vehicle through the electric motor based on the battery SoC and corresponding pulses are transmitted to one of the semiconductor switches. However, the final decision to either buck or boost is determined on the load demand from the electric vehicle. But, in instances where the control does not receive adequate signal from the electric vehicle to make an informed decision, the battery SoC is used as the determining factor

to either operate in the buck or boost mode. Furthermore, if the fuel cell power is equal to the load demand from the electric vehicle, then the battery will be disconnected momentarily.

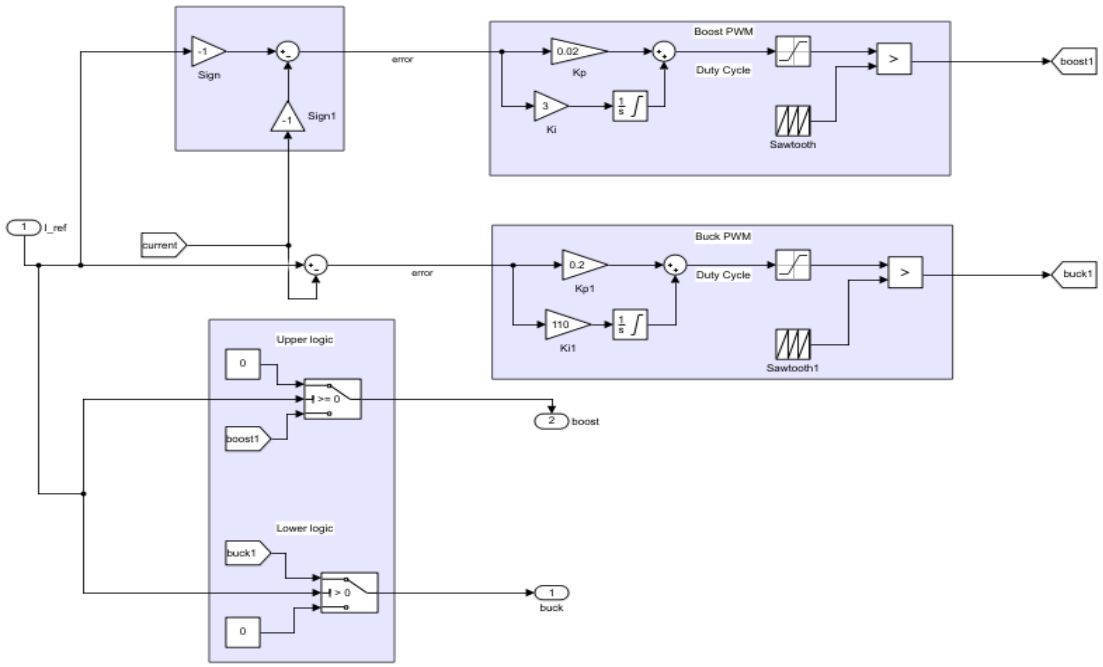

Figure 3.15: Bidirectional converter controller

3.5.3.3 DC-AC Inverter

In this study, a three-phase inverter as shown in Figure 3.16 was used to converts the DC power from both the fuel cell and the lithium-ion battery through the unidirectional and bidirectional converters to a corresponding AC power able of driving the electric motor (EM) at an acceptable power factor of 0.8.

The inverter regulates the voltage at the DC link by ensuring that an adequate reference AC current at the output and the magnitude are obtained and aligned to the electric motor standard. This was achieved by using a simple PI loop that generates the current magnitude and compares it to the reference value of the DC link voltage while the phase locked loop was used to provide details of the voltage phase angle. Again, for a negative error, the PI controller generates a negative reference current and for a positive error, it generates a positive reference current and controls the DC bus voltage. An increase in the DC bus voltage is an indication that an additional energy has been added to the DC bus. This extra energy is then sent to the EM to provide additional power to the electric vehicle demand or used to charge the lithium-ion battery if the SOC is less than 80%.

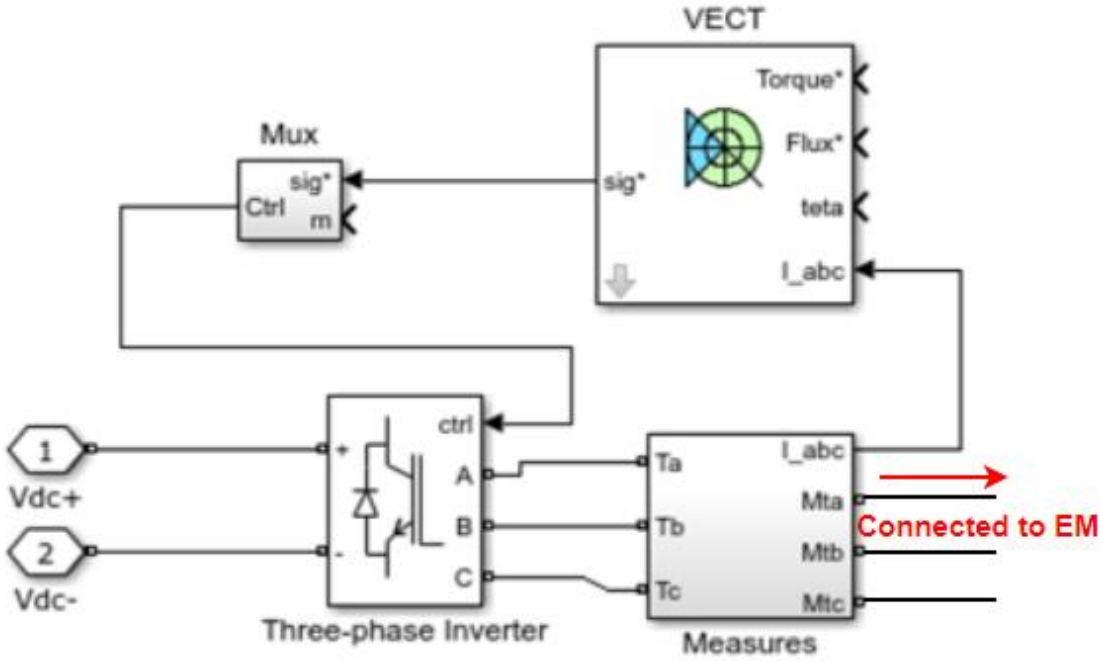

Figure 3.16: Three-phase inverter

To control the PWM input to the inverter, a controlled PWM voltage source scheme is added as shown in Figure 3.17. The controlled PWM voltage scheme represents a PWM voltage source supplied by the longitudinal driver. The PI generates a positive reference current while using the three-phase inverter and ensures acceleration, braking and reverse operations. Furthermore, obtaining a positive error proves that the reference value is higher than the current hence, the controller moves the clock pulses to a higher value and switches OFF the inverter to prevent short circuit and power shortage.

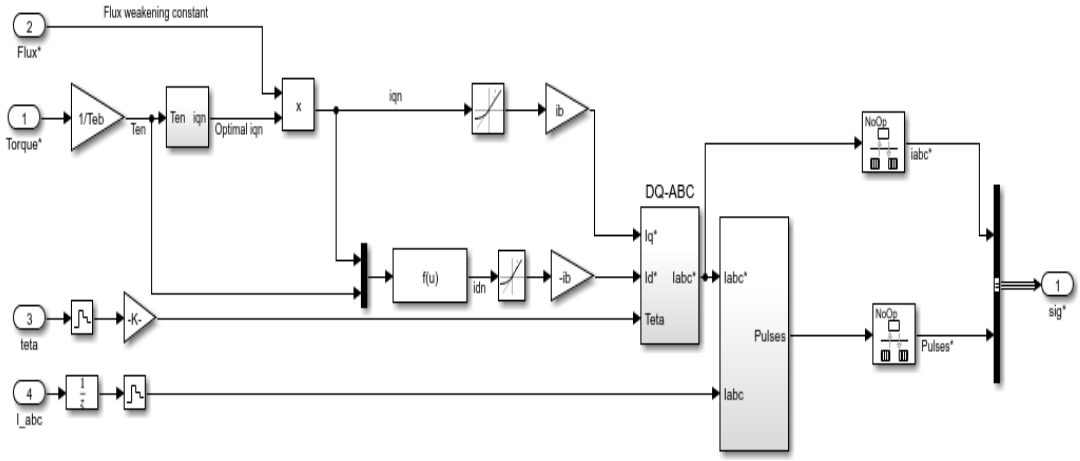

Figure 3.17: Controlled PWM voltage source for the three-phase inverter

3.5.3. Lithium-ion battery

In this study, lithium-ion (Li-ion) battery was selected because of its high energy density, low self-discharge rate, long cycle life and increased temperature range (Gao, Jin, Zhang, et al., 2016). These characteristics makes it more suitable for vehicular applications when compared to other conventional lead acid batteries. A high energy lithium-ion battery is used for energy storage and carefully modelled as a voltage source connected in series with a resistance as shown in Figure 3.18.

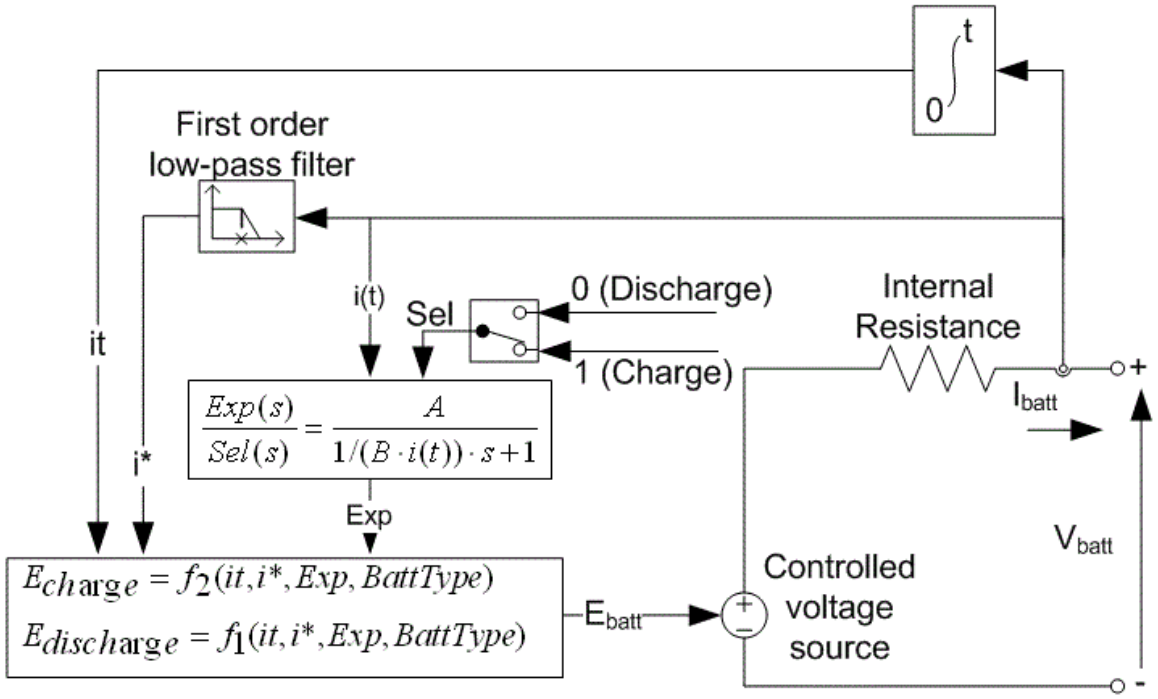

Figure 3.18: Lithium-ion battery equivalent circuit

The battery output voltage (V_{bat}) is obtained using equation 3.27 as follows (Alloui et al., 2013; Grammatico et al., 2010):

$$V_{Bat} = E_{Bat} - r_{Bat} i_{Batt} \tag{3.27}$$

Where:

E_{Bat} = no load voltage (V)

r_{Bat} = internal resistance (Ω)

i_{Batt} = battery current (Ω)

The internal resistance value of the battery changes during charging and discharging or based on the battery current but it is always assumed to be constant to avoid complex calculations (George, 2018).

Again, the open circuit voltage of the battery depends on the state of charge (SoC), battery current and hysteresis losses of the battery while ignoring the effects of temperature. Therefore, the characteristics model of this battery includes two fundamental components: a charge mode model and discharge mode model which are used to determine the operating modes (Showers, 2019).

The voltage in the discharge mode ($i^* > 0$) is given as:

$$f_1(it, i*) = E_o - K.\frac{Q}{Q - it}.i* - K.\frac{Q}{Q - it}.it + A.\exp(-B.it) \quad (3.28)$$

The voltage during charge mode ($i^* < 0$) is given as:

$$f_2(it, i*) = E_o - K.\frac{Q}{it + 0.1.Q}.i* - K.\frac{Q}{Q - it}.it + A.\exp(-B.it) \quad (3.29)$$

Where:

E_o = constant voltage (V)

K = polarization constant (V/A h)

Q = maximum battery capacity (Ah)

i^* = low frequency current dynamics (A)

B = exponential capacity (Ah^{-1})

A = exponential voltage (V)

it = extracted capacity (Ah)

i = battery current (A)

exp = exponential zone dynamics (V).

The battery state of charge (SoC) is represented using equation 3.30 as:

$$Q(t) = Q(0) - \int_0^1 i_{Batt} dt \quad (3.30)$$

Again, the rate of charging and discharging of the battery is described using the C rate and it is defined as:

$$C_{rate} = \frac{i_{Batt}}{Q/h} \tag{3.31}$$

The battery discharge curve operated under normal conditions in the MATLAB/Simulink environment expressed as a function of time (hours) is shown in Figure 3.19. The battery experiences a rapid voltage drop in the charge saturation limits while the middle area shown in grey colour represents the area where the battery is operating optimally till its nominal voltage. The complete discharge of the battery happens in this area due to the exponential voltage drop that occurs after the nominal discharge voltage. Again, larger loads associated with higher currents drawn, reduces the battery state-of-charge accordingly as shown in Figure 3.20. However, the battery can be adjusted to a voltage suitable for any chosen operation in the MATLAB/Simulink environment where, the battery state-of-charge (SOC) indicates the original state of charge of the battery at the initial stage expressed in percentage.

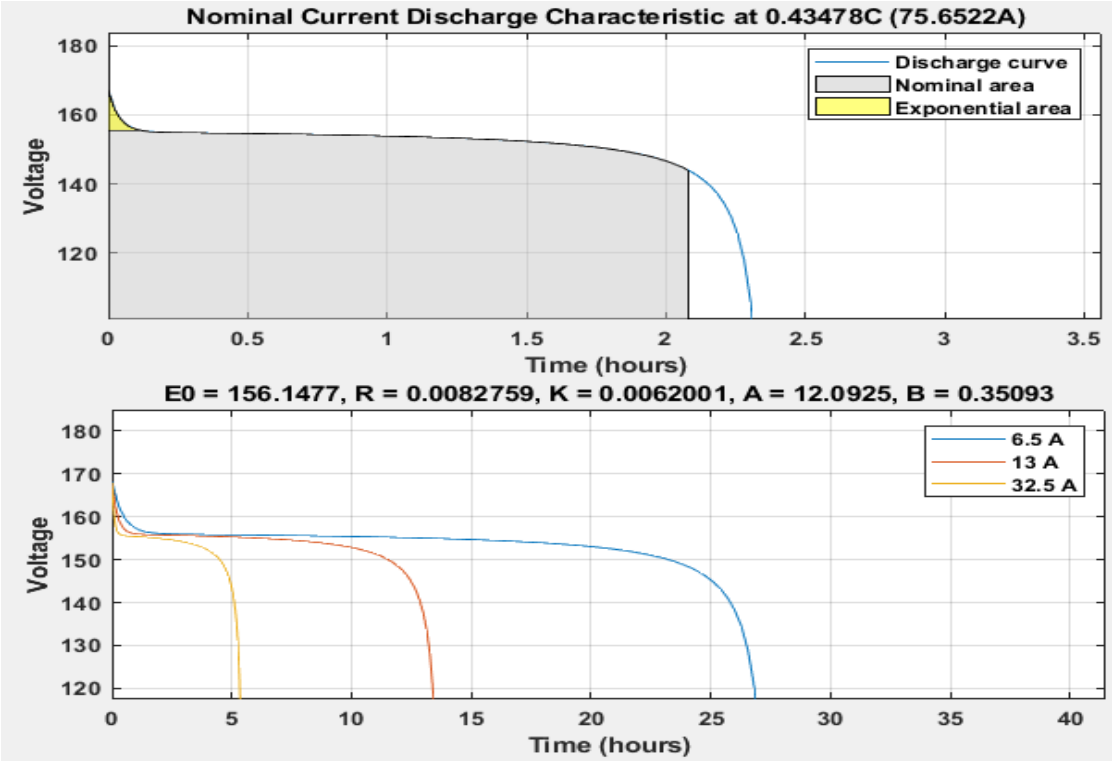

Figure 3.19: Battery discharge characteristics expressed as a function of time

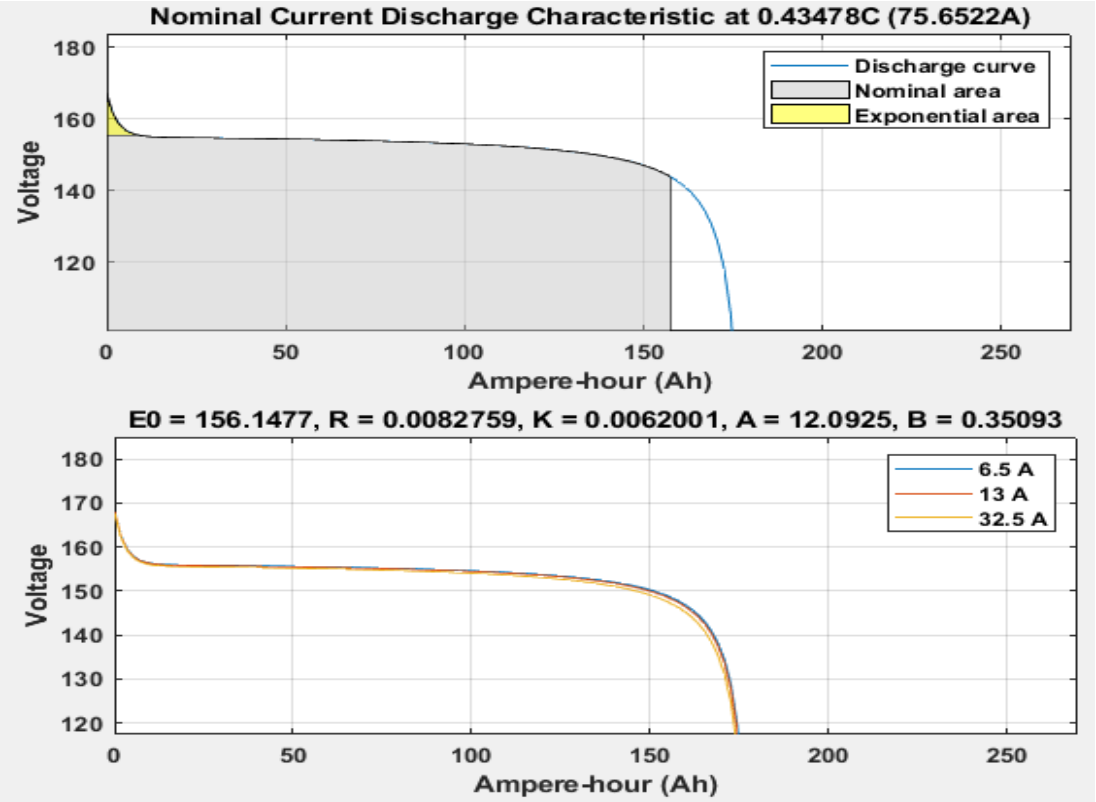

Figure 3.20: Battery discharge characteristics expressed in Ampers-hour

The battery is rated at 30 kW which is approximately 33.3% of the power supply capacity when compared to the fuel cell. Again, the choice of the battery is also to ensure performance delivery and to provide increased flexibility with constant energy supply and extended error margin. The Li-ion battery parameters are presented in Table 3.7.

Table 3.7: Battery specifications

Parameter	**Value**
Chemistry	Li-ion
Nominal Voltage	144 V
Nominal capacity	208.3 Ah
Nominal Power	30 kW
Initial battery SoC	90 %
Response time	1 s
Nominal temperature	25 ℃

Li-ion battery has high energy density and consistent charge-discharge performance that makes it preferable for vehicular applications. Although, there are few disadvantages shown by Li-ion batteries in relation to EMS such as fidelity in battery charging and discharging limits considered crucial for operational and safety reasons. It is essential to note that the battery is not a self-generating device rather an energy storage device that only produces the same amount of energy stored previously (Showers, 2019). The primary working principle of Li-ion battery is based on transfer of lithium-ions in between the positive and negative electrodes to generate or store energy. In both charging and discharging conditions, electrons flow in the opposite direction to the ions present in the electrolyte which serves as an effective barrier for electrons orbiting the outer circuit. The voltage control is according to the charge and discharge dynamics of the battery pack (Erensoy, 2018). Furthermore, aging effects and temperature are crucial to the battery performance but in this study, they were both ignored due to modelling complexities and computational challenges including the fact that it is not central to this study. However, the model presented is detailed enough to provide the relation between current and voltage over a wide state-of-charge that is sufficient for this study.

3.5.4 Electric Motor

The characteristics of electric motor which include its efficiency, mode of operation, torque and speed is provided in the literature review in sections 2.3.4 and 2.3.5 respectively. Electric motors have high efficiency of up to 95% if properly connected to an efficient energy converter. Although, when the electric motor is operating at steady state and less operational power is required, maximum torque can still be produced. In this study, a Permanent-Magnet Synchronous Motor (PMSM) as shown in Figure 3.21 was used because it has higher efficiency, higher starting torque, low noise and higher power density when compared to other available electric motors such as brushless DC Electric Motor (BLDC), etc. Physically, PMSM and BLDC motors are similar with both having field windings in the stator and permanent magnet on the rotor. The major difference is that the PMSM operates on a smooth continuous sinusoidal AC current while the BDLC uses a DC current that switches various windings “ON” and “OFF’’ at intervals to spin the permanent magnet. Again, the rotor speed in PMSM is the same as the magnetic field speed in the windings thereby eliminating torque ripple and improving efficiency. A PMSM has both stator and a rotor like other any other motor, but its functionality differs from DC motors because it uses AC current. The rotor is the moving component of the motor and has a permanent magnet while the stator is the stationary component and has coil windings. When current is supplied to the coils, it creates a magnetic field between the coils and the magnets then creates a corresponding torque that further enables rotation. The magnets spin around a fixed armature that removes the fundamental requirement for commutator to link the current to a rotating armature. The motor controller normally has three pairs of coil and every moment during operation, two pairs of the coil are

energised to move against the rotor magnets and position of the magnet. This action is measured using an ideal rotational motion sensor enabled by the controller as shown in Figure 3.21. The controller supplies the triggering pulses that triggers the electronic switches that magnetises the stator and the rotor magnets spins in the same magnitude. However, the only disadvantage of the PMSM is that it creates “back electromotive force” (EMF) during low speed with the potential to cause drag and heat but the energy during this stage is recovered through regenerative braking used to charge the battery (Gang et al., 2006; Gielniak & Shen, 2004; Panday & Bansal, 2014; Grammatico et al., 2010).

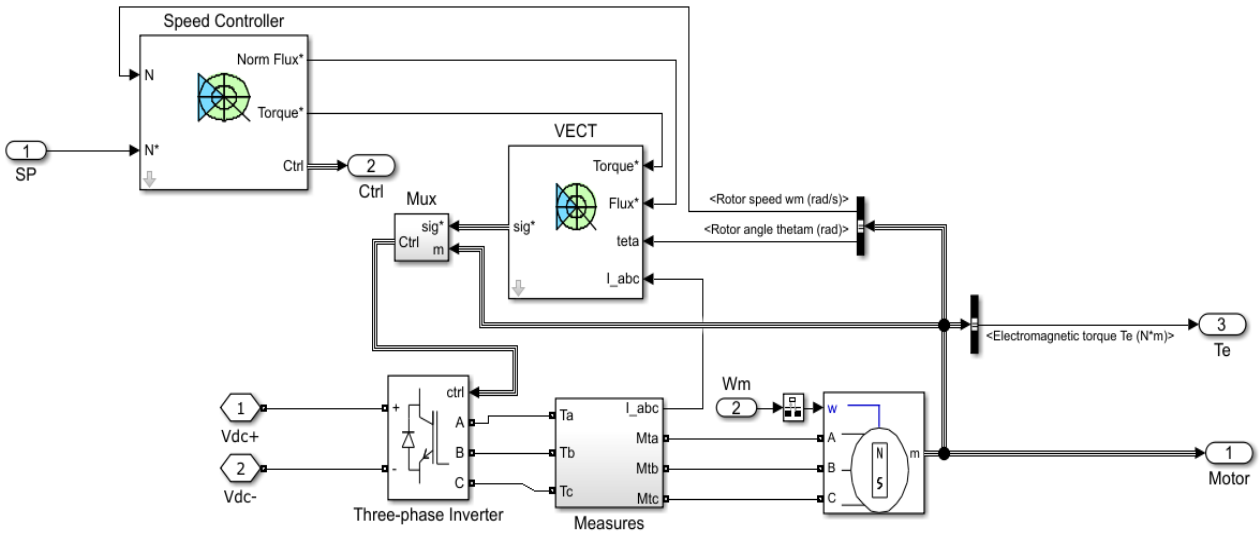

Figure 3.21: PMSM connected to a speed controller

PMSM operation requires little maintenance, it is noise-free and smooth, has advanced safety mechanism and less electromagnetic interference with less weight and size. For this specific study, the reduced size noise-less characteristics were considered as the primary deciding factors. The EM is a 100 kW PMSM with a nominal no-load speed of 4000 rpm while other parameters are shown in Figure 3.22. However, the performance limits and safety measures are assumed to be perfect without getting into the details such as differential equations associated with EM modelling which generates boundary errors in performance.

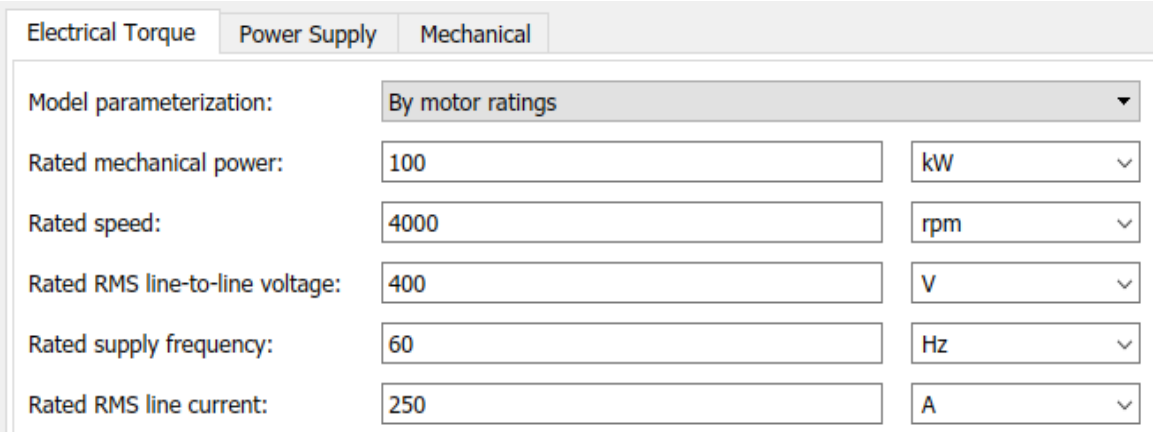

Figure 3.22: PMSM parameters

The primary purpose of the EM model is to calculate available torque delivered according to the transmission system load and thereafter establish the efficiency of a specific performance load and utilizes the mechanical load exerted on the EM to determine the electrical load on the fuel cell and battery system respectively. Using the information needed for a particular rotation rate and corresponding load on the system based on the drive cycle implemented, the EM establishes the performance and electrical energy demand and specific current load using dynamically measured DC bus voltage.

In addition, the EM output power is absorbed by the load on the transmission system and the vehicle speed which must correspond to the drive cycle at that specific time. But the spinning shaft ensures effective transmission of power and the rotation speed. This means that the EM torque must correspond to the vehicle speed and drive cycle condition. However, for a constant torque, the EM torque must be proportional to the rotational speed to ensure affective operation.

3.6 Summary

This chapter presented the drive-cycle block, longitudinal driver model, and mathematical modelling of the different components that make up the FCHEV. These components include the electric vehicle body, the powertrain components such as PEMFC, power electronic converters such as DC to DC buck converter (unidirectional converter), DC to DC bidirectional converter, DC to AC inverter and an energy storage system (lithium-ion battery). An electric motor (PMSM) was also presented in detail.

CHAPTER 4: ENERGY MANAGEMENT SYSTEM ALGORITHM

4.1 Introduction

In this chapter, a high-level energy management system (EMS) for a fuel cell/lithium-ion powered electric vehicle is developed and implemented according to a set of performance criteria. The FCHEV EMS was designed and developed using state-flow logical programming language under the MATLAB/Simulink environment. State-flow is a graphical language that comprises flow charts, state transition tables, truth tables and state transition diagrams. A complete model of the FCHEV and the EMS algorithm is shown in Figure 4.1 while the Battery management system and EMS subsystem are shown in Appendix 1 and 2 respectively.

The EMS uses the reference current of the fuel cell to ensure that the fuel cell is operated optimally and also meeting the load demand. The parameters that regulate EV speed and operation mode are also adjusted according to the battery SOC, power demand, the drive cycle conditions similar to South African road conditions including driver behaviour in order to improve the energy efficiency of the EV.

There are four control systems developed for the operation of this FCHEV. The control that ensures effective operation of the fuel cell voltage for the selected bus voltage that is adequate for tracking the reference with a minimum error. This is to ensure that ripples are rejected during transient load under single degree of freedom such as the frequency and duty cycle. To optimise the system, a separate control system is developed for the lithium-ion battery that controls the charge and discharge of the battery system determined by the load demand and state-of-charge (SOC). A special control that monitors the vehicle speed, load demand and supplies and a corresponding power is designed for the EM. Lastly, is the central control that integrates the individual controls into a central control. The central control makes decision based on signals received from the other three aforementioned controls.

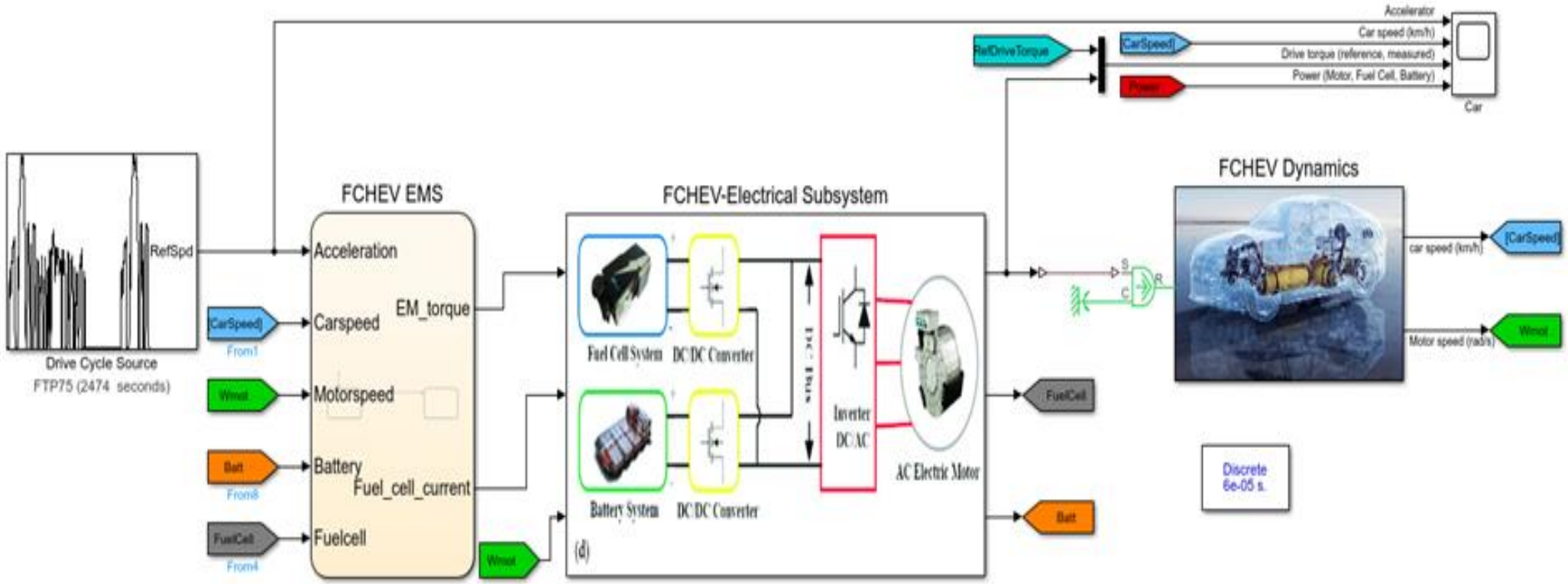

Figure 4.1: FCHEV with the EMS

Developing an effective EMS for a fuel cell and lithium-ion battery hybrid EV will result in fuel cell stack downsizing which will have a positive impact on the system because the fuel cell can better respond to the load demand for a specific drive cycle and increase the travel range. It will also result in smaller fuel cell system and smaller hydrogen tank thereby reducing parasitic loss and less weight (Showers & Raji, 2022). Effective EMS will also address the problem of poor dynamic response of the fuel cell created by lag in auxiliary components, oxygen shortage caused by increased load demand that might cause dead spots and short circuits. Furthermore, adding an energy storage system (ESS) will ensure regenerative energy recovery which is used to charge the battery (Erensoy, 2018). The importance of effective EMS cannot be overemphasised as it will enable effective load distribution between the fuel cell and the energy storage system with the potential to store the excess power during regenerative braking and idle moments.

4.2 Control algorithm

In the fuel cell/lithium-ion hybrid model, developing and effective EMS ensures proper distribution of the average power supplied by the fuel cell and transient load balancing by the lithium-ion battery. The fuel cell serves as the main source of power while the battery is used for load levelling. This means that battery is charged in the event that the load demand is less than the average fuel cell power output and discharged when the load demand is greater than the average fuel cell power output. Ideally, the average load demand corresponds to an effective operation time of the fuel cell power. This has a significant impact on the power-train and the EMS design (Yue, 2019; Koot et al., 2015).

The developed EMS improves the travel range and battery lifespan where the primary target of the fuel cell is achieved based on the load requirement and battery SOC. The control of the hydrogen flow rate using the fuel cell delivery system is determined by the fuel cell reference current which regulates the fuel cell power output. Hence, the power distribution is achieved by using the battery to augment the difference between the fuel cell power output and the load demand. Furthermore, the EMS algorithm is designed to monitor the fuel cell output power, battery SOC and the load demand under the selected drive cycle (FTP-75). Therefore, the EMS control algorithm based on effective power distribution between the fuel cell and battery system should ensure the following objectives:

- The load demand is always met by the power output of the EM.
- Optimal operation of the fuel cell and battery system; the set minimum and maximum currents and considered
- Effective power distribution between the fuel cell and battery system to avoid deep discharge of the battery and fuel cell during transient loads.

- Reduce fuel consumption

The central controller is required to track the different dynamic parameters in order to ascertain the operational requirements of the FCHEV determined by the drive cycle as shown in Figure 3.2. The central controller uses the fuel cell power P_{fc}, battery SOC ($Batt_{SOC}$), EM load demand and vehicle speed to achieve the anticipated vehicle performance while the other sub-controllers use a closed-loop system that focuses on the primary objectives without exhibiting direct connection with the central controller. The central controller of the EMS configuration used in the simulation is shown in Figure 4.2.

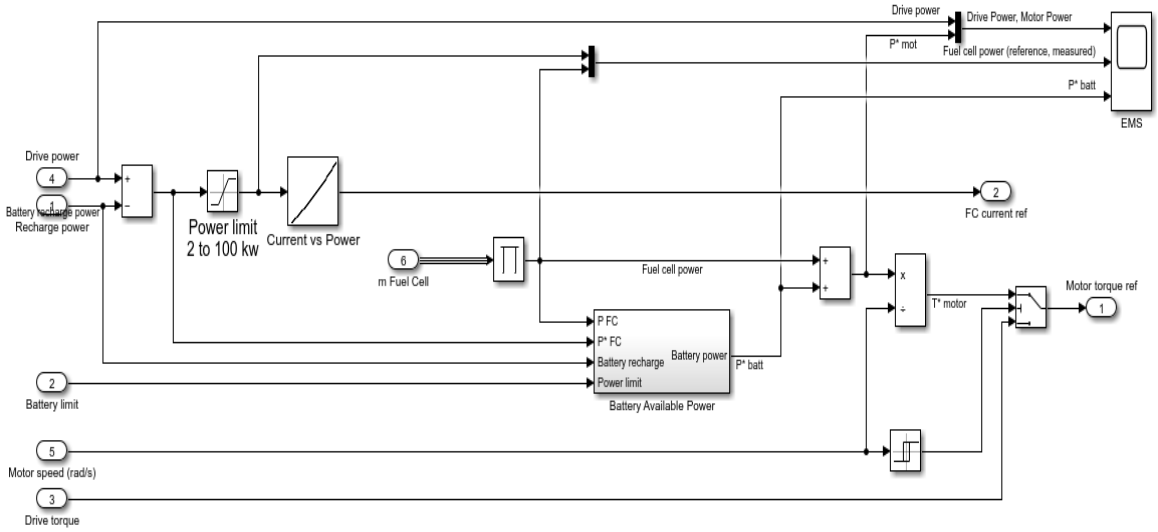

Figure 4.2: EMS configuration

Firstly, in deciding on the mode of operation, the central control receives relevant signal from the other three controls such as battery SOC, available battery charge and discharge based on the battery set limits determined by the value of the voltage and the EM load demand. This information is then evaluated using the set conditions in state flow in the MATLAB/Simulink environment. Because the primary purpose of the EMS is optimization, the algorithm first searches for the most optimal and efficient condition of operation of the fuel cell and battery system considering the vehicle speed at that point. That condition is then assessed based on the set conditions. However, the operation of the fuel cell is not temperature dependent rather its turning “ON” and “OFF” depends on the vehicle speed and the battery SOC. Thermostatic control of fuel cell is not included in this research, but studies have shown that it has influence on the efficiency of the fuel cell and reduces its life span (Panday & Bansal, 2014). Again, the EMS has the capacity to stop the vehicle in a situation where the load demand is higher than the combined power provided by the fuel cell and battery system.

The low and high regions of the battery SOC ensures that its operating condition is set based on the different drive cycle requirements, vehicle speed and the EM load demand. However,

in this study, limits were established to ensure efficient energy storage while operating the battery optimally and prioritizing the EMS. The battery is charged and discharged according to load demand determined by vehicle speed but does not exceed the set threshold to avoid deep discharge. To obtain high performance based on the set criteria, five input variables are measured: acceleration, car speed, EM power (P_{EM}), battery power (P_{batt}), fuel cell (P_{fc}). These parameters are compared with the defined battery set limits and the load demand to establish the optimal fuel cell operation mode. The load limit is defined based on the drive cycle requirement, battery capacity and the fuel cell capacity. The fuel cell provides little amount of power when the battery SOC is greater than or equal to 40% and supplies maximum power when the battery SOC is less than 40% and the load demand is above 30 kW.

To achieve effective power distribution between the fuel cell and the lithium-ion battery system using the load demand by the EM, the following driving modes are considered:

i. Starting mode: During this mode, the fuel cell is switched “OFF” and the battery is switched “ON” (discharging). The power balance during this mode is expressed as:

$$P_{Batt} = P_{EM\ and}\, P_{fc} = 0 \tag{4.1}$$

ii. Traction mode (fuel cell “ON” and battery is charging): During this mode, the fuel cell is switched “ON” and the battery is charging. The power balance is experessed as:

$$P_{fc} = P_{EM} + P_{Batt} \tag{4.2}$$

iii. Traction mode (fuel cell is switched “ON” and baterry is switched “ON”): During this mode, the load demand is greater than the fuel cell power output and the battery is discharging to augument for the power deficit. Therefore, the power balance can be expresed as:

$$P_{EM} = P_{fc-max} + P_{Batt} \tag{4.3}$$

iv. Regenerative braking mode: During this mode, the fuel cell is switched “OFF”, the battery is charging and the EM is operated as a generator used to charge the battery.

The EMS is developed by using information such as the vehicle speed, EM power demand, minimum operating power of the fuel cell stack and battery SOC. These parameters are controlled and operated at different modes that is determined by the drive cycle requirement and available power to produce sufficient power to meet the EM load demand. The decisions are made using the flowchart shown in Figure 4.3 based on equations 4.1 to 4.3. Irrespective of the complex implementation of the EMS algorithm and selecting the approriate driving mode, the overall function of the EMS startegy is to ensure effective power distribution between the

fuel cell and battery system in a way that ensures sufficient power to meet the driver's torque load demand.

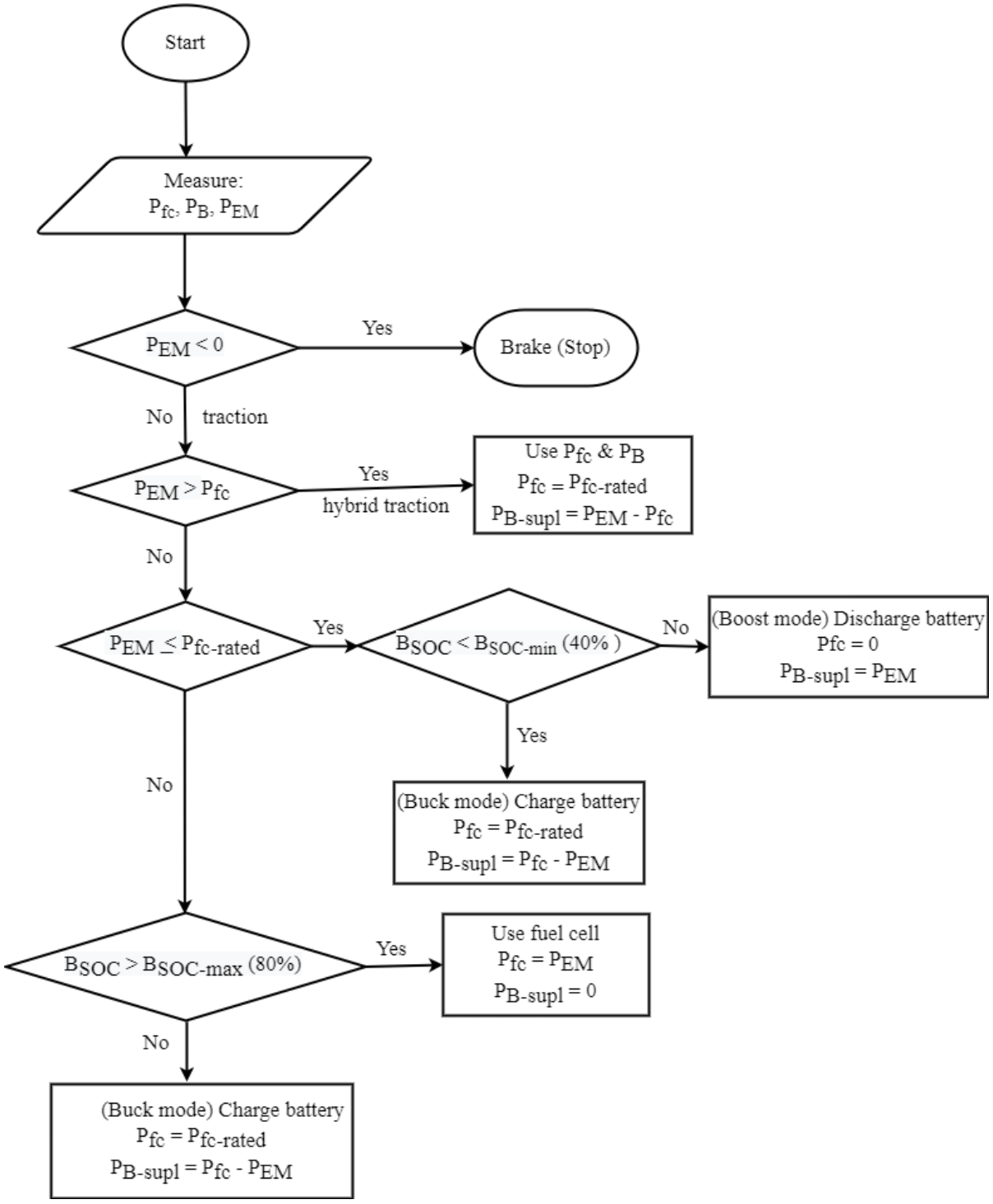

Figure 4.3: FCHEV EMS flowchart

Where:

P_{EM} = EM power (load demand)

$P_{fc-rated}$ = fuel cell rated power

P_{fc} = fuel cell power

P_{fc-MIN} = fuel cell minimum power

P_{B-spl} = power supplied by the battery

P_B = battery power

B_{SOC} = battery SOC

$B_{SOC-min}$ = minimum level of battery SOC

$B_{SOC-max}$ = maximum level of battery SOC

4.3 Summary

This chapter exclusively presented the FCHEV EMS algorithm. The EMS was developed using information such as the fuel cell power output, battery SOC and electric motor load demand (torque). These parameters were carefully controlled to ensure effective implementation of the set objective of effective power distribution between the fuel cell and battery system determined by the drive cycle requirement and EM load demand. A MATLAB/Simulink model indicating individual components that comprises the FCHEV EMS, electrical subsystem (fuel cell, battery, converters and EM) and vehicle dynamics connected to the stateflow were presented.

CHAPTER 5: RESULTS AND DISCUSSION

5.1 Introduction

This chapter presents the simulation results, associated interpretation and discussions of the results. An EMS for a FCHEV is implemented using state-flow logical programming language under the MATLAB/Simulink environment as shown in Figure 4.1. The fundamental purpose of the EMS is to ensure effective power distribution between the fuel cell, lithium-ion battery system and the EM load demand based on the drive cycle requirement. However, to ascertain the effectiveness of the EMS, its performance and power supply are evaluated during transient load demand situations and idle moments using the drive cycle details. This includes the response of the fuel cell stack and battery system, the bidirectional converter and EM response during regenerative braking. Furthermore, battery system charging and fuel cell and battery response during idle moments when the total load demand is zero are used to measure the effectiveness of the EMS. Lastly, the response of the powertrain during dynamic load using the drive cycle requirement is evaluated.

5.2 Simulation results and performance of the fuel cell stack under no-load

The output voltage of the fuel cell stack is shown in Figure 5.1. This output voltage serves as the input to the DC-DC boost (unidirectional) converter. From the simulation result, the output voltage of the fuel cell stack is 350 V_{DC}.

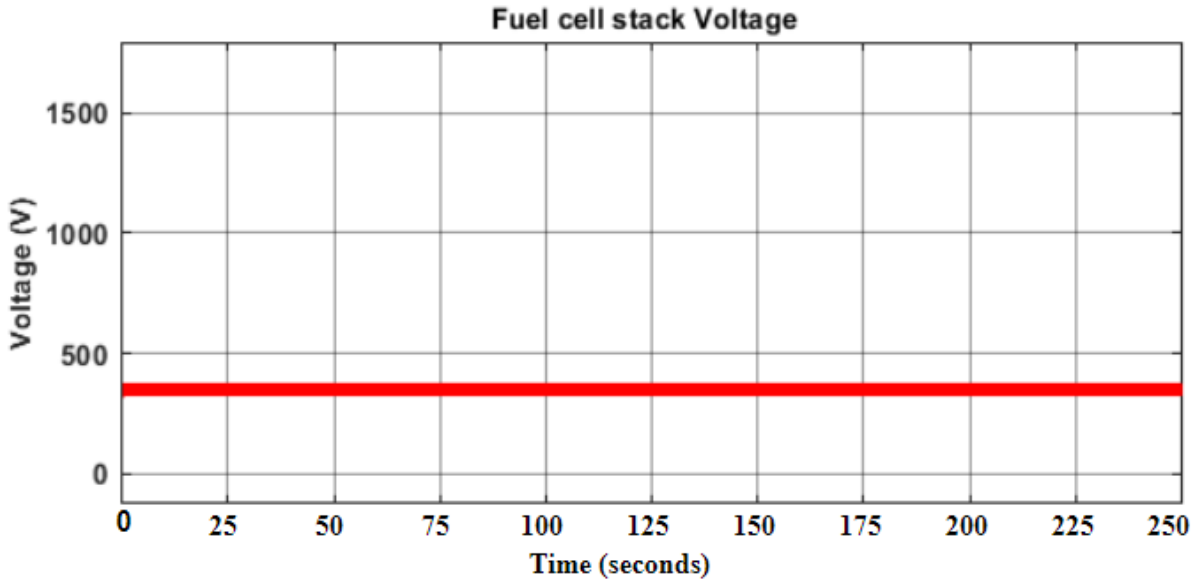

Figure 5.1: Fuel cell stack voltage

Again, the fuel cell stack current and efficiency are shown in Figure 5.2 (a) and (b) respectively. The values are maintained at 285.7 A and 45 % during the entire simulation period because all the parameters are kept constant.

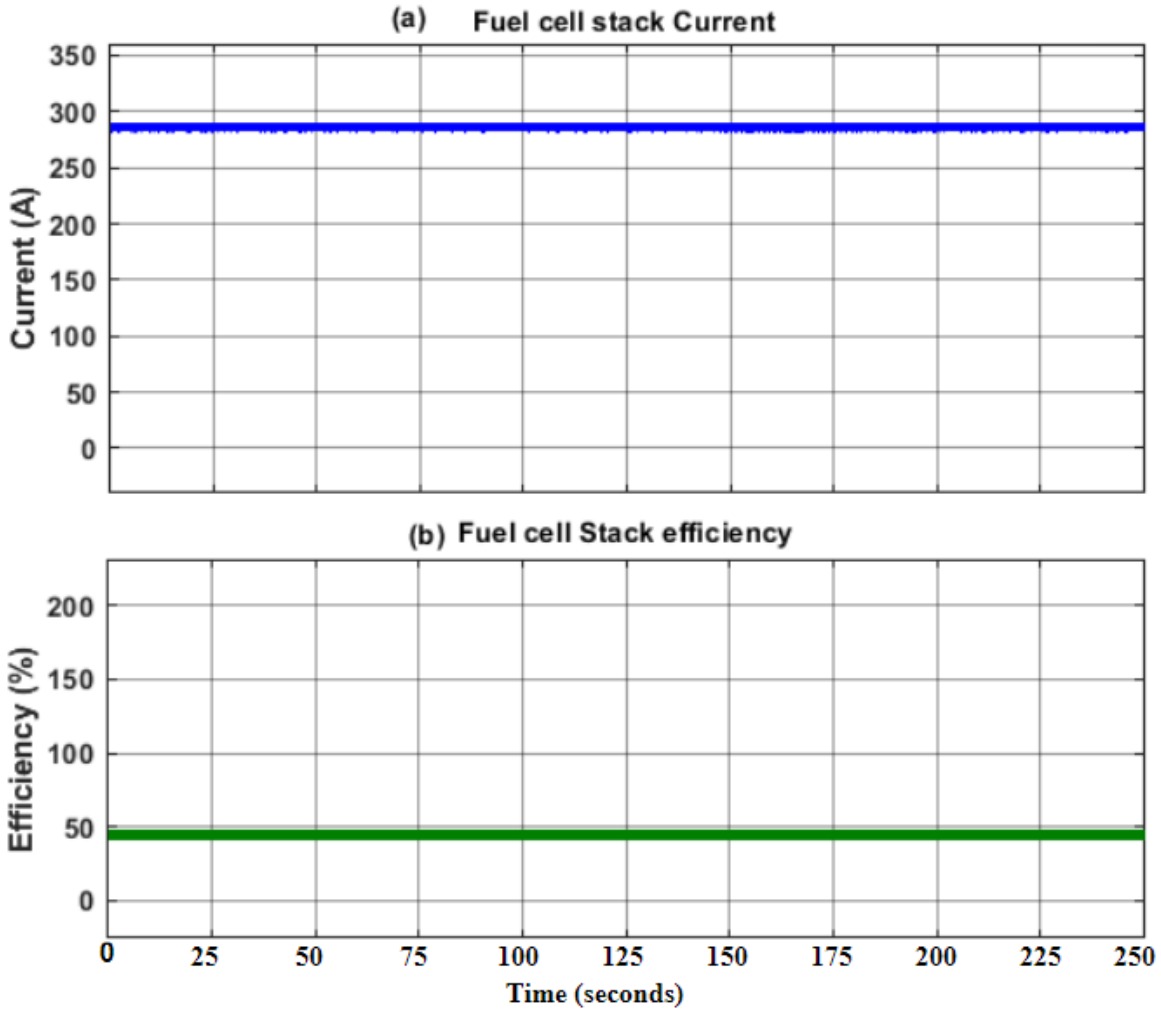

Figure 5.2: Fuel cell stack current and efficiency

The simulated power output of the fuel cell stack is shown in Figure 5.3. The power during the period is constant at 99.995 kW. This value is approximated to 100 kW for easy simulation and design purposes.

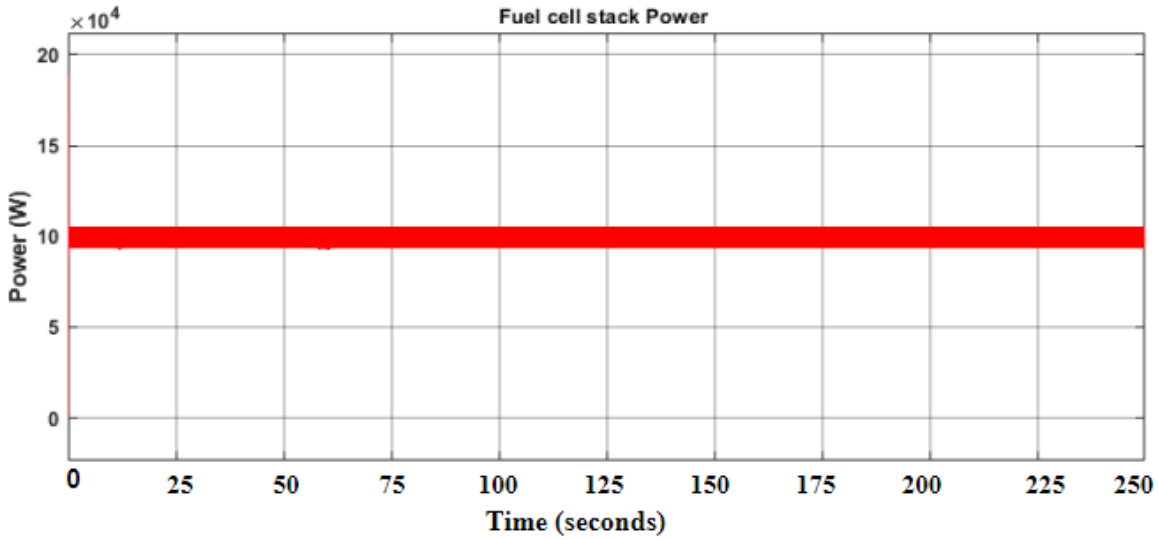

Figure 5.3: Fuel cell stack power output

5.3 Simulation result of the fuel cell DC-DC boost converter

The fuel cell voltage is fed directly to a DC-DC boost converter in order to boost the fuel cell voltage to the same level as the DC bus voltage of 400 V_{DC}. The current and boosted voltage after the boost converter is shown in Figure 5.4 (a) and (b) respectively. The current dropped to 250 A and the voltage boosted to 400 V to ensure that the 100 kW power is maintained. The duty cycle ensured that the voltage is controlled and kept constant at 400 V. However, any change in the value of the input voltage will result to a corresponding change in the duty cycle but the DC bus voltage is kept constant.

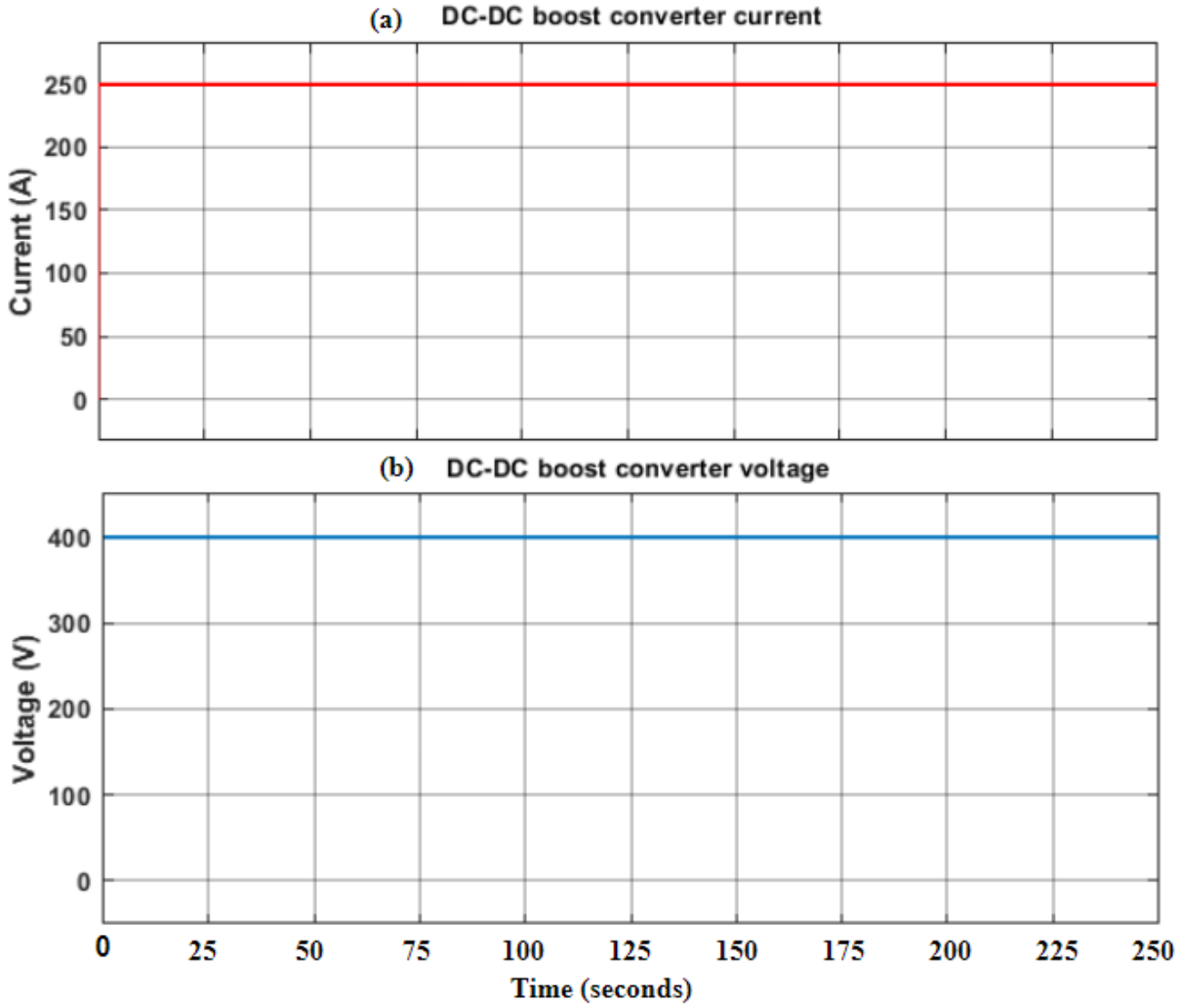

Figure 5.4: Boost converter (a) current (b) Voltage

5.4 EMS performance under the drive cycle

The simulation results and evaluation of the FCHEV EMS is presented under three different sections (vehicle standstill, traction and regenerative braking). The mechanical load demand exerted by the electric motor using the drive cycle data shown in Figure 3.2 under section 3.2 is distributed under 2474 seconds. The computational complexity associated with a simulation of this magnitude is very high and time consuming for a 64-bits operating system at 3.40 GHz CPU. Therefore, the drive cycle time was down-sample by 1/10 (10%) to accommodate the load demand dynamics in a more compressed and concise time. This unavoidable decision puts the FCHEV under a more demanding condition because the load demand changes in more shorter intervals that requires faster response from the power sources. From the flow chart shown in Figure 5.5, it is seen that the vehicle in on standstill during this period because the electric motor power (P_{EM}) is less than zero, vehicle speed is less than zero, the fuel cell power (P_{fc}) is greater than the electric motor power and the battery state-of-charge ($Batt_{SOC}$) is less than 20%. This transition is determined by the input parameters as indicated and it can

be seen that the flow chart displays the standstill mode in blue to show that the operating mode is fulfilled. In addition, the compressed drive cycle, vehicle speed, drive torque, electric motor power, fuel cell power, battery power with associated load demand is presented in Figure 5.6. It can be seen that the peaks and associated drive cycle demand are preserved with a combination of the fuel cell power and battery power. The electric vehicle power which is determined by the load demand and corresponding drive cycle is zero in the first 20 seconds but accelerates afterwards.

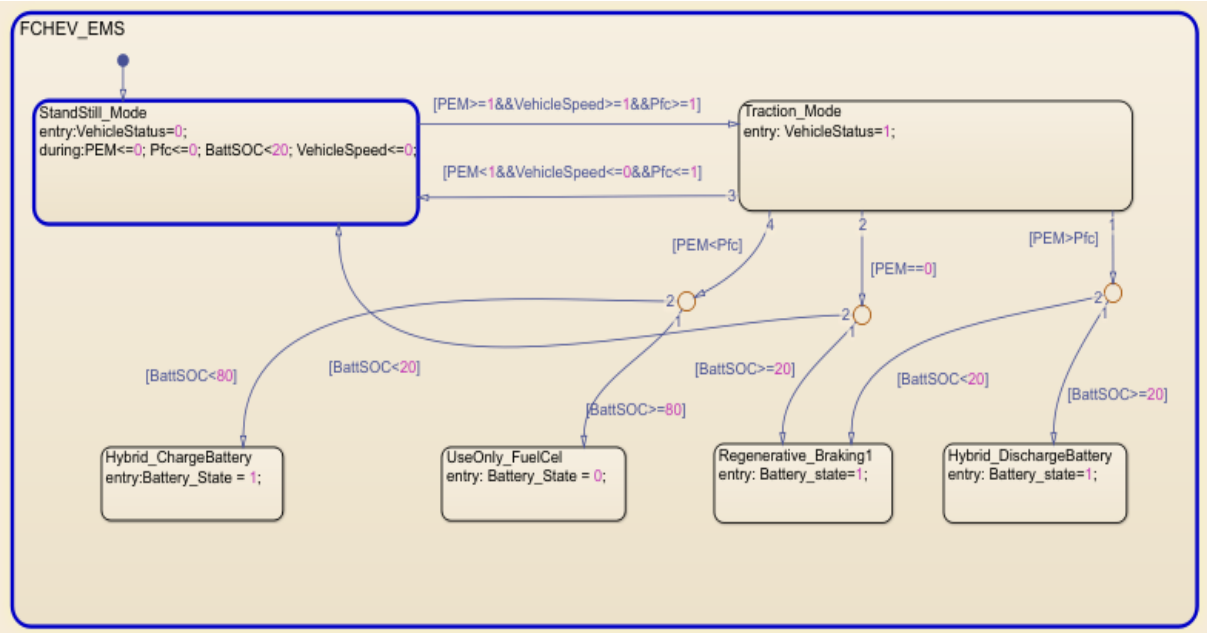

Figure 5.5: Transition state indicating vehicle standstill

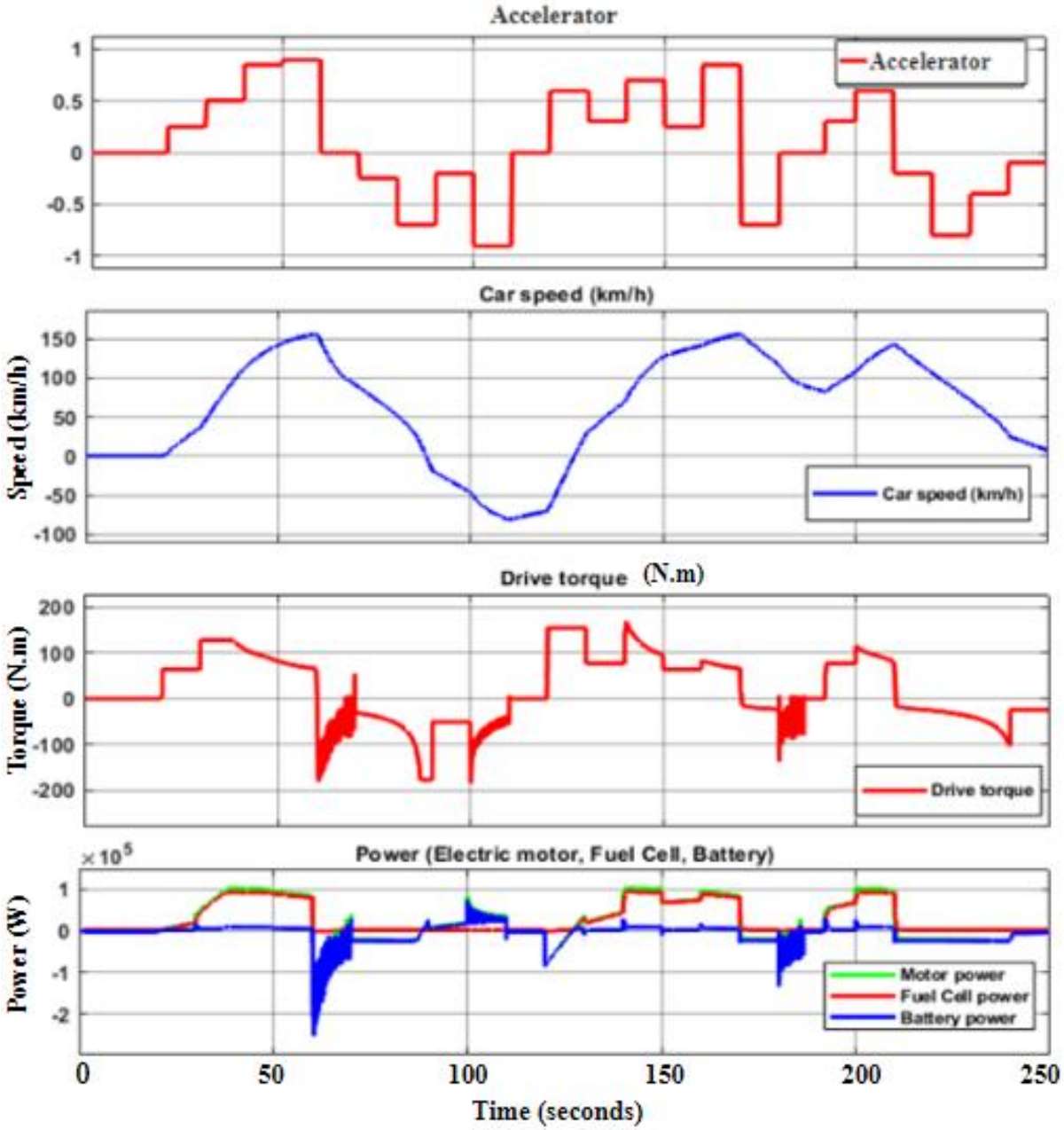

Figure 5.6: Power train performance and power supply to the load

5.4.1 EMS performance at zero load (when P_{fc} is greater than P_{EM})

The load demand and battery state-of-charge (SOC) are critical parameters used to determine the amount of power demand from the FCHEV and the power supply hence, in this simulation, the initial state of charge is kept at 80% and the load demand is maintained at zero using the drive cycle down-sampled. This section focuses on a portion of the drive cycle where the load demand is zero and the battery SOC is less than 80% to proof the workability of the EMS. The first 20 seconds was extracted because it satisfies the requirement. The load demand from the electric motor (P_{EM}) which is determined by the drive cycle is adequately supplied by the power delivered by the fuel cell (P_{fc}) and the battery power (P_{batt}) as shown in Figure 5.7 and further

demonstrated on the transition state flow chart shown in Figure 5.8. In addition, the load demand during the first 20 seconds is less than the fuel cell power (P_{fc}) and the battery power is negative which shows that the battery is charging as shown in Figure 5.9, hence, the EMS is in hybrid mode where the excess power produced by the fuel cell is used to charge the battery. This situation also occurred between 70 – 80 seconds, 120 – 130 seconds, 170 – 180 seconds and 240 – 250 seconds respectively. The result showed that the load demand is met during these periods and the EMS is functioning effectively as demonstrated. The fuel cell power is equal to the negative battery power because the there was no demand from the EV and the entire power from the fuel cell is used to charge the battery system as shown in figure 5.9.

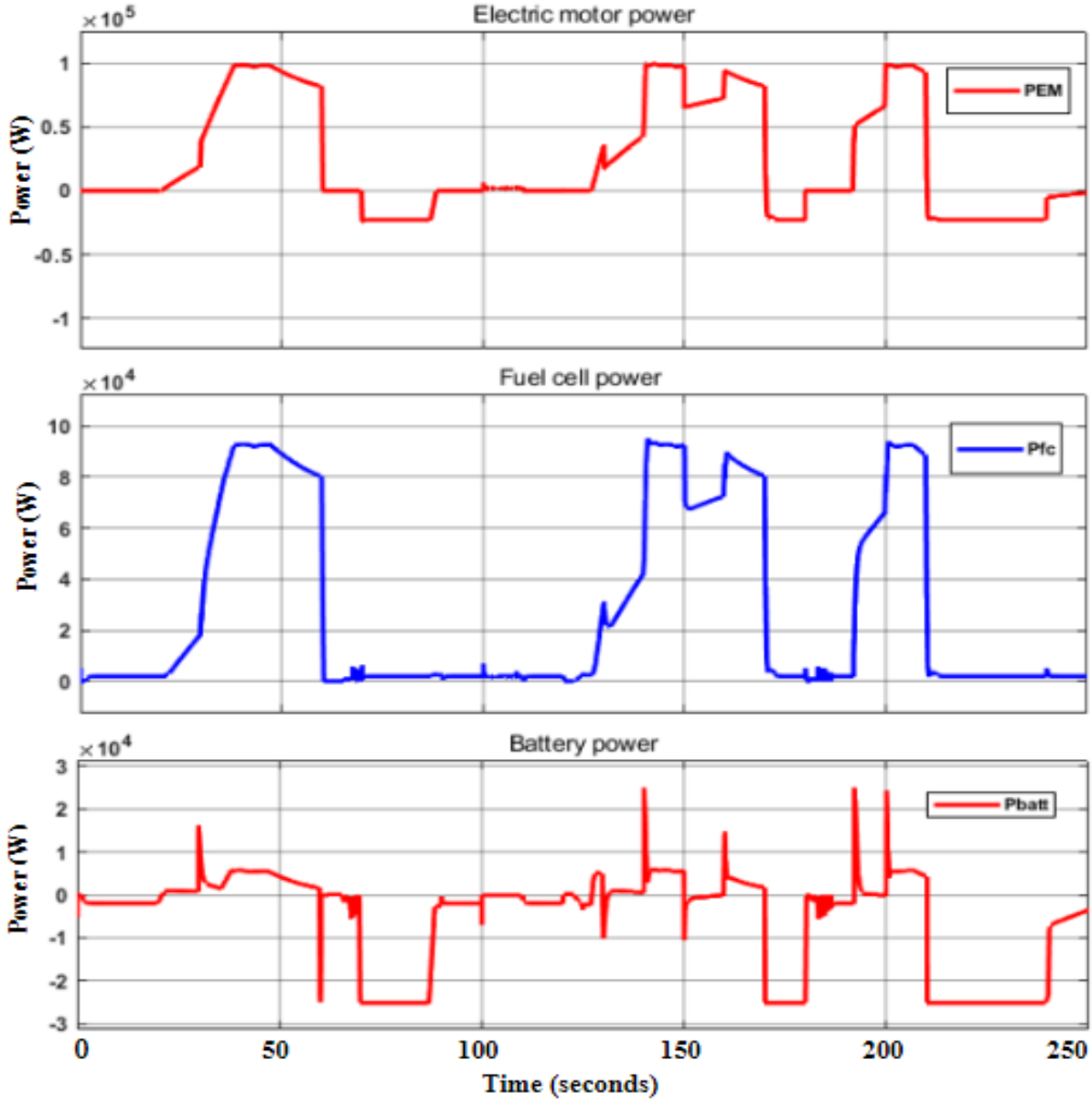

Figure 5.7: Power distribution using the down-sampled drive cycle

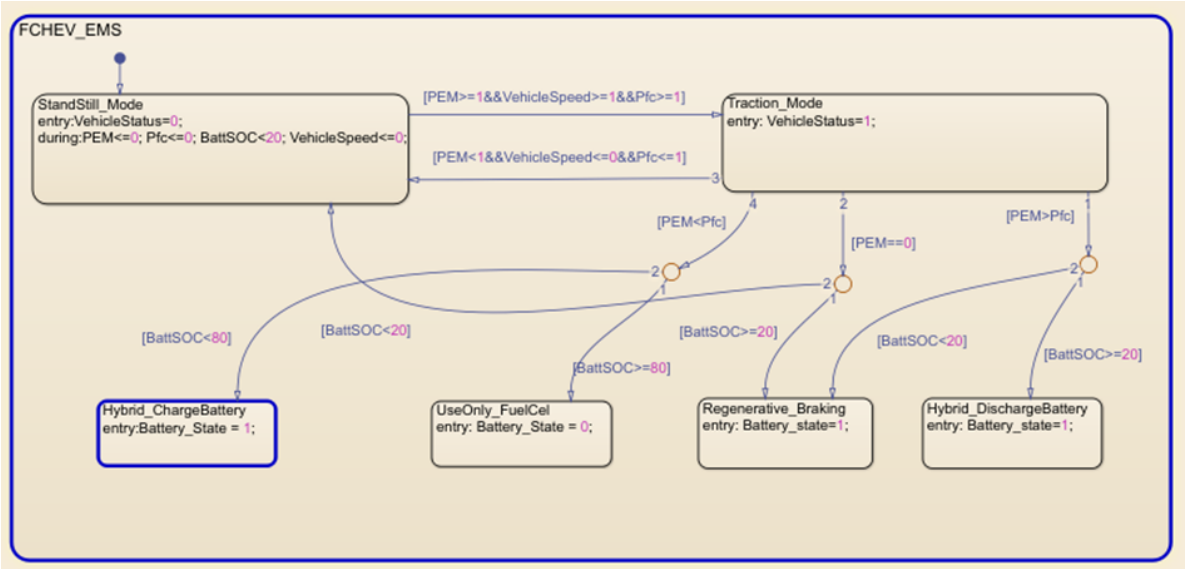

Figure 5.8: Hybrid mode-ChargeBattery

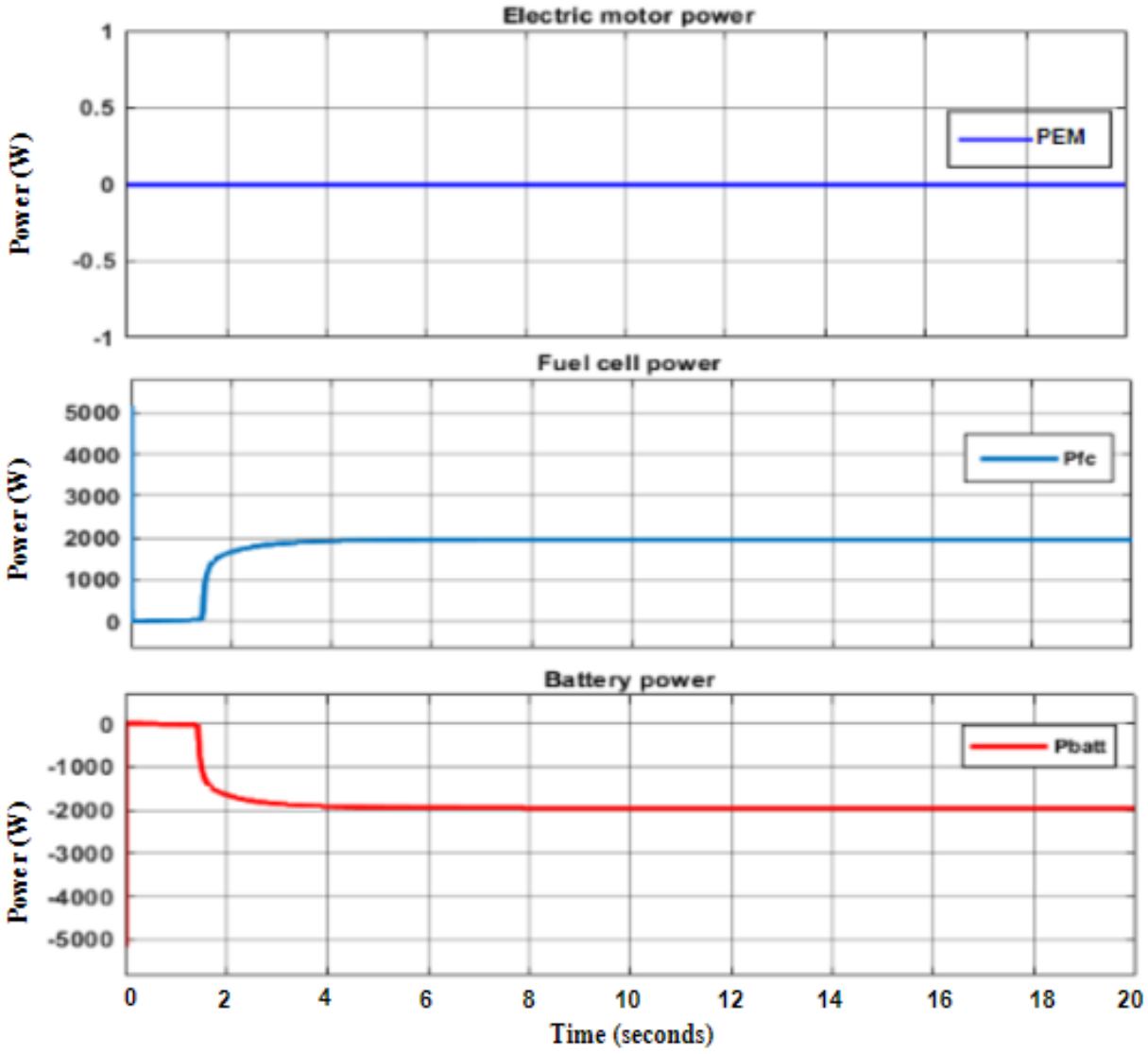

Figure 5.9: Load demand, fuel cell power, battery power during first 20 seconds

The initial state-of-charge (SOC) of battery state is set at 80% but it increased to 80.24% due to charging by the fuel cell power during this period as shown in Figure 5.10. This result further proves the functionality of the EMS considering the power supplied by the fuel cell, battery power and the load demand determined by the drive cycle during this period.

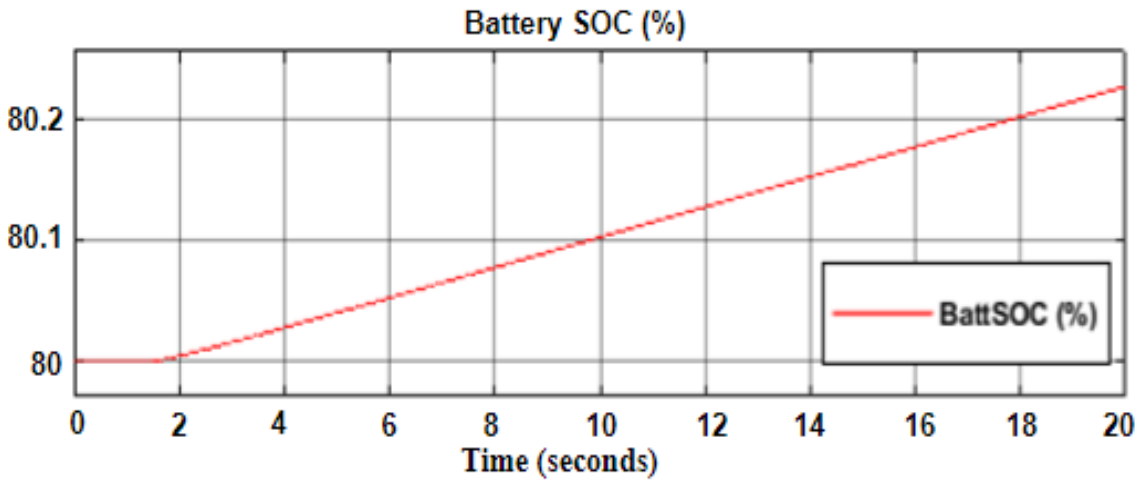

Figure 5.10: Battery SOC during first 20 seconds

5.4.2 EMS performance when P_{EM} is greater than P_{fc}

As indicated earlier in section 5.4, this is one of the conditions under traction mode. In this portion, the load demand from the vehicle (PEM) is greater than the fuel cell power output (Pfc) due to high acceleration of the EV. This has a significant impact on the fuel cell and the energy storage system (lithium-ion battery). The fuel cell is the primary source of power, and the lithium-ion battery is designed to store and release energy based on the prevailing power demand and its SOC. These major accelerations occurred between 35 – 55 seconds, 140 – 150 seconds and 200 – 210 seconds respectively. This is highlighted with a green square in Figure 5.11. During these periods, the power demand was 100 kW, but the fuel cell supplied approximately 95 kW and the lithium-ion battery augmented 5 kW as shown in Figure 5.11. The discharge rate was constant based on the power demand and the transition state of the stateflow indicating the battery discharge state is shown in Figure 5.12.

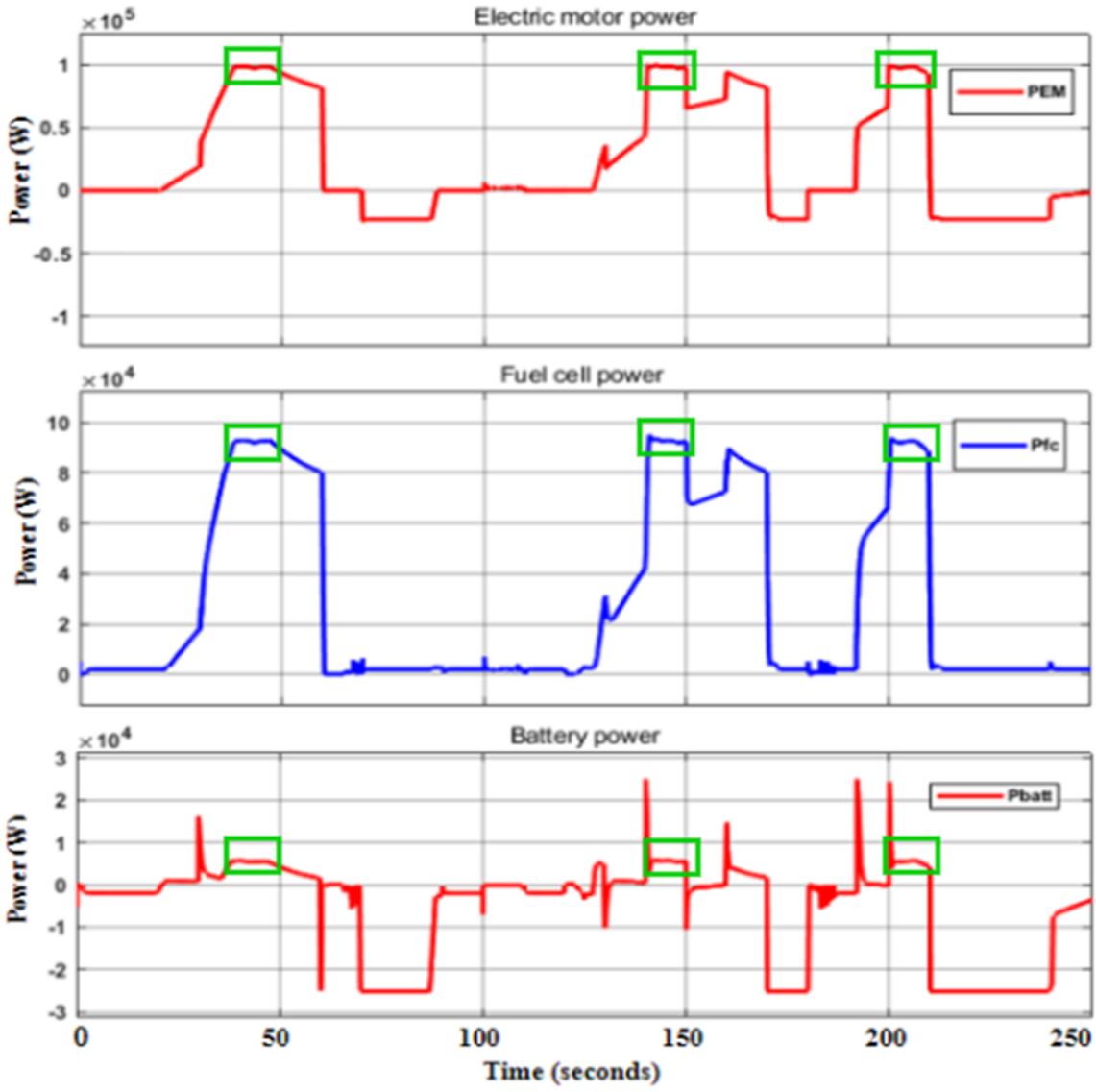

Figure 5.11: Hybrid mode - battery discharging

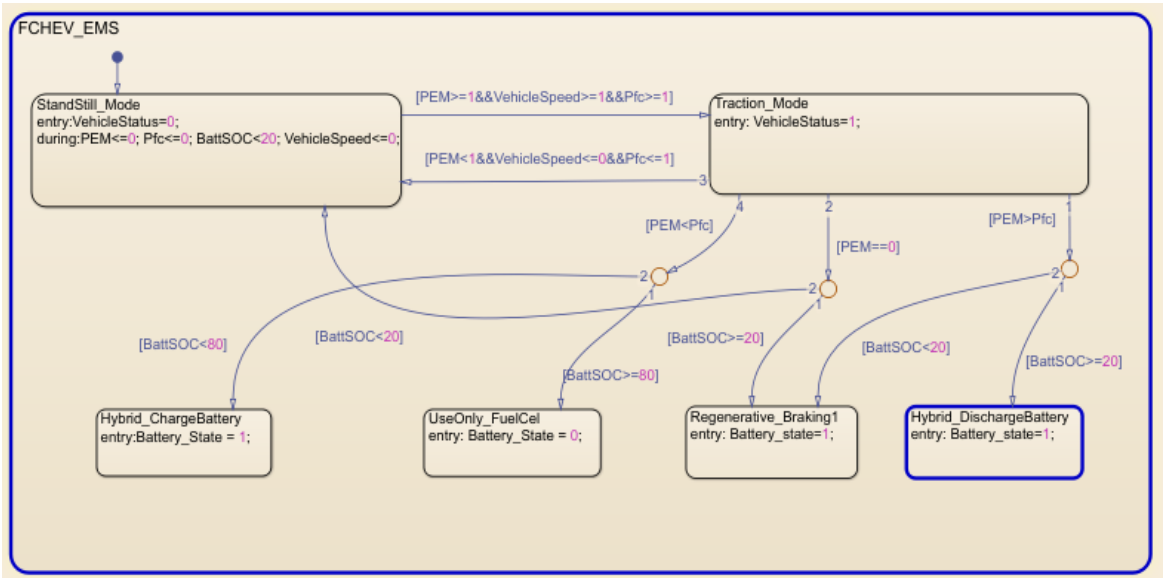

Figure 5.12: Transition state from the Stateflow chart

5.4.3 EMS performance during regenerative braking

The regenerative braking occurred between 65 – 85 seconds, 170 – 185 seconds and 210 – 240 seconds respectively. This is highlighted with a green dotted square as shown in Figure 5.13. During these periods, the regenerative power was 2.5 kW and is used to charge the lithium-ion battery. Furthermore, during this period the electric motor functioned as a generator and generated 2.5 kW and the transition state of the stateflow indicating regenerative braking is shown in Figure 5.14. The fuel cell during these periods is disconnected to ensure the smooth flow of power from the electric motor to the battery.

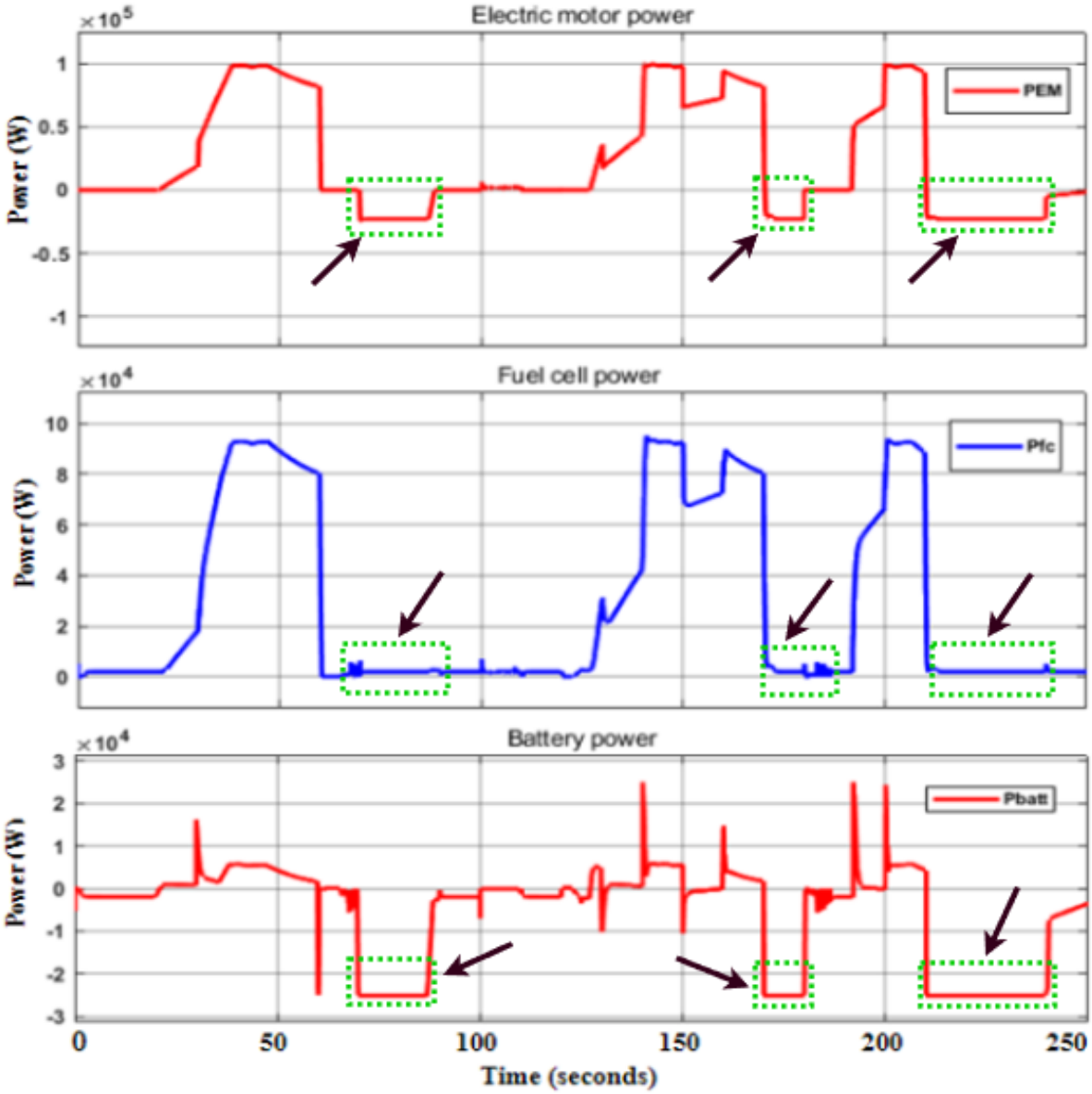

Figure 5.13: Regenerative braking mode

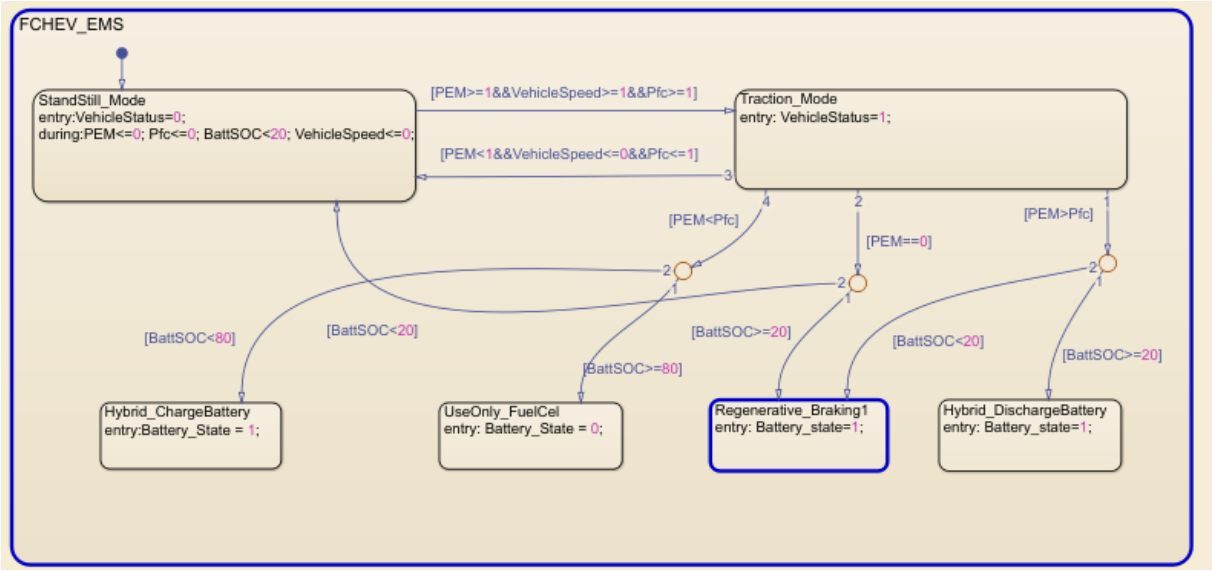

Figure 5.14: Transition state indicating regenerative braking

5.4.4 EMS performance using only fuel cell

This occurs when the electric vehicle power demand is equal to the power generated by the fuel cell. The battery system during this period is disconnected because it is fully charged. It occurred between 20 – 35 seconds, 110 – 120 seconds and 190 – 200 seconds under the drive cycle to clearly ascertain the effectiveness of the EMS. The stateflow transition is shown in Figure 5.15.

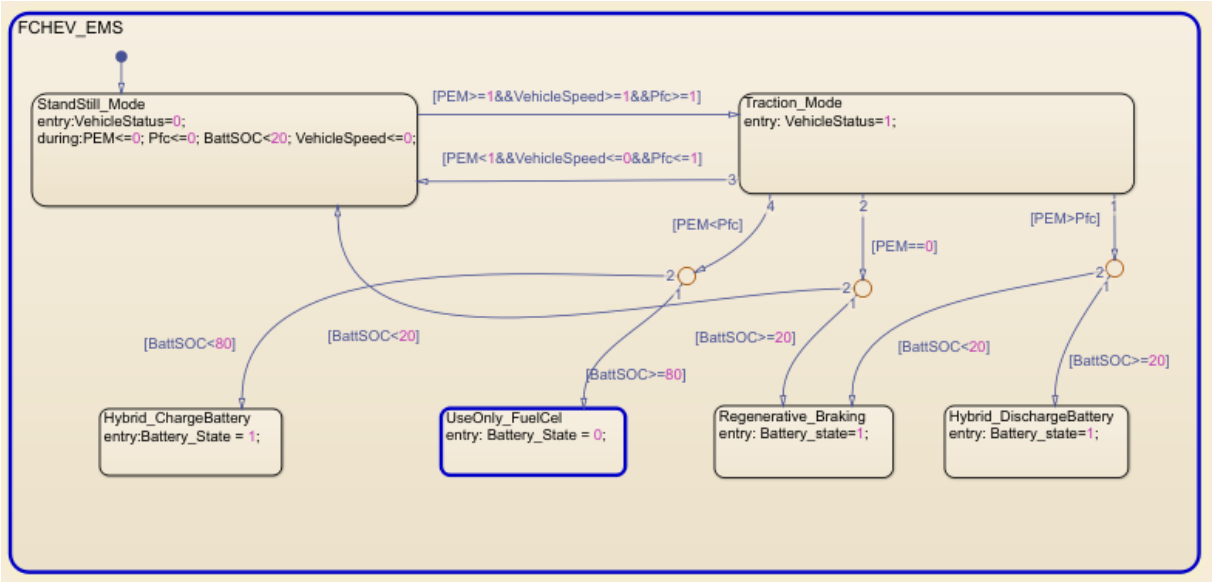

Figure 5.15: Transition state - Use only fuel cell

Furthermore, “use only fuel cell” mode is highlighted with a green dotted square with an arrow pointing towards it as shown in Figure 5.16. The battery power is zero because it is disconnected.

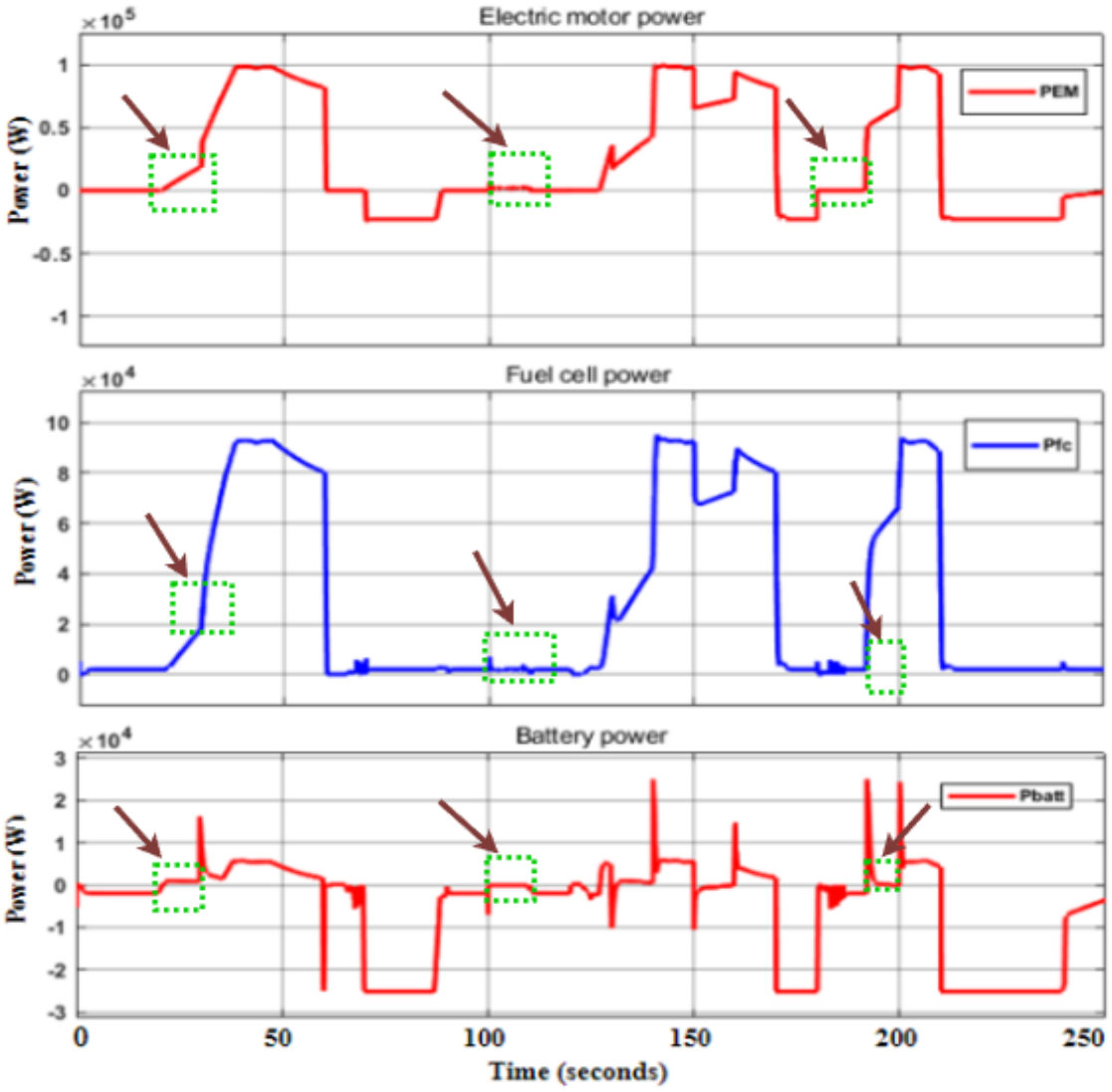

Figure 5.16: Use only fuel cell mode

To validate the effectiveness of the EMS and the model, the FCHEV was run under the selected drive cycle (FTP-75) as presented in previous sections. Some results including bidirectional DC-DC converter current, fuel cell and battery voltage, fuel cell and battery current and the battery SOC are shown in Figure 5.17. The bidirectional DC-DC converter current peaked at 300 A and the V_{DC} bus voltage at 400 V. In addition, the current peaked at 250 A as shown. However, the aforementioned parameters and associated values at any point in the drive cycle depends on the power demand and the availability of power from both sources (fuel cell, battery).

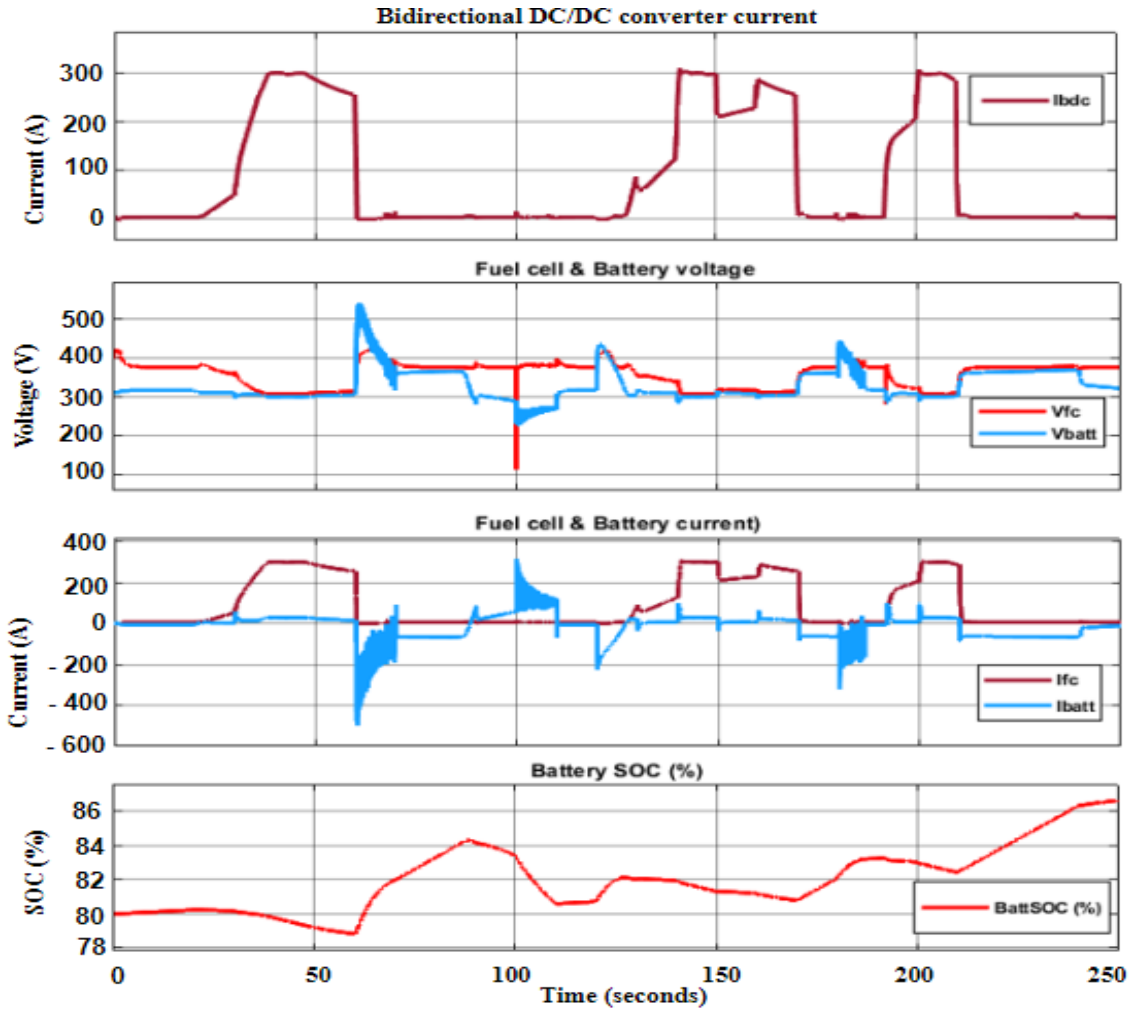

Figure 5.17: BDC current, V_{fc}, V_{batt}, I_{fc}, I_{batt}, $Batt_{SOC}$ under MATLAB/Simulink

Other parameters such as the electromagnetic torque, electric motor rotor speed (rpm), mechanical power, current and voltages are presented in Figure 5.18. The values are determined by the drive cycle and correspond to the initial calculations.

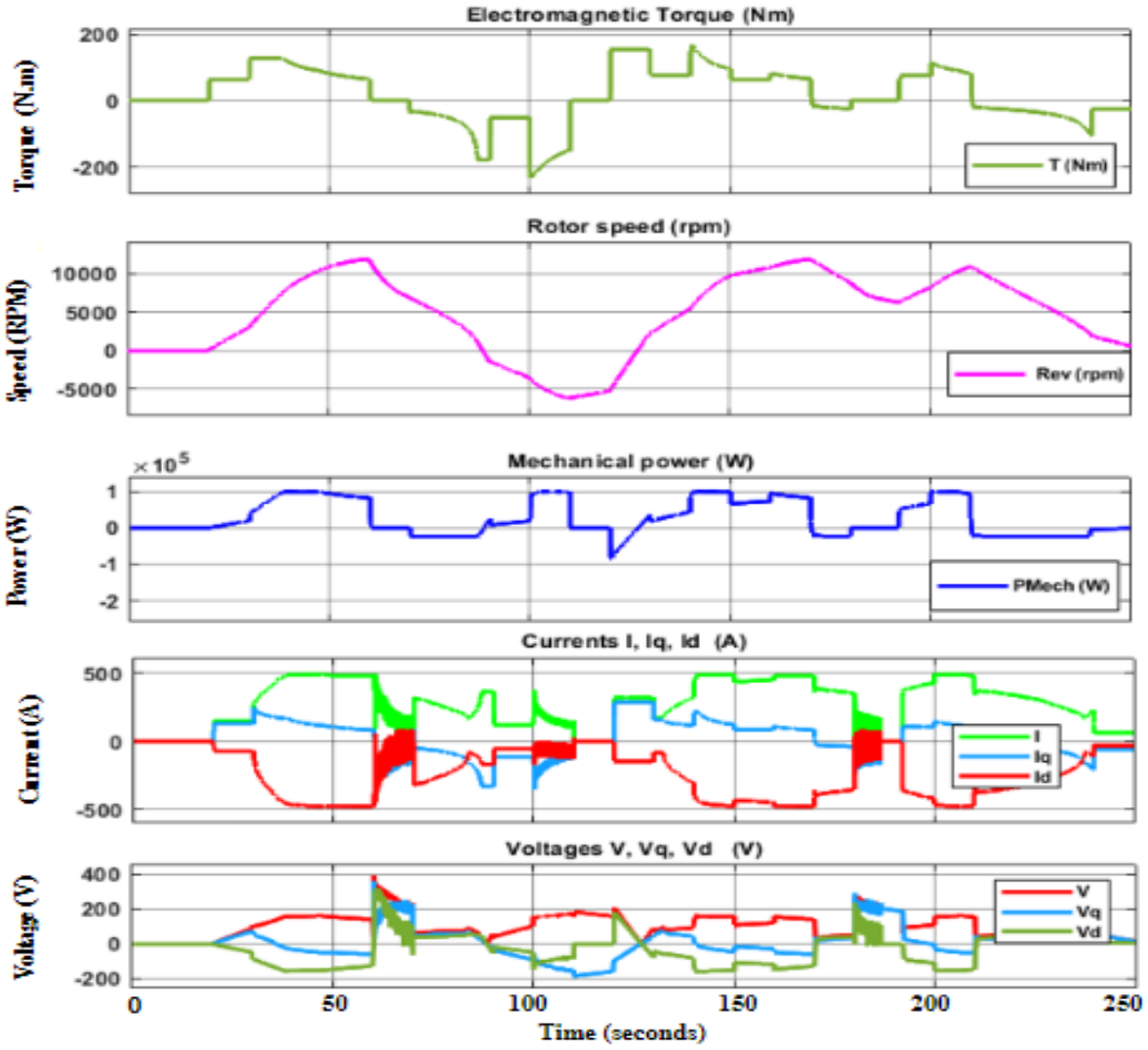

Figure 5.18: Electromagnetic torque, Rotor speed, Mechanical power, Current, Voltage

In conclusion, the proposed EMS responded swiftly to all three conditions (standstill, battery charging, battery discharging and use fuel cell only) determined by the fuel cell power, battery SOC and EV load demand. This is properly represented in Figure 5.7 where the EV load demand was less than the fuel cell power. This condition was recorded between 0 - 20 seconds, 70 – 80 seconds, 120 – 130 seconds, 170 – 180 seconds and 240 – 250 seconds respectively. However, between 0 – 20 seconds, the battery SOC increased from 80% to 80.24%. Again, when the fuel cell power (P_{fc}) was less than the EV load demand (P_{EM}), the battery SOC decreased. During this condition, the battery supplied between 5 kW and 28 kW depending on the EV load demand, fuel cell power and battery SOC. The battery SOC increased during deceleration and decreased during acceleration to further authenticate the effectiveness of the proposed EMS. The EV power demand was met at all times during its operation and the battery SOC was correctly adjusted throughout the drive cycle.

5.5 Experimental Validation using Typhoon HIL software

After the modelling and simulation of the FCHEV and results obtained, the study needed to validate the control system and the proposed energy management system that was implemented using a real time simulator. Hence, Typhoon HIL software referred to as “Typhoon HIL control center” is used to validate the functionality of the proposed EMS considering the practical constraints inherent in real-time simulators. The menu software platform that presents the Typhoon HIL software list of tools and functionalities which include a Schematic Editor, HIL SCADA, Typhoon Test IDE, Waveform Generator, Signal Analyser, Script Editor, Firmware Manager, Test and Calibration, LUT Extraction Tool are shown in Figure 5.19.

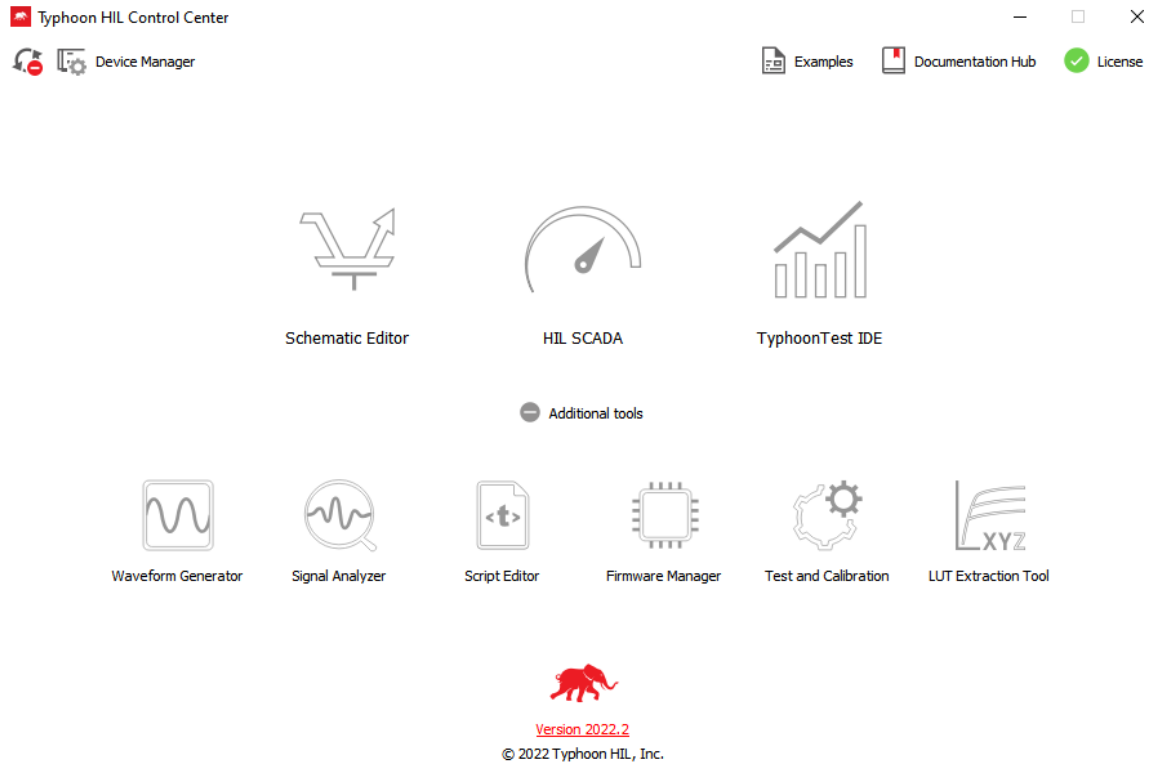

Figure 5.19: Typhoon HIL control center structure

5.5.1 Schematic Editor

The Schematic Editor is used to create high-fidelity models that emulate the real-time functions. It is used to implement models that can be represented in real-time and standard graphic representation of electrical systems as shown in Figure 5.20. This tool provides options such as model settings, design shortcut button, compilation button, initialisation script editor and regular file management features. Effective modelling of the system requires selecting an appropriate HIL device that will be used to emulate the model including, setting the simulation step and discretisation method for the solver. Again, on the bottom left of the Schematic Editor

page is the Library Explorer where all the components needed for the model is selected for implementation.

The electrical circuit part of the model is designed and displayed at the center of the page in black while the signal processing part is in blue as shown in Figure 5.20. In Typhoon HIL control center, the signal processing parts are used to represent a control which is implemented separately from the hardware controller but used to represent it in the model correctly. It can also be used to test the functionality of a controller design that requires pre-validation before simulation and it is a critical component in virtual mode simulation (Bastien, 2022).

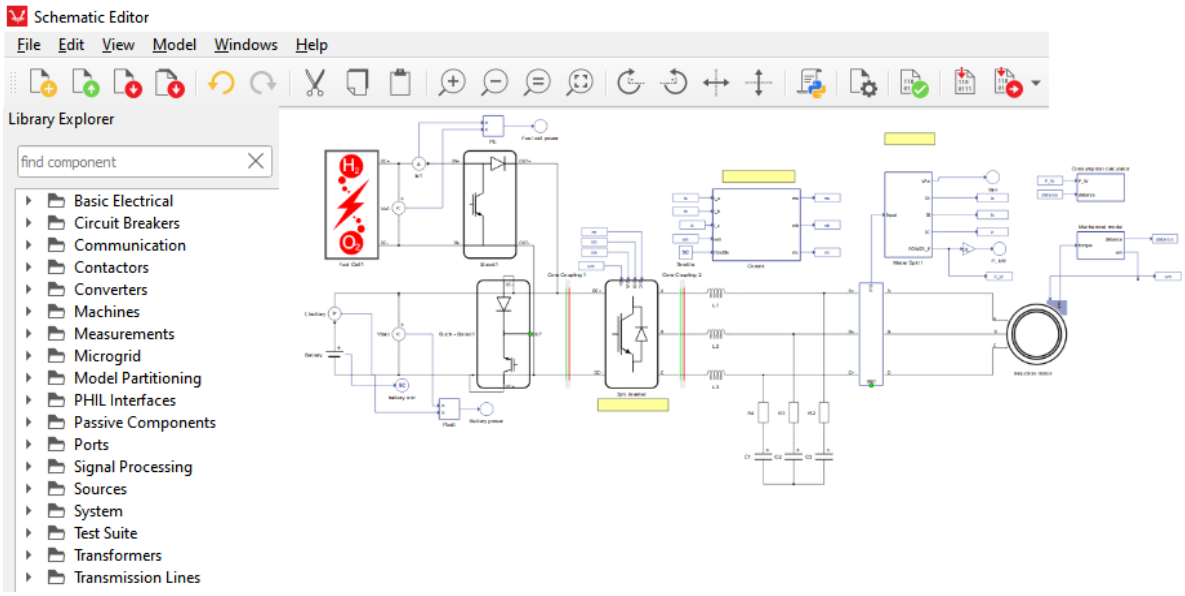

Figure 5.20: Schematic Editor

5.5.2 HIL SCADA

HIL SCADA is the software component of Typhoon HIL software that handles the simulation and evaluation of widgets with the capacity to display readings, activate relays, regulate control gains, control reference signals including many other functions (Bastien, 2022). HIL SCADA is basically implemented by first designing/creating and compiling the model in the Schematic Editor then opened in the HIL SCADA. Thereafter, the compiled model is loaded on the HIL device if it is connected to the computer or run virtually on the virtual HIL environment if not connected. When operating on the virtual HIL environment, the computer CPU will emulate the presence of the HIL device but does not receive signals from the actual hardware. Again, simulations implemented in the virtual HIL environment are not operated in real-time hence, the time step is significantly increased. However, a HIL device which is the hardware component of Typhoon HIL software, is required to execute HIL simulation and other operations. But the complexity of the model depends on the knowledge of the computer specification and capacity. Widgets are used to monitor and evaluate the simulation after

loading the model. The monitoring panels are user-friendly but not required to obtain simulation data rather automated testing including automatic data recovery is achievable using Typhoon Test IDE. This tool is not elaborated in this thesis because it was not used during the simulation.

In addition, prior to launching the simulation, the HIL SCADA permits the configuration of initial parameters of the model such as the battery state-of-charge, voltage value, status of relays, switching device, etc. The digital and analogue configuration of the signal output can also be controlled under the SCADA environment.

5.5.3 Hardware component

The simulation requires an additional computational device to enable it run in real-time which is basically an interface that is capable of transmitting signals between the software and hardware promptly with high fidelity. Hence, Typhoon HIL has included the HIL device as the hardware component. These comprises of FPGAs that permits real-time resolve of the model known as the execution speed of the device. The HIL device has inbuilt significant Deutsches Institut für Normung (DIN) connecters that has a number of pins with the capacity to send and receive signals in both analogue and digital format (Bastien, 2022).

A HIL device has 3 basic computing sections (Typhoon FPGA solver, System CPU, User CPU) as shown in Figure 5.21. The Typhoon FPGA solver is a dedicated multi-core processor responsible for accurate and precise simulation of all electrical domain models and the most vital processor in the HIL device. It is incharge of resolving the differential equations present in the electrical circuit at each junction of the model and establishes the simulation time step (Bastien, 2022; Trovao et al., 2017).

The System CPU is an all-purpose processor used to simulate low dynamic functionalities of specific electrical domain components or responsible for effective sharing of signals between communication protocol stacks. Lastly, the User CPU similar to System CPU is an all-purpose processor that implement sub-models made up of signal processing components. It also simulates all the non-electrical domain components such as thermal or mechanical models. In addition, the time step in a particular HIL device is determined by the number of User CPUs present and must be significantly higher than the simulation step (Bastien, 2022).

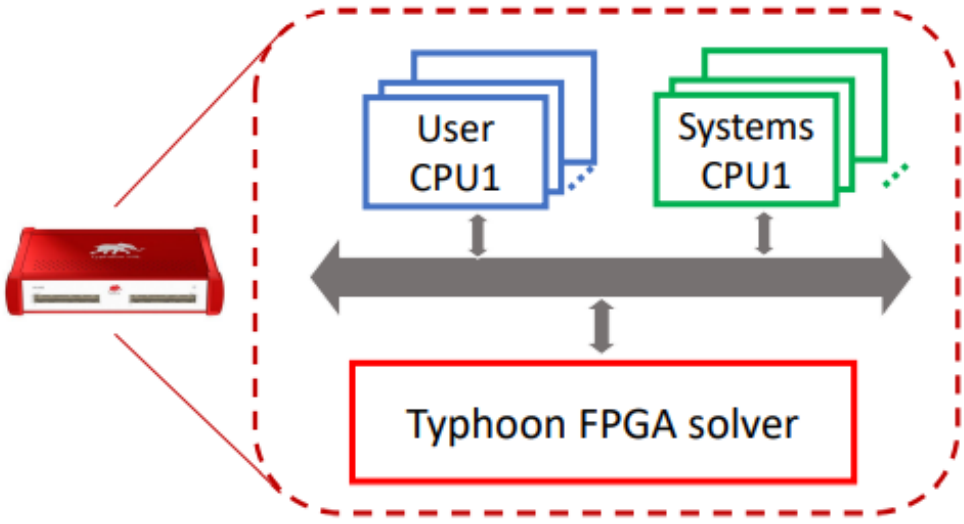

Figure 5.21: Typhoon HIL device processors architecture

The allocation of the model components based on responsible computing units and individual functionalities is shown in Figure 5.22. The blue section shows the User CPUs component such as original controller, the red section represents the System CPU components such as non-linear synchronous electrical motor and RMS measurements and the other section of the model (black) is supported by the FPGA solver.

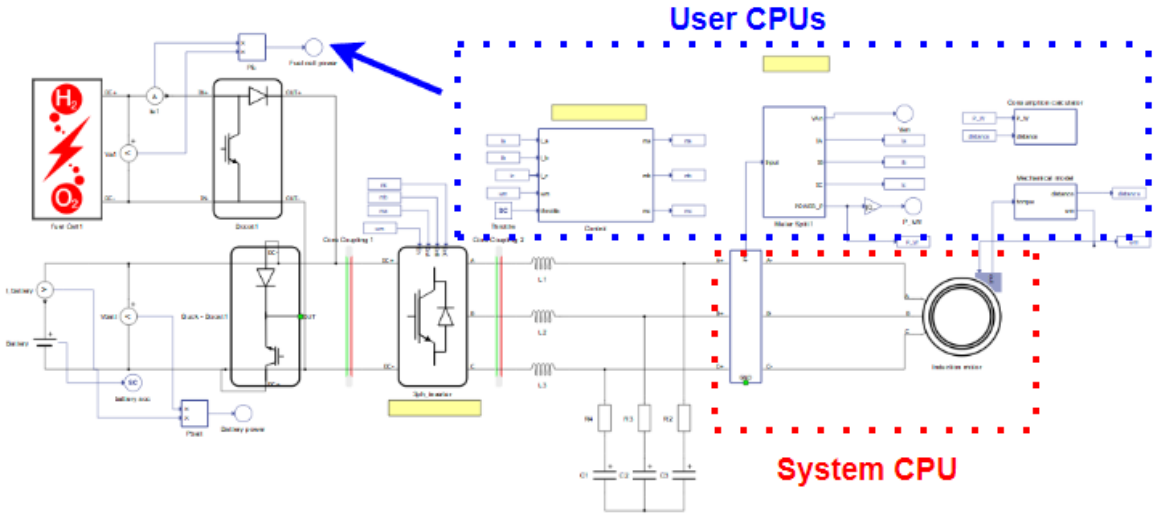

Figure 5.22: Components allocation according to responsible computing unit

5.5.4 Hardware-in-the-Loop (HIL) simulator

The primary purpose of implementing this model in Typhoon HIL using a high-power simulation is to validate the results obtained in the MATLAB/Simulink environment. This includes the supply system control loop of available energy sources, power demand and energy management system algorithm using the drive cycle requirement. The down-sampled step is adopted to validate the performance of the energy management system algorithm and the

effective hybridization of both energy sources (fuel cell, battery system). However, based on the down-sampled approach adopted previously, the hybridization of the EMS and the traction motor-drive are incorporated in the simulation and evaluated using a reduced method approach of power variation strategy (Trovão et al., 2014).

In this study, a high-power HIL platform is modelled to a reduced scale of 1:4 (25%) based on the full scale and time spread of the drive cycle while the DC bus was maintained at 400 V (+-20%). The maximum power demand exerted by the electric vehicle is 100 kW, the fuel cell stack maximum power was set at 100 kW, lithium-ion battery was maintained at 30 kW maximum power, but the state-of-charge was varied to evaluate the performance of the EMS. An electric motor is used to emulate the down-sampled powertrain load demand exerted by the electric vehicle as seen in (Trovão et al., 2014) and a bidirectional converter is used to track the reference power demand. However, the controller simulates in real-time the electric vehicle traction system to evaluate the DC bus reference power using a control loop of the inductor current.

Furthermore, the battery system is connected to a DC/DC bidirectional converter then to the DC bus at a switching frequency of 20 kHz. The levelling inductances of 1.35 mH are connected to the battery system (buck side) of the converter to ensure that ripples are reduced and a filter capacitor of 3300 µF is connected on the common DC bus. The electric vehicle model includes the connection logic, measurement devices, control elements and mechanical blocks using internal modulator of the three-phase inverter. In this study, the fuel cell power, battery power and its state-of-charge and the DC bus voltage are evaluated using the down-sampled drive, vehicle speed and corresponding electrical motor power. This is implemented in the Typhoon HIL schematic editor platform and evaluated in the HIL SCADA environment using the power availability and load demand as shown in Figure 5.23 and 5.24 respectively.

Figure 5.23: External structure of the FCHEV in Schematic Editor

The powertrain control module (PCM) of the FCHEV is implemented using an indirect field-oriented control (IFOC) method with regenerative abilities incorporated into it. This made it possible to recover power from the electric motor to charge the battery during regenerative braking because the electric motor functions as a generator during this period.

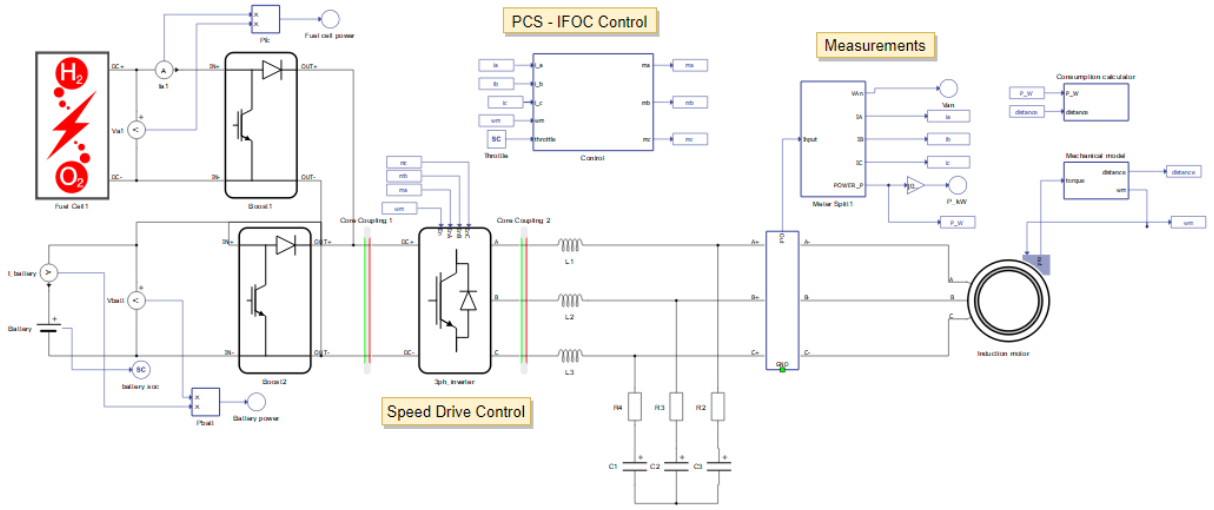

Figure 5.24: Internal configuration of the FCHEV model

5.5.5 EV powertrain control system (PCS)

The powertrain control system generates the PWM reference signals ma, mb and mc as presented in Figure 5.25. A three-phase measurement system is used to measure the active power and current flow from the inverter to the electrical motor and vice versa, depending on the load demand and power availability. The PCS uses a simplified IFOC dependent method to transform the measured three-phase current to equivalent direct current (i_d) and quadrature components (i_q) before using adjusted PI controllers. Furthermore, the machine

flux connected to the i_d and the EM torque linked to the i_q where, the electrical motor parameters, measured currents and rotor speed (RPM) are achieved using the IFOC method.

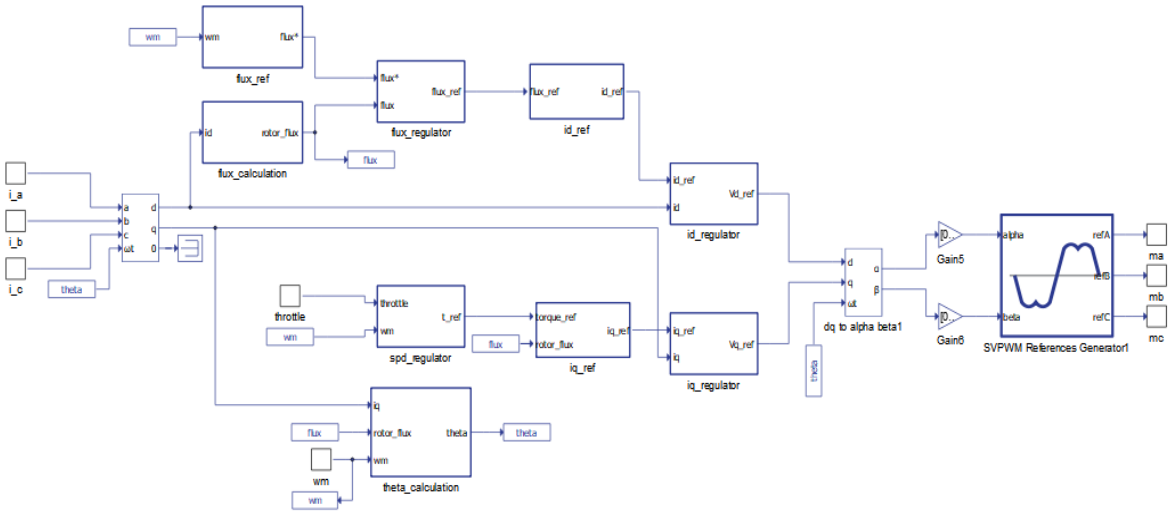

Figure 5.25: EV powertrain control system

5.5.6 Experimental results

The value of the fuel cell stack current, voltage and power output before the boost convert as modelled in Typhoon HIL schematic editor is shown in Figure 5.26. The current is approximately 285.8 A, voltage is 350 V and the power output is 100 kW as shown in (a), (b) and (c) respectively. These values correspond to the ones obtained in the MATLAB/Simulink environment.

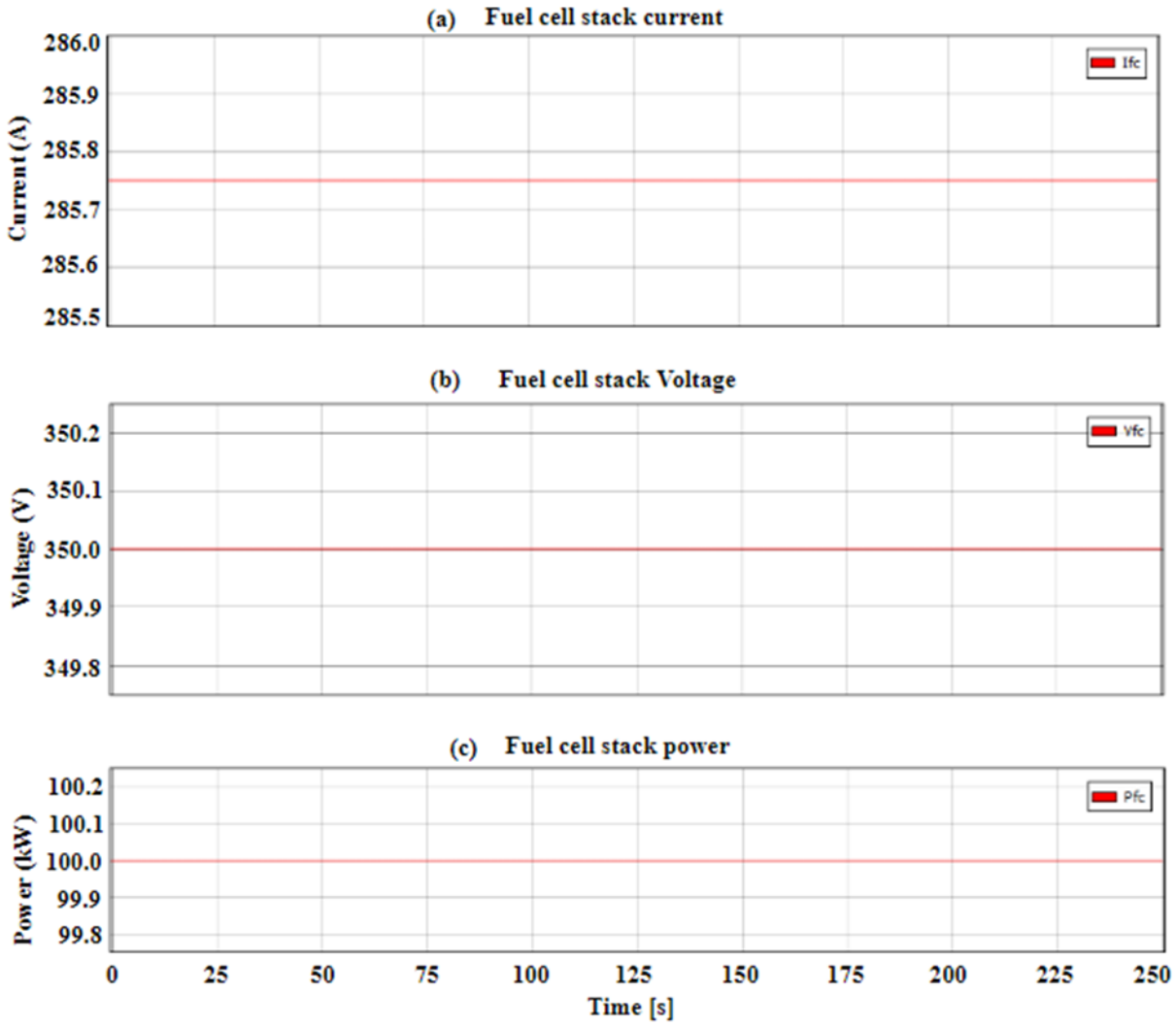

Figure 5.26: Fuel cell stack values obtained in Typhoon HIL SCADA

Furthermore, the fuel cell voltage is boosted to 400 V to meet the $V_{DC\text{-}bus}$ voltage. This is to ensure that the current is maintained at 250 A while the power output remained unchanged at 100 kW. The current, boosted voltage and power output of the fuel cell after the DC-DC boost converter is shown in Figure 5.27 (a), (b) and (c) respectively.

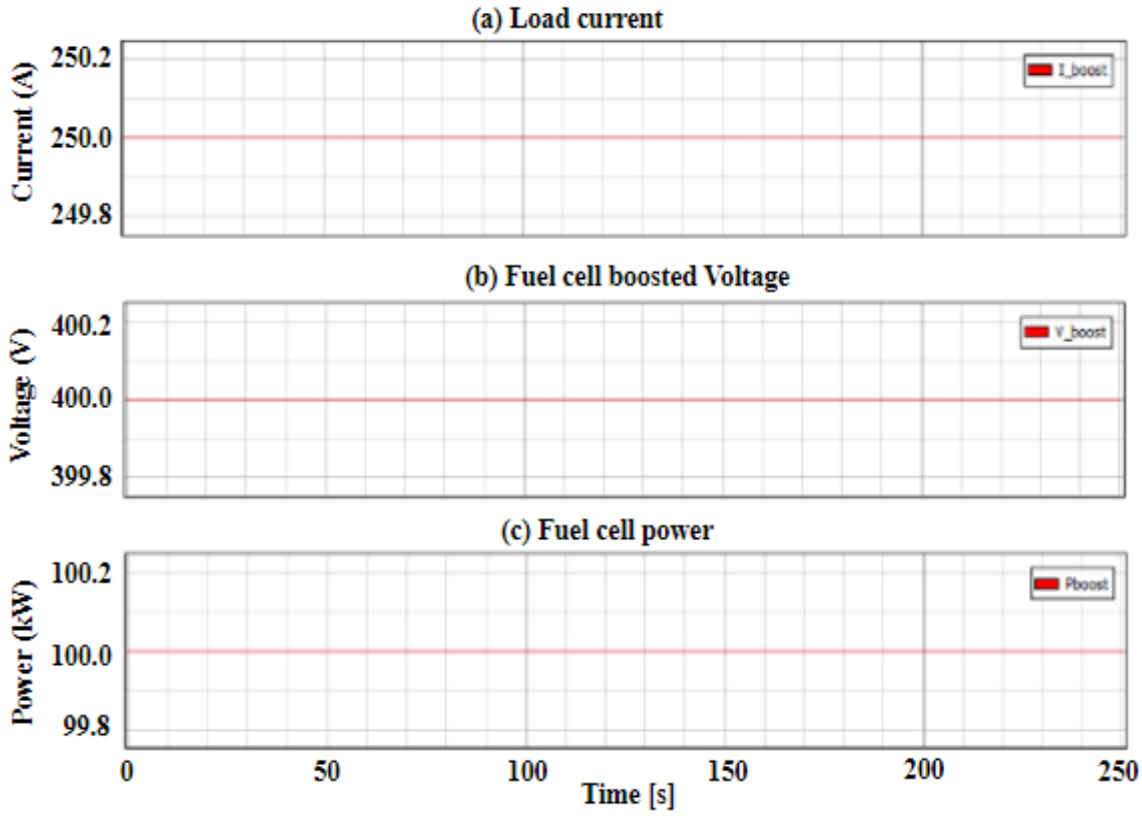

Figure 5.27: Fuel cell current, voltage, and power after the boost converter

5.5.6.1 EMS Performance at no load

The simulation started with an initial load demand of the electric vehicle at zero. During this period the fuel cell power is used to charge the battery system because its SOC is less or equal to 80%. The DC bus voltage is maintained at the nominal value of 400 V, the load demand from the EV powertrain is kept at zero and the battery SOC is approximately 80% as shown in Figure 5.28. This is an indication that the electric vehicle is on standstill while the fuel cell power is used to charge the battery system. In addition, the mechanical torque, electrical torque, and mechanical speed are all zero. When the electric vehicle is not in motion, the power demand is normally zero. These results corresponded with the ones presented in the MATLAB/Simulink environment in the previous sections. This is an indication that the closed-loop control system and the proposed energy management system responded accordingly.

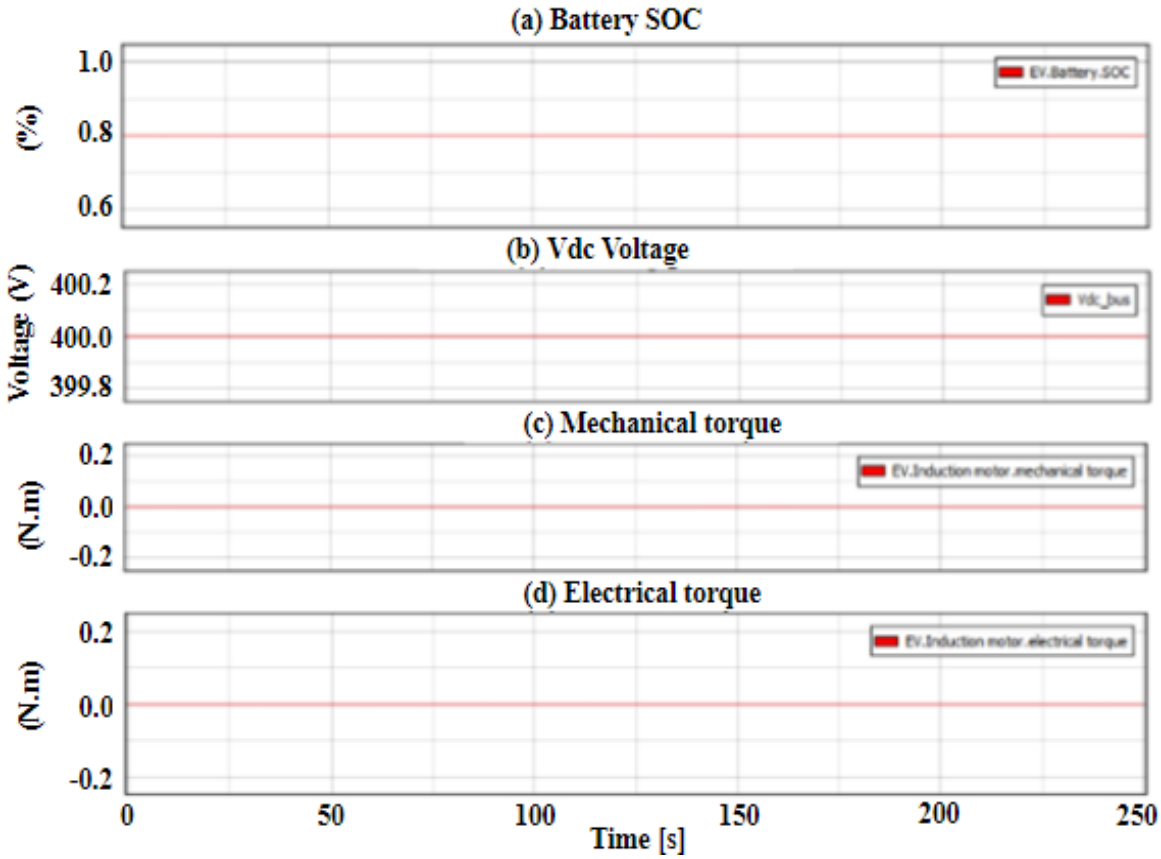

Figure 5.28: Experimental results when EV is on standstill

The phase current is around 250 A as shown in Figure 5.29 (a), while the phase voltages V_{an}, V_{Bn}, an V_{Cn} is around 400 V as shown in Figure 5.29 (b). These values are coherent with the calculations presented in chapter four. However, these values change based on the load demand informed by the drive cycle at any specific point, but the EMS ensures that enough power is always supplied to meet the load demand using both energy sources (fuel cell, battery system).

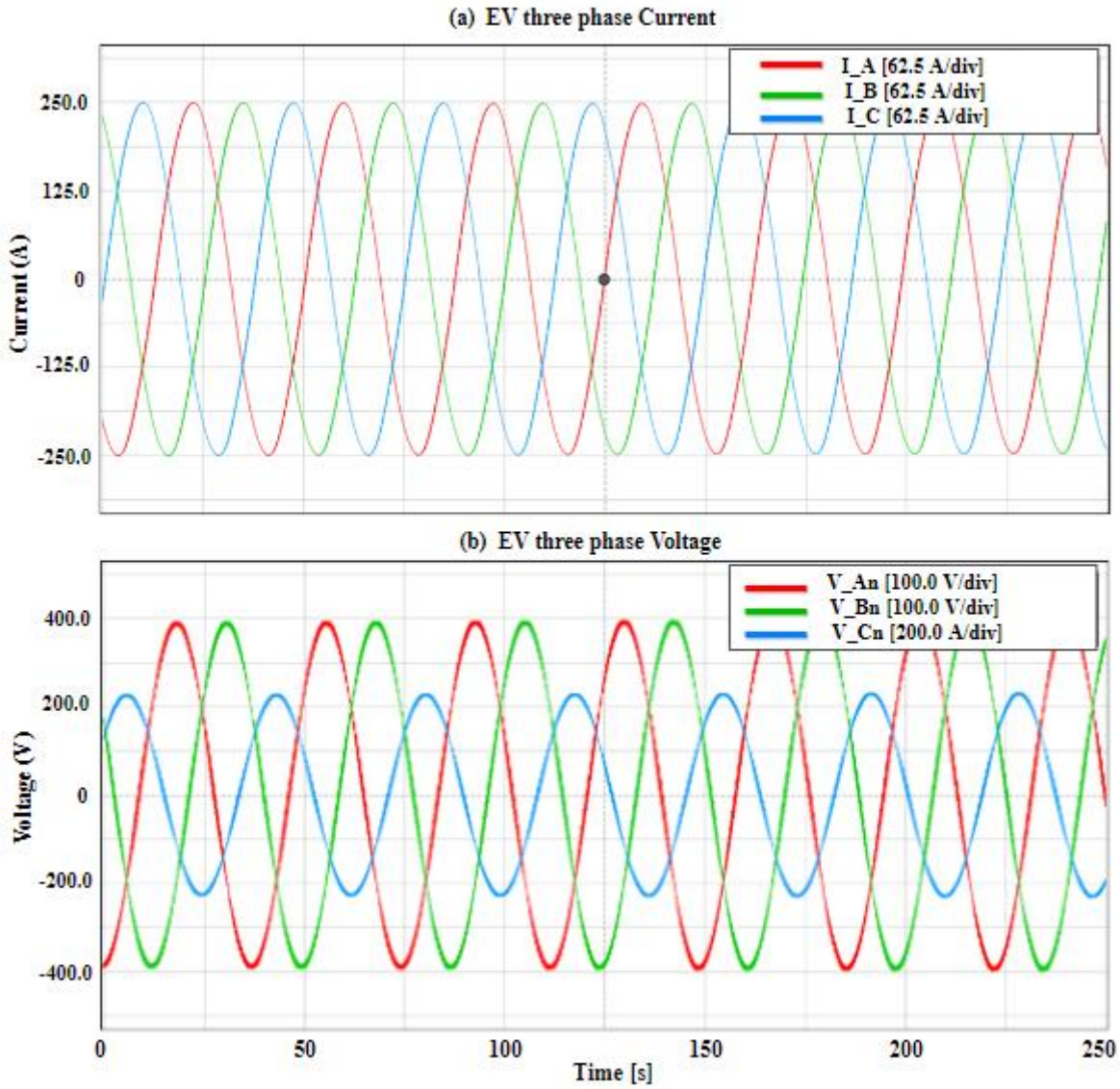

Figure 5.29: Phase current (a), Phase Voltage (b)

5.5.6.2 Power results for FTP-75 drive cycle under Typhoon HIL

The down-sampled drive cycle detail and corresponding Typhoon HIL experimental results scale approach are presented in Figure 5.30 and 5.31 respectively. The lithium-ion battery SOC was 80% at the beginning of the simulation as shown in Figure 5.32 but, the entire spectrum of the drive cycle showed various parts such as standstill, acceleration and deceleration of the FCHEV. This impacted significantly on the fuel cell behaviour which led to fluctuations in the battery output power and SOC. As previously indicated in chapter 4, the fuel cell is the primary source of power to the EV while the battery is expected to store and supply power to the EV according to the load demand. From the result shown in Figure 5.30, the EV was on standstill during the first 20 minutes and the load demand was zero but, the power out from the fuel cell was used to charge the battery pack to 80.24%. Thereafter, there was a

power demand of 20 kW due to acceleration (0 to 40 Km/hr in 10 seconds) of the EV during this period.

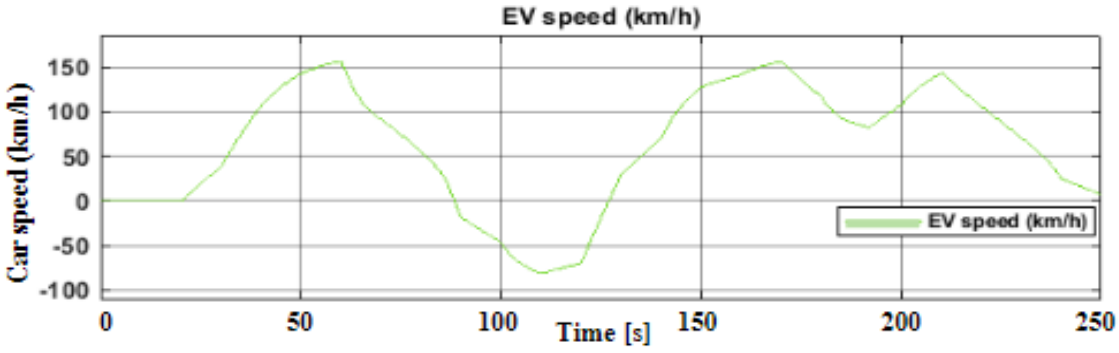

Figure 5.30: Down-sampled drive cycle

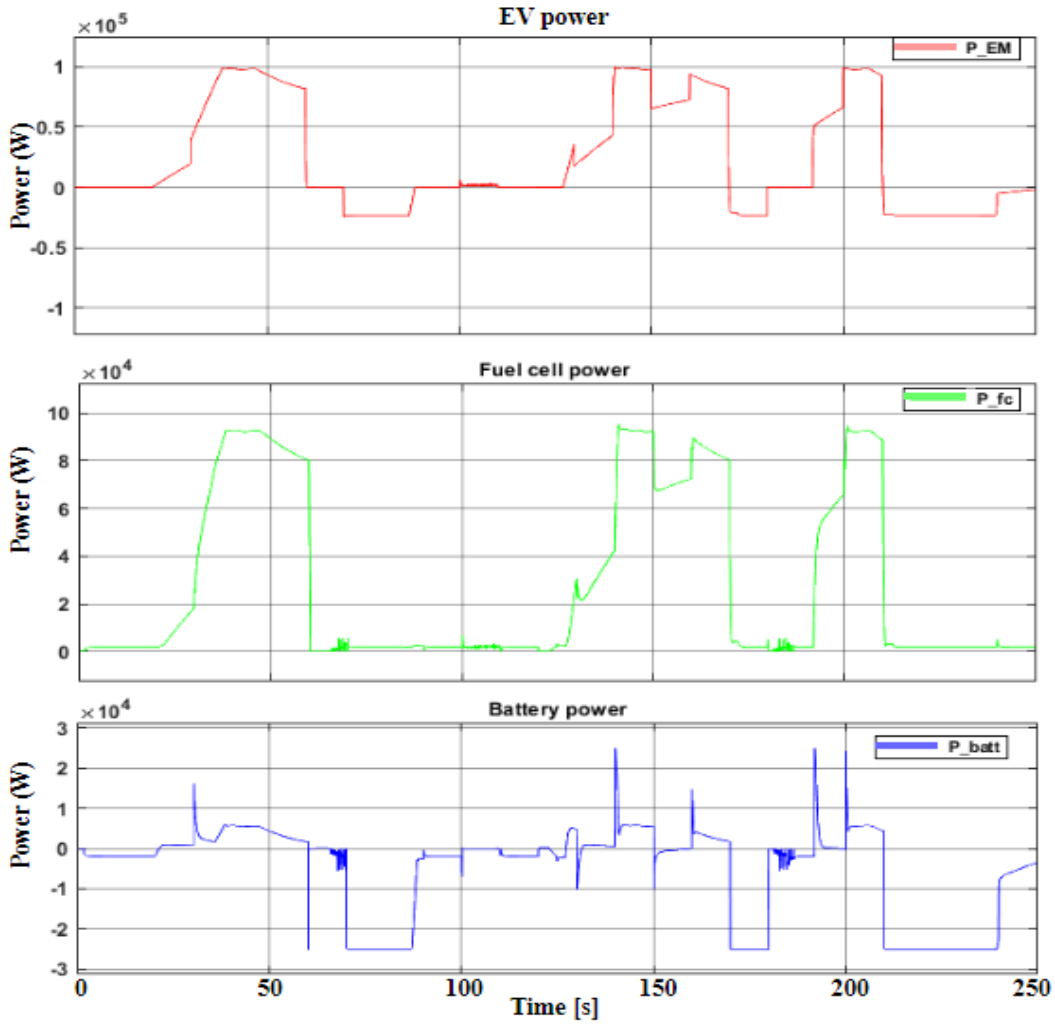

Figure 5.31: Experimental result under Typhoon HIL

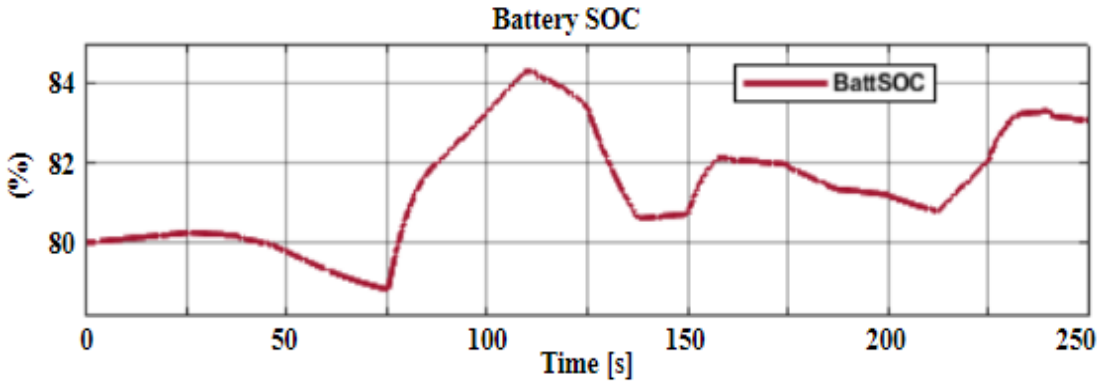

Figure 5.32: Battery SOC

The acceleration continued to 150 km/h in 55 seconds and the power demand increased to 100 kW. During this period, the fuel cell supplied 80 kW while the lithium-ion battery augmented the extra 20 kW. However, as the lithium-ion battery discharges during this first acceleration period, its SOC decreased and dropped to 79% from 80.24% obtained initially. Thereafter, the EV experienced a deceleration in the next 50 seconds and the fuel cell supply reduced but, as the lithium-ion battery SOC is still operating within its acceptable threshold region, the EMS triggers a controlled mechanism to charge the battery. Hence, the power from the fuel cell is used to charge the battery and its SOC increased to 84.1%. This was systematically executed to ensure that the battery is ready to supply enough power during the next acceleration. A new phase of acceleration (150 km/h) occurred in the next 60 seconds, where the EV power demand was increased to 100 kW which is greater than the fuel cell power supply of 75 kW at that moment and the battery augmented with 25 kW. This happened until somewhere around the 170 second mark and the battery SOC reduced to 82%. Furthermore, the EV speed dropped to 80 km/h in the next 30 seconds close to the 200 seconds mark. During this period, the fuel cell supplied enough power (around 85 kW) to meet the load demand and the battery was disconnected.

Again, from the result as it can be seen, the energy management system adjusted adequately to the two main power demands where the battery pack supplied enough power to augment the power supply from the fuel cell during high acceleration and high-power demand. This will help increase the lifecycle of the fuel cell and the battery system as aging is a major challenge in battery system. Furthermore, the result showed that the battery SOC reduced during acceleration and increased during deceleration respectively.

The results shown in Figure 5.31 are coherent with the ones obtained in the MATLAB/Simulink environment. This is an indication that the inner-control loop system and the proposed energy management system functioned effectively by maximising the impact of the battery system and charged it during deceleration periods (moments of less power demand). The EV power

demand was not compromised at any moment during its operation and the battery SOC was properly adjusted throughout the drive cycle.

5.6 Summary

This chapter presented the results obtained from both MATLAB/Simulink and Typhoon HIL software. The first was the result obtained from the MATLAB/Simulink environment and associated discussions on the meaning of the results. Thereafter, real-time Typhoon HIL results were presented with corresponding discussions. These were properly presented and discussed to demonstrate the effectiveness of the proposed EMS and its capacity to handle complex EV configuration.

CHAPTER 6: CONCLUSION AND FUTURE WORK

6.1 Conclusion

The primary purpose of this research was to develop an energy management system for a Fuel Cell Hybrid Electric Vehicle (FCHEV) because fuel cell has been seen as a dependable alternative that will solve environmental pollution associated with ICE vehicles and general transportation. This is because hydrogen fuel cell does not emit greenhouse gases from the vehicle and hence do not contribute to environmental pollution. Again, there is an urgent need to reduce fossil fuel-based vehicles as the global population continues to increase and rather operate more eco-friendly vehicles.

Unfortunately, hydrogen fuel cell vehicles have shown some setbacks such as slow response time, high cost, swift response during transient load and durability which has affected its competitiveness to ICE vehicles. Swift response is essential in vehicular applications and performance and in most instances considered more important than efficiency because responding swiftly to transient load demand and random electric load is critical for effective operation. Therefore, to mitigate fuel cell slow response time which is associated with its mass and heat balances within and outside the fuel cell, it is imperative to combine it with battery to form a hybrid power system. Available literature has shown that hybridisation of fuel cell and lithium-ion battery will reduce the harmful transitions that creates oxygen shortage, led to increased fuel cell efficiency and reduce vehicle weight.

Therefore, this research designed, modelled and analysed the effectiveness of an EMS for a fuel cell/lithium-ion hybrid electric vehicle by combining a DC-DC converter, a bidirectional converter and an inverter for a series connected configuration. The FCHEV comprises of a fuel cell, lithium-ion battery, converters, electric motor (permanent magnet synchronous motor) and vehicle body (chassis). The EMS ensured optimal power balancing between the primary source (fuel cell) and the secondary source (lithium-ion battery) by considering the slow response of the fuel cell but not underrating or miscalculating its transient capacity.

The EMS was first developed and implemented using state-flow logical programming language under the MATLAB/Simulink environment and validated in real-time using experimental result in Typhoon HIL software. The inner-control loop system of the lithium-ion battery and fuel cell stack linked with the overall EMS ensured a smart power sharing between both sources during standstill mode, deceleration mode and acceleration mode. The EMS ensured that the battery system utilised minimal power determined by the load demand and fuel cell power output. Furthermore, the real-time experimental results obtained in Typhoon HIL software showed a good performance following the results obtained in the MATLAB/Simulink environment using stateflow logical language. It was subjected to all three conditions (standstill, deceleration,

acceleration) using the drive cycle conditions and it proved very effective. Both results were similar and operated based on the vehicle load demand, fuel cell power and battery SOC. The battery responded swiftly and instantaneously during transient loads and was equally recharged during deceleration. Power was effectively shared between the fuel cell and lithium-ion battery during acceleration which ensured optimal operation of both sources.

6.2 Recommendations and future work

Further research should concentrate on the following:

- The EMS should be expanded to include a combination of hybrid power sources such as: fuel cell-supercapacitor, fuel cell-battery-supercapacitor or battery-supercapacitor.
- Available literatures have shown that the battery lifespan, cost of installation, mass and discharge rate are critical factors in selecting any battery for vehicular applications. Furthermore, battery capacity, chemistry and technology have significant impact on the response time and the amount of power it can supply therefore, fuel cell should be combined with other types of battery chemistry such as lead-acid, Nickel Cadmium, Alkaline battery, Carbon Zinc battery, Silver Oxide battery, Zinc Air battery.
- The proposed EMS should be tested on trains, trucks and tricycles.
- To extract long term benefits of the proposed EMS, research should be expanded to implement same EMS on other hybrid EV topologies such as parallel topology, double parallel and series-parallel topology.
- Transient performances and control restrictions are common with PEMFC because it depends on the air flow system for effective operation hence, other fuel cell technologies should be investigated with specific focus on the air supply system because it affects the EV size, weight and the overall fuel cell performance.
- The drive cycle determines the amount of power demand by the vehicle hence, the EMS should be implemented on another drive cycle

REFERENCES

Abd El Monem, A.A., Azmy, A.M. & Mahmoud, S.A. 2014. Effect of Process Parameters on the Dynamic Behavior of Polymer Electrolyte Membrane Fuel Cells for Electric Vehicle Applications. *Ain Shams Engineering Journal*, 5(1): 75–84. http://dx.doi.org/10.1016/j.asej.2013.05.001.

Alharbi, A. 2013. *Impact of Plug-in Electric Vehicle Battery Charging on a Distribution System Based on Real-Time Digital Simulator*. University of Tennessee at Chattanooga, Chattanooga, Tennessee.

Alloui, H., Achour, Y., Marouani, K. & Becherif, M. 2015. Energy Management Based on Frequency Decoupling: Experimental Results with Fuel Cell-Electric Vehicle Emulator. *IEEE Vehicular Technology Conference*, 2015: 1–5.

Alloui, H., Becherif, M. & Marouani, K. 2013. Modelling and Frequency Separation Energy Management of Fuel Cell-Battery Hybrid Sources System for Hybrid Electric Vehicle. In *21st Mediterranean Conference on Control and Automation, MED*. Crete, Greece: IEEE: 646–651.

Arabul, F.K., Senol, I., Arabul, A.Y. & Boynuegri, A.R. 2015. Providing Energy Management of a Fuel Cell-Battery Hybrid Electric Vehicle. *International Journal of Electrical, Computer, Energetic, Electronic and Communication Engineering*, 9(8): 975–979.

Arcos-Vargas, A. 2021. *Green Energy and Technology The Role of the Electric Vehicle in the Energy Transition : A Multidimensional Approach*. A. Arcos-Vargas, ed. Seville, Spain: Springer. http://www.springer.com/series/8059.

Ates, Y., Erdinc, O., Uzunoglu, M. & Vural, B. 2010. Energy Management of an FC/UC Hybrid Vehicular Power System Using a Combined Neural Network-wavelet Transform Based Strategy. *International Journal of Hydrogen Energy*, 35(2): 774–783. http://dx.doi.org/10.1016/j.ijhydene.2009.11.021.

Azidin, F.A. 2016. *Energy Mangement System for Three-Wheel Light Electric Vehicle using Multi-Sources Enrgy Models*. Universiti Kebangsaan Malaysia Bangi.

Bastien, E. 2022. *Digital twin of a power converter : using hardware-in-the-loop for the design and evaluation of digital control algorithms*. UNIVERSITÉ DE LIÈGE FACULTÉ DES SCIENCES APPLIQUÉES.

Becherif, M., Claude, F., Hervier, T. & Boulon, L. 2015. Multi-stack Fuel Cells Powering a Vehicle. *Energy Procedia*, 74: 308–319. http://dx.doi.org/10.1016/j.egypro.2015.07.613.

Behdani, A. & Naseh, M.R. 2017. Power Management and Nonlinear Control of a Fuel Cell–Supercapacitor Hybrid Automotive Vehicle with Working Condition Algorithm. *International Journal of Hydrogen Energy*, 42(38): 24347–24357. http://dx.doi.org/10.1016/j.ijhydene.2017.07.197.

Bendjedia, B., Alloui, H., Rizoug, N., Boukhnifer, M., Bouchafaa, F. & Benbouzid, M.E. 2016. Sizing and Energy Management Strategy for hybrid FC/Battery Electric Vehicle. In *IECON Proceedings (Industrial Electronics Conference)*. Florence, Italy: IEEE: 2111–2116.

Bendjedia, B., Rizoug, N., Boukhnifer, M. & Bouchafaa, F. 2017. Hybrid Fuel Cell/Battery Source Sizing and Energy Management for Automotive Applications. *IFAC-PapersOnLine*, 50(1): 4745–4750. https://doi.org/10.1016/j.ifacol.2017.08.869.

Benyahia, N., Denoun, H., Badji, A., Zaouia, M., Rekioua, T., Benamrouche, N. & Rekioua, D. 2014. MPPT Controller for an Interleaved Boost dc-dc Converter used in Fuel Cell Electric Vehicles. *International Journal of Hydrogen Energy*, 39(27): 15196–15205. http://dx.doi.org/10.1016/j.ijhydene.2014.03.185.

Berrueta, A., Ursua, A., Martin, I.S., Eftekhari, A. & Sanchis, P. 2019. Supercapacitors: Electrical Characteristics, Modeling, Applications, and Future Trends. *IEEE Access*, 7: 50869–50896.

Bidault, F. & Middleton, P.H. 2012. Alkaline Fuel Cells. Theory and Application. In *Comprehensive Renewable Energy*. Elsevier Ltd: 179–202.

Böhme, T.J. & Benjamin, F. 2017. *Hybrid Systems , Optimal Control and Hybrid Vehicles*. M. J. Grimble & M. A. Johnson, eds. Cham, Switzerland: Springer Nature.

Borkow, G. & Gabbay, J. 2018. *Advances in Power Systems and Energy Management*. http://link.springer.com/10.1007/978-981-10-4394-9.

Carnevali, M.L.S. 2017. *Modelling and Control of PEM Fuel Cells*. Universitat Politecnica de Catalunya. https://mat-web.upc.edu/people/carles.batlle/fitxers/thesis_MLSC.pdf.

Chaibet, A., Boukhnifer, M., Ouddah, N. & Monmasson, E. 2020. Experimental Sensorless Control of Switched Reluctance Motor for Electrical Powertrain System. *Energies*, 13(12): 1–15.

Chang, W.-Y. 2013. The State of Charge Estimating Methods for Battery: A Review. *ISRN Applied Mathematics*, 2013(1): 1–7.

Choudhury, S.R. 1989. Phosphoric Acid Fuel Cell Technology. , 229(1).

Corral-Vega, P.J., García-Triviño, P. & Fernández-Ramírez, L.M. 2019. Design, Modelling, Control and Techno-Economic Evaluation of a Fuel Cell/Supercapacitors Powered Container Crane. *Energy*, 186.

Das, H.S., Tan, C.W. & Yatim, A.H.M. 2017. Fuel Cell Hybrid Electric Vehicles: A Review on Power Conditioning Units and Topologies. *Renewable and Sustainable Energy Reviews*, 76(March): 268–291. http://dx.doi.org/10.1016/j.rser.2017.03.056.

Du, Y., Zhou, X., Bai, S., Lukic, S. & Huang, A. 2010. Review of Non-Isolated Bi-Directional DC-DC Converters for Plug-in Hybrid Electric Vehicle Charge Station Application at Municipal Parking Decks. *Conference Proceedings - IEEE Applied Power Electronics Conference and Exposition - APEC*, (1): 1145–1151.

Dusmez, S. & Khaligh, A. 2014. A Supervisory Power-Splitting approach for a New Ultracapacitor-Battery Vehicle Deploying two Propulsion Machines. *IEEE Transactions on Industrial Informatics*, 10(3): 1960–1971.

EG&G Technical Services, I.U. 2004. *Cell components*. Seventh. Morgantown, West Virginia: U.S. Department of Energy, Office of Fossil Energy National Energy Technology Laboratory.

Ehsani, M., Gao, Y. & Emadi, A. 2010. *Modern Electric, Hybrid Electric, and Fuel Cell Vehicles*. Second. New York: CRC Press, Taylor & Francis Group.

Ehsani, M., Gao, Y., Longo, S. & Ebrahimi, K. 2018. *Modern Electric, Hybrid Electric, and Fuel Cell Vehicles*. Third. London: CRC Press, Taylor & Francis Group.

Erensoy, S.C. 2018. *Simulation and Energy Management Strategy Development for a Fuel Cell Hybrid Electric Powertrain of a Zero-Emission Boat*. Tecnico Lisboa.

Fan, B.S. 2011. *Multidisciplinary Optimization of Hybrid Electric Vehicles : Component Sizing and Power Management Logic*. University of Waterloo. http://resonance.uwaterloo.ca/p/alumni/thesis/b_fan_T.pdf.

Felgenhauer, M., Witzmann, I.R., Felgenhauer, M. & Witzmann, I.R. 2016. *Battery and Fuel Cell Electric Vehicles in the Context of the Energy Transition*. Technical University of Munich. https://mediatum.ub.tum.de/doc/1327434/document.pdf%0Ahttps://mediatum.ub.tum.de/1327434.

Fernandez, A.M.I., Kandidayeni, M., Boulon, L. & Chaoui, H. 2020. An Adaptive State Machine Based Energy Management Strategy for a Multi-Stack Fuel Cell Hybrid Electric Vehicle.

IEEE Transactions on Vehicular Technology, 69(1): 220–234.

Feroldi, D. 2012. Energy Management Strategies for Fuel Cell Hybrid Systems. *Green Energy and Technology*, 87: 233–258.

Fletcher, T. 2017. *Optimal Energy Management Strategy for a Fuel Cell Hybrid Electric Vehicle*. Loughborough University. https://dspace.lboro.ac.uk/2134/25567.

Fletcher, T., Thring, R. & Watkinson, M. 2016. An Energy Management Strategy to Concurrently Optimise Fuel Consumption & PEM Fuel Cell Lifetime in a Hybrid Vehicle. *International Journal of Hydrogen Energy*, 41(46): 21503–21515. http://dx.doi.org/10.1016/j.ijhydene.2016.08.157.

Fonseca, R.N. da. 2013. *Optimization of the Sizing and Energy Management Strategy for a Hybrid Fuel Cell Vehicle Including Fuel Cell Dynamics and Durability Constraints*. Institut National des Sciences Appliquées de Lyon-INSA Lyon.

Gang, S., Yuanwei, J., Aidong, X. & Jia, M. 2006. Study and Simulation of Based-Fuzzy-Logic Parallel Hybrid Electric Vehicles Control Strategy. In *International Conference on Intelligent Systems Design and Applications*. Jinan, China: IEEE, Computer Society: 280–284.

Gao, D., Jin, Z., Liu, J. & Ouyang, M. 2016. An interleaved step-up/step-down converter for fuel cell vehicle applications. *International Journal of Hydrogen Energy*, 41(47): 22422–22432. http://dx.doi.org/10.1016/j.ijhydene.2016.09.171.

Gao, D., Jin, Z., Zhang, J., Li, J. & Ouyang, M. 2016. Comparative Study of Two Different Powertrains for a Fuel Cell Hybrid Bus. *Journal of Power Sources*, 319: 9–18. http://dx.doi.org/10.1016/j.jpowsour.2016.04.046.

Gao, J., Li, M., Hu, Y., Chen, H. & Ma, Y. 2019. Challenges and Developments of Automotive Fuel cell hybrid Power System and Control. *Science China Information Sciences*, 62(5): 2–26.

George, S.S. 2018. *A Modular Multi-Level Converter for Energy Management of Hybrid Storage System in Electric Vehicles*. San Jose State University.

Gielniak, M.J. & Shen, Z.J. 2004. Power Management Strategy Based on Game Theory for Fuel Cell Hybrid Electric Vehicles. In *IEEE Vehicular Technology Conference*. Los Angeles, CA, USA.: IEEE: 4422–4426.

Gou, B., Ki Na, W. & Diong, B. 2010. *Fuel Cells: Modelling, Control, and Applications*. London:

CRC Press, Taylor & Francis Group.

Grammatico, S., Balluchi, A. & Cosoli, E. 2010. A Series-Parallel Hybrid Electric Powertrain for Industrial Vehicles. *2010 IEEE Vehicle Power and Propulsion Conference, VPPC 2010*: 0–5.

Greeshma, M.S. & Nayana, J. 2016. Isolated Bidirectional Dc-Dc Converters in Fuel Cell Electric Vehicle. *International Research Journal of Engineering and Technology (IRJET)*, 3(5): 1719–1724.

Han, J., Charpentier, J.F. & Tang, T. 2014. An Energy Management System of a Fuel Cell/Battery Hybrid Boat. *Energies*, 7(5): 2799–2820.

Herb, F., Akula, P.R., Trivedi, K., Jandhyala, L., Narayana, A. & Wöhr, M. 2013. Theoretical Analysis of Energy Management Strategies for Fuel Cell Electric Vehicle with respect to Fuel Cell and Battery Aging. In *World Electric Vehicle Symposium and Exhibition, EVS 27*. Barcelona, Spain: EVS27: 1–9.

Hernandez, J.C., Mira, M.C., Sen, G., Thomsen, O.C. & Andersen, M.A.E. 2014. Wide Operating Voltage Range Fuel Cell Battery Charger. *Elektronika ir Elektrotechnika*, 20(5): 97–103.

Hosseini, S.E. & Butler, B. 2020. An Overview of Development and Challenges in Hydrogen Powered Vehicles. *International Journal of Green Energy*, 17(1): 13–37. https://doi.org/10.1080/15435075.2019.1685999.

Hosseinzadeh, E. 2012. *Modeling and Design of Hybrid PEM Fuel Cell Systems for Lift Trucks*. Technical University of Denmark.

Howell, J. 2014. Aerodynamic drag in a windy environment. In *International Vehicle Aerodynamics Conference*. Loughborough, UK: Elsevier: 1–200.

Hu, J., Jiang, X., Jia, M. & Zheng, Y. 2018. Energy Management Strategy for the Hybrid Energy Storage System of Pure Electric Vehicle Considering Traffic Information. *Applied Sciences (Switzerland)*, 8(8).

IEA. 2020. *Global EV Outlook 2020*.

IEA. 2022. *Global EV Outlook 2022 Securing supplies for an electric future*. https://iea.blob.core.windows.net/assets/ad8fb04c-4f75-42fc-973a-6e54c8a4449a/GlobalElectricVehicleOutlook2022.pdf.

Jain, S. & Kumar, L. 2018. *Power Electronics Handbook*. Fourth. M. Rashid, ed. Oxford, United Kingdom: Butterworth-Heinemann. http://publications.lib.chalmers.se/records/fulltext/245180/245180.pdf%0Ahttps://hdl.handle.net/20.500.12380/245180%0Ahttp://dx.doi.org/10.1016/j.jsames.2011.03.003%0Ahttps://doi.org/10.1016/j.gr.2017.08.001%0Ahttp://dx.doi.org/10.1016/j.precamres.2014.12.

Jeon, B. 2020. *Energy Management System in Naval Submarines*. Arizona State University.

Kamarudin, S.K., Achmad, F. & Daud, W.R.W. 2009. Overview on the Application of Direct Methanol Fuel Cell (DMFC) for Portable Electronic Devices. *International Journal of Hydrogen Energy*, 34(16): 6902–6916. http://dx.doi.org/10.1016/j.ijhydene.2009.06.013.

Khayyer, P. 2008. *Design and Performance Analysis of Electric Vehicles Fed by Multiple Fuel Cells*. West Virginia University.

Kolli, A., Gaillard, A., De Bernardinis, A., Bethoux, O., Hissel, D. & Khatir, Z. 2015. A Review on DC/DC Converter Architectures for Power Fuel Cell Applications. *Energy Conversion and Management*, 105: 716–730. http://dx.doi.org/10.1016/j.enconman.2015.07.060.

Koot, M., Kessels, J.T.B.A., Jager, B. de, Heemels, W.P.M.H., Bosch, P.P.J. van den & Steinbuch, M. 2015. Energy Management Strategies for Vehicular Electric Power Systems. *IEEE Transactions on Vehicular Technology*, 54(3): 771–782.

Li, C.Y. & Liu, G.P. 2009. Optimal Fuzzy Power Control and Management of Fuel Cell/Battery Hybrid Vehicles. *Journal of Power Sources*, 192(2): 525–533.

Lorf, C.F. 2014. *Optimum Battery Capacity for Electric Vehicles with Particular Focus on Battery Degradation*. Imperial College London.

Lu, J. 2013. *Modeling and Control of Proton Exchange Membrane Fuel Cell*. James Cook University.

Luta, D.N. 2019. *An Energy Management System for a Hybrid Reversible Fuel cell / Supercapacitor in a 100 % Renewable Power System*. Cape Peninsula University of Technology.

Manoharan, Y., Hosseini, S.E., Butler, B., Alzhahrani, H., Senior, B.T.F., Ashuri, T. & Krohn, J. 2019. Hydrogen Fuel Cell Vehicles; Current Status and Future Prospect. *Applied Sciences (Switzerland)*, 9(11): 2–17.

Mehmeti, A., Santoni, F. & Della, M. 2017. Life Cycle Assessment of Molten Carbonate Fuel Cells : State of the Art and Strategies for the Future. *Journal of Power Sources*,

308(January 2016): 97–108. http://dx.doi.org/10.1016/j.jpowsour.2015.12.023.

Miao, Y., Hynan, P., Von Jouanne, A. & Yokochi, A. 2019. Current li-ion battery technologies in electric vehicles and opportunities for advancements. *Energies*, 12(6).

Minh, N.Q. 2004. Solid Oxide Fuel Cell Technology — Features and Applications. , 174: 271–277.

Mkhize, S.M. 2019. *Impacts and Solutions on Vehicle to Grid (V2G) Infrastructure*. University of KwaZulu-Natal.

Mokrani, Z., Rekioua, D., Mebarki, N. & Rekioua, T. 2016. Energy Management of Battery-PEM Fuel Cells Hybrid Energy Storage System for Electric Vehicles. , (November): 1–70.

Mokrani, Z., Rekioua, D. & Rekioua, T. 2014. Modeling, Control and Power Management of Hybrid Photovoltaic Fuel Cells with Battery Bank Supplying Electric Vehicle. *International Journal of Hydrogen Energy*, 39(27): 15178–15187. http://dx.doi.org/10.1016/j.ijhydene.2014.03.215.

Noel, L., Zarazua de Rubens, G., Kester, J., Sovacool, B.K., Noel, L., Zarazua de Rubens, G., Kester, J. & Sovacool, B.K. 2019. *Vehicle-to-Grid, A Sociotechnical Transition Beyond Electric Mobility*. D. Elliott & G. Wood, eds. Stirling, UK: Palgrave macmillan.

Odeim, F., Roes, J. & Heinzel, A. 2015. Power Management Optimization of an Experimental Fuel Cell/Battery/Supercapacitor Hybrid System. *Energies*, 8(7): 6302–6327.

Okba, K. 2015. *Control and Energy Management of an Electrical Vehicle*. Mohamed Khider University of Biskra.

Ong, B.C., Kamarudin, S.K. & Basri, S. 2017. Direct Liquid Fuel Cells: A Review. *International Journal of Hydrogen Energy*, 42(15): 10142–10157. http://dx.doi.org/10.1016/j.ijhydene.2017.01.117.

Opila, D.F., Wang, X., McGee, R., Gillespie, R.B., Cook, J.A. & Grizzle, J.W. 2014. Real-world Robustness for Hybrid Vehicle Optimal Energy Management Strategies Incorporating Drivability Metrics. *Journal of Dynamic Systems, Measurement and Control, Transactions of the ASME*, 136(6).

Panchal, S. 2014. *Impact of Vehicle Charge and Discharge Cycles on the Thermal Characteristics of Lithium-ion Batteries*. University of Waterloo.

Panday, A. & Bansal, H.O. 2014. A Review of Optimal Energy Management Strategies for

Hybrid Electric Vehicle. *International Journal of Vehicular Technology*, 2014: 1–18.

Panday, A. & Bansal, H.O. 2016. Energy Management Strategy for Hybrid Electric Vehicles Using Genetic Algorithm. *Journal of Renewable and Sustainable Energy*, 8(015701). http://dx.doi.org/10.1063/1.4938552.

Patel, N., Bhoi, A.K., Padmanaban, S. & Holm-Nielsen, J.B. 2021. *Electric vehicles*. N. Patel, A. K. Bhoi, S. Padmanaban, & J. B. Holm-Nielsen, eds. Gateway East, Singapore: Springer Nature.

Pittini, R. 2014. *High Efficiency Reversible Fuel Cell Power Converter*. Technical University of Denmark.

Placca, L. & Kouta, R. 2011. Fault Tree Analysis for PEM Fuel Cell Degradation Process Modelling. *International Journal of Hydrogen Energy*, 36(19): 12393–12405. http://dx.doi.org/10.1016/j.ijhydene.2011.06.093.

Pukrushpan, J.T., Stefanopoulou, A.G. & Peng, H. 2006. *Control of Fuel Cell Power Systems": Principles, Modeling, Analysis and Feedback Design*. London: Springer. http://scholar.google.com/scholar?hl=en&btnG=Search&q=intitle:Advances+in+Industrial+Control+-+Practical+PID+Control#9.

Rosario, L. 2007. *Power and Energy Management of Multiple Energy Etorage Systems in Electric Vehicles*. Cranfield University.

Roscher, M.A., Assfalg, J. & Bohlen, O.S. 2011. Detection of Utilizable Capacity Deterioration in Battery Systems. *IEEE Transactions on Vehicular Technology*, 60(1): 98–103.

Rousseau, A., Sharer, P. & Ahluwalia, R. 2004. *Energy Storage Requirements for Fuel Cell Vehicles*.

Sahu, A.V. 2017. *Exploring the Role of Battery Electric and Fuel Cell Electric Vehicles in a Sustainable Smart City*. Delft University of Technology.

Salet, T. 2018. *Fuel cell and Battery Electric Vehicles as Power Plants- a Techno-Economic Scenario Analysis in two Climates for Smart Cities*. Delft University of Technology.

Samrat, N.H., Ahmad, N. Bin, Choudhury, I.A. & Taha, Z. Bin. 2014. Modeling, Control, and Simulation of Battery Storage Photovoltaic-wave Energy Hybrid Renewable Power Generation Systems for Island Electrification in Malaysia. *Scientific World Journal*, 2014: 1–22.

Sanguesa, J.A., Torres-Sanz, V., Garrido, P., Martinez, F.J. & Marquez-Barja, J.M. 2021. A Review on Electric Vehicles: Technologies and Challenges. *Smart Cities*, 4(1): 372–404.

Shang, J. 2013. *The Role of Hydrogen and fuel Cells for Ultra Low Carbon Vehicles*. University of Birmingham. http://etheses.bham.ac.uk/5101/%5Cnhttps://trid.trb.org/view/1331972.

Shi, L. & Crow, M.L. 2008. Comparison of Ultracapacitor Electric Circuit Models. *IEEE Power and Energy Society 2008 General Meeting: Conversion and Delivery of Electrical Energy in the 21st Century, PES*, (June).

Showers, S.O. 2019. *Enhanced Frequency Regulation of a Grid-Connected PV System*. Cape Peninsula University of Technology.

Showers, S.O. & Raji, A.. 2022. State-of-the-art review of fuel cell hybrid electric vehicle energy management systems. *AIMS Energy*, 10(3): 458–485.

Smithson Bell, J.K. 2016. *Design and Control of a Hydrogen Fuel Cell Vehicle*. University of California, IRVINE.

Sorlei, I., Bizon, N., Thounthong, P., Varlam, M., Carcadea, E., Culcer, M., Iliescu, M. & Raceanu, M. 2021. Fuel Cell Electric Vehicles—A Brief Review of Current Topologies and Energy Management Strategies. *Energies*, 14(1): 2–27.

Souleman, N.M., Tremblay, O. & Dessaint, L.A. 2009. A generic fuel cell model for the simulation of fuel cell power systems. In *2009 IEEE Power and Energy Society General Meeting, PES*. Dearborn, Michigan, USA: IEEE: 1722–1729.

Soylu, S. 2011. *Electric Vehicles – Modeling and Simulations*. Rijeka, Croatia: INTECH.

Strahl, S. 2014. *Experimental and Model-Based Analysis for Performance and Durability Improvement of PEM Fuel Cells*. Universitat Politecnica De Catalunya. http://www.tesisenxarxa.net/handle/10803/285240.

Suh, K.W. 2006. *Modeling, Analysis and Control of Fuel Cell Hybrid Power Systems*. University of Michigan, Ann Arbor, Michigan.

Sulaiman, N., Hannan, M.A., Mohamed, A., Ker, P.J., Majlan, E.H. & Wan Daud, W.R. 2018. Optimization of Energy Management System for Fuel-cell Hybrid Electric Vehicles: Issues and Recommendations. *Applied Energy*, 228(May): 2061–2079. https://doi.org/10.1016/j.apenergy.2018.07.087.

Sulaiman, N., Hannan, M.A., Mohamed, A., Majlan, E.H. & Wan Daud, W.R. 2015. A Review

on Energy Management System for Fuel Cell Hybrid Electric Vehicle: Issues and Challenges. *Renewable and Sustainable Energy Reviews*, 52: 802–814.

Sun, D., Lin, X., Qin, D. & Deng, T. 2012. Power-Balancing Instantaneous Optimization Energy Management for a Novel Series-Parallel Hybrid electric bus. *Chinese Journal of Mechanical Engineering (English Edition)*, 25(6): 1161–1170.

Sundmacher, K., Schultz, T., Zhou, S., Scott, K., Ginkel, M. & Gilles, E.D. 2001. Dynamics of the Direct Methanol Fuel Cell (DMFC): Experiments and Model-Based Analysis. *Chemical Engineering Science*, 56(2): 333–341.

Sundström, O. & Stefanopoulou, A. 2006. Optimal power split in fuel cell hHybrid electric vehicle with different battery sizes, drive cycles, and objectives. In *IEEE International Conference on Control Applications*. Munich: 1681–1688.

Tazelaar, E., Veenhuizen, B., Jagerman, J. & Faassen, T. 2013. Energy Management Strategies for Fuel Cell Hybrid Vehicles; an Overview. In *EVS27 International Battery, Hybrid and Fuel Cell Electric Vehicle Symposium*. Barcelona, Spain: EVS27: 1–12.

Trovão, J.P., Machado, F., Silva, M.A. & Neves De Melo, H. 2014. Reduced-scale hardware-in-the-loop simulation to study several hybridization rates of electric vehicles. In *IEEE Vehicle Power and Propulsion Conference, VPPC*. IEEE Xplore.

Trovao, J.P.F., Roux, M.A., Menard, E. & Dubois, M.R. 2017. Energy- and power-split management of dual energy storage system for a three-wheel electric vehicle. *IEEE Transactions on Vehicular Technology*, 66(7): 5540–5550.

Uzunoglu, M. & Alam, M.S. 2007. Dynamic Modeling, Design and Simulation of a PEM fuel cell/Ultra-Capacitor Hybrid System for Vehicular Applications. *Energy Conversion and Management*, 48(5): 1544–1553.

Vaz, W.S. 2015. *Energy Management in Electric Vehicles: Development and Validation of an Optimal Driving Strategy*. Missouri University of Science and Technology. https://search.proquest.com/docview/1721711343?accountid=14166%0Ahttp://xg9ax2jm9j.search.serialssolutions.com?ctx_ver=Z39.88-2004&ctx_enc=info:ofi/enc:UTF-8&rfr_id=info:sid/ProQuest+Dissertations+%26+Theses+Global&rft_val_fmt=info:ofi/fmt:kev:mtx:dissert.

Waag, W., Fleischer, C. & Sauer, D.U. 2014. Critical Review of the Methods for Monitoring of Lithium-Ion Batteries in Electric and Hybrid Vehicles. *Journal of Power Sources*, 258: 321–339. http://dx.doi.org/10.1016/j.jpowsour.2014.02.064.

Wang, C. 2006. *Modelling and Control of HybridWind/Photovoltaic/Fuel Cell Distributed Generation Systems*. Montana State University.

Wang, Z., Huang, B., Li, W. & Xu, Y. 2006. Particle swarm optimization for operational parameters of series hybrid electric vehicle. In *IEEE International Conference on Robotics and Biomimetics, ROBIO*. Kunming, China: IEEE: 682–688.

Weyers, C. & Bocklisch, T. 2018. Simulation-Based Investigation of Energy Management Concepts for Fuel cell – Battery – Hybrid Energy Systems in Mobile Mobile Applications. *Energy Procedia*, 155: 295–308. https://doi.org/10.1016/j.egypro.2018.11.048.

Williamson, S.S. 2013. *Energy Management Strategies for Electric and Plug-in Hybrid Electric Vehicles*. London: Springer.

Wu, B. 2014. *Fuel Cell Hybrid Electric Vehicle Powertrain Modelling and Testing*. Imperial College London.

Wu, J., Yuan, X.Z., Martin, J.J., Wang, H., Zhang, J., Shen, J., Wu, S. & Merida, W. 2008. A Review of PEM Fuel Cell Durability: Degradation Mechanisms and Mitigation Strategies. *Journal of Power Sources*, 184(1): 104–119.

Xu, L., Mueller, C.D., Li, J., Ouyang, M. & Hu, Z. 2015. Multi-objective component sizing based on optimal energy management strategy of fuel cell electric vehicles. *Applied Energy*, 157: 664–674. http://dx.doi.org/10.1016/j.apenergy.2015.02.017.

Yuan, X.Z., Li, H., Zhang, S., Martin, J. & Wang, H. 2011. A Review of Polymer Electrolyte Membrane Fuel Cell Durability Test Protocols. *Journal of Power Sources*, 196(22): 9107–9116. http://dx.doi.org/10.1016/j.jpowsour.2011.07.082.

Yue, M. 2019. *Contribution of Developing a Prognostics-based Energy Management Strategy for Fuel Cell Hybrid System - Application to a Fuel cell / Battery Hybrid Electric Vehicle*. Université Bourgogne Franche-Comté.

Zeiaee, M. 2016. *An Intelligent Cell-Level Battery / Ultracapacitor Hybrid*. McMaster University.

Zhang, Q. & Li, G. 2019. A Game Theory Energy Management Strategy for a Fuel Cell/Battery Hybrid Energy Storage System. *Mathematical Problems in Engineering*, 2019.

Zhang, S., Yuan, X., Wang, H., Mérida, W., Zhu, H., Shen, J., Wu, S. & Zhang, J. 2009. A review of accelerated stress tests of MEA durability in PEM fuel cells. *International Journal of Hydrogen Energy*, 34(1): 388–404.

Zhang, W., Li, J., Xu, L. & Ouyang, M. 2017. Optimization for a Fuel Cell/Battery/Capacity Tram with Equivalent Consumption Minimization Strategy. *Energy Conversion and Management*, 134: 59–69. http://dx.doi.org/10.1016/j.enconman.2016.11.007.

Zhi-ling, J., Wei-rong, C., Zhi-jian, Q., Chao-hua, D. & Zhan-li, C. 2010. Energy Management for a Fuel Cell Hybrid Electrical Vehicle. In *Asia-Pacific Power and Energy Engineering Conference*. Chengd: IEEE: 1–6.

APPENDICES

Appendix 1: Battery management system

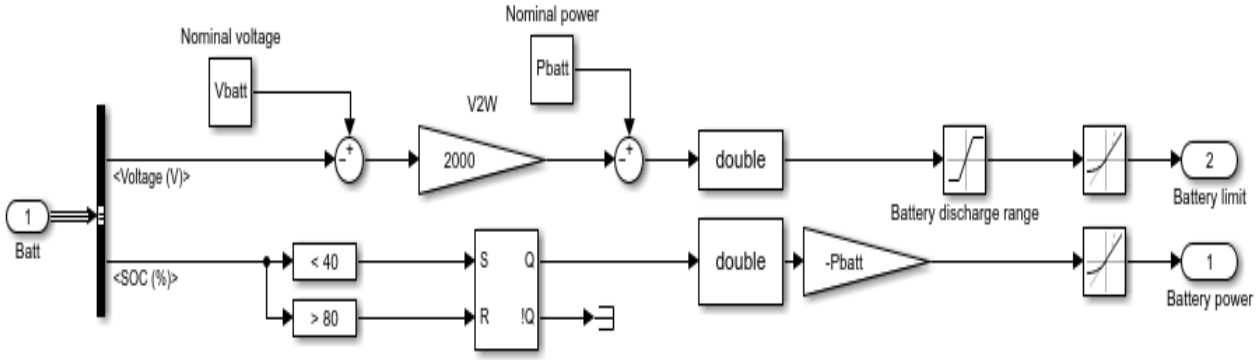

Appendix 2: EMS subsystem